A Comprehensive Investigation of New Planar Wideband Antennas

Seong-Youp Suh

Dissertation submitted to the Faculty of the Virginia Polytechnic Institute and State University in partial fulfillment of the requirements for the degree of

Doctor of Philosophy
In
Electrical and Computer Engineering

Dr. Warren L. Stutzman, Chair
Dr. William A. Davis
Dr. Ahmad Safaai-Jazi
Dr. Sanjay Raman
Dr. Tao Lin

July 29, 2002
Blacksburg, Virginia

Keywords: Wideband Antenna, Planar, Low Profile, Dual-Polarization, Ultra-wideband (UWB)

A Comprehensive Investigation of New Planar Wideband Antennas

Seong-Youp Suh

(ABSTRACT)

Broadband wireless communications require wideband antennas to support large number of users and higher data rates. Desirable features of a wideband antenna are low-profile, dual-polarization and wide bandwidth in a compact size. Many existing wideband antennas are large in size and some have only circular polarization. On the other hand low-profile, dual-polarized antennas frequently have limited bandwidth. This dissertation reports on results from original research into several new wideband antennas. All are compact and planar, and many are low-profile and dual-polarized.

Since 1994, Virginia Tech Antenna Group (VTAG) has performed research on the wideband, low-profile and dual-polarized antennas of compact size. This research resulted in the following antenna innovations: the Fourpoint, Fourtear, PICA (Planar Inverted Cone Antenna), diPICA (dipole PICA) and LPdiPICA (Low-Profile diPICA) antennas. They are all planar in geometry so one can easily construct them in a compact size. The antennas were characterized and investigated with extensive simulations and measurements. The computed and measured data demonstrates that some of the antennas appear to have the characteristics of the self-complementary antenna and most of the proposed antennas provide more than a 10:1 impedance bandwidth for a VSWR < 2. Patterns, however, are degraded at the high end of the frequency. Several tapered ground planes were proposed to improve the radiation pattern characteristics without degrading the impedance performance. A simulation result proposed a possibility of another antenna inventions providing 10:1 pattern bandwidth with the 10:1 impedance bandwidth.

Research into wideband antennas demonstrated that the newly invented antennas are closely related each other and are evolved from a primitive element, PICA. Not only the comprehensive investigation but also a practical antenna design has been done for commercial base-station array antennas and to phased array antennas for government applications. This dissertation presents results of comprehensive investigation of new planar wideband antennas and its usefulness to the broadband wireless communications.

DEDICATION

To my wife,

Hyunhee

and to my three sons

David (Chanyoung), Jonathan (Chanwoo), and Joseph (Chaneui)

ACKNOWLEDGEMENTS

Above all, I give thanks to my heavenly Father, God, my Savior, Jesus Christ, and my Comforter, Holy Sprit. Many of the idea in this dissertation came along with the relationship with God during prayer. He gave me a wisdom how to solve and to optimize the antenna performance whenever I confronted with difficult problem. God surely lead my research to a right direction and I was able to experience God through the research. I praise and worship God, my creator and my Lord! Hallelujah!

I appreciate every effort made by committee members throughout this research. Particularly I would like to thank to my advisor, Professor Warren Stutzman for his guidance and funded support with my research. He didn't hesitate to give a fruitful advice and didn't forget to say "good job" whenever I brought an idea. The word "good job" was a great encourage to me during my research. Thanks to Professor William Davis for his warm concern and creative input to this dissertation. I would also like to thank to Professors. Ahmad Safaai-Jazi, Sanjay Raman and Tao Lin for their sincere advice and support. Their comments on my research were very helpful for enhancing the dissertation quality.

I also thank to Randall Nealy for his help in building the antenna and measurement. Thanks to Koichiro Takamizawa for his support and contribution of time for sharing my idea. Thanks to Derek Wells for being a good friend. I would like to thank to all antenna group members for their help: Mike Barts, Carl Dietrich, Melba Morrozoff, Taeyoung Yang, Josh Arritt, Carey Buxton, Nathan Cummings, Kai Dietze, Eric Caswell, Christopher Hearn, Minh-Chau Huynh, Gayrav Joshi, Byung-Ki Kim, Stani Licul, Laure Mousselon, Kevin Mescher, and Melanie Jennelle, and to those who encouraged me through this research.

Thanks to Drs. ByungSil Jun, JongKyo Kim, WoonChul Ham, HeungKi Baek, JoonHwan Lee, and MoonHo Lee who are professors at ChonBuk National University in Korea. I also thanks to my previous work members at Agency for Defense Development (ADD) in Korea. Special thanks to SeungYul Ahn, MooDo Kim, JoonBok Park, BonSoon Koo, MyungJin Jang, and TaeIn Choi who were my bosses at the research center, ADD. Thanks to my friends in Korea as follows: SeungGoo Lee, NamGyoon Yoon, JongGyoo Park, SangKi Chung, JeongSoo Yoo, SangHwan Kweon, TaeGeun Bong, YoungHo Choi, SeungHyun Lee, HyunSeung Kim, SukBin Lee, JongIn Ko, and their families.

I would like to thanks to JaeWoo Lee, HyungJin Lim, WanSoo Jeong, JongGwan Cho, JaeMoon Kang, ChoongHwan Cho and to the brothers and sisters at Navigator in Jeonju who helped and prayed for me to grow in Jesus Christ. I cannot forget the beautiful moments sharing my life with them, preaching the gospel to students in campus, studying the bible, and having lunch at the bench under a tree. I deeply thanks to all of them.

I would like to give special thanks to my pastor, Hyun David Chung and his family for their continuous prayer and lovely concern. Thanks to praise team for their encourage and lovely friendship as follows: Heejeong Kim, Kanguook Lee, Misun Chung, Sangwon Park, Junhyung Kim, Hyunjeong Lee, Hanna Shin, Seungyeon Han and Yoojin Hwang. I also thank to sincere brothers in Jesus Christ who prayed for me: KyoungKyoon Bae, Yonggul Lee, Jeonghoi Koo, Sukwon Kim, Hongman Kim, Yunhyun Kim, and Jeonghoon Kim, and to every brothers and sisters in Korean Baptist Church of Blacksburg (KBCB). Thanks to the alumni of KBCB as follows: SangGyoon Kim, ByungMoon Song, ByungKi Ahn, HeungKweon Shin, SungWon Kang, DongWoo Sohn, and HyungSuk Oh.

During the research period, God allowed me to teach the bible to college students in Virginia Tech, which is my sacred privilege. I would like to thank to all the college students and alumni in Korea Campus Crusade for Christ (KCCC) for their enthusiastic encourage and prayer. Special thanks to YoungJoo Kim who helped with the drawing figures in the dissertation. I also thank to JeongHoon Kim, Iksoo Hong, Byungsun Choi, Jooback Lee, Youngil Kang, Sungmin Lee and every leaders in VT KCCC: KunEui Kang, JoonTaek Lee, YoungUook Kim, JooHan Lee, MinSoo Park, SeMin Kim, SooHyung Lee, ChanWon Park, KeunBae Kim, NakHyun Kim, SukHan Song, UnJoo Hwang, HyunYoung Lim, YunHa Lee, JiEun Song, MinJeong Kim, HyunKyung Koo, Gina Song, YoungJoo Lim, MyungJoo Ji. And I would like to thanks to every VT KCCC alumni.

I am grateful to my mother, JeongJi Gweon who prayed for me every day and patiently waited this Ph.D. dissertation in Korea. Thanks to my siblings, Bong-Geum, Haeyoung,and Sungil, and their families. I also thank to my father, Yongki Suh who are in heaven. I would like to thank to my parent-in-law, Doo-Ok Kim and Jeong-Soon Yoon for their support and lovely care. I also thank to brother- and sister-in-law, Hyuntae, Hyunah, Yoonhee and KyungTae, and their families. Thanks to my three sons, David (Chanyoung), Jonathan (Chanwoo), and Joseph (Chaneui) who are my precious treasures. I am deeply grateful to my wife, Hyunhee who is my eternal lover mated by my heavenly Father, God. Without her support and prayer, I cannot finish my dissertation at all.

CONTENTS

LIST OF FIGURES

LIST OF TABLES

Chapter 1

Introduction

1.1 Motivation

The demand for wireless wideband communications is rapidly increasing due to the need to support more users and to provide more information with higher data rates. Wideband antennas are essential for providing wireless wideband communications. Many wireless, wideband communication devices require features of low-profile, linear polarization and unidirectional patterns in a compact size. Another desirable feature is that of dual-polarization to support polarization diversity, polarization frequency reuse, or polarization agile operation. Many existing wideband antennas, however, are electrically large and provide a single circular polarization.

Wideband antennas are useful for the wideband scanning array antennas in military applications. Such applications require several features such as wide scan, security, high speed communication and high reliability in a compact size. Note that the element size is a critical parameter in determining the scan angle in an array antenna [1.1, pp. 130-133]. Small size is desirable for the array antenna. Specifically, a low-profile

geometry is much more desirable for a space-limited mobile vehicle. Many military vehicles, however, contain many protruding antennas for multiple communication links. There are many applications in both industry and government for a wideband, low-profile, polarization diverse antenna.

Since 1994, Virginia Tech Antenna Group (VTAG) has performed research on wideband, low-profile and dual-polarized antennas of compact size. Two antennas-the Foursquare antenna [1.2] and the Trimmed Foursquare antenna [1.3]-have been patented as a result of the research. The Foursquare antenna provides excellent features of a low-profile geometry, dual-linear polarization, unidirectional pattern and wideband (about 50 % bandwidth); all being desirable for wideband communications in industry and military applications.

This dissertation presents investigation results for several new wideband antenna inventions. They are: Fourpoint antenna (Chapter 3), Fourpoint antenna with tuning plate (Chapter 4), Fourtear antenna (Chapter 5), PICA antenna (Chapter 6) and low-profile dipole PICA antenna (Chapter 7). Provisional patents are filed for three of these antennas - the PICA antenna [1.4], the Fourpoint antenna [1.5] and the Fourtear antenna [1.6].

The newly invented antennas can be used in wideband phased array antennas to provide wide-scan, low-profile and dual-polarization features. In addition to phased array antenna applications, the newly invented antennas are promising candidate antennas for dual-band, dual-polarization base-station array antennas covering AMPS, GSM, DCS and PCS bands.

1.2 Overview

In Chapter 2, several wideband antennas are reviewed. Most of them have planar geometry except for the spheroidal antenna [1.7, pp. 480-482], teardrop antenna [1.8, pp. 9] and biconical antenna [1.1, pp. 242-243]. The concept of the teardrop antenna was largely used in antenna inventions. Monopole disc antennas are also extensively reviewed in Chapter 2 because they are fundamental to the development of the Planar Inverted Cone Antenna (PICA). The Foursquare antenna is also reviewed in detail due to the direct relationship to the Fourpoint antenna.

The Fourpoint antenna, discussed in Chapter 3, improved the performance of the Foursquare antenna dramatically without increasing mechanical size. A tuning plate was added to the Fourpoint antenna to enhance the impedance bandwidth by extending the high frequency performance. The idea of the performance enhancement is discussed extensively with computed data and measured data from two hardware test models. A circularly polarized Fourpoint antenna was simulated and the results demonstrate that the Fourpoint antenna is able to provide not only dual-linear polarization but also circular polarization.

In Chapter 4, the effect of the tuning plate is presented for both Foursquare and Fourpoint antennas. The computed impedance characteristics are compared for cases with and without the tuning plate. The simulation results demonstrate that the tuning plate enhances the impedance bandwidth of the both Foursquare and Fourpoint antennas toward the high end of the frequency band.

In Chapter 5, the gap in the Fourpoint antenna was investigated to enhance the impedance bandwidth further. The Fourtear antenna was invented as a result of this investigation. The Fourtear antenna, however, has an asymmetrical geometry, giving impedance characteristics that are different for each feed configuration. A modified Fourtear antenna with hexagonal geometry was developed and measured in an attempt to minimize the impedance difference for each feed configuration. The measured results demonstrate that the modified Fourtear antenna provides similar impedance characteristics for each feed configuration.

A newly invented PICA antenna is discussed in Chapter 6. The PICA antenna evolved from the monopole disc antennas discussed in Chapter 2. The PICA antenna was examined using several hardware test models. The results demonstrate that the PICA antenna enhances the radiation pattern bandwidth significantly compared to the monopole disc antennas reviewed in Section 2.5. Moreover, the PICA has smaller size than conventional monopole disc antennas.

In Chapter 7, a modified PICA antenna is presented. The dipole PICA (diPICA) was simulated and the results demonstrate that the diPICA antenna has extremely wide impedance and pattern bandwidth. The diPICA antenna was modified further forming a low-profile diPICA (LPdiPICA) with a unidirectional pattern. The LPdiPICA was measured at the Virginia Tech Antenna Group providing wide impedance. The LPdiPICA antenna was found to suffer a degrading radiation pattern as the frequency increases. To enhance the radiation pattern at high frequencies, an exponentially tapered ground plane was simulated. The simulation results demonstrate that the tapered ground plane enhances the radiation performance at high frequencies.

In Chapter 8, the investigation results of this dissertation are summarized and possible future work is proposed.

References

[1.1] W. L. Stutzman and G.A. Thiele, *Antenna Theory and Design 2nd edition*, John Wiley & Sons, New York, 1998.

[1.2] J. R. Nealy, "Foursquare Antenna Radiating Element," *U.S. Patent No. 5,926,137*, July 20, 1999. VTIP Ref. 96-056. http://www.vtip.org.

[1.3] Randall Nealy, Warren Stutzman, J. Matthew Monkevich, William Davis, "Improvements to the Foursquare Radiating Element-Trimmed Foursquare," *U.S. Patent No. 6,057,802*, May 2, 2000. VTIP Ref. 98-001. http://www.vtip.org.

[1.4] Seong-Youp Suh and Warren L. Stutzman, "*A Planar Inverted Cone Antenna*," VTIP disclosure No. 00-130, http://www.vtip.org/Licensing/disclosures/00-130.htm, September 8, 2000

[1.5] Seong-Youp Suh and Warren L. Stutzman, "*A Fourpoint Antenna*," VTIP disclosure No. 00-141, http://www.vtip.org/Licensing/disclosures/00-141.htm, September 28, 2000

[1.6] Seong-Youp Suh and Warren L. Stutzman, "*A Fourtear Antenna*," VTIP disclosure No. 01-078, http://www.vtip.org/Licensing/disclosures/01-078.htm, July 17, 2001

[1.7] S. Ramo and J. R. Whinnery, *Fields and Waves in Modern Radio*, New York, 1944.

[1.8] J. D. Kraus, *Antennas*, McGraw Hill, New York, 1950.

Chapter 2

Literature Review

The IEEE (Institute of Electrical and Electronics Engineers) standard [2.1, pp. 5] defines the bandwidth of an antenna as "the range of frequencies within which the performance of the antenna, with respect to some characteristics, conforms to a specific standard." In this dissertation, the bandwidth is defined for impedance and radiation pattern separately. The impedance bandwidth is defined for a VSWR less than 2. The radiation pattern bandwidth, however, is hard to define with a specific criterion, so it is simply taken to be the frequency range within which the patterns are acceptable for a specific application.

The bandwidth can be denoted as a percent of the center frequency B_p as follows:

$$B_p = \frac{f_U - f_L}{f_C} \times 100\% . \tag{2-1}$$

where $f_c = \frac{f_L + f_U}{2}$ and f_U and f_L are the upper and lower frequencies of operation for which satisfactory performance is obtained [2.2, pp.225].

Bandwidth may also be defined as a ratio B_r by [2.2, pp.225]

$$B_r = \frac{f_U}{f_L} . \tag{2-2}$$

Basic wideband antenna structures have been investigated since the early 1940's. Stratton and Chu [2.3], [2.4] proposed the spheroidal antenna in 1941. Their study of spheroidal antennas was obtained by a straightforward solution of Maxwell's equation. However, spheroidal antenna analysis cannot be applied to general antennas of arbitrary shape.

In 1943, Schelkunoff proposed a biconical antenna which can be easily explained with Maxwell's equations [2.4] [2.5]. He also extended his analysis results for the biconical antenna to antennas of general shape. He presented analytical formulas for antenna impedance characteristics for several antenna shapes. The biconical antenna is still widely used for wideband antenna applications and its variations, including the discone antenna and the bow-tie antenna, are popular antennas for wideband applications.

In 1947, a wideband antenna concept was proposed by the staff of the U.S. Radio Research Laboratory at Harvard University [2.9]. The concept of a wideband antenna evolves from a transmission line that gradually diverges while keeping the inner and outer conductors ratio constant. Several variations of the concept were developed, such as the teardrop antenna, sleeve antenna and inverted trapezoidal antenna, etc.

In 1950's, the spiral antenna was introduced in the class of frequency independent antennas. The equiangular spiral and Archimedean spiral antennas are the most well

known spiral antennas. Spiral antennas have about a 10:1 bandwidth, providing circular polarization in a low-profile geometry [2.12].

In 1982, R. H. Duhamel invented the sinuous antenna, which provides dual-linear polarization plus wide bandwidth in a compact, low-profile geometry [2.15]. The sinuous antenna is more complicated than the spiral antenna. However, it provides dual orthogonal linear polarizations so that it can be used for polarization diversity or for transmit/receive operation. Also, the two two-arm pair outputs can be combined to produce simultaneous LHCP and RHCP [2.2].

Several monopole disc antennas have been invented since 1992 [2.16]-[2.20]. They produce very wide bandwidth with a simple structure such as circular, elliptical or trapezoidal shapes. The radiating elements are mounted orthogonal to a ground plane and are fed by a coaxial cable. The monopole disc antennas are promising antennas for Ultra Wideband (UWB) applications.

In 1999, the Foursquare antenna was invented and patented by Virginia Tech Antenna Group (VTAG). Even though the Foursquare antenna does not offer as much bandwidth as other elements discussed in this chapter, it has its unique characteristics such as unidirectional pattern, dual-polarization, low-profile and compact geometry [2.21], [2.22]. The compact geometry of the Foursquare antenna is one of a desirable feature for wide-scan, phased array antenna. The scanning performance of the array is generally determined by the element spacing, which is limited by the element size. For wideband antennas the operating band is very broad, making the electrical distance between the elements larger as the frequency increases. Ideally, less than $\lambda/2$ spacing is desired over the frequency band. When the element size is large, the spacing will easily exceed the $\lambda/2$ spacing at high frequency so the scanning performance of the array is degraded. Therefore small size antenna such as offered by the Foursquare antenna is desirable for a wideband array antenna. The remainder of this chapter discusses many of the wideband antennas.

2.1 Spheroidal Antenna [2.3] [2.4]

In 1941, Stratton and Chu presented solutions not only for spherical antennas but also for prolate spheroidal antennas as shown in Fig. 2.1. Figure 2.1 shows the evolution from a sphere to a thin spheroidal wire dipole. Axial symmetry is assumed, and the excitation voltage is applied across a very small gap at the center.

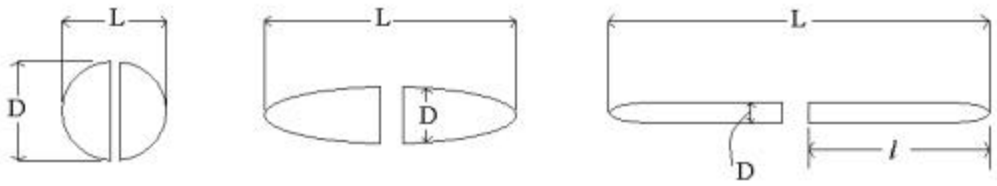

(a) Spherical wire (b) Spheroidal wire (c) Thin wire.

Figure 2.1 Transition from 3D sphere to the thin 3D spheroidal wire dipole.

Stratton and Chu noted that spheroidal antenna characteristics are quite similar in nature but different in magnitude from the results for the sphere. They found that large eccentricity (large ratios of length to diameter) generate sharp resonances in contrast to the broad resonance of the sphere. They mentioned that zero reactance occurs when the antenna length is slightly less than a half wavelength for long thin wires (about 0.49 λ or 98 % of the antenna length). However, for fatter wires zero reactance may occur when the antenna length is greater than a half wavelength. For a spherical conductor there is no place at which input reactance is zero; there is always a capacitive component.

It was evident that the fatter antenna makes the impedance curve broader, and thus provides wider bandwidth.

2.2 Biconical Antenna [2.2] - [2.7]

In 1943, Schelkunoff proposed a biconical antenna as shown in Fig. 2.2 [2.4] [2.5]. The biconical antenna concept is based on the fact that thicker wire provides wider impedance bandwidth than that for a thin wire dipole antenna [2.2]. This concept can be extended to further increase bandwidth if the conductors are flared to form the biconical structure in Fig. 2.2. The biconical antenna can be analyzed as transmission line if the biconical antenna is flared out to infinity. The infinite biconical antenna, as shown in Fig. 2.2 (a), acts as a guide for a spherical wave. It was proved that there is only a TEM mode in the infinite biconical antenna [2.2].

The input impedance of the infinite biconical antenna can be computed from the ratio of terminal voltage and current. The terminal voltage and current can be computed by integrating E_q and H_f respectively [2.2]:

$$V(r) = \int_{?_h}^{p-?_h} E_? \, r \, d? = \frac{?H_0}{2p} e^{-j\beta r} \ln\left(\cot\frac{?_h}{2}\right) \tag{2-3}$$

$$I(r) = \int_0^{2p} H_f \, r \sin ? \, df = 2prH_f \sin ? = \frac{H_o}{2} e^{-jb\,r}. \tag{2-4}$$

The characteristic impedance at any point r, from (2-1) and (2-2), is

$$Z_o = \frac{V(r)}{I(r)} = \frac{?}{p} \ln\left(\cot\frac{?_h}{2}\right). \tag{2-5}$$

Since this is not a function of distance r, the antenna input impedance must also be equal the characteristic impedance. Thus, (2-5) gives the input impedance:

$$Z_A = Z_o = 120 \ln\left(\cot\frac{?_h}{2}\right) \quad O \tag{2-6}$$

where $h/p \cong 120$ was used.

For q_h less than 20°,

$$Z_A = Z_o \approx 120 \ln\left(\frac{2}{?_h}\right) \quad O \tag{2-7}$$

where q_h is in radians.

The input impedance of the infinite biconical antenna is real valued because there is only a pure traveling wave. In other words, the infinite structure has no discontinuities and does not cause reflections that, in turn, set up standing waves, which generate a reactive component in the impedance [2.2].

The practical form in the biconical antenna family is the finite biconical antenna shown in Fig. 2.2(b) and formed by finite sections of the two infinite cones. The discontinuity at the ends of the cones causes higher order modes, which introduce a reactive component and increase the standing wave ratio. However, experimental results by G. H. Brown revealed that for large angle q_h (see the Fig. 2.2 (b)) the reactive component is reduced and the bandwidth is wider [2.6].

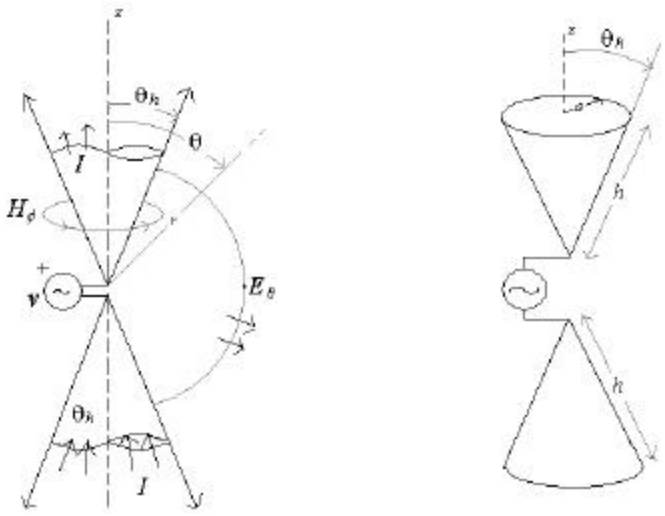

(a) Infinite biconical antenna. (b) Finite biconical antenna.

Figure 2.2 Biconical Antenna [2.2].

A variation of the finite biconical antenna, called the discone antenna, was developed by Kandoian in 1945 [2.7]; see Fig. 2.3. A disc-shaped ground plane is used instead of a cone on top of the finite biconical antenna shown in Fig. 2.3. There are many useful applications for the discone antenna.

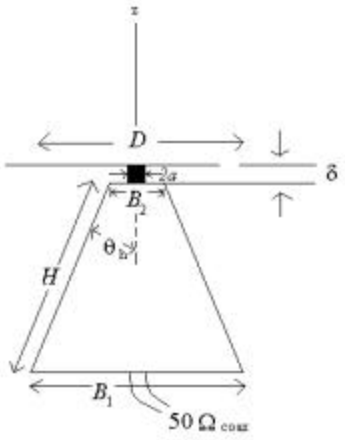

Figure 2.3 Discone antenna. Typical dimensions are $H \sim 0.7?$, $B \sim 0.6?$, $D \sim 0.4?$ *and* $d \langle\langle D$ [2.2].

2.3 Bow-tie Antenna [2.6] [2.8]

The bow-tie antenna is a planar version of the finite biconical antenna discussed in Section 2.2 and is a much simpler geometry as shown in Fig. 2.4. It offers less weight and less cost to build, but has a somewhat more frequency sensitive input impedance than the finite biconical. The bow-tie antenna provides a dipole-like omni-directional pattern with broad main beams perpendicular to the plane of the antenna. Since the currents are abruptly terminated at the ends of the fins, the antenna bandwidth is limited to about 2:1 [2.6].

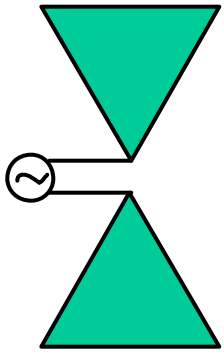

Figure 2.4 The bow-tie antenna.

The bow-tie antenna has been used in a planar array for aircraft flight test and evaluation of an UHF radiometer system [2.8]. Basically, the same bow-tie antenna element studied in [2.6] was applied to the radiometer system. But it was operated over a conducting ground plane to provide a unidirectional radiation pattern. The bow-tie antenna element shown in Fig. 2.5 has the flare angle of 60° and it employs a balun to feed the elements with a coaxial cable. The best wideband impedance characteristic was obtained for a dipole length of about 0.3λ (L) and height of about 3/8λ (H) at the center frequency. The simple bow-tie antenna achieved a bandwidth (VSWR < 2) of 37 % at the 50-Ω coaxial cable input; see Fig. 2. in [2.8]. The measured radiation patterns in [2.8] demonstrate the effect of the separation of the dipole and ground plane; see Figs. 3 and 4. in [2.8]. A slight depression was observed at the bore-sight direction of radiation patterns at upper frequency. The depression deepens as the frequency increases. However, the

distortion disappears when the separation between the element and ground plane is decreased; but the reduced height causes high VSWR so the impedance bandwidth may be reduced. This is the trade-off relationship between VSWR and radiation pattern in the bow-tie antenna with a ground plane.

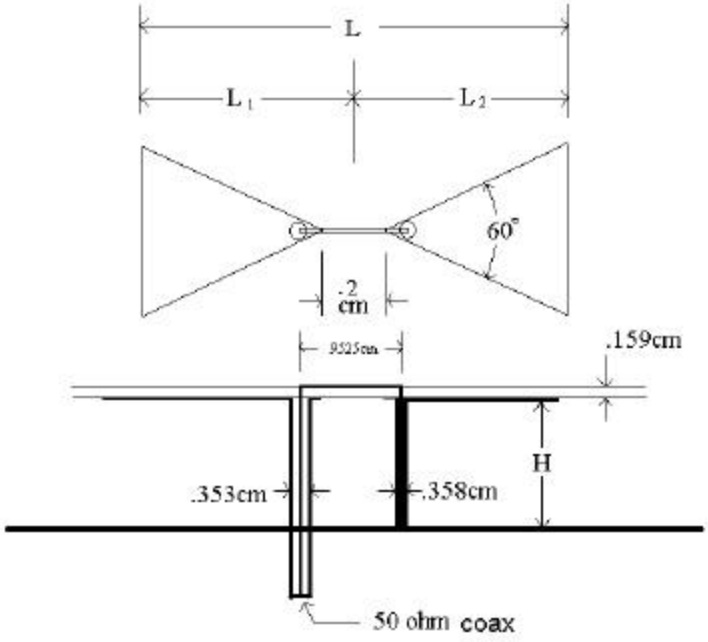

Figure 2.5 Geometry of a bow-tie antenna element with a ground plane [2.8].

2.4 Teardrop Antenna [2.9] - [2.11]

An antenna may be defined as a structure associated with the region of the transition between a guided wave and a free space, or vice versa. The transmission line acts as a guide for a plane wave and it has constant impedance over a broadband of frequencies.

Figure 2.6(a) shows a coaxial transmission line flared out while maintaining the ratio of the conductor diameter D/d constant [2.10]. Thus, the characteristic impedance of the line is constant along the transmission line. If the taper is gradual and D is large where the line ends, this device radiates with little reflection over very wide bandwidth as shown in Fig. 2.6 (b) [2.9]. Several variations from the wideband antenna concept are presented in Figs. 2.7 [2.9] and 2.8 [2.10]. Note that many antennas among the variations designed in 1940's are used in industry today.

The teardrop antenna shown in Fig. 2.8(b) was designed by shaping the top of the conductor shown in Fig. 2.8(a). The impedance bandwidth of the teardrop antenna is nearly as wide as that of the device in Fig. 2.8(a) and it radiates a guided wave into free space. The teardrop antenna was extensively studied by L. E. Lindenblad in 1941 to employ the antenna concept in a television antenna at the Empire state building television station [2.11]. Experimental results presented in [2.11] demonstrate that the shape of the teardrop antenna is a major factor in determining the bandwidth; see Fig. 11 in [2.11]. The optimum ratio of the teardrop antenna dimensions obtained experimentally are shown for the antenna in Fig. 2.9. Based on the teardrop antenna element, the television antenna was built on Empire State Building. The information on how the antenna works is not clearly described in the article. However, the concept of the teardrop antenna was employed in the television antenna of the Empire state building to obtain a wide bandwidth.

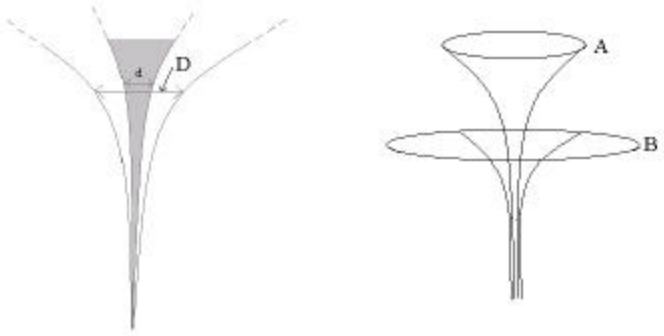

(a) A flared out transmission line [2.10]. (b) A wideband antenna [2.9].

Figure 2.6 Concept of the evolution of a wideband antenna from a tapered transmission line**.**

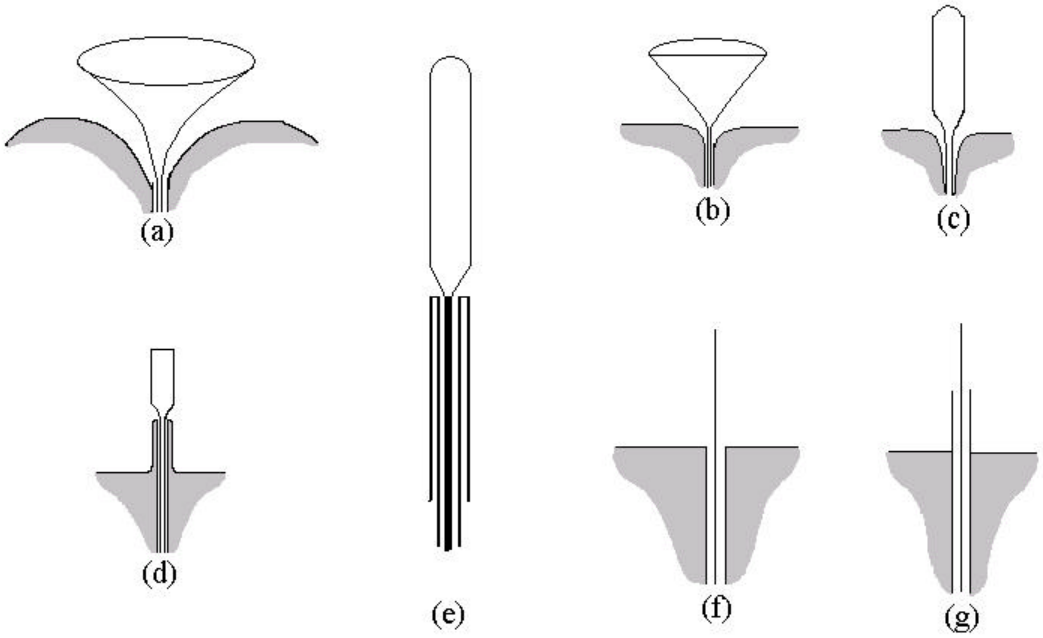

Figure 2.7 Various form of monopole wideband antenna in [2.9].

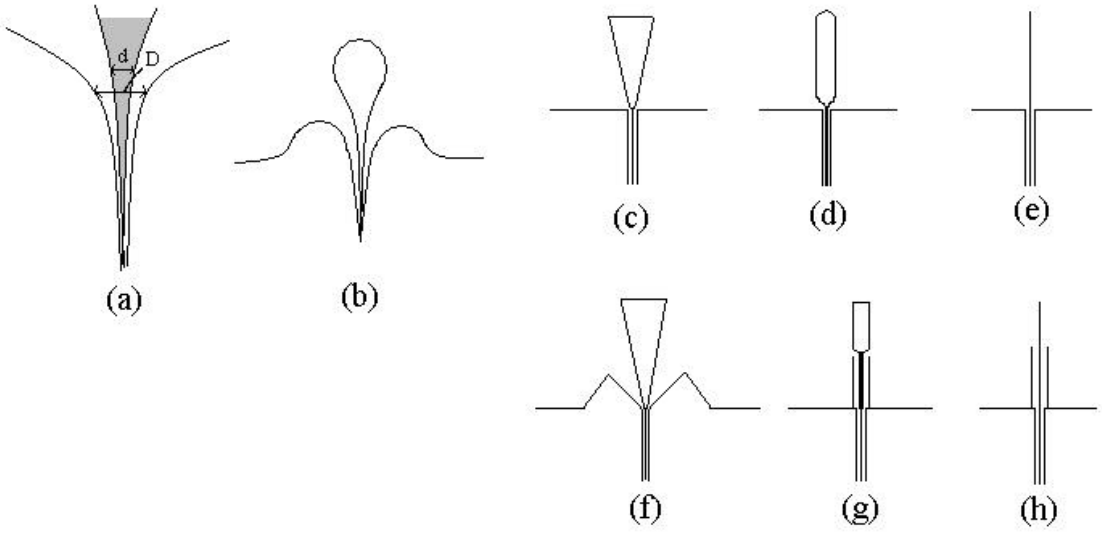

Figure 2.8 Various form of monopole wideband antenna in [2.10].

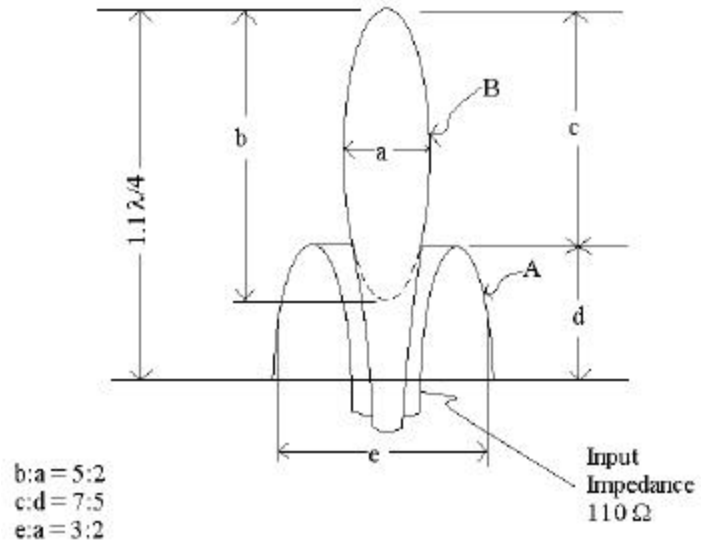

Figure 2.9 The optimum teardrop antenna by N. E. Lindenblad [2.11].

2.5 Spiral Antennas [2.2], [2.12] – [2.14]

Spiral antennas belong to the class of planar frequency independent antennas and are formed from a spiraled two-wire transmission line that gradually transforms itself into a radiating structure. An equiangular spiral antenna published by J. D. Dyson in 1959 is the earlist spiral antenna [2.12]. The spiral antenna design and its operation have been explained in many references that will not be cited here; see [2.2]. Several variations of the equiangular spiral antenna have been developed such as Archimedean spiral antenna. The Archimedean spiral antenna shown in Fig. 2.10 has the form of a self-complementary antenna, in which arm metallization is as thick as the space between arms. In theory, the self-complementary antenna has about 188.5-Ω input impedance [2.13]. However, the experimental data revealed that the impedance ranges from 120 to 200-Ω [2.14]. It is generally well known that the Archimedean spiral antenna produces a broad main beams perpendicular to the plane of spiral [2.2]. The broad main beam can be converted to the unidirectional beam by backing the spiral with a ground plane, which is desirable in most applications. The cavity-backed Archimedean spiral antenna employing a metallic cavity behind the spiral is popular for producing a unidirectional beam. In most commercial products, absorbing materials are loaded in the cavity to reduce the resonance effects; however, this introduces loss and consequent gain reduction. Typical performance parameters for the cavity-backed Archimedean spiral are Half Power Beam Width = 75°, |Axial Ratio| = 1 dB, Gain = 5 dB over a 10:1 bandwidth or more. The input impedance is about 120-Ω and is nearly real. The performance of the equiangular spiral is similar to that of the Archimedean [2.2].

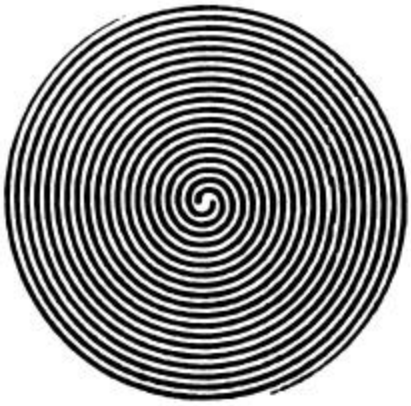

Figure 2.10 A geometry of an Archimedean spiral antenna [2.4, pp.256].

2.6 Sinuous Antenna [2.14], [2.15]

The sinuous antenna shown in Fig. 2.11, invented by R. H. Duhamel in 1982, is the most recent frequency independent antenna. It offers several advantages such as wide bandwidth and dual-linear or dual-circular polarization with low-profile geometry as [2.15]. The sinuous antenna has a four arm self-complementary structure that is fed in a balanced manner; and its diameter is about $0.4?_{L}$ at lowest operating frequency. Based on the self-complementary antenna theory, the sinuous antenna should have an input resistance of 188.5-Ω and an input reactance of 0-Ω over its bandwidth of operation in free space. However, measured data reveals that it has lower impedance than the theoretical value [2.14]. The measured input resistance was between 160-Ω and 190-Ω for substrate $(e_r = 2.33)$ thicknesses of 30 mils and 5 mils, respectively, keeping the input reactance near 0-Ω [2.15]. The substrate material also affects the characteristics of the sinuous antenna.

Most antenna applications require a ground plane to be used with low-profile antennas, such as the sinuous antenna, in order to produce a unidirectional beam. But the ground plane usually changes the antenna impedance characteristics over the operating band. Thus, the performance of frequency independent antennas, such as the sinuous, is greatly altered when used with a ground plane.

Figure 2.11 Geometry of a sinuous antenna [2.4, pp.258].

2.7 Disc Antennas [2.16]-[2.20]

Several disc type antennas have been invented since 1992. Disc antennas are named for their thin disc radiating structure which can be circular, elliptical, trapezoidal, or crossed half disc antenna. This section reviews several disc antennas.

2.7.1 Circular Disc Antenna [2.16], [2.17]

A flat circular disc antenna was proposed as a TV antenna operating at 90-770 MHz in 1992 [2.16]. The circular disc antenna is composed of a flat circular disc mounted above a ground plane as shown in Fig.2-12.

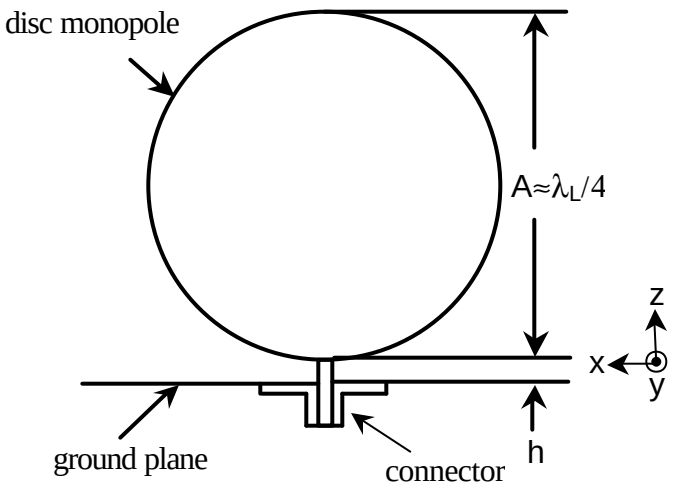

Figure 2.12 Circular disc antenna over a ground plane.
(λ_L is wavelength at the lowest operating frequency.)

The circular disc antenna has a very large impedance bandwidth, about 10:1. A circular disc antenna of diameter A=25 mm, made of 0.5 mm thick brass plate mounted at height h=0.7 mm over a square ground plane (30 cm x 30 cm) yielded acceptable impedance (VSWR<2) over the operating band from 2.25 to 17.25 GHz for a bandwidth of 7.7:1. [2.17] However, the radiation patterns of the circular disc antenna degrade at the high end of the band. The direction of the conical beam maxima in the E-plane pattern vary from 30° to 60° in elevation as frequency increases from 2.5 to 9.0 GHz, whereas in the H-plane the pattern remains somewhat omni-directional with maximum variation in azimuth increasing from 4 to 7 dB over the band. [2.17]

2.7.2 Modified Flat Monopole Antennas [2.18]

Several modified flat monopole antennas were proposed in [2.18] to obtain better impedance bandwidth. They are elliptical, square, rectangular, and hexagonal shaped flat monopoles. An elliptical disc monopole antenna having an ellipticity ratio of 1.1 yields the best performance. [2.18] However, the modified flat monopole antennas still suffer from radiation pattern degradation in E-plane.

2.7.3 Trapezoidal Flat Monopole Antenna [2.19]

The trapezoidal shape flat monopole antenna shown in Fig. 2.13 has been proposed as a variation of square flat monopole antenna. [2.19] The impedance bandwidth of the antenna was optimized by tapering the lower base near the ground plane. However, the trapezoidal flat monopole antenna does not solve the problem of variations in tilt angle of the E-plane pattern peak. [2.19]

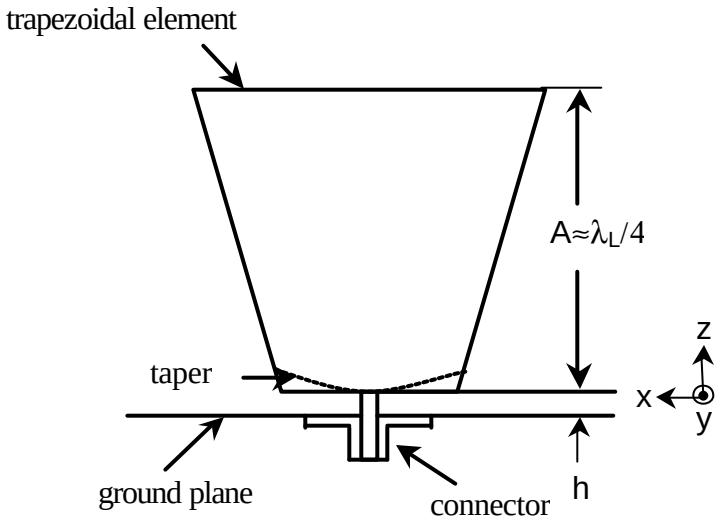

Figure 2.13 Trapezoidal planar monopole antenna above a ground plane.
(λ_L is wavelength at the lowest operating frequency.)

2.7.4 The Crossed Half-Disc Antenna [2.20]

The crossed half-disc antenna shown in Fig. 2.14 was proposed as a variation of the crossed bow-tie antenna. [2.20] The crossed flat (i.e. planar) elements improve the antenna pattern over the impedance bandwidth compared to a single half disc element. The dotted circle inside of the half disc in Fig. 2.14 represents the size of a circular disc having similar impedance bandwidth. The crossed half-disc antenna has about twice the maximum dimension of the circular disc antenna.

Typical specifications for omni-directional antennas from 0.5 to 18 GHz require ±2.0 dB pattern variation from omni-directional, 0 dBi gain, and 3:1 Voltage Standing Wave Ratio (VSWR). The crossed half-disc antenna maintains the pattern and gain specifications over wide bandwidth, with a 2:1 VSWR from 0.5 to 18 GHz [2.20]. However, cross polarization can be high.

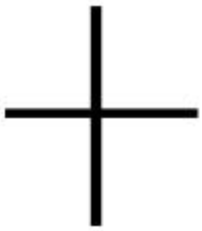

(a) Top view

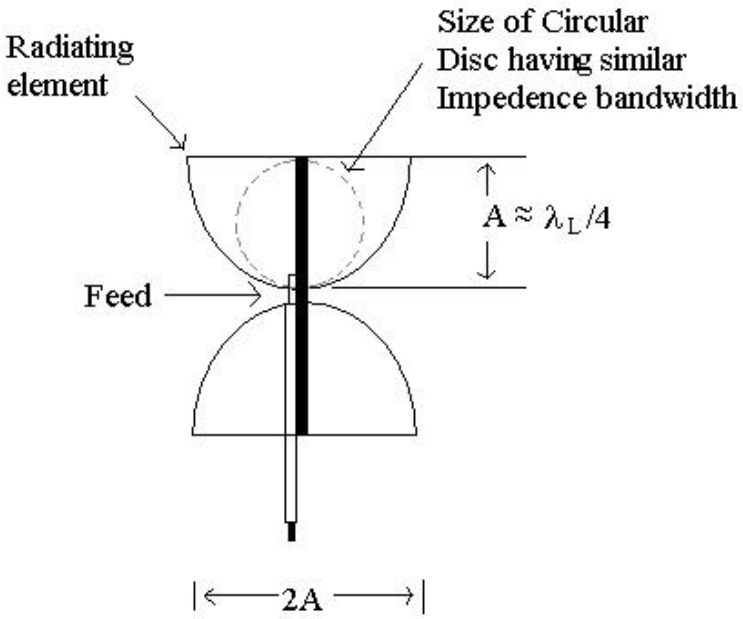

(b) Side view

Figure 2.14 Crossed half disc antenna.

(λ_L is wavelength at the lowest operating frequency.)

2.8 Foursquare Antenna [2.21] - [2.23]

The Foursquare antenna was patented by VTAG in 1999 [2.21]. Since it is the motivation for the Fourpoint antenna, which is one of main contributions in this dissertation, we describe the Foursquare antenna in detail here.

2.8.1 The Antenna Structure

The Foursquare antenna provides wideband performance and several practical advantages for commercial and military applications. Its features are a low-profile geometry, dual-polarization, compact radiating element size, making it ideal for use as an array element. The Foursquare antenna consists of four square-shaped flat radiating "squares" etched on a dielectric substrate and positioned above a ground plane as shown in Fig. 2.15. Opposing squares are fed with equal amplitude and opposite phase. The Foursquare provides dual, orthogonal linear polarizations naturally, but these polarization outputs can be processed to produce any polarization state(s). In this section, we present the dual-linear polarization configuration.

The diagonal length of the antenna $\sqrt{2}\,A$ is about $?_L/2$ and the height 'h' of the element above the ground plane is about $?_U/4$, where $?_L$ and $?_U$ represent wavelength at the lower and upper operating frequencies f_L and f_U [2.21], [2.22].

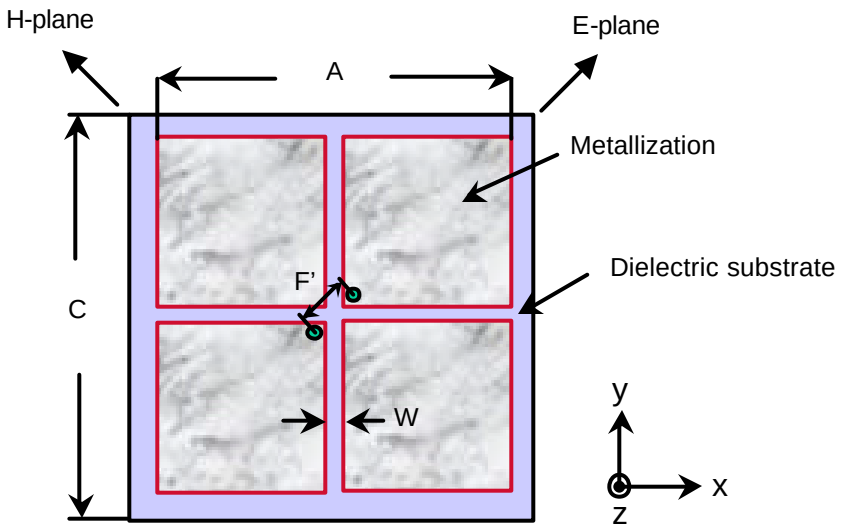

(a) Top view of the Foursquare antenna.

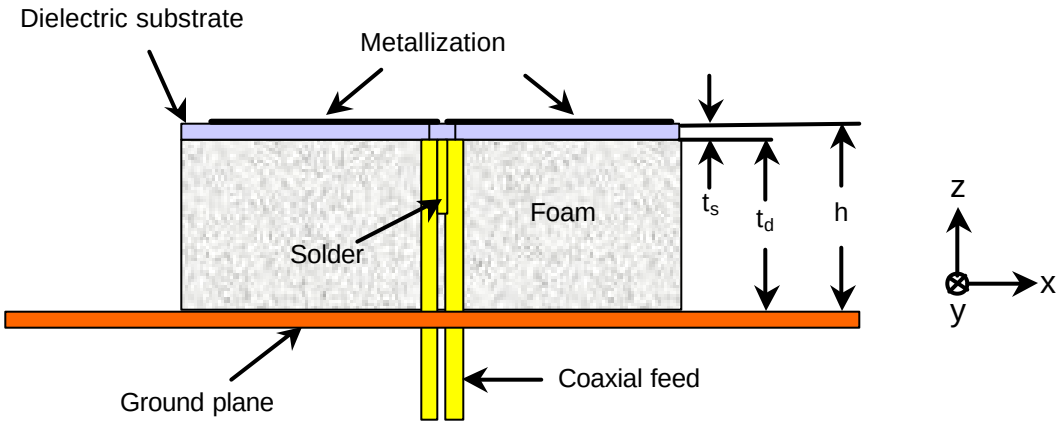

(b) Side view of the Foursquare antenna

Figure 2.15 Geometry of the Foursquare antenna [2.21].

2.8.2 Hardware Test model of the Foursquare antenna

A hardware test model of the Foursquare antenna was constructed and tested with the dimensions listed in Table 2.1 [2.21].

Table 2.1

Geometry of the Foursquare Antenna of Fig. 2.15 [2.21].

Description	**Symbol**	**Size**
Element side length	A	21.3 mm (0.84”)
Substrate side length	C	21.8 mm (0.86”)
Gap width	W	0.25 mm (0.01”)
Substrate thickness	t_s	0.7 mm (0.028”)
Foam thickness	t_d	6.4 mm (0.25”)
Element height above ground plane	h	7.06 mm (0.278”)
Feed positions distance	F’	4.3 mm (0.17”)

A dielectric constant 2.33 of the dielectric substrate was used in both simulation and measurement. Both the input impedance and the radiation patterns were measured at Virginia Tech Antenna Group. The Foursquare antenna was also simulated using both the Fidelity code (FDTD) from Zeland software [2.23] and the Agilent HFSS (High-Frequency Structure Simulator) code (FEM) from Agilent Technologies [2.24].

2.8.2.1 Antenna Input Impedance [2.25]

Input impedance of an antenna is the ratio of the voltage to current at the antenna terminals. The input impedance is composed of real and imaginary parts. Maximum power is radiated from the antenna at frequencies where the input impedance is closed to real value. Usually antenna is fed by transmission line such as coaxial cable, microstrip line, etc. The goal is to match the antenna impedance to the characteristic impedance of the connecting transmission line. However, a standing wave is caused by the impedance mismatch between the antenna and the transmission line. VSWR(Voltage Standing Wave Ratio) is measured with the ratio of the maximum voltage to the minimum voltage of the standing wave; VSWR=1 implies that the antenna and the transmission line are perfectly matched.

Foursquare antenna employs a balanced coaxial feed system having double-coaxial cable of which outer conductors are soldered to each other (see Fig. 2.15(b)): they are fed with 180° phase difference. The balanced coaxial feed system is modeled as a two-port circuit in Fig. 2.16.

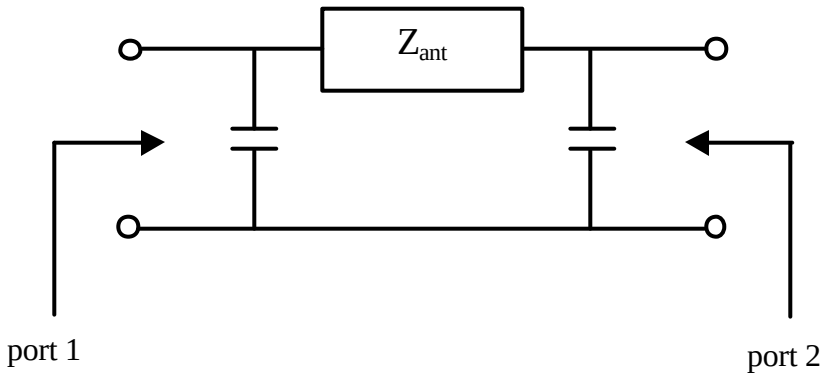

Figure 2.16 A two-port circuit model of a balanced-fed antenna.

The S-parameter of the two-port network will be obtained from measurement or simulation. Solving for Z_{ant} using the S-parameter gives

$$Z_{ant} = 2Z_0 \frac{1+S_{11}-S_{21}}{1-S_{11}+S_{21}}. \tag{2-6}$$

The input impedance of a hardware test model in Table 2.1 was measured using a HP 8510B network analyzer and was also computed using commercial codes, Fidelity and Agilent HFSS. Figure 2.17 shows the computed and measured impedance and VSWR (referenced to 50-Ω) curves of the Foursquare antenna in Fig. 2.15 and Table 2.1. They give similar results as shown in Fig. 2.17. The agreement between the measured and calculated results indicates that accurate studies can be performed by simulation. Note that the resistance of the antenna is about 50-Ω over the operating band and the reactance of the antenna is mostly inductive.

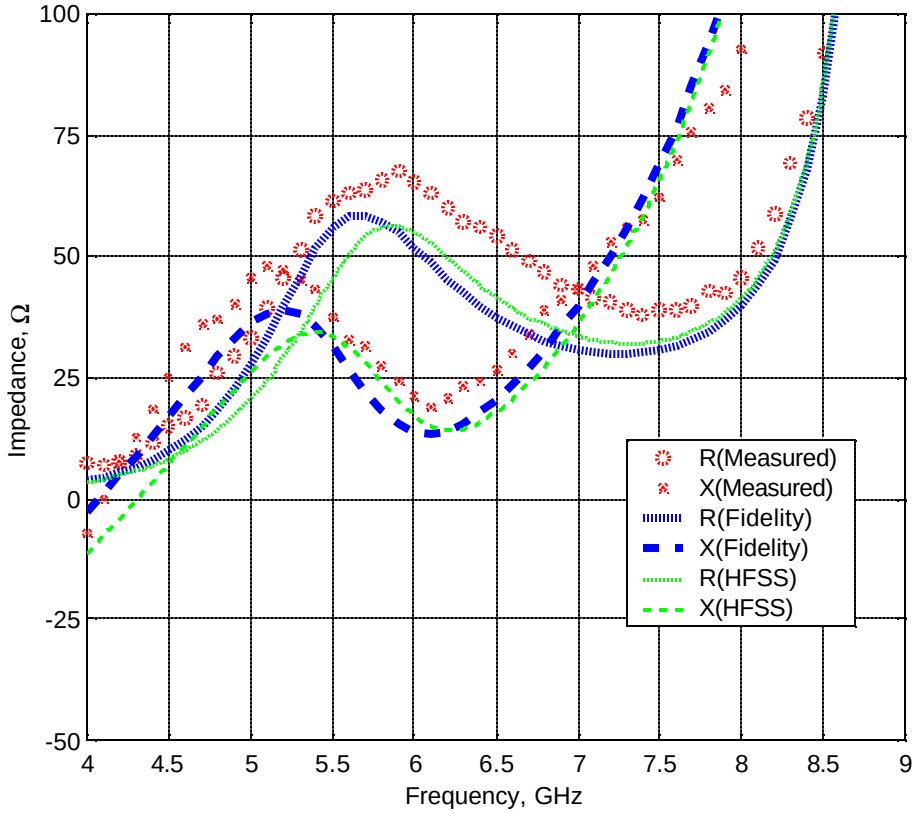

(a) Antenna Impedance (R: Resistance, X: Reactance).

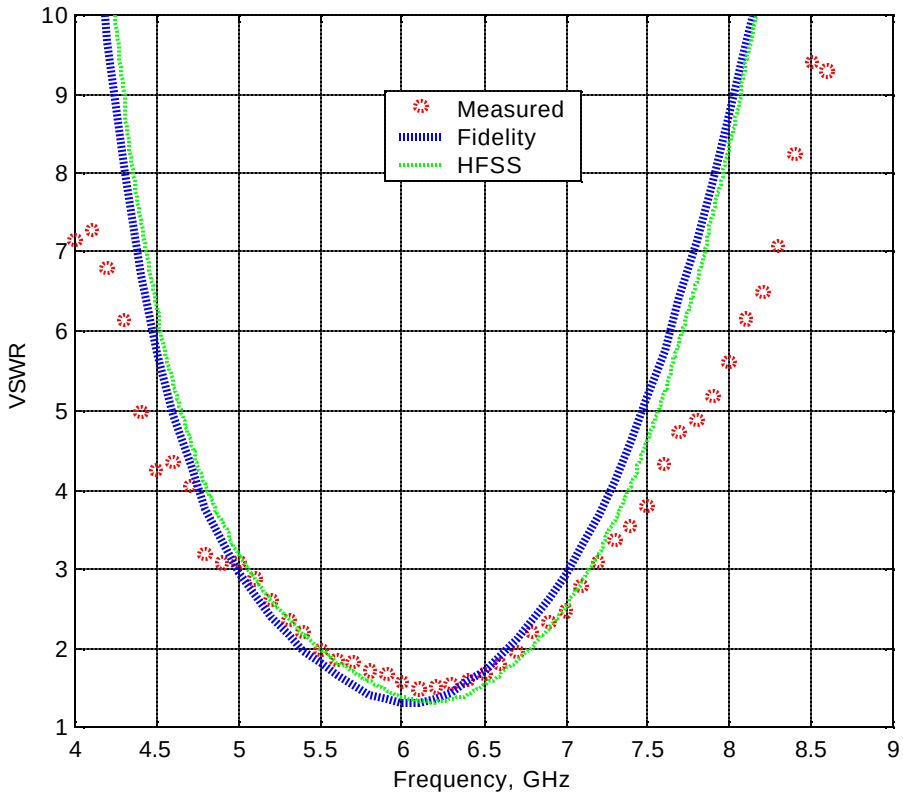

(b) VSWR referenced to 50-Ω.

Figure 2.17 Computed and measured impedance and VSWR (referenced to 50-Ω) curves of the Foursquare antenna in Fig. 2.15 with the dimensions of Table 2.1 [2.21].

2.8.2.2 Radiation Pattern

The radiation patterns of the Foursquare antenna was also measured on the outdoor range at Virginia Tech Antenna Group. In order to feed double coaxial cable, a 180° hybrid was used. The output ports of the hybrid are connected to each coaxial cable of the Foursquare antenna. Both E- and H- plane patterns are measured at several different frequencies: 4.5 GHz, 6.0 GHz and 7.25 GHz. The E-plane pattern is the radiation pattern measured in a plane containing feed; see Fig. 2.15 (a). The H-plane pattern is the radiation pattern in a plane orthogonal to the E-plane. They have similar radiation patterns over the frequencies, which is ideal for wideband antenna characteristic. Computed patterns from Agilent HFSS are compared with the measured patterns as shown in Fig. 2.18. They show very good agreement each other.

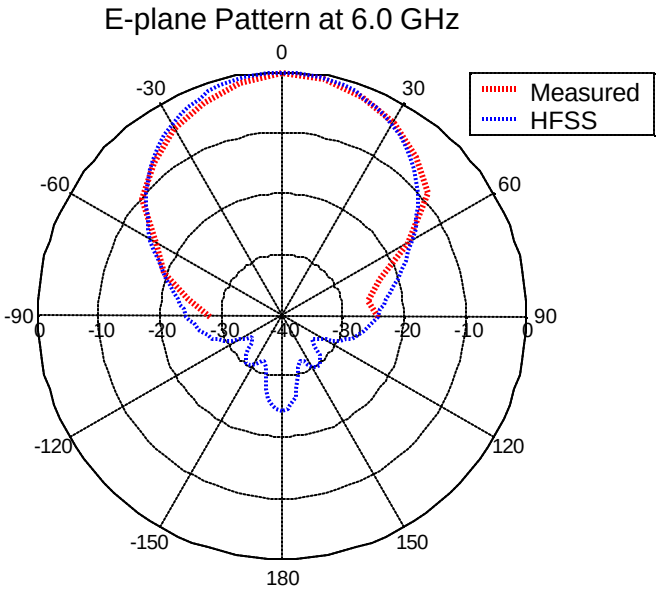

(a) Measured and computed E-Plane pattern at 6 GHz (10 dB/division).

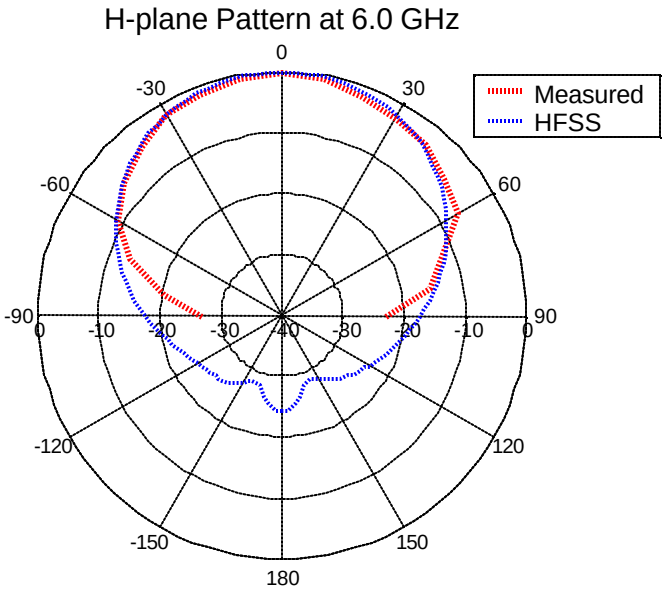

(b) Measured and computed H-Plane pattern at 6 GHz (10 dB/division).

Figure 2.18 Measured radiation patterns of the Foursquare antenna in Fig. 2.15 with the dimensions of Table 2.1 [2.21].

The measured and computed data of the Foursquare antenna are tabulated in Table 2.2. The Foursquare antenna has about 20 % bandwidth at VSWR ≤ 2 .

Table 2.2

Measured and Computed Performance of the Foursquare Antenna.

(Geometry: Figure 2.15; Performance curve: Figure 2.17; Pattern: Figure 2.18)

Description	**Symbol**	**Performance**	
		Measured [2.21]	**Simulated**
Lowest frequency at VSWR =2	f_L (VSWR=2)	5.5 GHz	5.4 GHz
Upper frequency at VSWR =2	f_U (VSWR=2)	6.7 GHz	6.65 GHz
Percent bandwidth	B_p	19.7 %	20.7 %
Element size in λ_L	A	0.39 λ_L	0.38 λ_L
Substrate size in λ_L	C	0.4 λ_L	0.39 λ_L
Height h in λ_L	h	0.13 λ_L	0.127 λ_L
Beam width of E-plane at f_L	HP_E at f_L	$\approx 60^\circ$	$\approx 60^\circ$
Beam width of H-plane at f_L	HP_H at f_L	$\approx 70^\circ$	$\approx 70^\circ$
Beam width of E-plane at f_U	HP_E at f_U	$\approx 60^\circ$	$\approx 60^\circ$
Beam width of H-plane at f_U	HP_H at f_U	$\approx 70^\circ$	$\approx 70^\circ$

2.8.3 Variation of the Foursquare antenna

A Cross-diamond antenna was also proposed in [2.21] as a second embodiment of the Foursquare antenna. The basic construction of the Cross-diamond antenna is the same as the Foursquare antenna. The Crossed-diamond radiating element as shown in Fig. 2.19 is composed with crossed four diamond shaped metal plates with included angles a_1 and a_2. That may be the same or different, depending on the applications. A test model with the same outer dimensions with the Foursquare antenna listed in Table 2.1 and with angles $a_1 = 60^\circ$ and $a_2 = 59.76^\circ$ was constructed and measured. The measured data demonstrated that the Cross-diamond antenna may be used in the same applications as the Foursquare antenna and has a bandwidth intermediate between conventional dipole antenna and the Foursquare antenna [2.21].

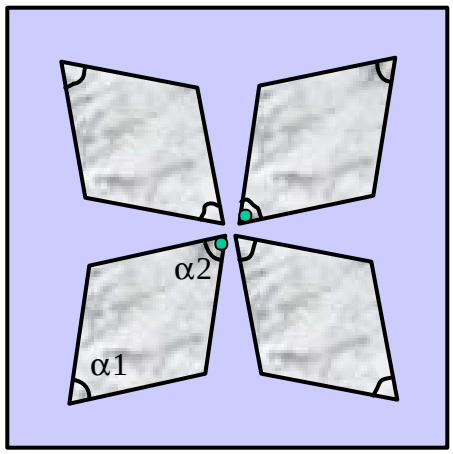

Figure 2.19 Geometry of the Cross-diamond antenna [2.21].
(Only top view is presented. Side view is same with the Fig. 2.15 (b).)

2.9 Summary

Several wideband antennas were reviewed in the historical discussion in this chapter. Since the spheroidal antenna has been developed in 1941, several wideband antennas have been developed in various forms. Three-dimensional geometric forms of wideband antenna were used in the early year, evolving into compact and low-profile geometries in 1980's, as needed for today commercial and government markets. Moreover, dual-linear polarization forms were achieved based on the single polarization forms with a low-profile geometry. Wideband, low-profile and dual-linear polarization antennas have in industry and government applications.

Recently, in addition to the wideband, low-profile and dual-linear polarization characteristics, many researches are investigating increases gain structure with a unidirectional radiation pattern. Generally, the unidirectional radiation pattern is achieved by employing a ground plane below the radiating element; however, this introduces the risk of degrading characteristics of the antenna. The unidirectional antenna with wide bandwidth and dual-polarization antenna in a low-profile geometry is useful for high performance base-station antennas for wireless communications and point-to-point communication applications, etc. Moreover dual-band or multi-band operation with those characteristics is the challenging technique in designing an antenna for wireless communications. Currently, commercial base-station antennas require high gain, dual-polarization and dual-band or multi-band operation covering AMPS/GSM and DCS/PCS characteristics in a low-profile geometry.

References

[2.1] Antenna Standards Committee of the IEEE Antennas and Propagation Society, *IEEE Standard Definitions of Terms for Antennas, IEEE Std 145-1993*, The Institute of Electrical and Electronics Engineers, Inc, New York, 1993.

[2.2] W. L. Stutzman and G.A. Thiele, *Antenna Theory and Design 2nd edition*, John Wiley & Sons, New York, 1998.

[2.3] Stratton and Chu, *Journal of Applied Physics*, March, 1941.

[2.4] S. Ramo and J. R. Whinnery, *Fields and Waves in Modern Radio*, New York, 1944, pp.480-482, Chap 11.

[2.5] Schelkunoff, "*Electromagnetic Waves*," Van Nostrand, 1943.

[2.6] George H. Brown and O. M. Woodward Jr., "Experimentally Determined Radiation Characteristics of Conical and Triangular Antennas," *RCA review*, vol. 13, pp.425-452, December 1952.

[2.7] A. G. Kandoian, "Three New Antenna Types and Their Applications," *Proc. IRE*, vol. 34, pp.70W-75W, Feb. 1946.

[2.8] M. C. Bailey, "Broad-Band Half-Wave Dipole," *IEEE Transactions on Antennas and Propagation*," Vol. AP-32, No. 4, pp. 410-412, April 1984.

[2.9] Radio Research Laboratory (U.S.), "*Very High-frequency Techniques*," McGraw Hill, New York, 1947, pp.1-25, Chap 1.

[2.10] J. D. Kraus, *Antennas*, McGraw Hill, New York, 1950, pp. 9, Chap 1.

[2.11] N. E. Lindenblad, "Antennas and Transmission Lines at the Empire State Television Station," *Communications*, pp.10-26, April, 1941.

[2.12] J. D. Dyson, "The Equiangular Spiral Antenna," *IRE Trans. Antennas & Propagation*, vol. AP-7, pp181-187, April 1959.

[2.13] Y. Mushiake, *Self-complementary Antennas*, Springer-Verlag, Berlin, 1996.

[2.14] R. Johnson, editor, *Antenna Engineering Handbook*, McGraw-Hill, 1993.

[2.15] R. H. Duhamel, "Dual Polarized Sinuous Antennas," *U.S. Patent 4,658,262*, April 14, 1987.

[2.16] S. Honda, M. Ito, H. Seki and Y. Jinbo, "A disc monopole antenna with 1:8 impedance bandwidth and omni-directional radiation pattern," *Proc. ISAP '92 (Sapporo, Japan)*, pp. 1145-1148, Sep. 1992.

[2.17] P. P. Hammoud and F. Colomel, "Matching the input impedance of a broadband disc monopole," *Electronics Letters*, Vol. 29, pp. 406-407, Feb. 1993.

[2.18] N. P. Agrawall, G. Kumar, and K. P. Ray, "Wide-band Planar Monopole Antennas," *IEEE Transactions on Antennas and Propagation*, Vol. 46, No. 2, pp.294-295, Feb. 1998.

[2.19] J. A. Evans and M. J. Ammann, "Planar Trapezoidal and Pentagonal monopoles with impedance bandwidth in excess of 10:1," *IEEE International Symposium Digest (Orlando)*, Vol. 3, pp. 1558-1559, 1999.

[2.20] R. M. Taylor, "A broadband Omni-directional Antenna," *IEEE Antennas and Propagation Society International Symposium Digest (Seattle)*, Vol. 2, pp. 1294 – 1297, June 1994.

[2.21] J. R. Nealy, "Foursquare Antenna Radiating Element," *U.S. Patent No. 5,926,137*, July 20, 1999. VTIP Ref. 96-056. http://www.vtip.org.

[2.22] Randall Nealy, Warren Stutzman, J. Matthew Monkevich, William Davis, "Improvements to the Foursquare Radiating Element-Trimmed Foursquare," *U.S. Patent No. 6,057,802*, May 2, 2000. VTIP Ref. 98-001. http://www.vtip.org.

[2.23] Fidelity User's Manual, Zeland Software Inc., Release 3, 2000.

[2.24] HFSS User's Manual, Agilent Technologies, September, 2000.

[2.25] Techniques for the Measurement of the Impedance of Wideband Balanced Antennas, W. A. Davis, J. R. Nealy, G. F. Riccardi, and W. L. Stutzman, *1995 Antenna Measurement Techniques Ass'n Symposium*, Nov 1995.

Chapter 3

The Fourpoint Antenna

3.1 Introduction

Foursquare antenna offers several advantages, including wide bandwidth, low-profile geometry, unidirectional pattern with high gain and dual-linear polarization [3.1]. During the investigation of the Foursquare antenna, it was found that the reactive component of the input impedance is mostly inductive over the operating band; see Fig. 2.17 (a). It was recognized that if the pure inductive reactance is replaced with a reactive component that is centered about zero reactance over the band, the impedance bandwidth could be increased in the upper part of band. Based upon this motivation, an antenna was newly invented that offers several advantages over the previous Foursquare antenna. The new antenna called the Fourpoint antenna is described in detail in this chapter [3.2].

3.2 The Antenna Structure

The geometry of the proposed Fourpoint antenna is shown in Fig. 3.1. It is based on the Foursquare antenna of Fig. 2.15, but provides significantly improved impedance bandwidth. It is an evaluation of the Foursquare formed by eliminating the corners of the Foursquare antenna introducing radiating structures that have four points rather than four squares. The indentation between the four points introduces capacitive reactance at upper part of the frequency band, balancing the inductive reactance component of the Foursquare antenna. Thus, the reactive components are equally distributed over the entire band in the Fourpoint antenna. The remainder of the geometry is same with the Foursquare antenna.

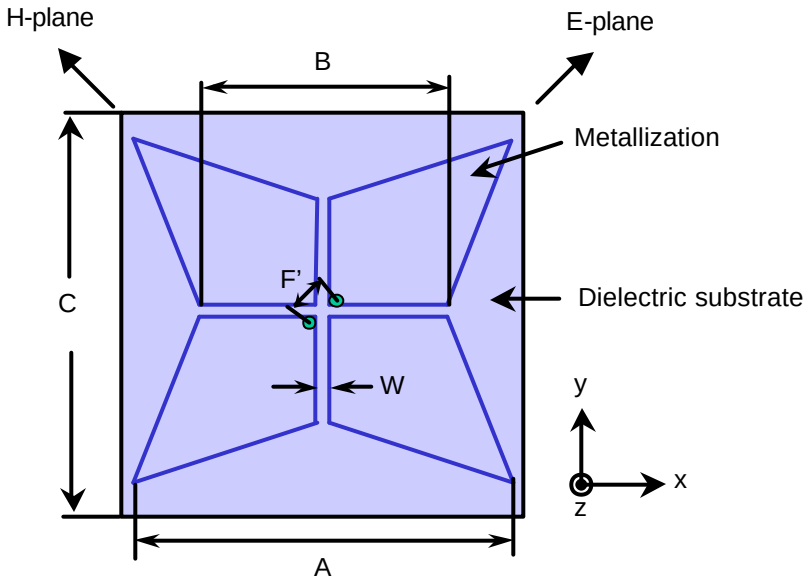

(a) Top view of the Fourpoint antenna.

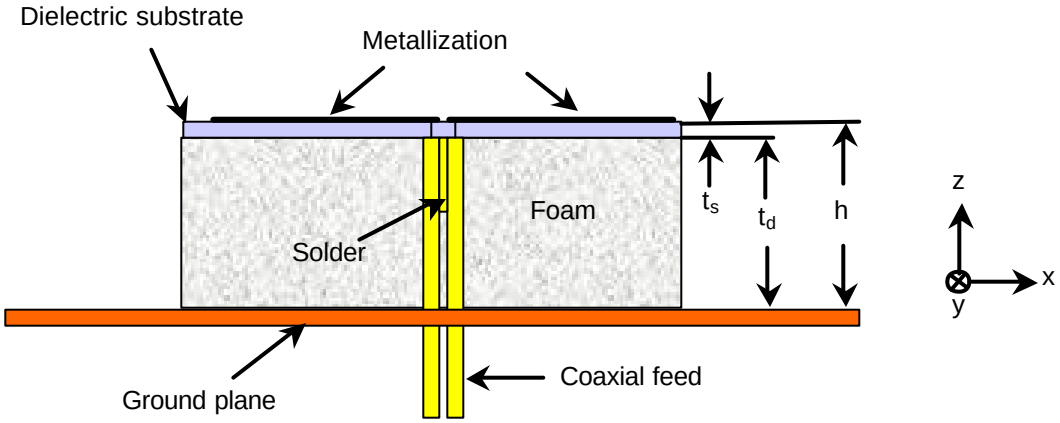

(b) Side view of the Fourpoint antenna.

Figure 3.1 Geometry of the Fourpoint antenna [3.2].

3.3 Simulation of the Fourpoint Antenna

The simulation model for the Fourpoint antenna in Fig. 3.1 was evaluated using both the Fidelity and HFSS codes [3.3], [3.4] to determine performance. The dimensions of the Fourpoint antenna are listed in Table 3.1. Simulating the antenna with two different commercial code increases the reliability of the computed results. For ease of comparison, the same outer dimensions of the Foursquare antenna in Fig. 2.15; that is, A is the same, were used for both simulation case.

Table 3.1

Geometry of the Fourpoint Antenna in Fig. 3.1.

Description	Symbol	Size
Element side length	A	21.3 mm (0.84”)
Length B	B	15.7 mm (0.62”)
Substrate side length	C	21.8 mm (0.86”)
Gap width	W	0.25 mm (0.01”)
Substrate thickness	t_s	0.7 mm (0.028”)
Foam thickness	t_d	6.4 mm (0.25”)
Element height above ground plane	h	7.06 mm (0.278”)
Feed positions distance	F’	4.3 mm (0.17”)

3.3.1 Antenna Impedance and VSWR

The same technique as described in Section 2.8.2.1 was used to find antenna impedance. In Fig. 3.2, shows the computed antenna impedance and VSWR curves for the Fourpoint antenna. The VSWR curves are referenced to 50-Ω input impedance. The data computed using two commercial codes Fidelity and HFSS agree very well with each other, adding confidence to the accuracy of the simulation approaches. Also shown in Fig. 3.2 are

measured results for the Foursquare antenna, permitting comparison of Fourpoint and Foursquare antenna performances.

The geometry characteristics and performance values of the Foursquare and the Fourpoint are tabulated in Table 3.2 for easy comparison.

Table 3.2

Performance Comparison of the Foursquare Antenna and Fourpoint antenna.

(Geometry: Figs. 2.15 & 3.1, VSWR curve: Figs. 2.17 & 3.2, Pattern: Figs. 2.18 & 3.3)

Description	**Symbol**	**Performance**	
		Foursquare (Measured [2.20])	**Fourpoint** (Computed using HFSS)
Lowest frequency at VSWR =2	f_L (VSWR=2)	5.5 GHz	5.3 GHz
Upper frequency at VSWR =2	f_U (VSWR=2)	6.7 GHz	8.0 GHz
Bandwidth	$\mathbf{B_p}$	**19.7 %**	**40.6 %**
Element size in λ_L	A	0.39 λ_L	0.38 λ_L
Substrate size in λ_L	C	0.4 λ_L	0.39 λ_L
Height h in λ_L	h	0.13 λ_L	0.125 λ_L
Beam width of E-plane at f_L	HP_E at f_L	$\approx 60^\circ$	$\approx 60^\circ$
Beam width of H-plane at f_L	HP_H at f_L	$\approx 80^\circ$	$\approx 80^\circ$
Beam width of E-plane at f_U	HP_E at f_U	$\approx 60^\circ$	$\approx 60^\circ$
Beam width of H-plane at f_U	HP_H at f_U	$\approx 80^\circ$	$\approx 80^\circ$

Based on these results, the Fourpoint antenna has enhanced performance over that for the Foursquare antenna. The impedance bandwidth of the Fourpoint antenna for VSWR ≤ 2 is 44 %, which is more than twice that of the Foursquare antenna bandwidth of 20 %. This is accomplished by just eliminating the corners of the Foursquare antenna squares. The impedance curves in Fig. 3.2(a) show that the Fourpoint antenna has much better impedance characteristics than the Foursquare antenna; that is, the reactive component of

the Fourpoint antenna impedance remains within a range of $\pm 25\text{-}\Omega$ and the resistive component is well matched to 50-Ω. The Foursquare antenna, however, is mostly inductive over the operating band. Therefore the Fourpoint antenna provides wider impedance bandwidth with the same outer dimensions.

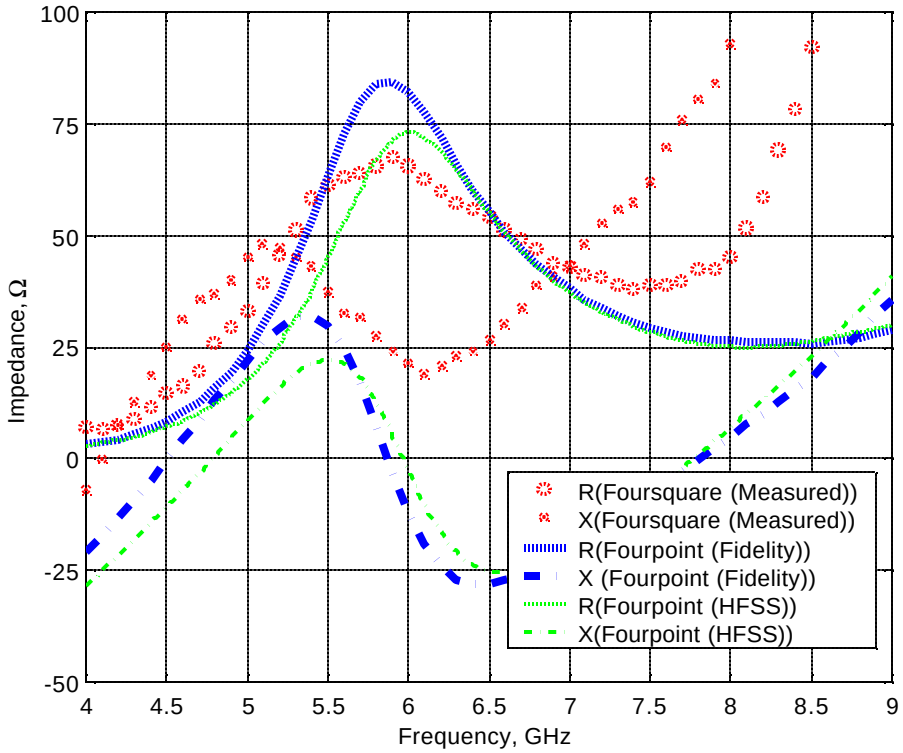

(a) Measured impedance curves of the Foursquare (circles and crosses) and computed impedance curves of the Fourpoint antenna (thick: Fidelity; thin: HFSS).

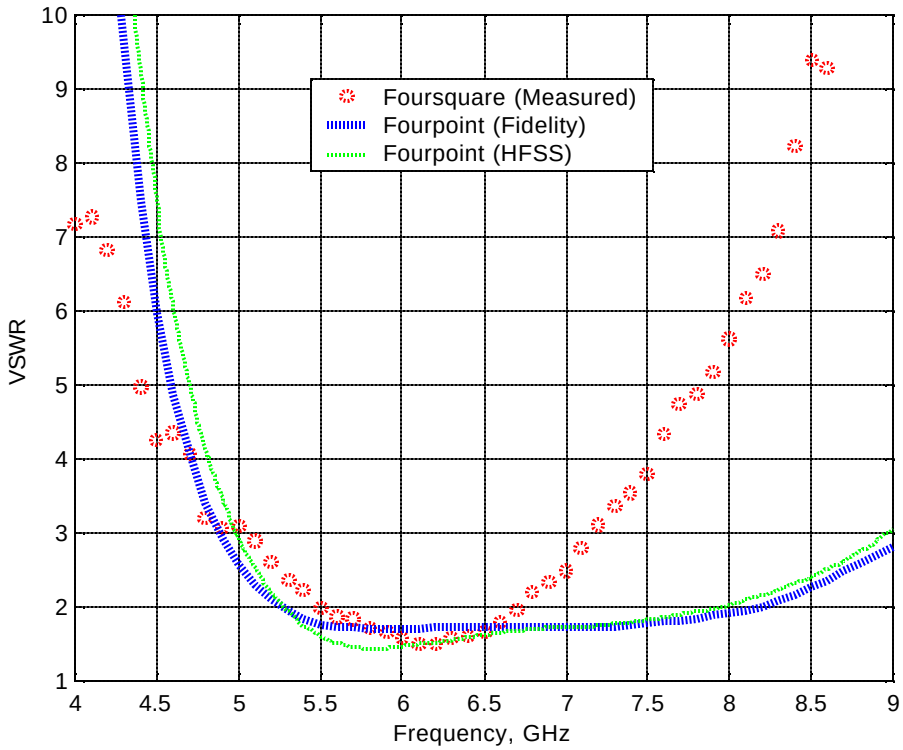

(b) Measured VSWR of the Foursquare (circles) and computed VSWR of the Fourpoint antenna.

Figure 3.2 Antenna impedance and VSWR (referenced to 50-Ω) for the Foursquare antenna (measured) in Fig. 2.15 and the Fourpoint antenna (computed) in Fig. 3.1 with the dimensions of Table 3.1. Note that the two antennas have the same outer dimensions.

3.3.2 Radiation Patterns

Radiation patterns of the Fourpoint antenna were computed at several frequencies using the commercial code Agilent HFSS. Figure 3.3 shows the computed E-plane and H-plane radiation patterns. The Fourpoint antenna has a beamwidth similar to that of the Foursquare antenna over the operating band. The level of cross polarization is not presented because they are negligibly small at all the frequencies for the Fourpoint antenna.

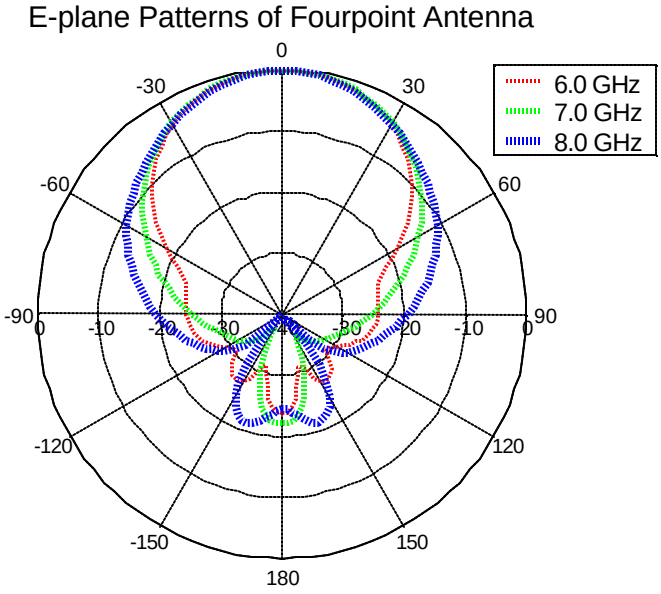

(a) Computed radiation patterns at E-plane at 6-8 GHz.

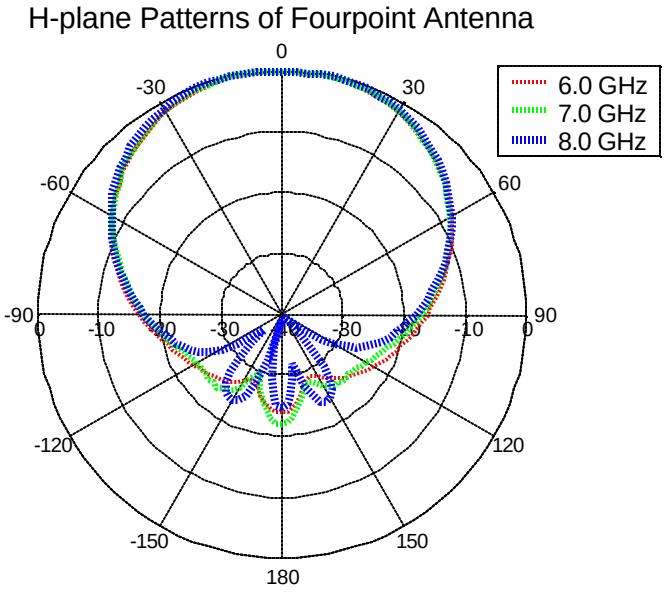

(b) Computed radiation patterns at H-plane at 6-8 GHz.

Figure 3.3 Radiation patterns of the Fourpoint antenna in Fig. 3.1 and the dimensions of Table 3.1 computed using HFSS. Note the cross-pol pattern is negligibly small at all frequencies.

3.4 The Fourpoint Antenna with a Tuning Plate

An extensive investigation was conducted with the goal of finding a geometry of the Fourpoint type of antenna with enhanced bandwidth. It was found that the bandwidth of the Fourpoint antenna is increased by adding a tuning plate on the bottom of the substrate as shown in Fig. 3.4 (b). The tuning plate can be constructed by etching it on the opposite side of the Fourpoint radiating element and the outer conductors of the coaxial cables are connected to the tuning plate. The tuning plate provides a second resonance at the high end of the operating band so that the bandwidth is significantly increased toward the high frequency. The tuning plate can be also used in the Foursquare antenna in the similar way. The tuning plate effect on the Foursquare antenna will be discussed in Chapter 4. S. A. Bokhari et al. [3.5] proposed a rotatable tuning plate with a microstrip patch antenna. The tuning plate was fabricated at a superstrate layer above the microstrip patch antenna so that mechanical tuning is easily achieved. They presented measured return loss, demonstrating that the tuning process is achieved by adjusting the tuning plate rotating angle.

In this section, some the tuning plate geometries are proposed and their effect is investigated. Two hardware test models were constructed and measured to verify the tuning plate effect.

3.4.1 Tuning Plate Geometries

Three tuning plate geometries are shown in Fig. 3.4 (b), (c) and (d) called square, star and circle. Each geometry has different impedance properties that can be used for optimizing the Fourpoint antenna a given application. Even though only three tuning plates are presented in this section, other geometries of the tuning plate also lead to acceptable performance. Generally, the size of the tuning plate is smaller than that of the radiating element so that it tunes the impedance at the high end of the operating band.

In addition to the shape of the tuning plate, the orientation of the tuning plate is a critical factor in determining the antenna impedance. The best performance was achieved with tuning plate rotated 45° from the radiating element vertices, as illustrated in Fig. 34 (a), (b), and (c); that is, the angle between vertices of the tuning plate and radiating

element is 45°. Additional tuning plates can be added between the radiating element and the ground plane as shown in Fig. 3.4 (f). Multiple tuning plates can tune the antenna impedance at several frequencies so that the impedance bandwidth is further enhanced.

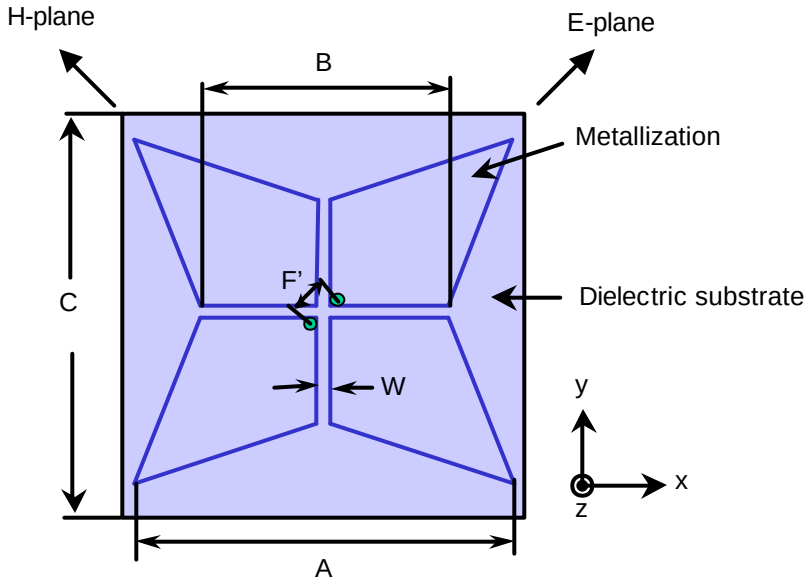

(a) Top view of the Fourpoint antenna.

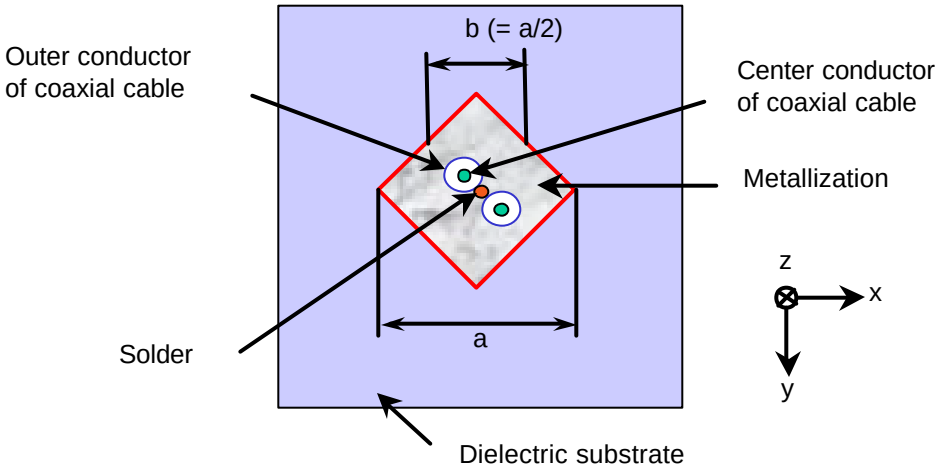

(b) A square-shaped tuning plate (Bottom view of the Fourpoint antenna).

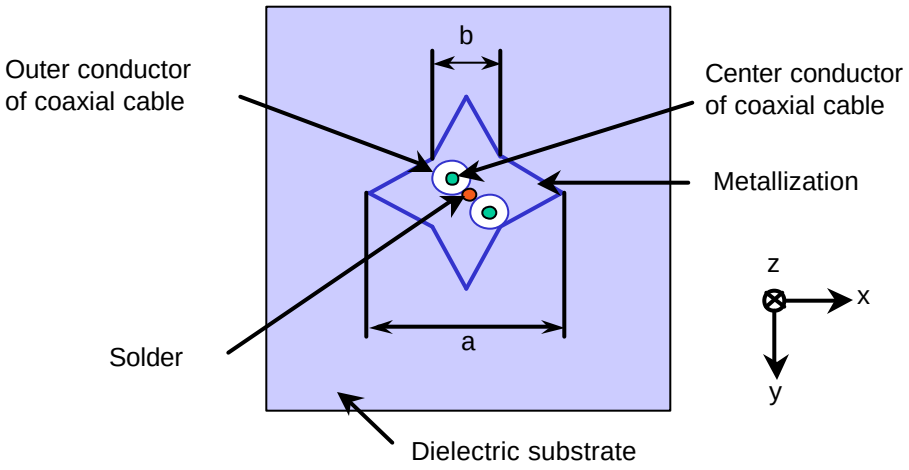

(c) A star-shaped tuning plate.

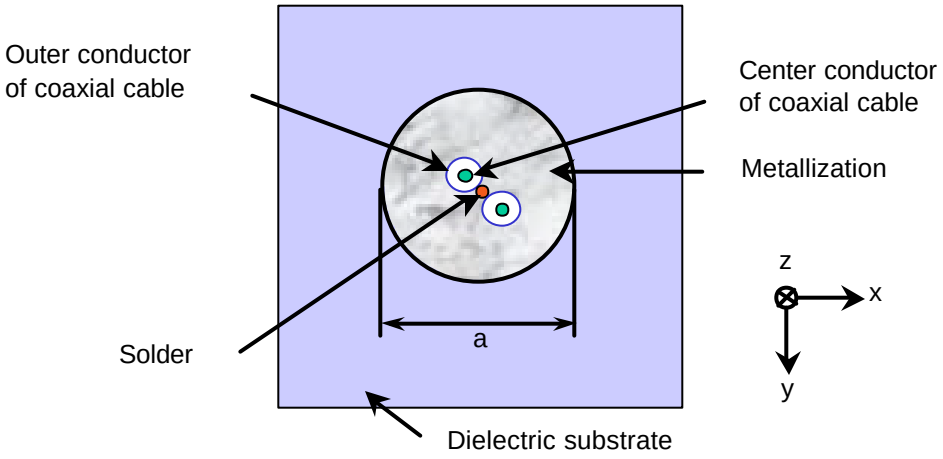

(d) A circular tuning plate.

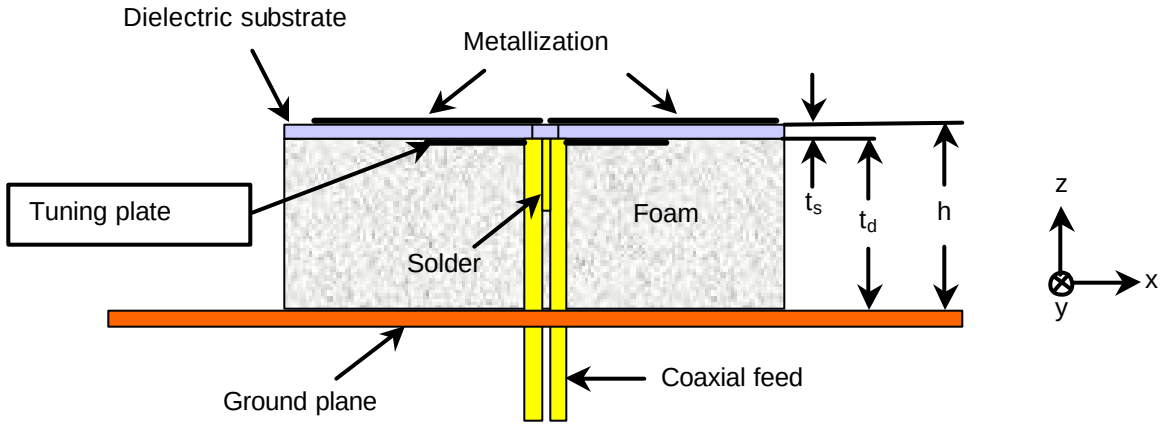

(e) Side view of the Fourpoint antenna with single tuning plate.

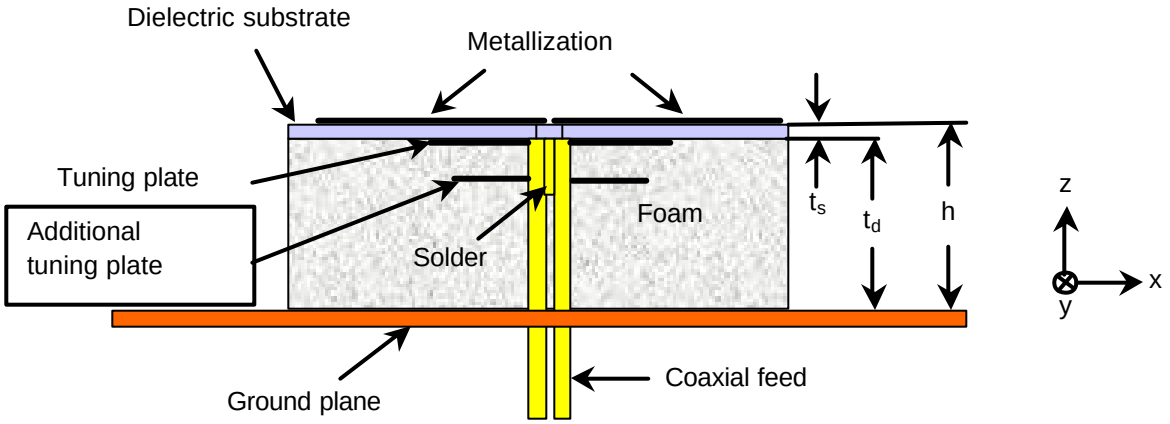

(f) Side view of the Fourpoint antenna with multiple tuning plates.

Figure 3.4 Geometries of the Fourpoint antenna with tuning plate. (The radiating element in Fig. 3.4(a) can be the Foursquare element in Fig. 2.15(a).)

3.5 Hardware test model of the Fourpoint antenna with a square–shaped tuning plate

The Fourpoint antenna with the geometry shown in Fig. 3.4 (a), (b), and (e) was investigated using both software simulation and hardware test models. A square-shaped tuning plate was employed for this investigation and the geometry dimensions of the antenna are listed in Table 3.3. The Fourpoint antenna with the square-shaped tuning plate was designed for covering AMPS, GSM, DCS and PCS bands simultaneously for use as a base-station antenna element. The commercial codes Fidelity and HFSS are used in simulation the Fourpoint antenna. The dielectric constant of 2.33 was used for the substrate in both simulations and measurements. In the simulations, an infinite ground plane was used because of the computational simplicity. In the measurements, however, a finite ground plane was used with the size of 431.8 mm x 431.8 mm (17" x 17"), which is much larger than the radiating element.

Table 3.3

Geometry of the Fourpoint Antenna of Fig. 3.4 (a), (b), and (e).

Description	Symbol	Size
Element side length	A	114.3 mm (4.5")
Length B	B	95.25 mm (3.75")
Substrate side length	C	117 mm (4.6")
Tuning plate outer dimension a	a	40.64 mm (1.6")
Tuning plate inner dimension b	b	20.32 mm (0.8")
Gap width	W	2.03 mm (0.08")
Substrate thickness	t_s	1.57mm (62 mils)
Foam thickness	t_d	62.48 mm (2.46")
Element height above ground plane	h	64.06 mm (2.522")
Feed positions distance	F'	5.03 mm (0.197")

3.5.1 Antenna Impedance and VSWR

Antenna impedance was computed using Fidelity and measured using an HP8720C vector network analyzer. The antenna impedance and VSWR referenced to 50-Ω are presented in Fig. 3.5 for both simulations and measurements. The performance data are also summarized in Table 3.4. Note the excellent agreement in measured and computed results.

In Fig. 3.5 (a), dual-resonances are observed at the low and high end of the operating band, leading to an impedance level that is close to 50-Ω for the resistance and 0-Ω for the reactance. This Fourpoint antenna with a square tuning plate has 2.7:1 (92 %) bandwidth for $\text{VSWR} \leq 2$. This is a dramatic improvement over the Fourpoint antenna without tuning plate of Section 3.3, which has a bandwidth of 40.6 %. The wide bandwidth and compact size of the Fourpoint antenna makes it ideal as a multiple-band base-station antenna. For example, it is capable of covering all the AMPS, GSM, DCS, and PCS services as illustrated in Fig. 3.5(c). The Fourpoint antenna can also provide dual-linear polarization to achieve polarization diversity. To the author's knowledge, there is no antenna used in commercial or military applications that has 2.7:1 bandwidth and dual-linear polarization in a low-profile package.

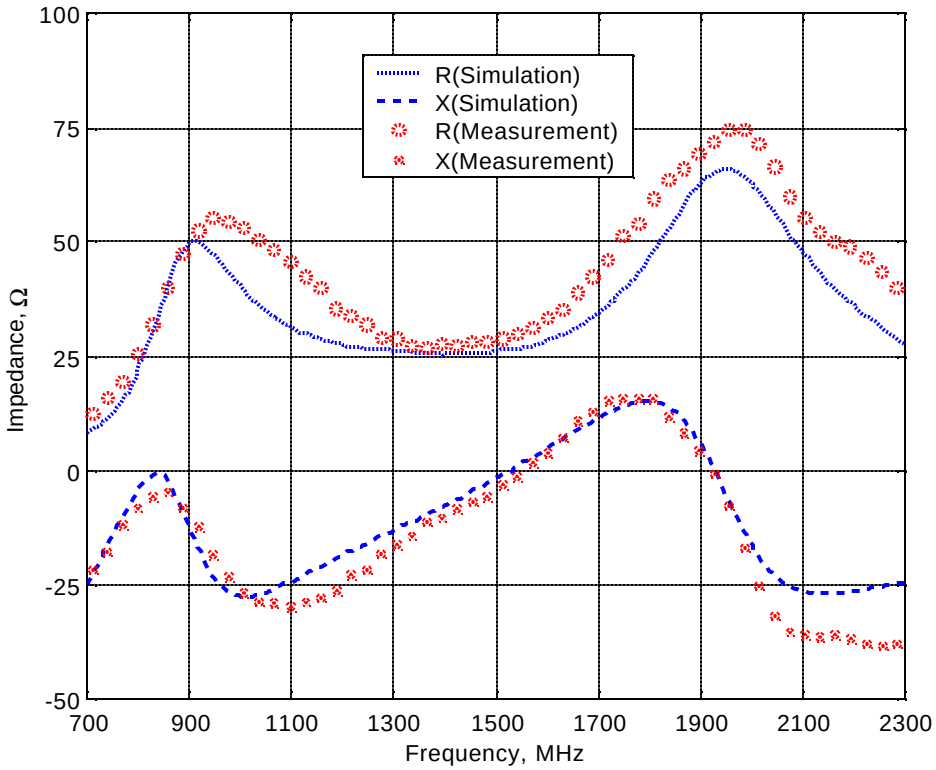

(a) Computed (solid and dashed curves) and measured (circles and crosses) antenna impedance.

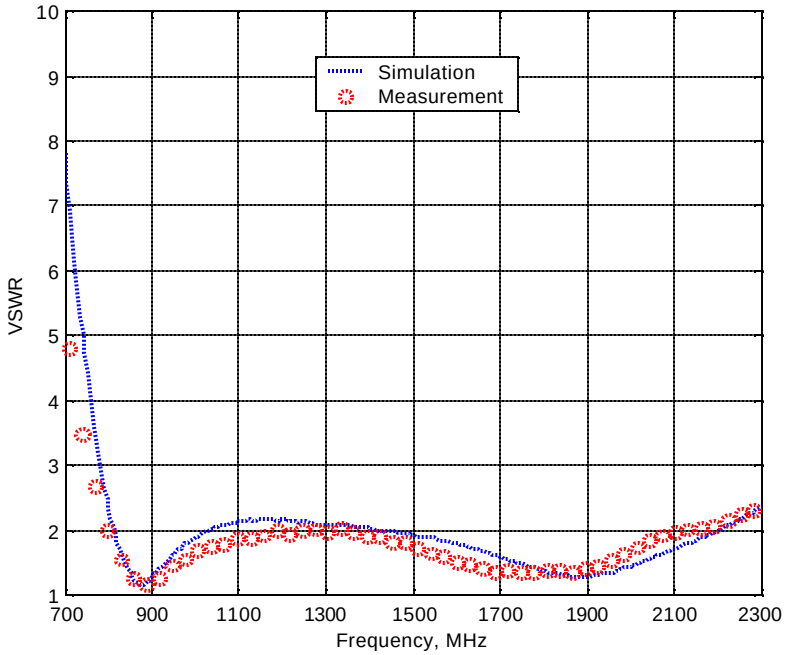

(b) Computed (solid curve) and measured (circles) VSWR (referenced to 50-Ω).

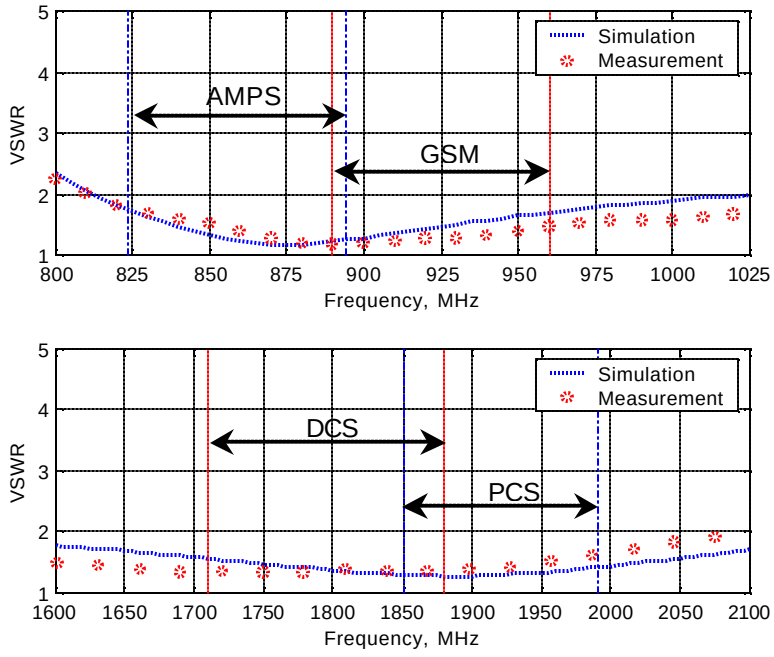

(c) VSWR plots together with AMPS, GSM, DCS, and PCS bands.

Figure 3.5 Computed and measured antenna impedance and VSWR (referenced to 50-Ω) for the Fourpoint antenna of Fig. 3.4 (a), (b), (e) with the dimensions of Table 3.3.

Table 3.4

Measured and Computed Performance for the Fourpoint Antenna with a Square Tuning Plate. (Geometry: Figure 3.4 (a), (b), (e); Performance curve: Figure 3.5; Pattern: Figure 3.6)

Description	**Symbol**	**Performance**	
		Measured	**Simulated**
Lowest frequency at VSWR =2	f_L (VSWR=2)	805 MHz	805 MHz
Upper frequency at VSWR =2	f_U (VSWR=2)	2190 GHz	2200 MHz
Percent bandwidth	B_p	92.5 %	92.9 %
Ratio bandwidth	B_r	2.72:1	2.73:1
Element size in λ_L	A	0.306 λ_L	0.306 λ_L
Substrate size in λ_L	C	0.314 λ_L	0.314 λ_L
Height h in λ_L	h	0.172 λ_L	0.172 λ_L
Beam width of E-plane at f_L	HP_E at f_L	$\approx 50^\circ$	$\approx 50^\circ$
Beam width of H-plane at f_L	HP_H at f_L	$\approx 65^\circ$	$\approx 65^\circ$
Beam width of E-plane at f_U	HP_E at f_U	$\approx 80^\circ$	$\approx 80^\circ$
Beam width of H-plane at f_U	HP_H at f_U	$\approx 150^\circ$	$\approx 150^\circ$

3.5.2 Radiation Patterns

Radiation patterns were measured at several frequencies in the anechoic chamber of Virginia Tech Antenna Group (VTAG) using a near field scanner operating in the spherical scan mode. The measured patterns are presented in Fig. 3.6 selected frequencies of 900 MHz, 950 MHz, 1800 MHz and 1900 MHz. Excellent unidirectional patterns are achieved at lower bands (900 MHz and 950 MHz) but a dip is present on bore-sight at upper bands (1800 MHz and 1900 MHz). The dip is due to the increased electrical height of the radiating element above the fixed ground plane [3.6]. Generally the electrical height of the radiating element should be about $\lambda/4$ above the ground plane to obtain good unidirectional patterns [3.6]. The patterns in Fig. 3.6 were obtained with the electrical heights of 0.19λ, 0.2λ, 0.39λ and 0.41λ at the frequencies of 900 MHz, 950 MHz, 1800 MHz and 1900 MHz, respectively. Note that the unidirectional patterns of Fig. 3.6 (a) and (b) were obtained with the electrical height close to $\lambda/4$. For larger electrical heights, a dip at the bore-sight is observed due to a wave cancellation.

An important feature that is highly desirable for many applications is the nearly balanced pattern of the Fourpoint antenna as demonstrated by the fact that the E- and H-plane patterns are not significantly different for all frequencies. The beam widths of the Fourpoint antenna are summarized in Table 3.4 and they are similar to those of the Foursquare antenna. Also, the E- and H-plane patterns are relatively broad, which is a useful property for commercial base-station array antennas and wide-scan phased array applications.

The gain of the Fourpoint antenna at bore-sight remains to be measured, but since the Foursquare antenna has about 8-9 dBi peak gain over the band, we expect the Fourpoint antenna to have similar peak gain values.

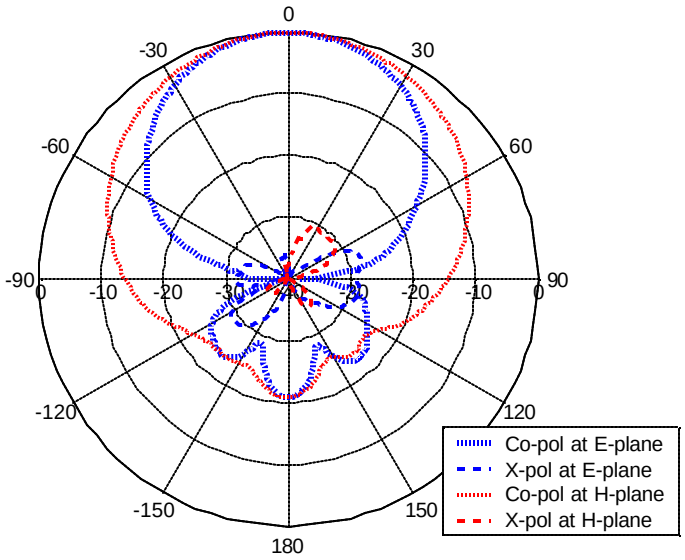

(a) Measured radiation patterns at 900 MHz.

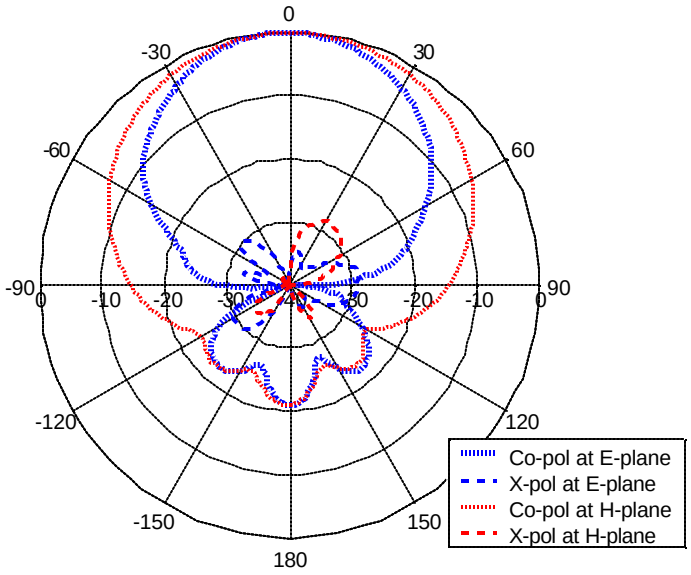

(b) Measured radiation patterns at 950 MHz.

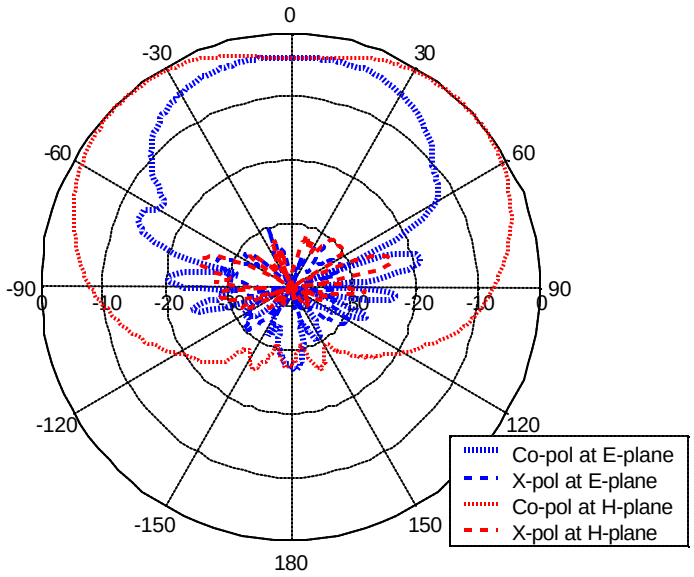

(c) Measured radiation patterns at 1800 MHz.

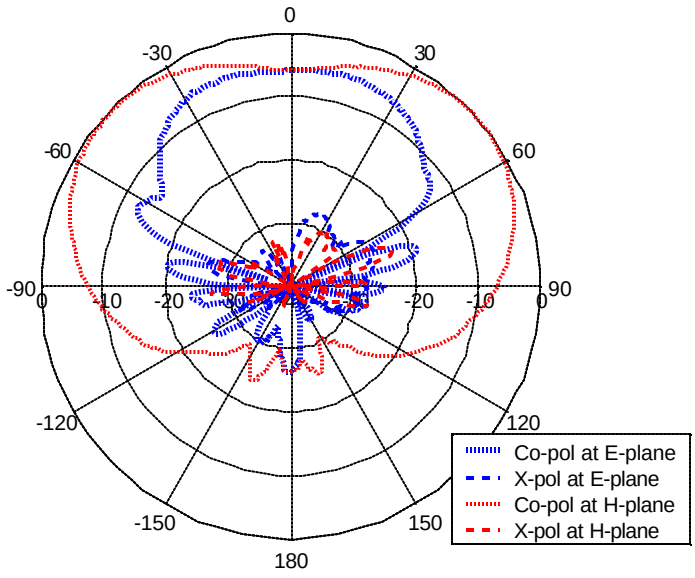

(d) Measured radiation patterns at 1900 MHz.

Figure 3.6 Measured radiation patterns for the Fourpoint antenna with a square-shaped tuning plate in Fig. 3.4 (a), (b), (e) with the dimensions of Table 3.3.

3.6 Hardware test model of the Fourpoint antenna with a star–shaped tuning plate

A second hardware test model was investigated that uses a star-shaped tuning plate. This Fourpoint antenna was designed at VTAG and was constructed and measured at Harris Co. The geometries of the radiating element with a star-shaped tuning plate are presented in Fig. 3.4(a), (c), and (e) and the dimensions are listed in Table 3.5. The antenna size is smaller because the Fourpoint antenna with the star-shaped tuning plate was designed for operation from 5.3 to 13.5 GHz. The element height above the ground plane, 'h', is about $0.27\lambda_C$ in the model, where λ_C represents wavelength at the center frequency of 9.25 GHz. A dielectric constant value of 2.33 was used for the substrate. Simulation and experimental evaluation were performed to investigate the Fourpoint antenna with the star-shaped tuning plate. A circular ground plane with a diameter of 127 mm (5.0") was used in the measurements of impedance, which are presented next. The radiation patterns were not measured, but were computed with the commercial code, HFSS. The performance of the Fourpoint antenna is summarized in Table 3.6. Again this antenna provides dual-polarization in a single antenna element.

Table 3.5

Geometry of the Fourpoint Antenna of Fig. 3.4 (a), (c), and (e).

Description	Symbol	Size
Element side length	A	17.02 mm (0.67")
Length B	B	13.97 mm (0.55")
Substrate side length	C	17.3 mm (0.68")
Tuning plate outer dimension a	a	11.18 mm (0.44")
Tuning plate outer dimension b	b	4.57 mm (0.18")
Gap width	W	0.508 mm (0.02")
Substrate thickness	t_s	0.787mm (31 mils),
Foam thickness	t_d	7.92 mm (0.312")
Element height above ground plane	h	8.71 mm (0.343")
Feed positions distance	F'	2.87 mm (0.113")

3.6.1 Antenna Impedance and VSWR

The antenna impedance and VSWR were computed at VTAG using the commercial code Fidelity. The measured data were provided by Harris co. Simulation and measurement results, compared in Fig. 3.7, show excellent agreement with each other. This Fourpoint antenna with the star-shaped tuning plate provides about 2.6:1 (87%) impedance bandwidth for VSWR ≤ 2 for VSWR referenced to 50-Ω.

Table 3.6

Measured and Computed Performance of the Fourpoint Antenna with a Star-shaped Tuning Plate. (Geometry: Figure 3.4 (a), (c), (e); Performance curve: Figures 3.7 and 3.8)

Description	**Symbol**	**Performance**	
		Measured	**Computed**
Lowest frequency at VSWR =2	f_L (VSWR=2)	5.3 GHz	5.8 GHz
Upper frequency at VSWR =2	f_U (VSWR=2)	13.5 GHz	13.3 GHz
Percent bandwidth	B_p	87 %	78.5 %
Element size in λ_L	A	0.3 λ_L	0.329 λ_L
Substrate size in λ_L	C	0.31 λ_L	0.334 λ_L
Height h in λ_L	h	0.154 λ_L	0.17 λ_L
Beam width of E-plane at 6 GHz	HP_E at f_L	N/A	$\approx 60^\circ$
Beam width of H-plane at 6 GHz	HP_H at f_L	N/A	$\approx 80^\circ$
Beam width of E-plane at 12 GHz	HP_E at f_U	N/A	$\approx 60^\circ$
Beam width of H-plane at 12 GHz	HP_H at f_U	N/A	$\approx 120^\circ$

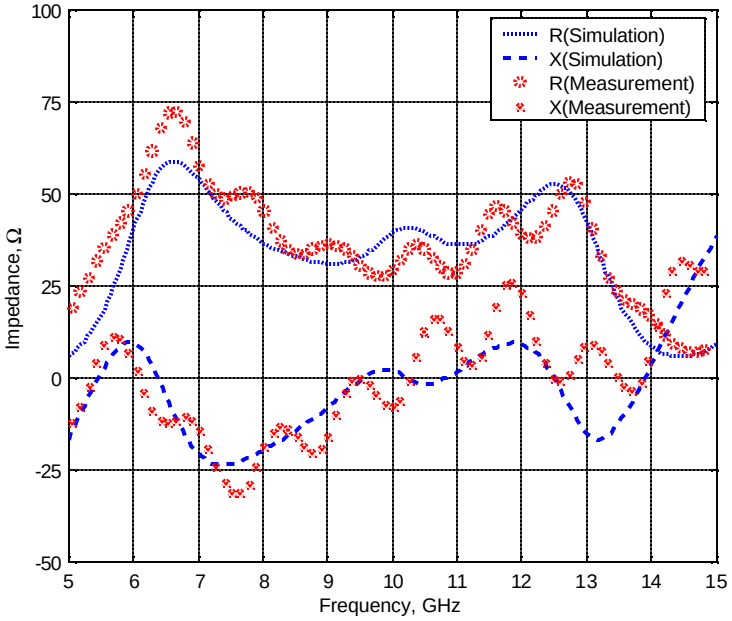

(a) Computed (solid and dashed) and measured (circle and cross) antenna impedance

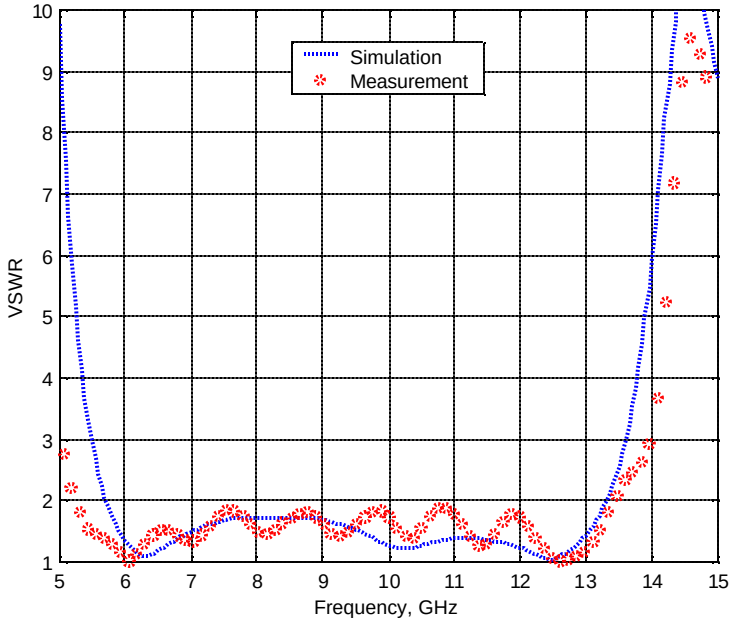

(b) Computed (solid) and measured (dotted) VSWR

Figure 3.7 Computed and measured antenna impedance and VSWR (referenced to 50-Ω) curves for the Fourpoint antenna with star-shaped tuning plate of Fig. 3.4 (a), (c), (e) with the dimensions of Table 3.5.

3.6.2 Computed Radiation Patterns

The radiation patterns of the Fourpoint antenna computed using Agilent HFSS code are presented in Fig. 3.8. Measured radiation patterns are not available but they will be very similar to the computed patterns based on the excellent agreement observed between computed and measured pattern for the Foursquare antenna discussed in Section 2.8.2.2. The computed patterns demonstrate that the Fourpoint antenna provides unidirectional patterns over the wideband.

Computed maximum gain vs. frequency plot is presented in Fig. B1 in Appendix B. Gain patterns can be directly obtained by adding the maximum gain number to the normalized radiation patterns.

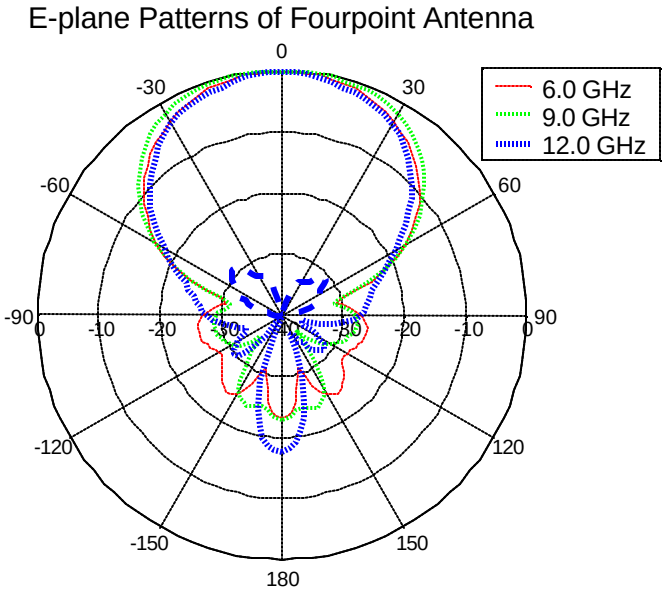

(a) Computed E-Plane normalized pattern at 6-12 GHz (10 dB/division).

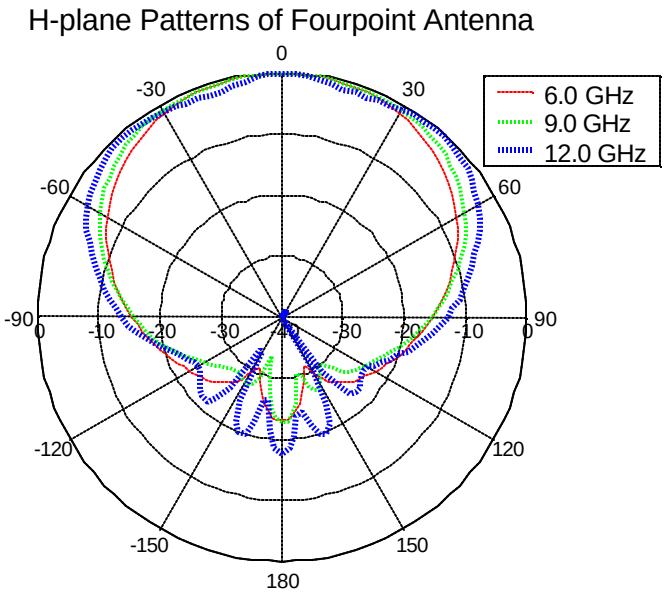

(b) Computed H-Plane normalized pattern at 6-12 GHz (10 dB/division).

Figure 3.8 Computed radiation patterns of the Fourpoint antenna in Fig. 3.4 (a), (c), and (e) with the dimensions of Table 3.5. The cross-pol pattern is not shown because it is negligible at all frequencies.

3.7 A Circularly-Polarized Fourpoint Antenna

In this section, the possibility and potential of the circularly-polarized Fourpoint antenna are demonstrated using a commercial code, Fidelity (FDTD). The CP Fourpoint antenna discussed in this section does not employ a tuning plate.

The geometry of the Fourpoint antenna is presented in Fig. 3.9 and its dimensions are listed in Table 3.7. A dual-linear polarized Fourpoint antenna can be modified for circular polarization (CP) using a hybrid combiner. A software test model of the CP Fourpoint antenna was designed for a frequency of 2.4 GHz. A feed concept with left hand circular polarization (LHCP) is presented in Fig. 3.10 with four coaxial feeds having a 90° phase difference.

In this section, the CP Fourpoint antenna was simulated with Fidelity. The simulation results are presented in Figs. 3.11 and 3.12.

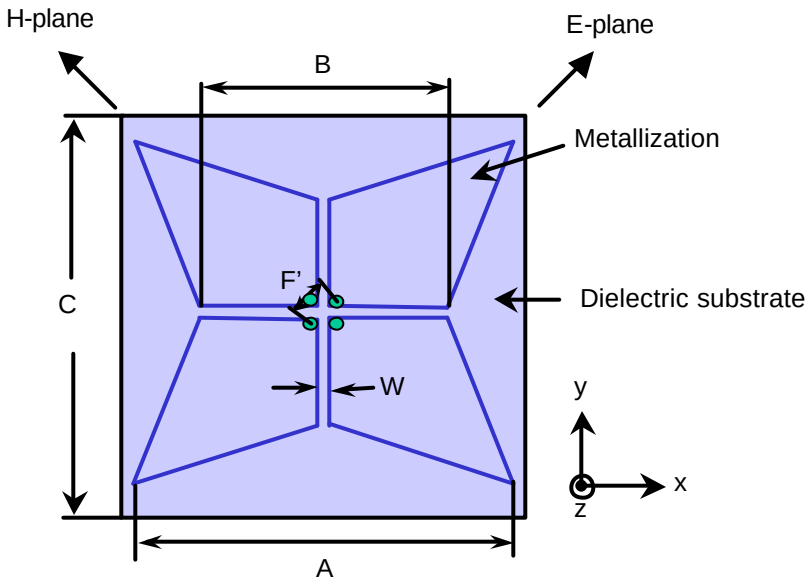

Figure 3.9 The CP Fourpoint antenna geometry. The side view is same with the one in Fig. 3.1 (b). Note that tuning plate is not included in the CP Fourpoint antenna.

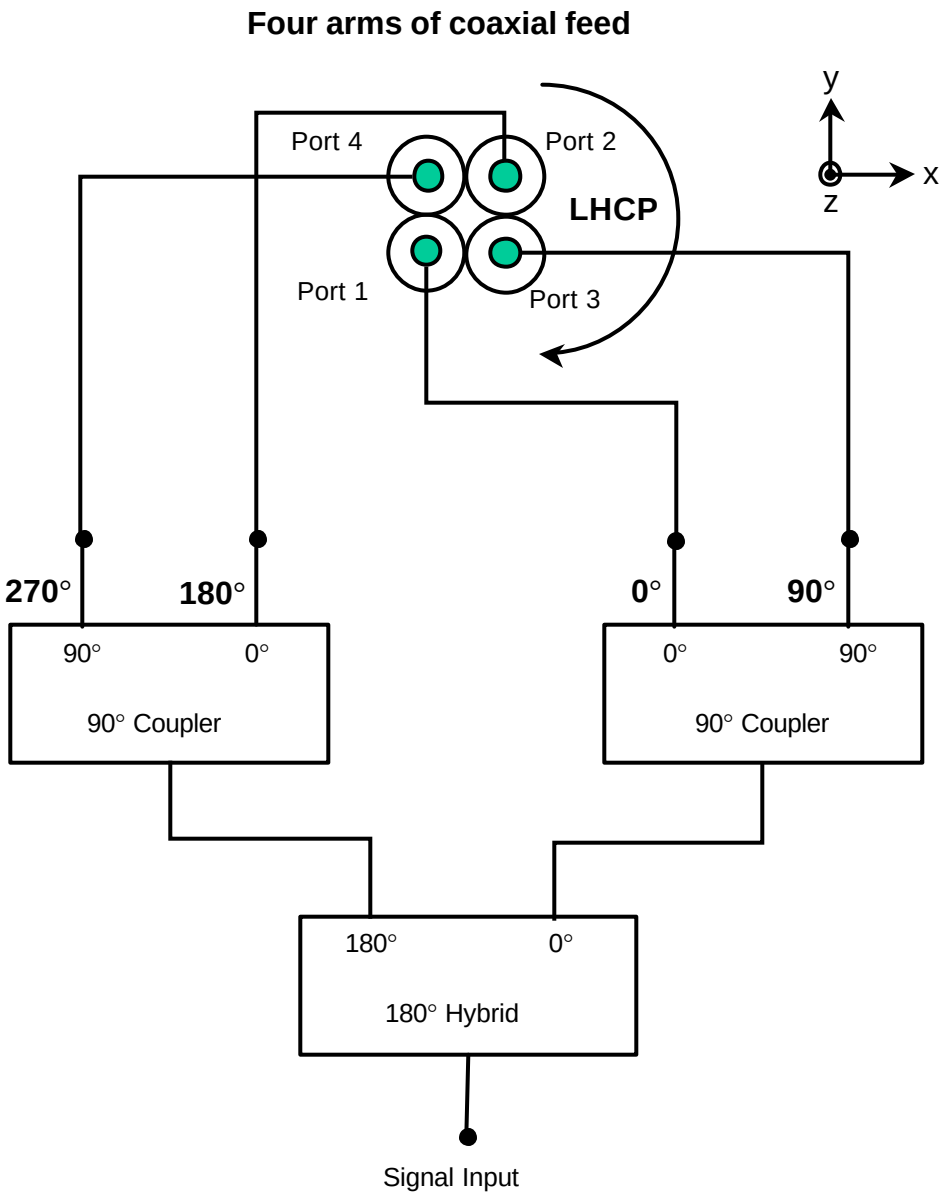

Figure 3.10 A feed network for the left-hand circular polarized (LHCP) Fourpoint antenna with wideband hybrids.

Table 3.7

Geometry of the Fourpoint Antenna of Figs. 3.9 and 3.1 (b).

Description	Symbol	Size
Element side length	A	50.8 mm (2.0”)
Length B	B	38.1 mm (1.5”)
Substrate side length	C	63.5 mm (2.5”)
Gap width	W	0.76 mm (0.03”)
Substrate thickness	t_s	0.76 mm (0.03”)
Foam thickness	t_d	26.7 mm (1.05”)
Element height above ground plane	h	27.4 mm (1.08”)
Feed positions distance	F’	2.87 mm (0.113”)

3.7.1 Reflection Coefficient and VSWR

The CP Fourpoint antenna was simulated with the commercial code Fidelity. In Fidelity four coaxial ports are modeled by feeding to the radiating element with 90° phase difference for each port. Reflection coefficients of the CP Fourpoint antenna were calculated using the S-parameter value obtained from Fidelity. In order to find the reflection coefficient, the S-parameters in the network can be reduced to a set of three values based on symmetric properties as follows:

$$r = S_{ii}, \quad c = S_{12} = S_{21} = S_{34} = S_{43}, \quad d = S_{13} = S_{31} = S_{14} = S_{41} = S_{23} = S_{32} = S_{24} = S_{42}. \tag{1}$$

And the simplified s-parameter can be described as

$$[S] = \begin{bmatrix} r & c & d & d \\ c & r & d & d \\ d & d & r & c \\ d & d & c & r \end{bmatrix} \quad and \quad \begin{bmatrix} b_1 \\ b_2 \\ b_3 \\ b_4 \end{bmatrix} = [S] \begin{bmatrix} a_1 \\ a_2 \\ a_3 \\ a_4 \end{bmatrix}. \tag{2}$$

The reflected wave at port 1 is

$$b_1 = r \cdot a_1 + c \cdot a_2 + d \cdot a_3 + d \cdot a_4. \tag{3}$$

For CP excitation, $a_1 = 1, a_2 = -1, a_3 = j, a_4 = -j$. So the final equation can be simplified to

$$b_1 = (r - c + j \cdot d - j \cdot d) \cdot a_1 = (r - c) \cdot a_1. \tag{4}$$

Hence the reflection coefficient at port 1 of the antenna can be obtained with computed s-parameter as follows:

$$|\Gamma| = \left| \frac{b_1}{a_1} \right| = |r - c| = |s_{11} - s_{21}|. \tag{5}$$

The reflection coefficient and VSWR value from the simulation are presented in Fig. 3.11. The CP Fourpoint antenna has impedance bandwidth of 53 % for VSWR<2 based on f_L=2.1 GHz, f_C= 2.85 GHz, f_U=3.6 GHz.

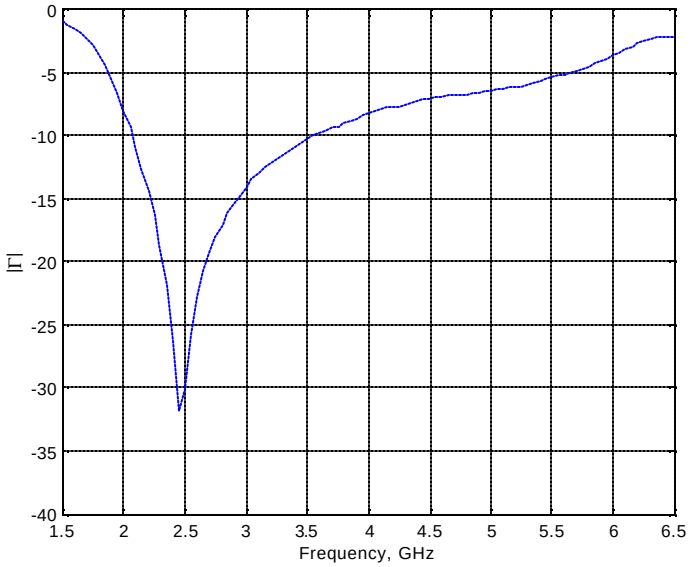

(a) Reflection coefficient at port 1 of the antenna.

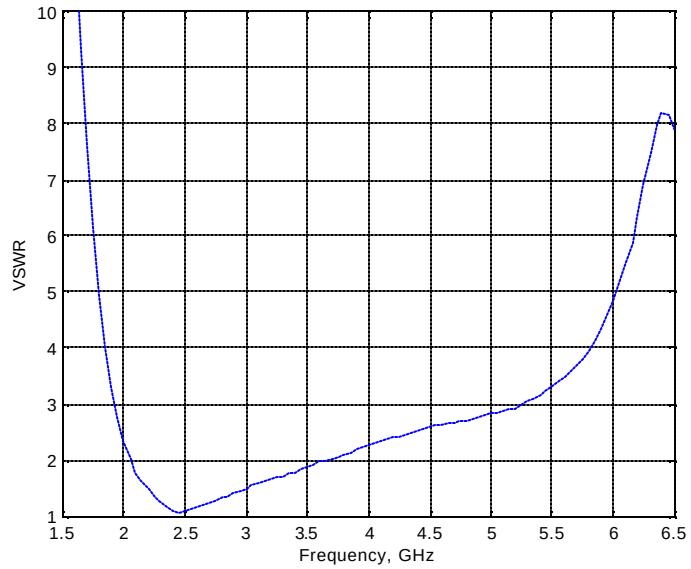

(b) VSWR referenced to 50-Ω.

Figure 3.11 Computed reflection coefficient and VSWR (referenced to 50-Ω) of the left-hand circular polarized (LHCP) Fourpoint antenna of Fig. 3.9 with the dimensions listed in Table 3.7.

3.7.2 Radiation Patterns

The radiation patterns of the LHCP Fourpoint antenna were computed at 2.4 GHz with the commercial code Fidelity. Figure 3.12 presents the elevation axial ratio patterns and the elevation patterns over the 180° in 5° increments. The cross-pol level is about 20 dB down at the bore-sight. The radiation patterns demonstrate that the CP Fourpoint antenna provides excellent CP patterns.

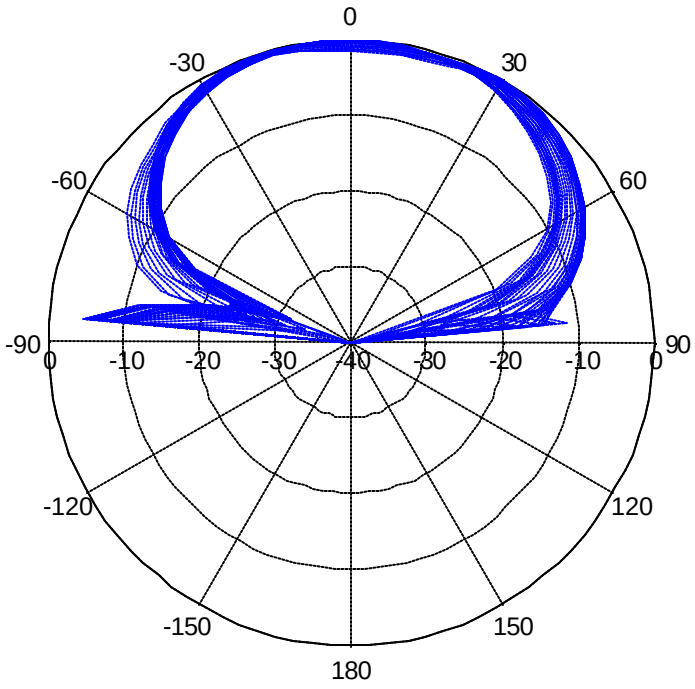

(a) Elevation axial ratio patterns in dB of the LHCP Fourpoint antenna at 2.4 GHz for all 180° azimuth angle by 5° increment.

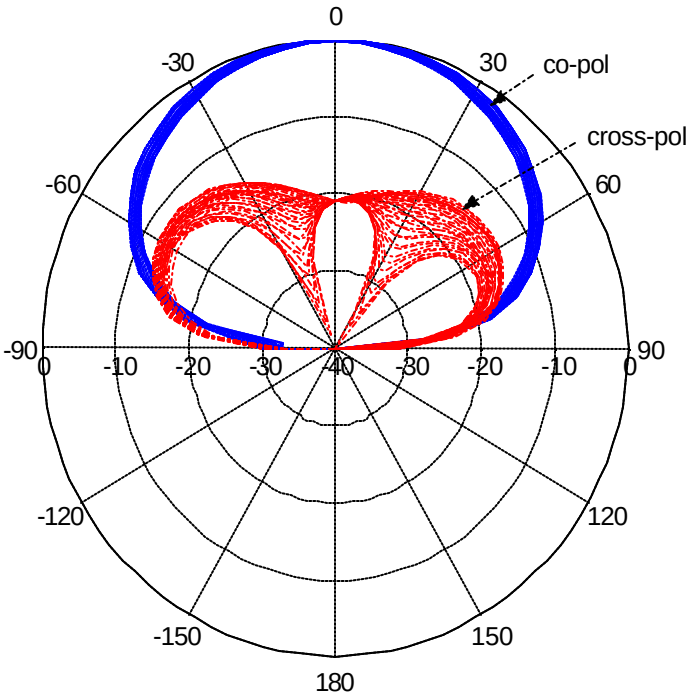

(b) Radiation patterns of the LHCP Fourpoint antenna at 2.4 GHz for all 180° azimuth angle by 5° increment.

Figure 3.12 Computed patterns of the LHCP Fourpoint antenna of Fig. 3.9 at 2.4 GHz**.**

3.8 Parametric Analysis of the Fourpoint Antenna

The Fourpoint antenna geometry parameters listed in Table 3.1 all influence its performance. An investigation was conducted to understand the parameter influences. The simulation code Fidelity was used. The investigations were made using the Fourpoint antenna in Fig. 3.1 and Table 3.1. Note that the tuning plate effect will be discussed in Chapter 4. The study was performed by computing the antenna impedance as a function of frequency. It is assumed that the radiation pattern is not greatly affected by parameter changes.

3.8.1 Parameter 'B' effect

The length parameter 'B' determines the second resonance frequency. The second resonate frequency was found to be inversely proportional to the length 'B' of the Fourpoint antenna. That is, increasing the length 'B' beyond the normal value of 15.77 mm reduces the second resonate frequency.

3.8.2 Parameter 'W' effect – Gap width effect between radiating element

The gap width between the radiating elements, 'W' influences the antenna impedance. Increasing the gap width causes the level of resistance to rise and increases the reactance variations.

3.8.3 Parameter 't_s' effect – Length of center conductor effect

The substrate serves only as a material to support the radiating element. Simulations demonstrated that the substrate has minimal effect on the antenna performance. This was determined through computations on a Fourpoint antenna with and without a substrate of dielectric constant of 2.33. The substrate thickness 't_s' determines the length of the interconnecting wire between coaxial feed and radiating element. The interconnecting wire length 't_s' increases the inductive reactance in the Fourpoint antenna.

3.8.4 Parameter 'h' effect – Height of the radiating element effect above the ground plane

Variation in the height above the ground plane, 'h' affects the variations of the antenna impedance at lower band of the operating band. Small height 's', cause high variation of impedance of the Fourpoint antenna. In addition to the effect on the impedance, 'h' also influences the shape of radiation pattern. By image theory radiating element should be located above the ground plane about quarter-wave length at a desired frequency for best pattern performance. When the height 'h' is smaller or larger than a quarter-wave length, there will be a destructive interference in the bore-sight direction (i.e. + z-direction). As a result it generates a dip at the bore-sight of the antenna. Therefore, an optimum height should be determined to avoid problems in a wideband ground plane antennas like the Fourpoint antenna.

3.8.5 Tuning plate effect

The addition of a tuning plate enhances the antenna performance dramatically without increasing antenna size. The tuning plate acts to distribute the impedance variations equally over the operating band. The plate shape is selected based on the application. The details of the tuning plate are discussed in Chapter 4.

3.9 Summary

A new antenna called the Fourpoint antenna was proposed for wideband applications. It is a low-profile and dual-polarized. The Fourpoint antenna evolved from the Foursquare antenna by enhancing the bandwidth through a modified geometry.

Several Fourpoint test models were designed and constructed along with computer simulations. The computed and measured data demonstrate that the Fourpoint antenna provides much better performance than a Foursquare antenna of the same size. Furthermore, a significant enhancement to the Fourpoint antenna was presented; see Section 3.4. A tuning plate increases the impedance bandwidth toward the high end of the operating band. The tuning plate can be etched on the bottom of the radiating element so no additional space is necessary. The antenna can be easily tuned by varying the tuning plates geometry and orientation. Several test models demonstrated that the tuning plate improves the antenna impedance. The tuning plates can be applied to the Foursquare antenna as well.

The Fourpoint antenna without tuning plate provides excellent unidirectional patterns over impedance bandwidth with broad beam width; see Sections 3.3 and 3.5. Although, the tuning plate in the Fourpoint antenna increases the impedance bandwidth, the radiation patterns at high end of the operating band are flattened near the bore-sight. This phenomenon is caused by the increased electrical height above the ground plane necessary for wide impedance bandwidth. The radiation patterns, however, are acceptable in most applications.

The dual-linearly polarized Fourpoint antenna was modified to a circularly polarized Fourpoint antenna using a software test model. The simulation results demonstrate that the Fourpoint antenna also has excellent CP characteristics. Thus, the Fourpoint antenna provides either linear or circular polarization and wide bandwidth in a low-profile physical package.

The geometry parameters are critical factor in determining the antenna performance. The effect of each parameter was investigated and summarized in Section 3.8. The effect of the tuning plate, however, is investigated in detail in Chapter 4.

References

[3.1] J. R. Nealy, "Foursquare Antenna Radiating Element," *U.S. Patent No. 5,926,137*, July 20, 1999. VTIP Ref. 96-056. http://www.vtip.org

[3.2] S.-Y. Suh and W. L. Stutzman, *"A Fourpoint Antenna," VTIP disclosure No. 00-141*, http://www.vtip.org/Licensing/disclosures/00-141.htm, September 28, 2000

[3.3] Fidelity User's Manual, Zeland Software Inc., Release 3, 2000.

[3.4] HFSS User's Manual, Agilent Technologies, September, 2000.

[3.5] S. A. Bokhari, Jean-Francois Z?rcher, Juan R. Mosig, Fred E. Gardiol, "A small Microstrip Patch Antenna with a Convenient Tuning Option," *IEEE Trans. Antennas Propagation*., vol. 44, No. 11, pp. 1521-1528, Nov. 1996.

[3.6] W. L. Stutzman and G.A. Thiele, *Antenna Theory and Design 2nd edition*, John Wiley & Sons, New York, 1998.

Chapter 4

Investigation of Tuning Plate Effects with Foursquare and Fourpoint Antennas

4.1 Introduction

It was shown in Chapter 3 that the impedance bandwidth of the Fourpoint antenna is increased dramatically by using a tuning plate. The tuning plate increases the impedance bandwidth of the Fourpoint antenna near the high frequency end of the operating band without increasing the antenna size. Various shapes of tuning plates can be used to tune the antenna impedance for a desired band [4.1]. Some test models of the Fourpoint antenna with a tuning plate that were presented in Chapter 3 demonstrated that significant bandwidth improvement is possible. The use of a tuning plate offers several advantages over the original Fourpoint antenna. In addition, the tuning plate can also be used in the Foursquare antenna.

In this chapter, the results of simulation studies into the effect of the tuning plates with both Foursquare and Fourpoint antennas are presented for two cases: with and without a tuning plate. Comparison using the Fidelity code with and without tuning plate

demonstrates that the tuning plate significantly enhances the impedance performance of both antennas without increasing the antenna size.

4.2 The Foursquare Antenna with a Tuning Plate

Since the tuning plate performed so well with the Fourpoint antenna (see Sections 3.4 - 3.6), the Foursquare antenna was examined to see if its performance could be similarly improved. In Figure 4.1 the Foursquare with the circular tuning plate is presented with the dimensions in Table 4.1. In order to investigate the effect of the tuning plate, the Foursquare antenna was simulated for two cases, with and without a tuning plate. The antennas have the same outer dimensions as listed in Table 4.1. The electrical height of the element above the ground plane was optimized to obtain unidirectional pattern over entire band, which produced antenna height of $0.31?_{U}$ and $0.24?_{U}$ with and without a circular tuning plate, respectively. The commercial code, Fidelity was used in simulating the antennas.

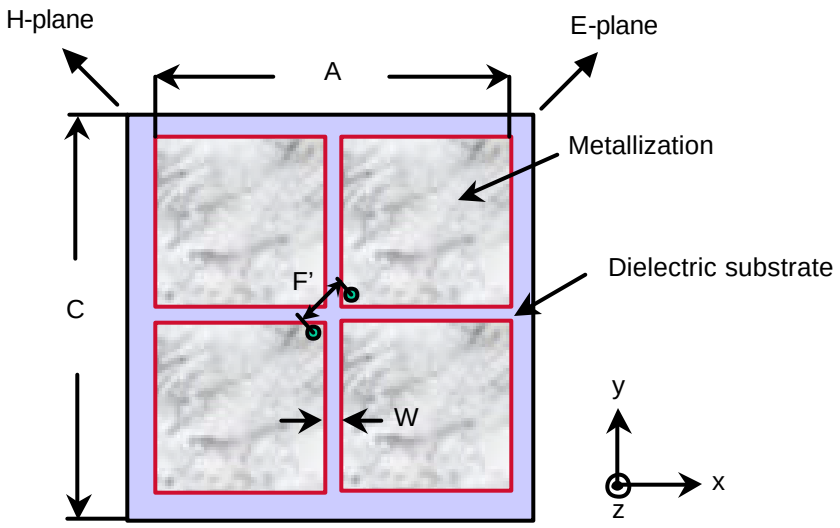

(c) Top view of the Foursquare antenna.

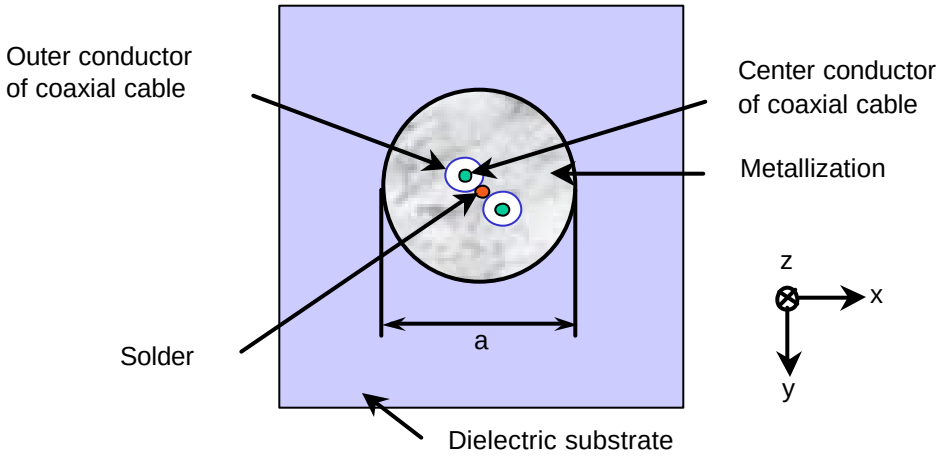

(d) Bottom view with a circular tuning plate.

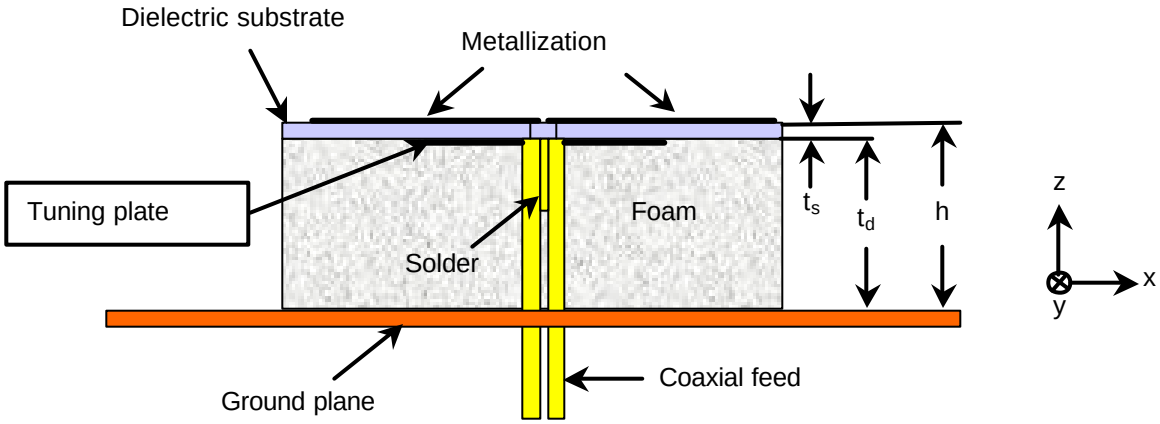

(e) Side view of the Fourpoint antenna with single tuning plate.

Figure 4.1 Geometry of the Foursquare antenna with a circular tuning plate.

Table 4.1

Geometry of the Foursquare Antenna with a Circular Tuning Plate in Fig. 4.1.

Description	Symbol	Size
Element side length	A	17.02 mm (0.67”)
Substrate side length	C	17.3 mm (0.68”)
Circular plate diameter	a	8.13 mm (0.32”)
Gap width	W	0.508 mm (0.02”)
Substrate thickness	t_s	0.787mm (31 mils),
Foam thickness	t_d	7.92 mm (0.312”)
Element height above ground plane	h	8.71 mm (0.343”)
Feed positions distance	F’	4.31 mm (0.17”)

The computed antenna impedance and VSWR (referenced to 50-Ω) are presented in Fig. 4.2 and the electrical performance and electrical size of the simulated Foursquare antenna are summarized in Table 4.2. The simulation results demonstrate that the tuning plate works well in the Foursquare antenna just with the Fourpoint antenna.

The circular tuning plate in the Foursquare antenna increased the bandwidth of the Foursquare antenna from 35 % to 60 % for $VSWR \leq 2$. The antenna impedance as shown in Fig. 4.2(a) demonstrates that the Foursquare antenna with the circular tuning plate is much more equally distributed over the band than the Foursquare antenna without the tuning plate.

The radiation patterns of the Foursquare antenna are not presented here, but it is expected that they will be similar to the patterns in Fig. 2.18.

Table 4.2

Electrical Performance and electrical size of the Foursquare Antenna with and without Circular Tuning Plate. (Geometry: Fig. 4.1; Performance curve: Figure 4.2)

Description	**Symbol**	**Performance (Computed)**	
		With circular tuning plate	**Without circular tuning plate**
Lowest freq. at VSWR =2	f_L (VSWR=2)	5.65 GHz	5.83 GHz
Upper freq. at VSWR =2	f_U (VSWR=2)	10.53 GHz	8.27 GHz
Impedance bandwidth	$B_p(VSWR \leq 2)$	60.3 %	34.6 %
Element size in λ_L	A	0.32 λ_L	0.331 λ_L
Substrate size in λ_L	C	0.325 λ_L	0.336 λ_L
Electrical height h in λ_L	h	0.164 λ_L	0.169 λ_L
Electrical height h in λ_U	h	0.31 λ_U	0.24 λ_U

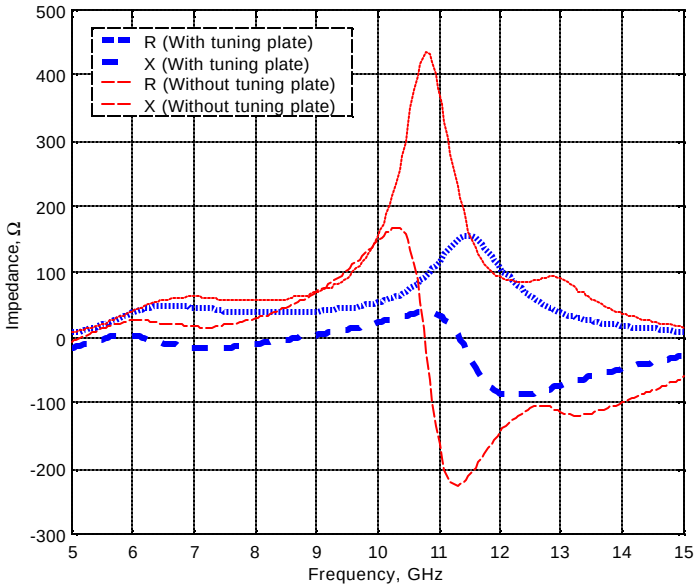

(a) Computed antenna impedance.

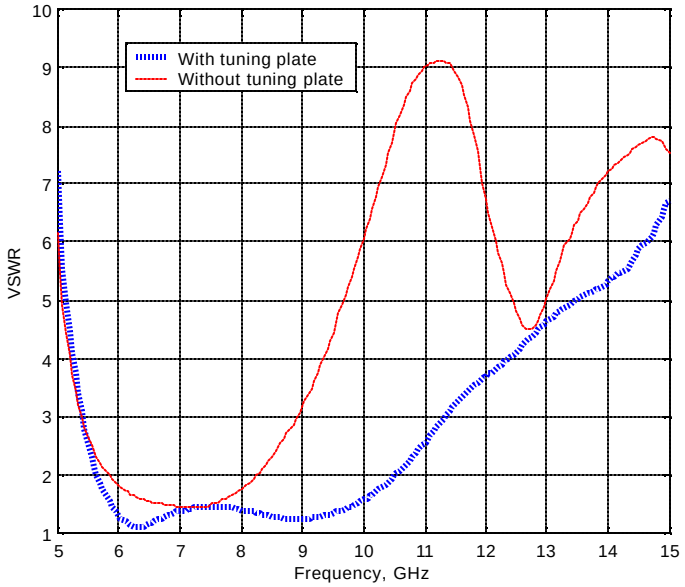

(b) Computed VSWR referenced to 50-Ω.

Figure 4.2 Antenna impedance and VSWR (referenced to 50-Ω) computed with Fidelity for the Foursquare antenna with and without a circular tuning plate as shown in Fig. 4.1 and with the dimensions of Table 4.1.

4.3 The Fourpoint Antenna with a Tuning Plate

The effect of the tuning plate was investigated with the Fourpoint antenna as well as the Foursquare antenna. The Fourpoint antenna of Fig. 3.4 (a), (c) (e) with the dimensions of Table 3.5 was compared with the Fourpoint antenna without the tuning plate. The Fourpoint antenna of Fig. 3.5 (a) without the tuning plate was computed with the commercial code Fidelity and the results are compared in Figure 4.3 for the two cases of with and without a tuning plate.

The computed results in Fig. 4.3 demonstrate that the tuning plate also plays an important role in enhancing the impedance of the Fourpoint antenna. The electrical performance and electrical size of the Fourpoint antenna are summarized in Table 4.3. Note that the impedance bandwidth increased from 54% to 79% for VSWR ≤ 2 through the use of the tuning plate, without increasing the antenna size. Based on the impedance curve in Fig. 4.3(a), the tuning plate distributes the impedance curve equally at high frequency.

Table 4.3

Electrical Performance and electrical size of the Fourpoint Antenna with and without Star-shaped Tuning Plate. (Geometry: Fig. 3.4(a), (c), and (e); Performance curve: Figure 4.3)

Description	**Symbol**	**Performance (Simulated)**	
		With star-shaped tuning plate	**Without star-shaped tuning plate**
Lowest freq. at VSWR =2	f_L (VSWR=2)	5.8 GHz	5.8 GHz
Upper freq. At VSWR =2	f_U (VSWR=2)	13.3 GHz	10.1 GHz
Percent bandwidth	B_p	78.5 % (B_r=2.3:1)	54.1 % (B_r=1.7:1)
Element size in λ_L	A	0.329 λ_L	0.329 λ_L
Substrate size in λ_L	C	0.334 λ_L	0.334 λ_L
Electrical height h in λ_L	h	0.17 λ_L	0.17 λ_L
Electrical height h in λ_U	h	0.39 λ_U	0.3 λ_U

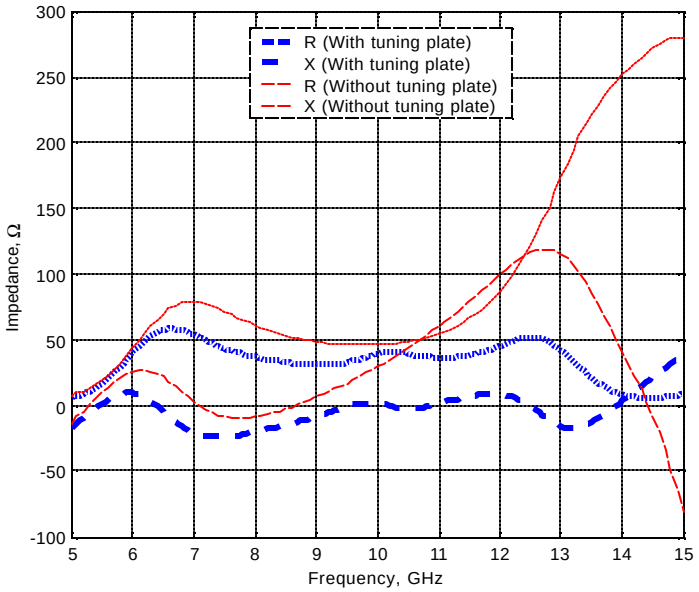

(a) Computed antenna impedance curves.

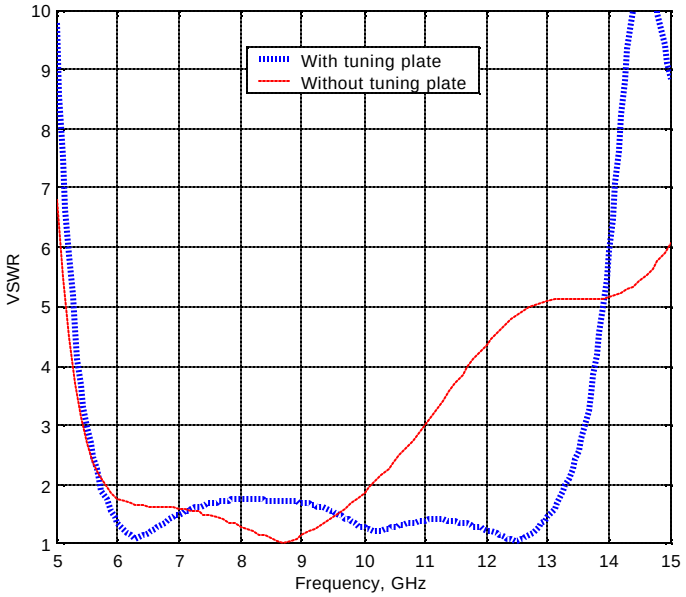

(b) Computed VSWR referenced to 50-Ω.

Figure 4.3 Antenna impedance and VSWR (referenced to 50-Ω) computed with Fidelity for the Fourpoint antenna with and without a star-shaped tuning plate, as shown in Fig. 3.4(a), (c), (e) with the dimensions of Table 3.5.

4.4 Summary

The effects of tuning plate were examined for both Foursquare and Fourpoint antennas. The same antennas were computed for the two cases of with and without tuning plate. The simulation results demonstrate that the tuning plate enhances the antenna impedance dramatically by increasing the impedance bandwidth toward the high frequency without increasing the antenna size.

The simulation results are summarized in Fig. 4.4 for the following antennas: 1) Foursquare antenna without tuning plate, 2) Foursquare antenna with a circular tuning plate, 3) Fourpoint antenna without tuning plate, 4) Fourpoint antenna with a star-shaped tuning plate. The modeled antennas have the same outer dimensions and are referenced to the same impedance of 50-Ω, so a direct performance comparison can be made. The tuning plate enhanced the impedance bandwidth of the Foursquare and Fourpoint antenna respectively. And significant impedance bandwidth enhancement with the Fourpoint antenna with the tuning plate was achieved, as shown in Fig. 4.4. Based on the simulation results, the impedance bandwidth was improved more than twice (from 35 % to 78.5 %) from the Foursquare antenna to Fourpoint antenna with tuning plate. Note that there is no size increment in the antenna evolution.

Tuning plates shapes in Fig. 3.4(b), (c), (d) such as square, circular and star, as well as other shapes, can be used for different the applications. Moreover, the tuning plate can be applied to any antenna with a geometry similar to the Foursquare or the Fourpoint antenna. Also, multiple tuning plates as in Fig. 3.4(f) can also be used to widen the antenna impedance bandwidth further.

Basic guidelines for the tuning plate design are as follows:

- The tuning plate should be smaller than the radiating element size. The size of about a = A/2 is a good starting dimension; see Fig. 3.4.
- The tuning plate geometry is determined by the radiating element geometry. If the radiating element geometry is sharp four points, star-shaped-tuning plate is recommended. But the element geometry is four squares, circular or square-shaped tuning plate is recommend.

- The height t_s between the element and tuning plate can be modified to obtain the optimum impedance characteristics. However, generally the height is determined by the thickness of the substrate.

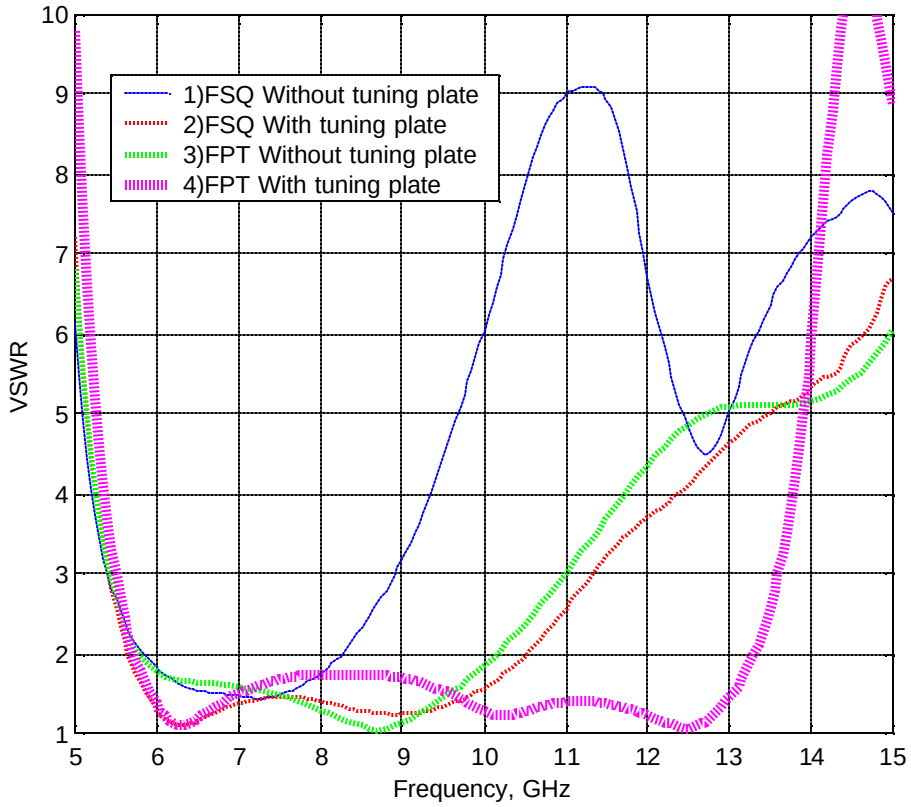

Figure 4.4 Computed VSWR (referenced to 50-Ω) curves of 1) the Foursquare antenna without tuning plate, 2) the Foursquare antenna with circular tuning plate, 3) the Fourpoint antenna without tuning plate and 4) the Fourpoint antenna with a star-shaped tuning plate. They have the same outer dimensions of 17.02 mm (0.67") as listed in Tables 3.5 and 4.1.

References

[4.1] S. A. Bokhari, Jean-Francois Z?rcher, Juan R. Mosig, Fred E. Gardiol, “A small Microstrip Patch Antenna with a Convenient Tuning Option,” *IEEE Trans. Antennas Propagation*., vol. 44, No. 11, pp. 1521-1528, Nov. 1996.

Chapter 5

Generalization of the Fourpoint Antenna: The Fourtear Antenna

5.1 Introduction

The effect of a tuning plate addition to the Fourpoint antenna was investigated extensively in previous chapters. The tuning plate improved impedance performance dramatically without increasing antenna size. In addition to the tuning plate, the gap width between the radiating elements, W, also influences the Fourpoint antenna performance. As an additional attempt to increase the impedance bandwidth of the Fourpoint antenna, the effect of the gap width between the radiating elements was investigated. Based on the results of the parametric study discussed in Section 3.8.2, it is expected that the Fourpoint antenna gap width, W, controls the antenna impedance, especially the resistance.

First we examine the uniform gap width effects on the Fourpoint antenna in Fig. 3.1 with the dimensions listed in Table 5.1. Two uniform gap widths of W=0.254 mm (0.01") and 0.508 mm (0.02") were examined to demonstrate the effect of the gap width on the Fourpoint antenna.

Table 5.1

Dimensions of the Fourpoint Antenna Geometry in Fig. 3.1.

Description	**Symbol**	**Size**	
		Wide Gap	**Narrow Gap**
Element side length	A	17.02 mm (0.67”)	Same
Length B	B	13.97 mm (0.55”)	Same
Substrate side length	C	17.3 mm (0.68”)	Same
Gap width	**W**	**0.508 mm (0.02”)**	**0.254 (0.01”)**
Substrate thickness	t_s	0.787mm (31 mils),	Same
Foam thickness	t_d	7.92 mm (0.312”)	Same
Element height above ground plane	h	8.71 mm (0.343”)	Same
Feed positions distance	F’	2.87 mm (0.113”)	Same

The simulation result of a Fourpoint antenna is presented in Fig. 5.1 demonstrating that the wider gap (thick line) yields higher resistance than the narrow gap. The dimensions of the Fourpoint antenna are listed in Table 5.1. Note that the Fourpoint antenna does not employ the tuning plate.

All of the previously discussed Foursquare and Fourpoint antennas employ uniform gap width. In this chapter, we investigate how the geometry of the gap affects the antenna characteristics.

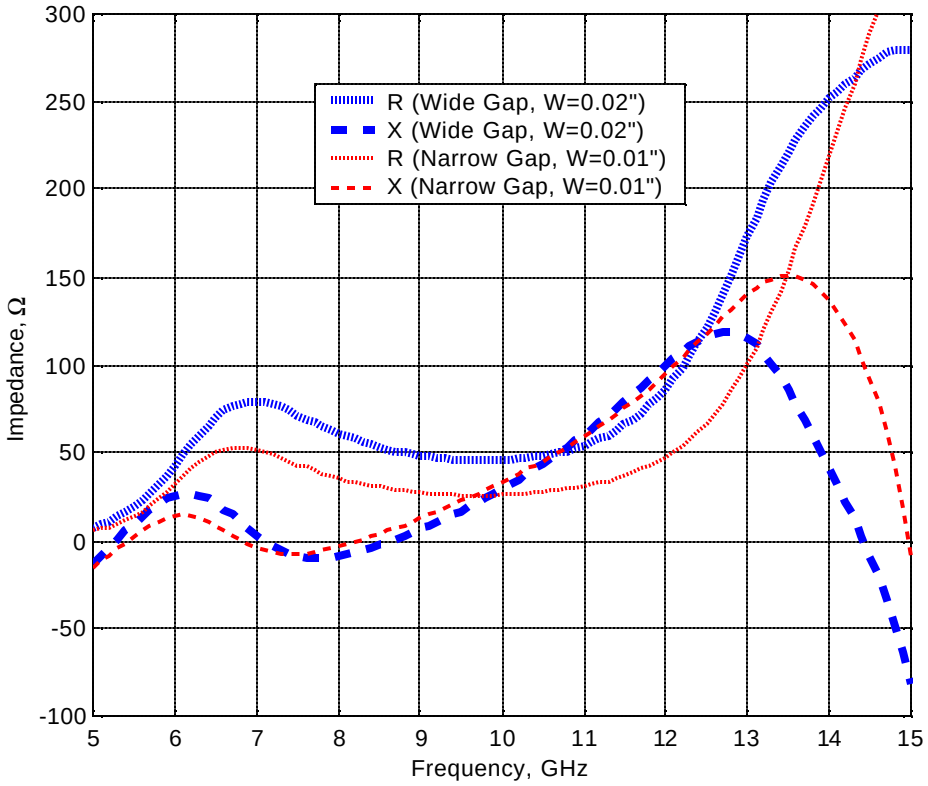

Figure 5.1 Input impedance of the Fourpoint antenna with the dimensions listed in Table 5.1 for two different uniform gap width.

5.2 Investigation of Gap Shape Effects

This section reports a numerical investigation with the effects of the Fourpoint antenna gap shape with the goal of increasing bandwidth. Both linearly and non-linearly tapered gaps were investigated.

5.2.1 Linearly Tapered Gap

The Fourpoint antenna in Fig. 3.1 with the dimensions of Table 3.1 was modified to the geometry in Fig. 5.2. The gap between the parasitic element and the metal containing the feed is changed to be slanted rather than straight. The gap width ratio, W2/W1=4 quantifies the rate of flare of the tapered edge gap. The simulation results shown in Fig. 5.3 reveal that the slanted edge provides improved antenna performance. The resistance level at low and mid-band frequencies is increased, while the resistance at the upper end of frequency band is decreased. Also, the reactive component was more equally distributed over a wide bandwidth with lower reactance level.

The linearly tapered gap improved impedance bandwidth of the Fourpoint antenna (with uniform gap) from 40% to 66% toward high end of band without increasing antenna size. The impedance bandwidth are calculated for VSWR < 2. Note that the Fourpoint antenna with linearly tapered gap does not employ the tuning plate.

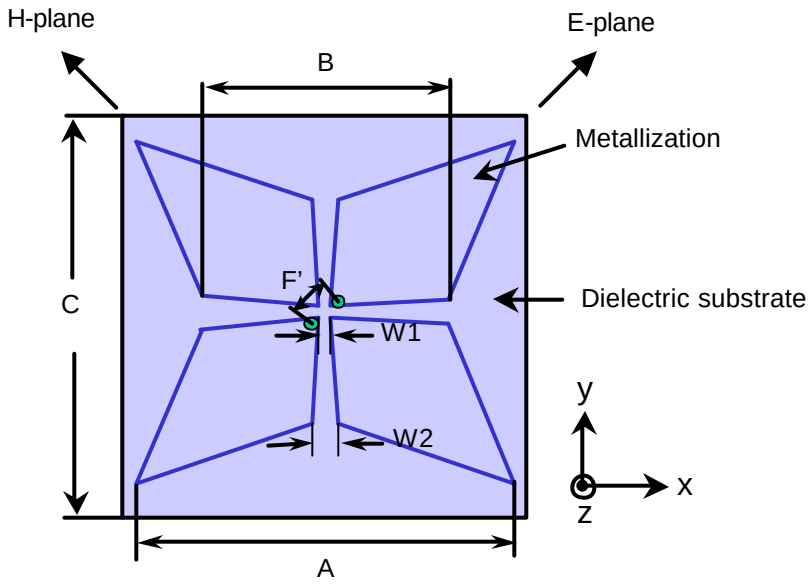

Figure 5.2 The Fourpoint antenna with tapered gaps and the dimensions listed in Table 5.1, except for the gap dimensions, W1=0.254 mm (0.01") and W2=1.02 mm (0.04").

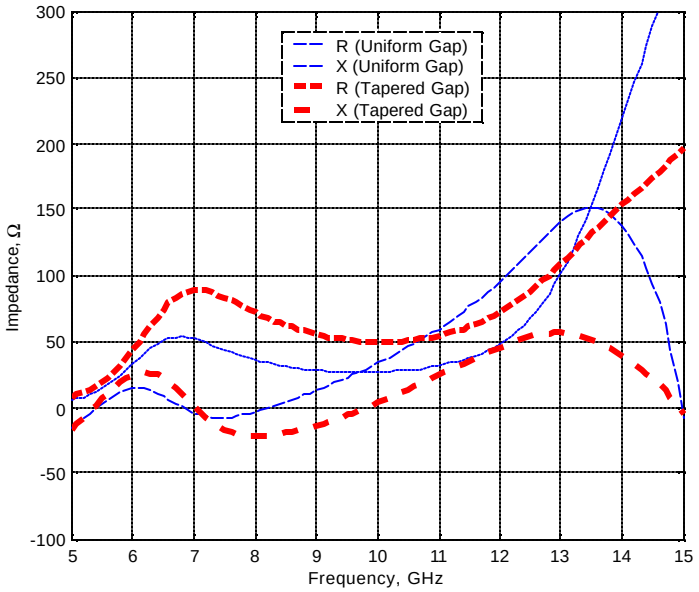

(a) Antenna Impedance.

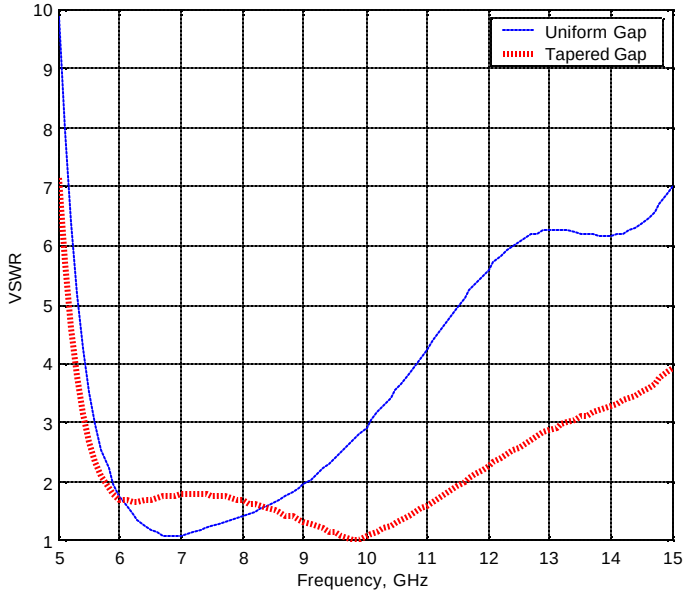

(b) VSWR referenced to 50-Ω.

Figure 5.3 Antenna impedance and VSWR (referenced to 50-Ω) for the Fourpoint antenna of Table 5.1 with uniform gap and the tapered gaps computed using the Fidelity code.

5.2.2 Non-linearly Tapered Gap

A non-linearly tapered gap effect was also investigated using the antenna geometry in Fig. 5.4. The gaps between the elements are non-linearly tapered, unlike the Fourpoint antenna or the antenna in Fig. 5.2. The geometry of the four radiating elements is identical, but the radiating element edges are piecewise linear, approximating a curved shape as shown in Fig. 5.4(a). The antenna was simulated for the dimensions listed in Table 5.2 using the FDTD code, Fidelity. The outer dimension is same for the Fourpoint antenna in Table 3.4. Note that no tuning plate was used in the antenna.

The simulation results are compared in Fig. 5.5 for two different feed configurations, a-a' and b-b'. The computed results demonstrate that the non-linearly tapered gap improves the performance of the Fourpoint antenna dramatically. But note that the antenna has different impedance characteristics for each of the two feed terminal pairs, a-a' and b-b'. The impedances for the two feeds are similar, but not identical, whereas the Foursquare and Fourpoint antennas have identical impedances for the two feed cases. The non-linearly tapered gap Fourpoint antenna has a resistance level of about 100-Ω over frequency band of 6 - 17 GHz as shown in Fig. 5.5 so that the VSWR is referenced to 100-Ω. Different impedance behavior for the two feed cases arises due to the asymmetrical geometry, which causes different current distributions for each feed cases. The antenna performance is compared in Table 5.3 for the Fourpoint antenna without a tuning plate as presented in Section 4.3 and the non-linearly tapered gap Fourpoint antenna discussed in this section.

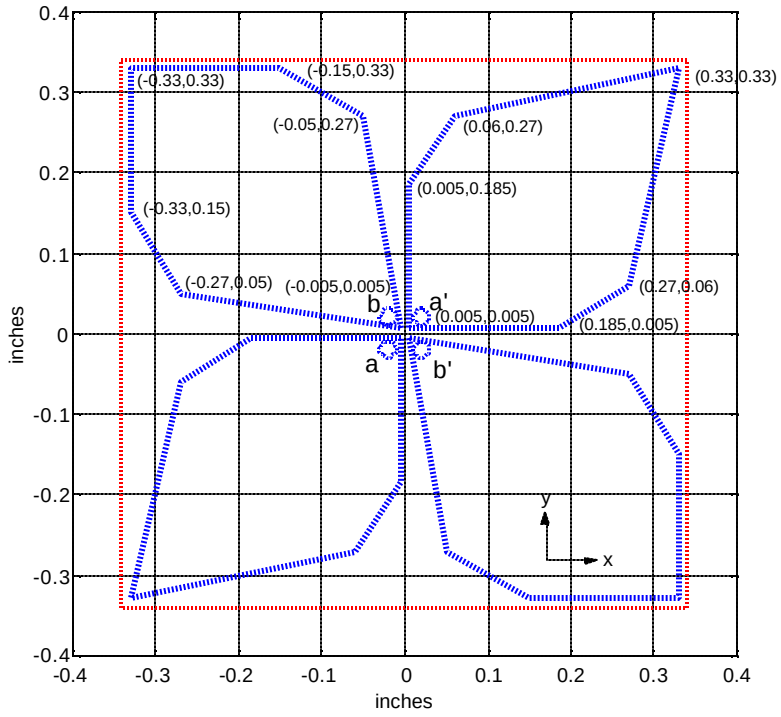

(a) Top view of the non-linearly tapered gap Fourpoint antenna.

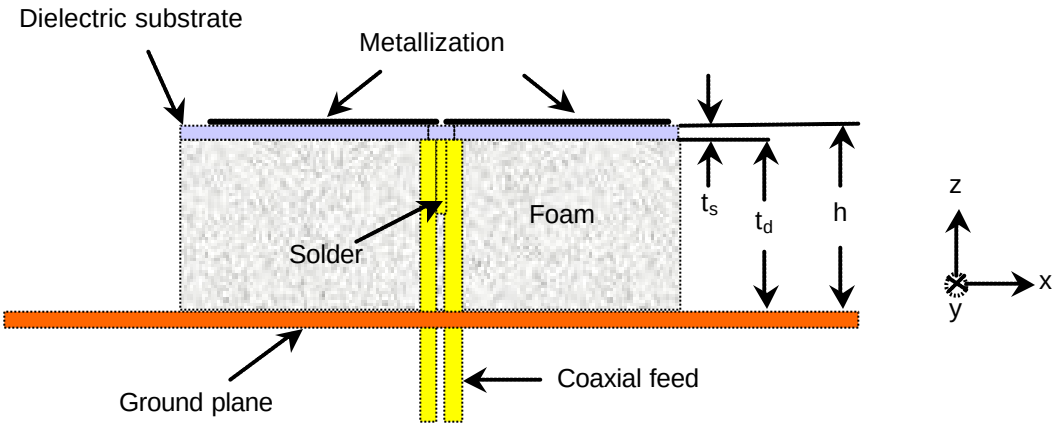

(b) Side view of the non-linearly tapered gap antenna.

Figure 5.4 Antenna geometry for a Fourpoint antenna with non-linearly tapered gap and the dimensions of the Table 5.2.

Table 5.2

Geometry of the Non-Linearly Tapered Gap Fourpoint Antenna of Fig. 5.4.

Description	**Symbol**	**Size**
Element side length	A	16.76 mm (0.66”)
Substrate side length	C	17.3 mm (0.68”)
Gap width	W	Non-linearly tapered
Substrate thickness	t_s	0.787mm (31 mils),
Foam thickness	t_d	7.92 mm (0.312”)
Element height above ground plane	h	8.71 mm (0.343”)
Feed positions distance	F’	2.87 mm (0.11”)

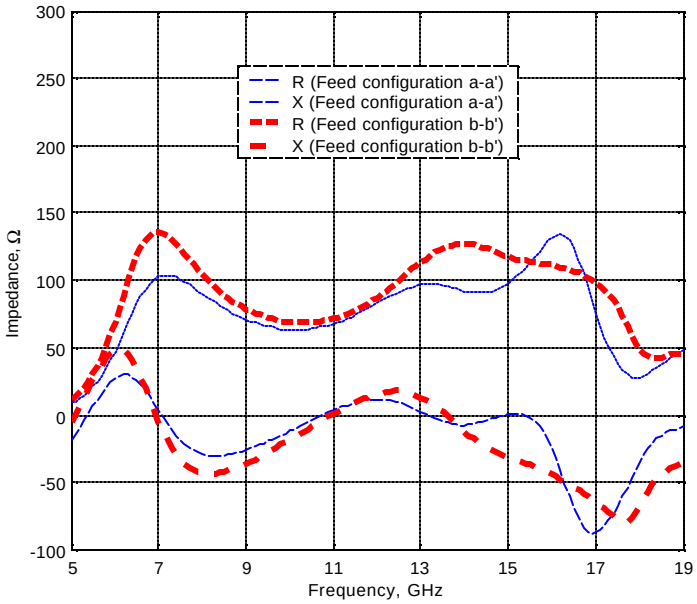

(a) Antenna impedance.

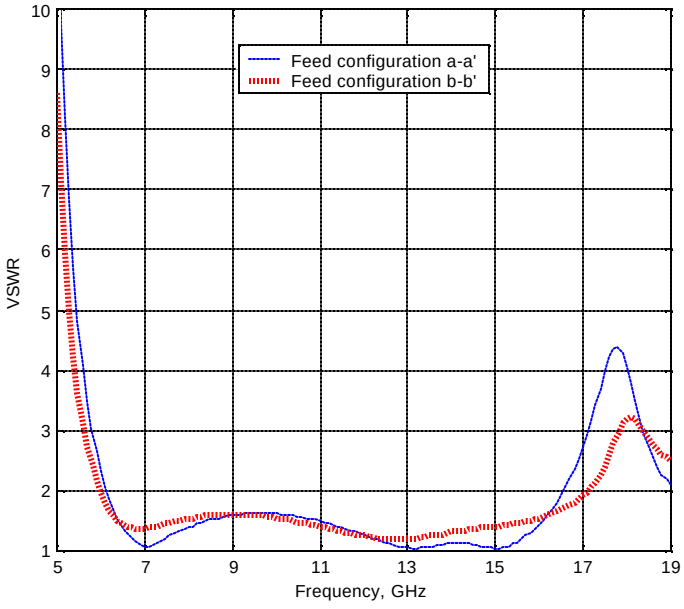

(b) VSWR referenced to 100-Ω.

Figure 5.5 Computed antenna impedance and VSWR (referenced to 100-Ω) of the non-linearly tapered gap Fourpoint antenna of Fig. 5.4 for two feed configurations.

Table 5.3

Computed Performance of the Non-Linearly Tapered Gap Fourpoint Antenna

(Geometry: Fig. 5.4; Performance curve: Figure 5.5)

Description	**Symbol**	**Performance (Simulated)**	
		a-a' feed	**b-b' feed**
Lowest freq. at VSWR =2	f_L (VSWR=2)	6.1 GHz	6.0 GHz
Upper freq. at VSWR =2	f_U (VSWR=2)	16.5 GHz	17.1 GHz
Impedance (VSWR ≤2) bandwidth	B_p	92.04 %	96.1 %
Ratio bandwidth	B_r	2.7:1	2.85:1
Element size in λ_L	A	0.341 λ_L	0.34 λ_L
Substrate size in λ_L	C	0.35 λ_L	0.35 λ_L
Height h in λ_L	h_L	0.177 λ_L	0.174 λ_L
Height h in λ_U	h_U	0.48 λ_U	0.5 λ_U

5.3 Radiating Element Design of the Fourtear Antenna

In this section, the non-linearly tapered gap Fourpoint antenna discussed in Section 5.2 is generalized into a new antenna called the Fourtear antenna. The Fourtear antenna is a logical evolution from the tapered gap Fourpoint antenna. The computed and measured data of the Fourtear antenna was presented in this section.

5.3.1 A solid Fourtear antenna

The Fourtear antenna discussion is started by reviewing some well-known classical antennas that are helpful in the development of the new antenna. Figure 5.6 shows the simple wire antennas evolved from monopole to crossed dipole antenna. These wire antennas are resonant antennas with narrow bandwidth. The monopole can be made in wide bandwidth from with the solid teardrop monopole antenna of Fig. 5.7 (a) [5.1]; see Section 2.4. The solid Teardrop antenna can be modified to form the solid Fourtear antenna shown in Fig. 5.7 [5.2]. This new antenna form is analogous to the crossed dipole antenna and can provide dual and diagonal linear polarizations over wide bandwidth.

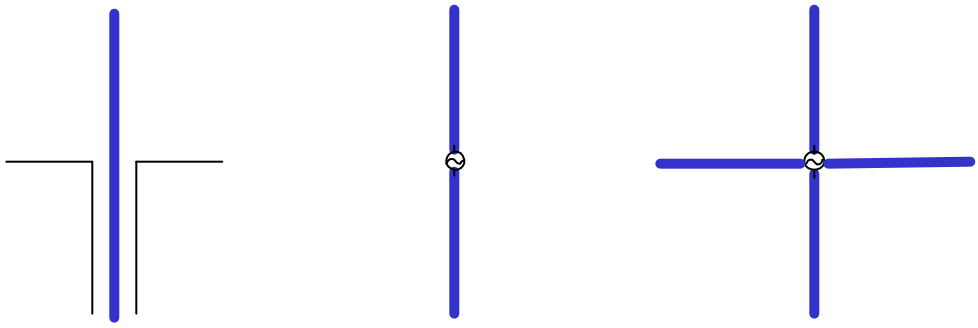

(a) Monopole. (b) Dipole. (c) Crossed dipole.

Figure 5.6 Evolution of crossed dipole antenna from monopole antenna.

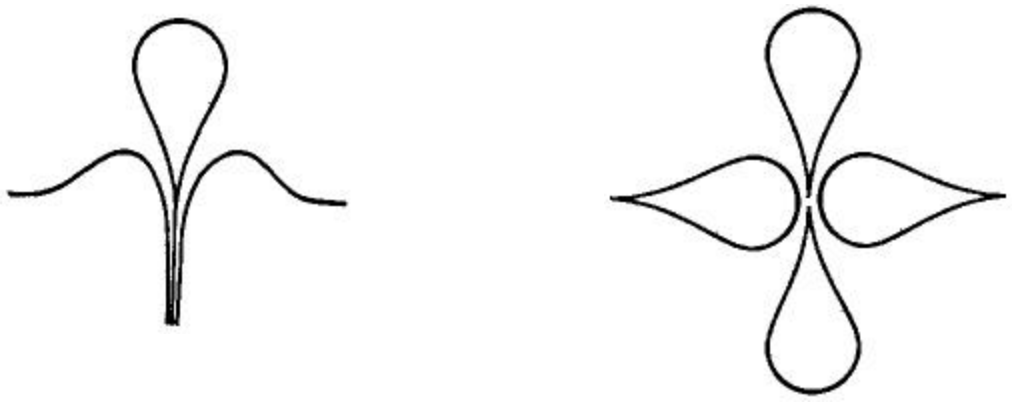

(a) Solid Teardrop antenna [5.1]. (b) Solid Fourtear antenna [5.2].

Figure 5.7 Evolution of the solid Fourtear antenna from the solid Teardrop antenna.

5.3.2 The Planar Fourtear antenna

The solid Fourtear antenna in Fig 5.7 (b) can be modified into the planar, low-profile geometry shown in Fig. 5.8. The planar Fourtear antenna has many geometric similarities to the Foursquare and Fourpoint antennas, so wide bandwidth is to be expected. The radiating element geometry is based on a circle of radius *r* together with a tip, as shown in Fig. 5.8 (a). Half of the circle is replaced with a smooth taper into the tip. The size and shape of the radiating element can be modified to control the operating band for the application. Generally, the dimension A is about $0.5?_L$ at the low end of the frequency band. Two feed configurations are possible in the Fourtear antenna and are denoted as a-a' and b-b'.

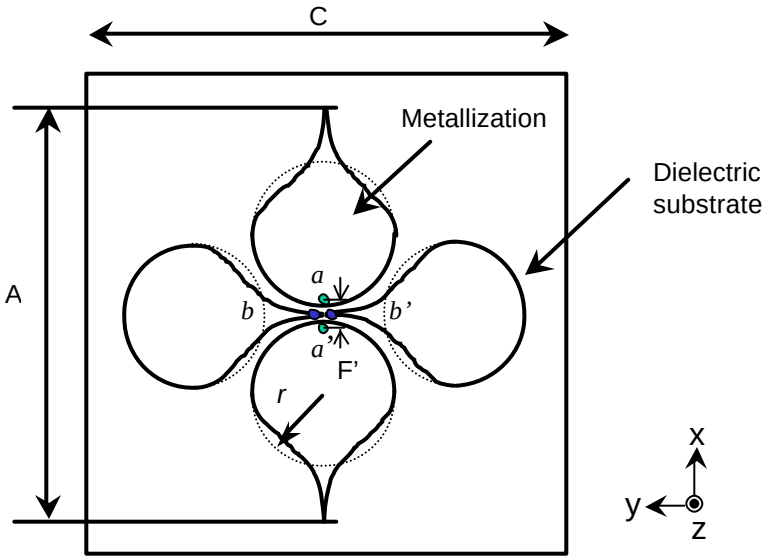

(a) Radiating element of the planar Fourtear antenna.

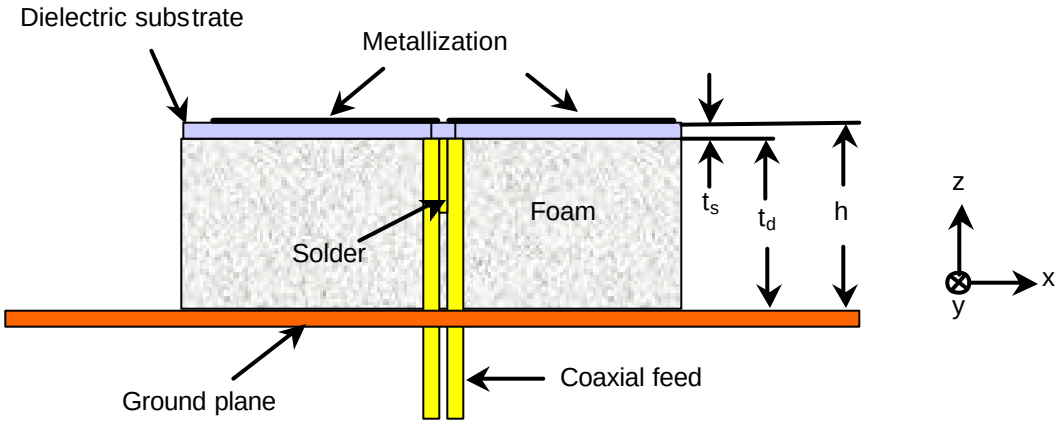

(b) Side view of the planar Fourtear antenna.

Figure 5.8 Geometry of the planar Fourtear antenna.

5.4 A Hardware Test Model of the Fourtear Antenna

The planar Fourtear antenna shown in Fig. 5.9 was constructed at Virginia Tech with the dimensions of Table 5.4. The radiating element was etched on a dielectric material, Duroid 5870 ($e_r = 2.33$) provided by Rogers Co. A semi-rigid cable of RG 405 /U was used as a coaxial feed with a characteristic impedance of 50-Ω. The outer diameter of the cable is about 2.2 mm (0.087"). The antenna was investigated using both simulation and measurement performed at the Virginia Tech Antenna Group. In computing the hardware test model, a commercial FDTD code, Fidelity was used. A HP8720C network analyzer and an Antcom near field scanner system were used for measuring the impedance and radiation patterns, respectively. An infinite ground plane was employed in simulations for computational simplicity and a 431.8 mm x 431.8 mm (17" x 17") aluminum ground plane was used in measurements. The electrical ground plane size is about 1.42 λ x 1.42 λ at the lowest antenna operating frequency of 1.0 GHz.

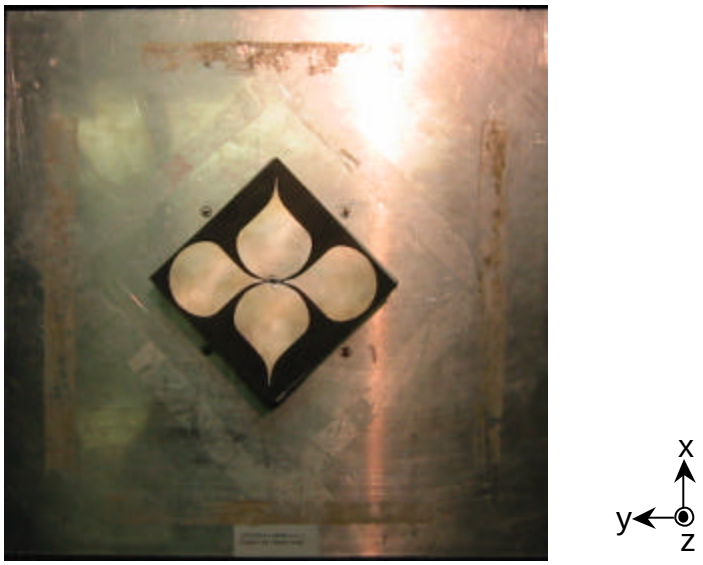

Figure 5.9 The hardware test model of the planar Fourtear antenna.

Table 5.4

Geometry of the Fourtear Antenna of Figs. 5.8 and 5.9.

Description	Symbol	Size
Element side length	A	154.9 mm (6.1")
Radius of circle	*r*	28 mm (1.1")
Substrate side length	C	165.1 mm (6.5")
Substrate thickness	t_s	0.79 mm (31 mils)
Foam thickness	t_d	37.34 mm (1.47")
Element height above ground plane	h	38.1 mm (1.5")
Feed positions distance	F'	3.56 mm (0.14")

5.4.1 The Fourtear antenna with the a-a' feed configuration

Unlike the Fourpoint antenna, the Fourtear antenna in Fig. 5.9 has different impedance characteristics for each feed configuration because of the asymmetric geometry in the radiating element. The Fourtear antenna with a-a' feed configuration performance was computed and measured and the results are presented in this section.

5.4.1.1 Antenna Impedance and VSWR

Antenna impedance and VSWR curves of the Fourtear antenna with a-a' feed configuration are shown in Fig. 5.10. The VSWR curves are referenced to a 100-Ω. The computed and measured data agree well. The resistive and reactive components are well matched with a value close to 100-Ω and 0-Ω over the whole band, respectively. The bandwidth based on VSWR < 2 is BW = f_U/f_L = 10. Based these simulations we see that more than 10:1 impedance bandwidth for VSWR < 2 is possible, except for the 2–3 GHz band. The impedance curves in Fig. 5.10 (a) demonstrate hat the Fourtear antenna has extremely wide impedance bandwidth.

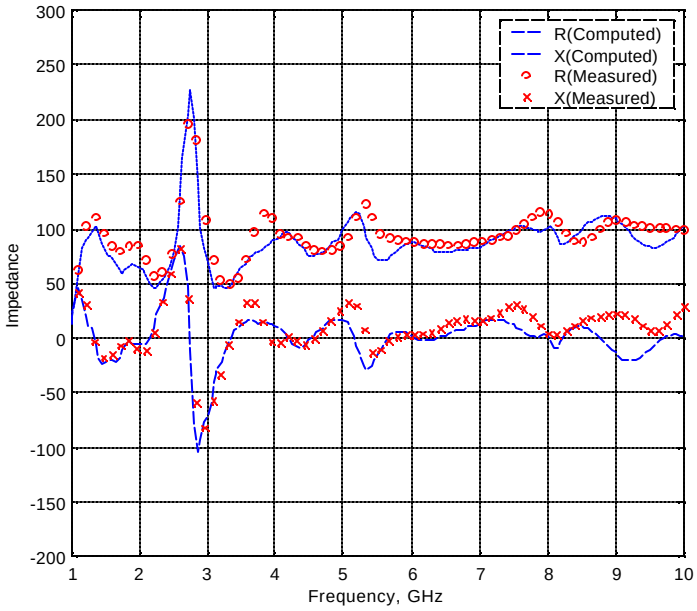

(a) Impedance curves of the Fourtear antenna with a-a' feed configuration.

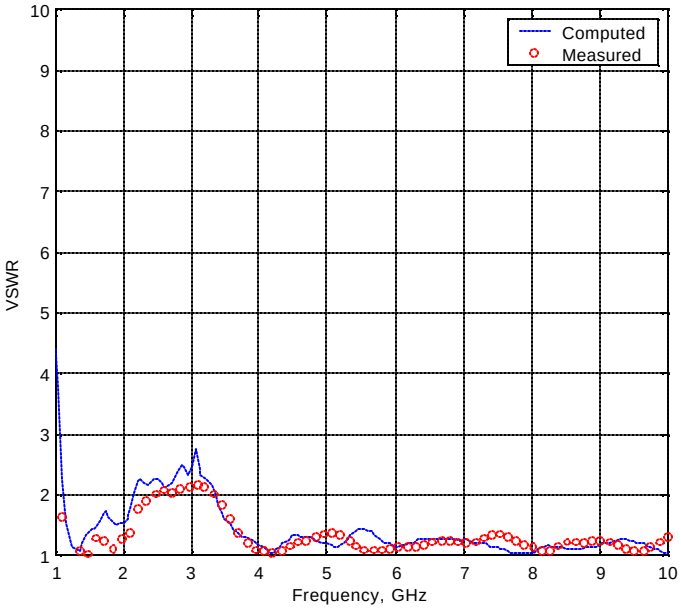

(b) VSWR curves referenced to 100-Ω of Fourtear antenna with a-a' feed configuration.

Figure 5.10 Computed and measured antenna impedance and VSWR (referenced to 100-Ω) for the Fourtear antenna in Figs. 5.8 and 5.9 with a-a' feed configuration and the dimensions of Table 5.4.

5.4.1.2 Radiation Patterns

The radiation patterns of the Fourtear antenna were measured with the near field scanner in the VTAG anechoic chamber. Patterns were measured at frequencies from 1.0 to 8.0 GHz. Some of the measured patterns are presented in Fig. 5.11 for several frequencies. The element height h above the ground plane, converted to the electrical height at the measurement frequency, is noted in parentheses. The radiation patterns change with frequency because the electrical height increases as frequency increases. Specifically, a dip occurs at 2.0 GHz in the bore-sight direction. And some lobes appear above 3.0 GHz. Generally, pattern degradation occurs when the electric height is more than $\lambda/4$ due to phase cancellation, as can be explained using image theory [5.3]. The effect is presented in [5.4] for an infinitesimal dipole antenna above a perfect ground plane. The patterns in Fig. 5.11, however, are quite different from the patterns of the infinitesimal dipole above a perfect ground plane because the Fourtear antenna has the parasitic element near the radiating element. Some lobes appear above 4.0 GHz where the electrical height is $\lambda/2$ and at 8.0 GHz the patterns become broken up. The radiation patterns were also measured at intermediate angle 45° and 135° and one of the patterns at 1.6 GHz are presented in Fig. 5.12. The co-pol patterns are consistent in all four plane cuts but the cross-pol levels are higher in the diagonal planes compared to the principal planes, especially near θ=45°. Note that the cross-pol at bore-sight is still very low, which is compatible with the cross-pol level of principal plane at bore-sight.

5.4.1.3 Summary

The Fourtear antenna with a-a' feed configuration has extremely wide impedance bandwidth, but the radiation patterns degrade as frequency increases. The radiation patterns are acceptable up to the 2:1 bandwidth. The patterns, however, can be improved using a ground plane modification. Investigation of the ground plane will be discussed in Chapter 7.

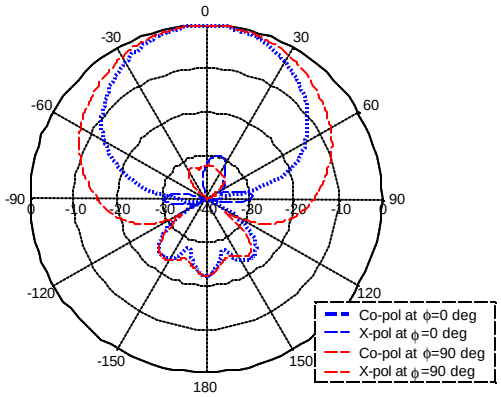

(a) 1.0 GHz (h = λ/8)

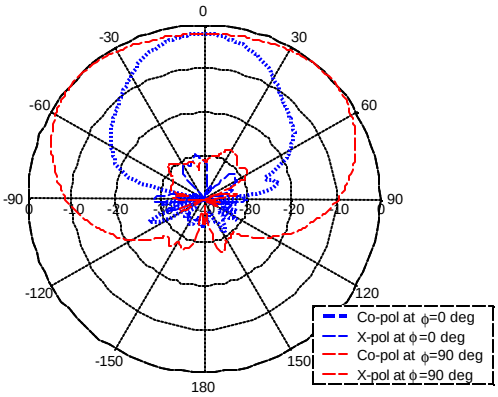

(b) 2.0 GHz (h = λ/4)

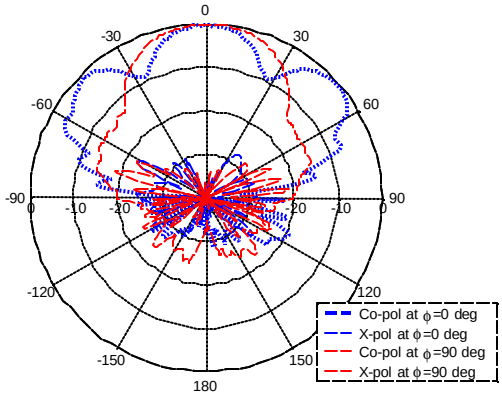

(c) 3.0 GHz (h = 3λ/8)

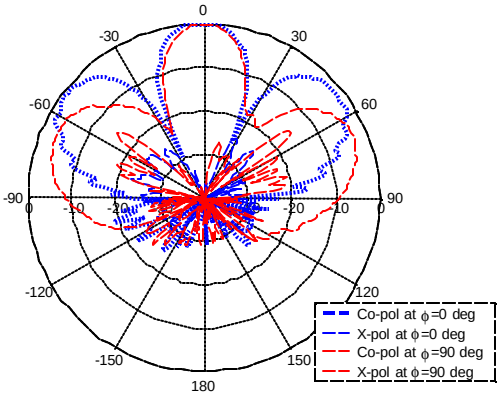

(d) 4.0 GHz (h = λ/2)

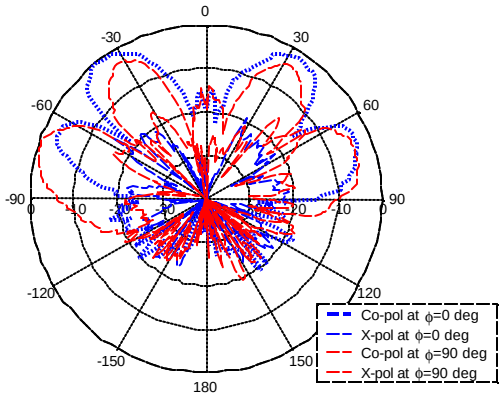

(e) 6.0 GHz (h = 3λ/4)

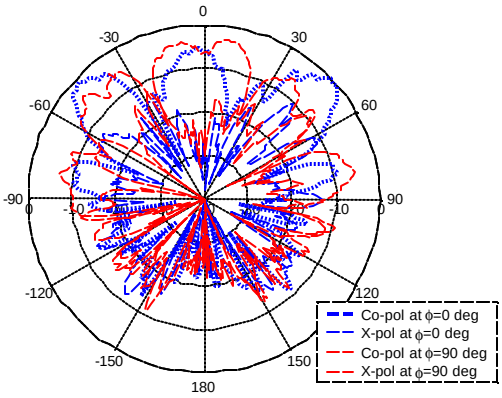

(f) 8.0 GHz (h = λ)

Figure 5.11 Measured radiation patterns of the Fourtear antenna in Fig. 5.9 with a-a' feed configuration with the dimensions of Table 5.4.

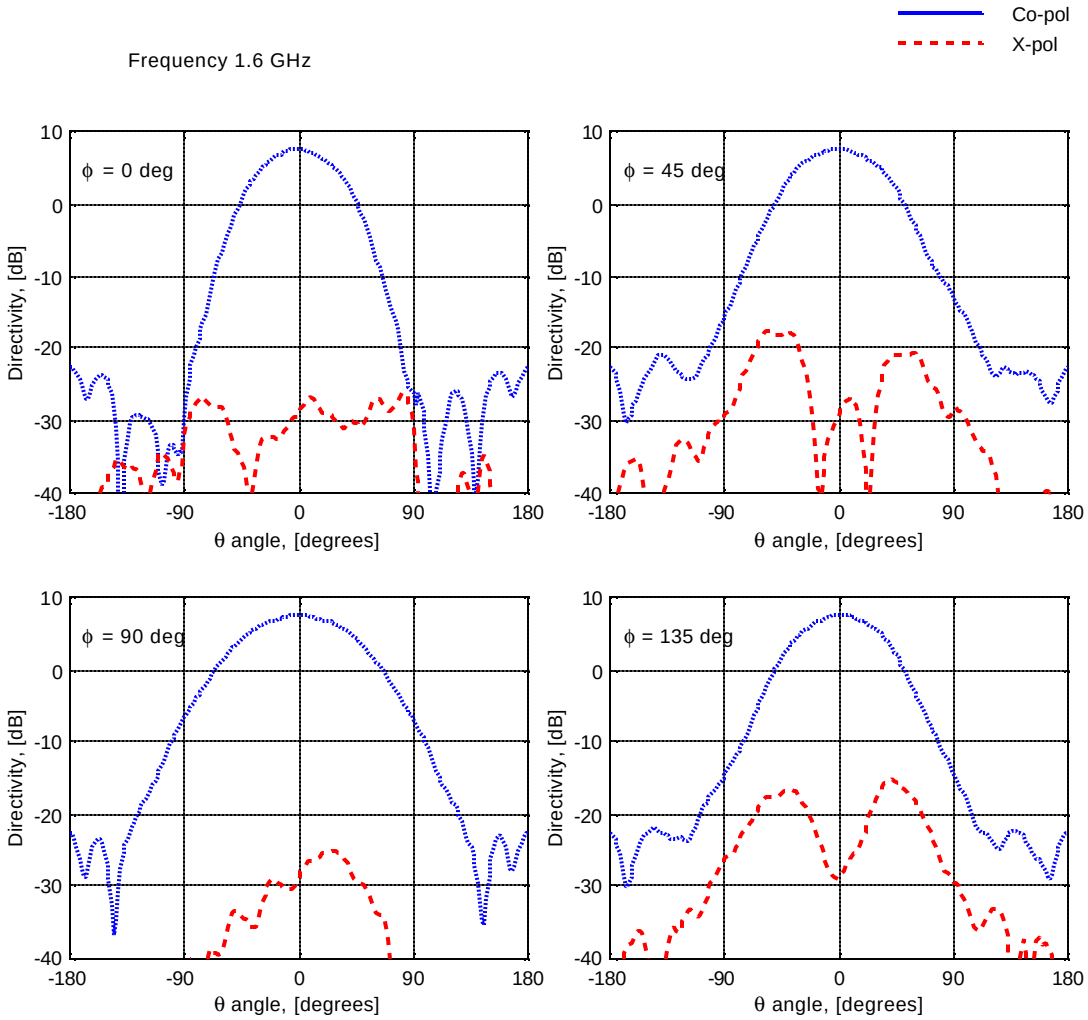

Figure 5.12 Measured radiation patterns of the Fourtear antenna in Figs. 5.8 and 5.9 with a-a' feed configuration with the dimensions of Table 5.4. The patterns are measured at four azimuth angles (ϕ = 0°, 45°, 90° and 135°) at a frequency of 1.6 GHz.

5.4.2 The Fourtear antenna with b-b' feed configuration

The Foursquare and Fourpoint antennas provide the same impedance characteristics when fed using either of their two feed configurations due to the symmetrical antenna geometry. However, the radiating element of Fourtear antenna in Fig. 5.8(a) is asymmetric, so the antenna characteristics are different for the two feed configurations.

5.4.2.1 Antenna Impedance and VSWR

Figure 5.13 shows the computed and measured impedance and VSWR referenced to 200-Ω for the Fourtear antenna fed using b-b' terminals. The resistance value for b-b' feed configuration is much higher (about double) that for the a-a' feed configuration in Fig.5.10 (a). And the reactance value of the b-b' feed configuration is also near the 0-Ω.

The overall level of the impedance for b-b' feed configuration remains constant over the band just as with the a-a' feed configuration, which is necessary for wideband operation. But the impedance level of the Fourtear antenna with the b-b' configuration is about double of the case of the a-a' feed configuration. The VSWRs in Fig. 5.13 (b) demonstrate that the Fourtear antenna with b-b' feed configuration also provide extremely wide impedance bandwidth more than 10:1 for VSWR < 2. At 2-3 GHz the VSWR, however, the slightly higher than VSWR=2.

The measured data demonstrate that the impedance of the Fourtear antenna has different impedance characteristics for two feed configurations. The Fourtear antenna with the a-a' feed configuration has half of the resistance level of the antenna with the b-b' feed configuration. Generally, in microstrip or stripline, the impedance is inversely proportional to the width of the microstrip or stripline [5.5]. Note that the width of the tip for a-a' feed configuration is much wider than the one for b-b' feed configuration, so the experimental results follow the transmission line trend.

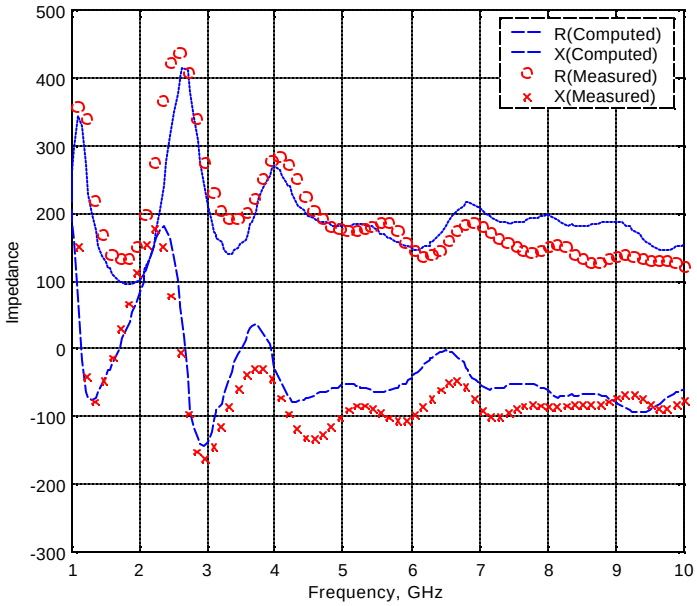

(a) Impedance curves of the Fourtear antenna with b-b' feed configuration.

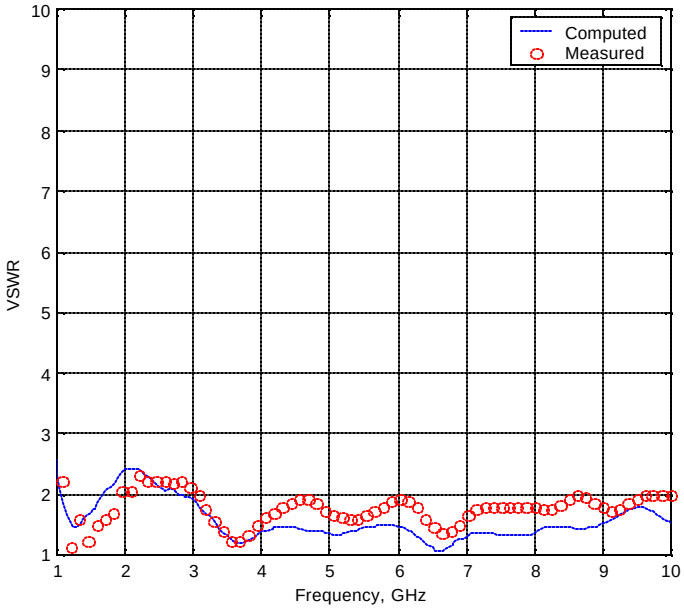

(b) VSWR curves referenced to 200-Ω for the Fourtear antenna with b-b' feed configuration.

Figure 5.13 Computed and measured antenna impedance and VSWR (referenced to 200-Ω) for the Fourtear antenna in Figs. 5.8 and 5.9 with b-b' feed configuration with the dimensions of Table 5.4.

5.4.2.2 Radiation Patterns

The radiation patterns of the Fourtear antenna were also measured for the case of b-b' feed configuration. The antenna elements shown in Fig. 5.8(a) were rotated 90° for the measurement so that the E-plane pattern is obtained at xz-plane (ϕ=0°) with b-b' feed configuration. The measured data are presented in Fig. 5.14 at several frequencies. Similar patterns are obtained like the case of the a-a' feed configuration. The patterns of the b-b' feed configuration, however, have a little better pattern shape than the ones of a-a' feed configuration. For b-b' feed configuration, the dip is not presented in the pattern at 2.0 GHz, unlike the patterns for a-a' feed configuration. In order to check at what frequency the dip begins to appear, the patterns are measured in Fig. 5.15 from 2.2 to 2.8 GHz. A very small dip appears at a frequency of 2.4 GHz. A noticeable dip is shown at a frequency of 2.6 GHz and additional lobes are also observed.

The measured radiation patterns in the diagonal planes (ϕ = 45° and 135°) are also presented in Fig. 5.16 for a frequency of 1.6 GHz. The diagonal plane patterns are consistent with the principal plane patterns, as it was observed for the a-a' feed configuration. The cross-pol level in the diagonal plane is a little higher than the cross-pol level in the principal planes, which was also observed for the case of the a-a' feed configuration.

5.4.2.3 Summary

The measured impedance and radiation patterns differ for two different feed configurations. This is due to the fact that they have different current distributions. Based on the investigation, the b-b' feed configuration has better performance than that for the a-a' feed configuration. The Fourtear antenna cannot be used for dual-linear polarization or circular polarization applications due to the different antenna characteristics for each feed. The Fourtear antenna, however, provides single linear polarization with wide bandwidth in a low-profile geometry.

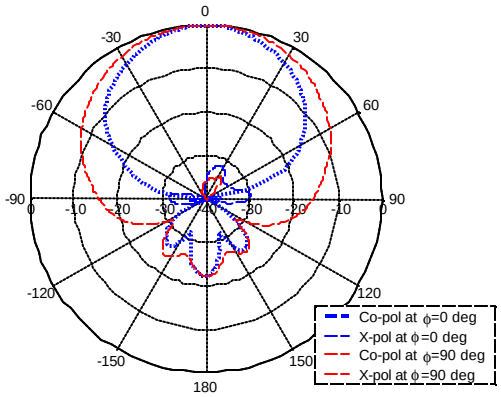

(a) 1.0 GHz (h = λ/8)

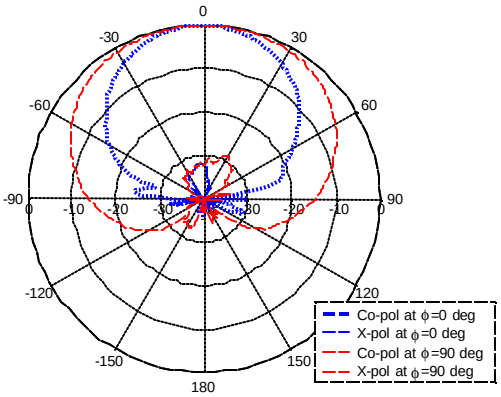

(b) 2.0 GHz (h = λ/4)

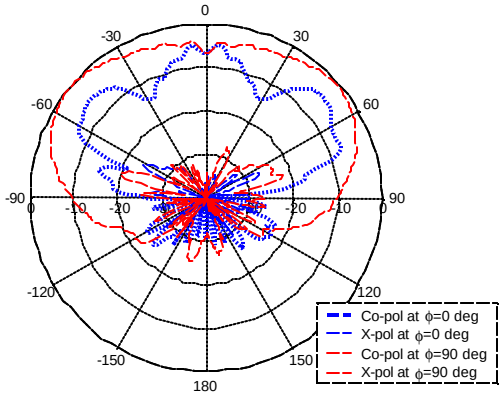

(c) 3.0 GHz (h = 3λ/8)

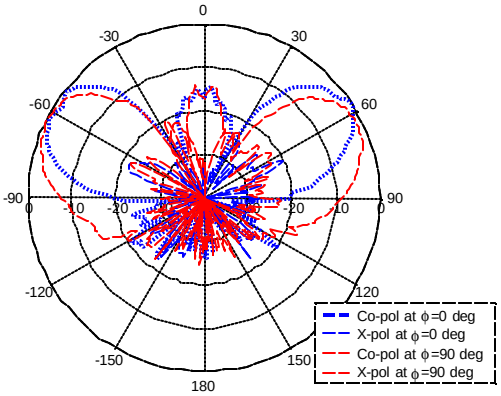

(d) 4.0 GHz (h = λ/2)

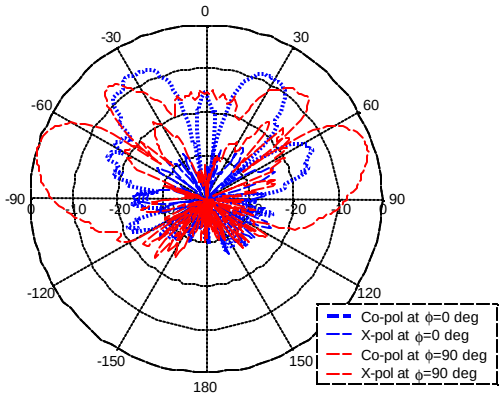

(e) 6.0 GHz (h = 3λ/4)

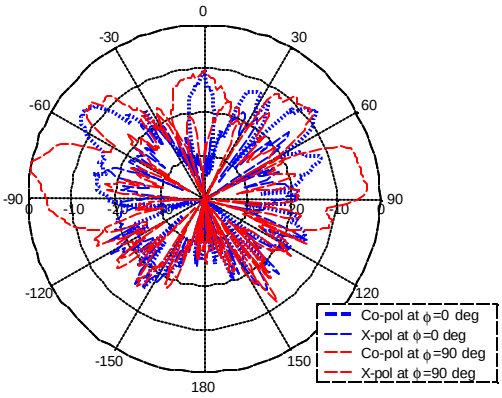

(f) 8.0 GHz (h = λ)

Figure 5.14 Measured radiation patterns of the Fourtear antenna in Fig. 5.9 with b-b' feed configuration with the dimensions of Table 5.4.

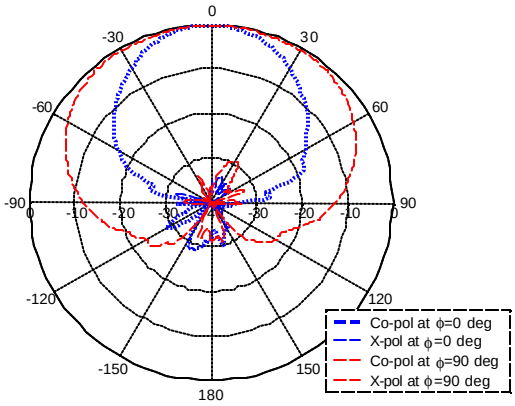

(a) 2.2 GHz

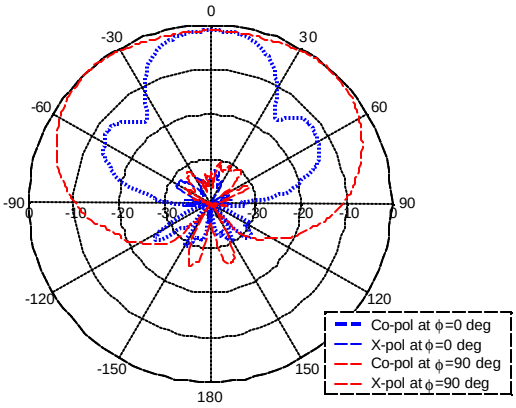

(b) 2.4 GHz

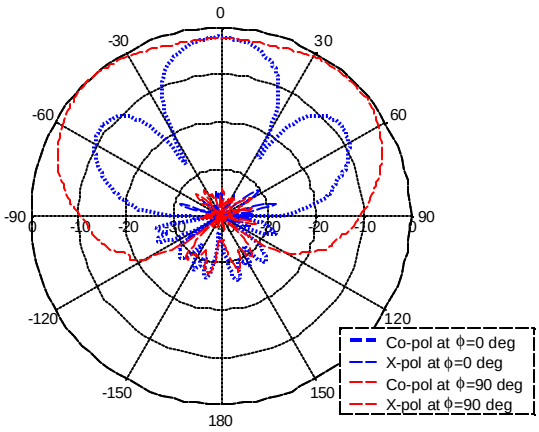

(c) 2.6 GHz

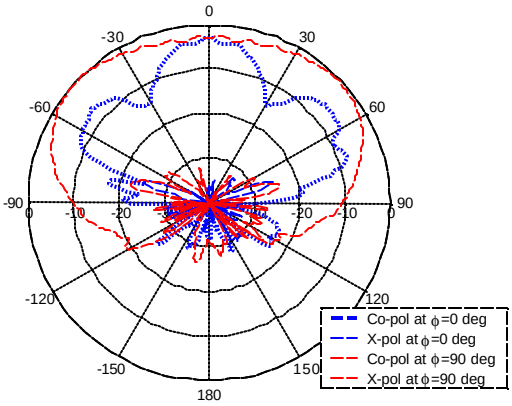

(d) 2.8 GHz

Figure 5.15 Measured radiation patterns of the Fourtear antenna in Fig. 5.8 from 2.2 to 2.8 GHz with b-b' feed configuration with the dimensions of Table 5.4. The radiating elements are rotated 90° from the Fig. 5.8 (a) to obtain the E-plane pattern in the direction of the feed direction.

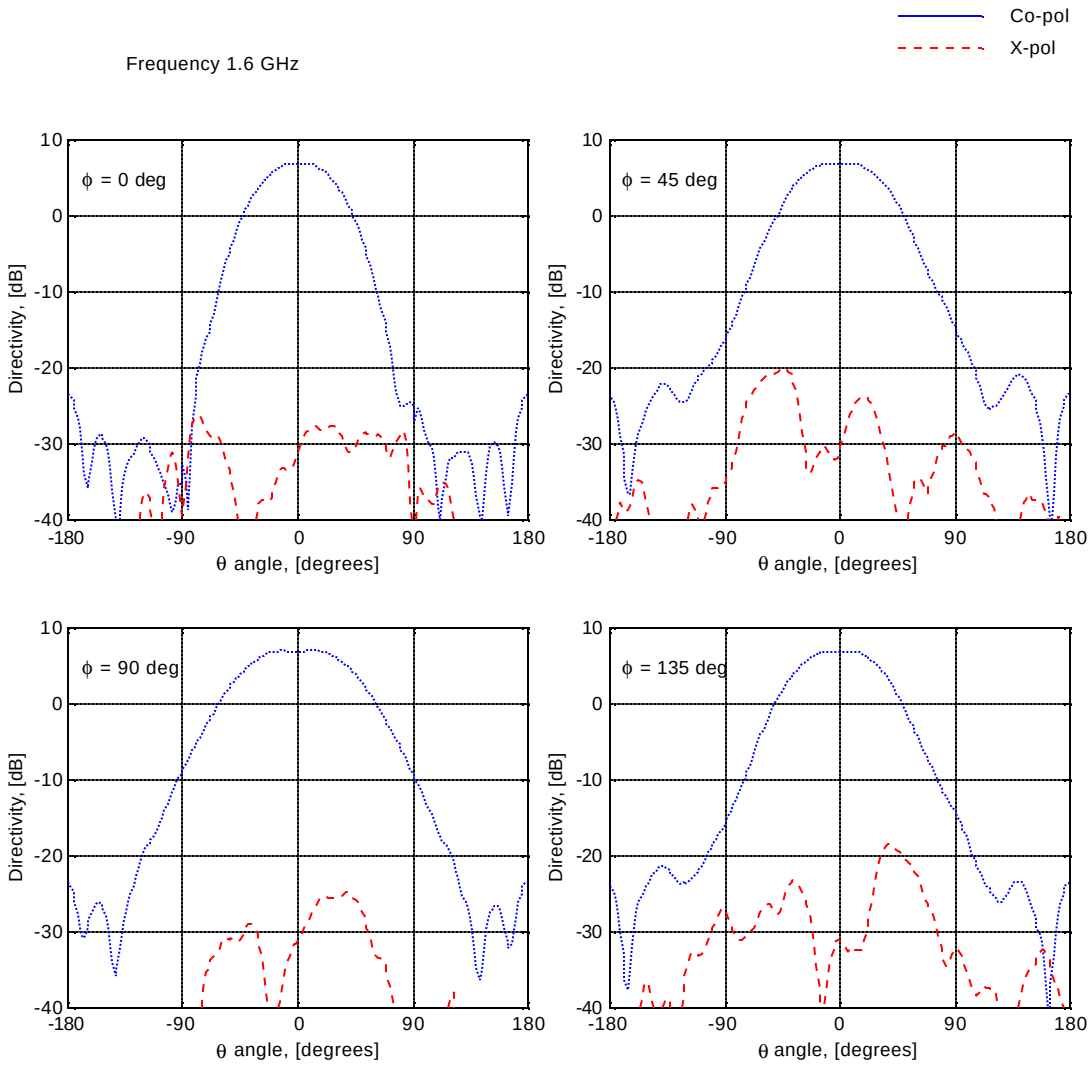

Figure 5.16 Measured radiation patterns of the Fourtear antenna in Figs. 5.8 and 5.9 with b-b' feed configuration with the dimensions of Table 5.4. The patterns are measured at four azimuth angles (ϕ = 0°, 45°, 90° and 135°) at a frequency of 1.6 GHz.

5.5 A Hardware Test Model of a Modified Fourtear Antenna

Even though the Fourtear antenna provides extremely wide impedance bandwidth, the asymmetric geometry of the Fourtear antenna causes different antenna characteristics for each feed configuration. With the goal of finding symmetric performance for the two feed cases, a modified Fourtear antenna was designed and constructed at VTAG as shown in Fig. 5.17. The geometry details of the modified Fourtear antenna are shown in Fig. 5.18 (a), which has a hexagonal shape that approximately a teardrop. The hexagonal radiating elements are not exactly identical in shape, but opposing pairs are identical mirror images. The hexagon helps to minimize the asymmetrical shape of teardrop by gradually changing the curve of teardrop into a straight line. The modified Fourtear antenna with the dimensions listed in Table 5.5 was simulated and measured. Same measurement techniques and set-up were employed as the Fourtear antenna was measured.

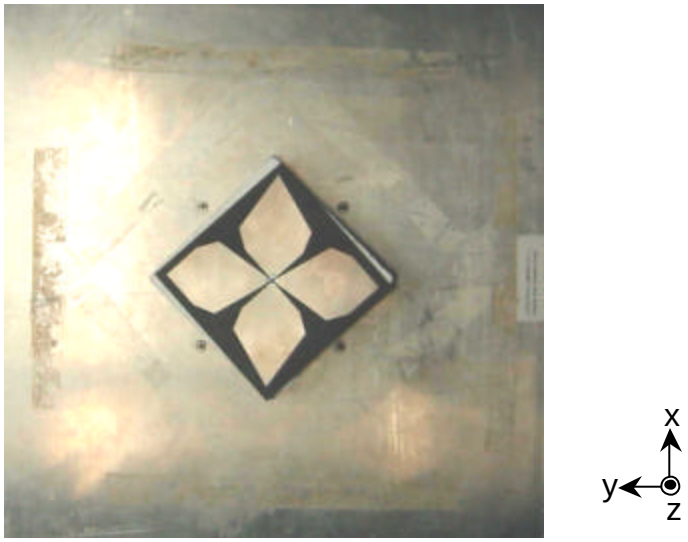

Figure 5.17 The hardware test model of the modified Fourtear antenna.

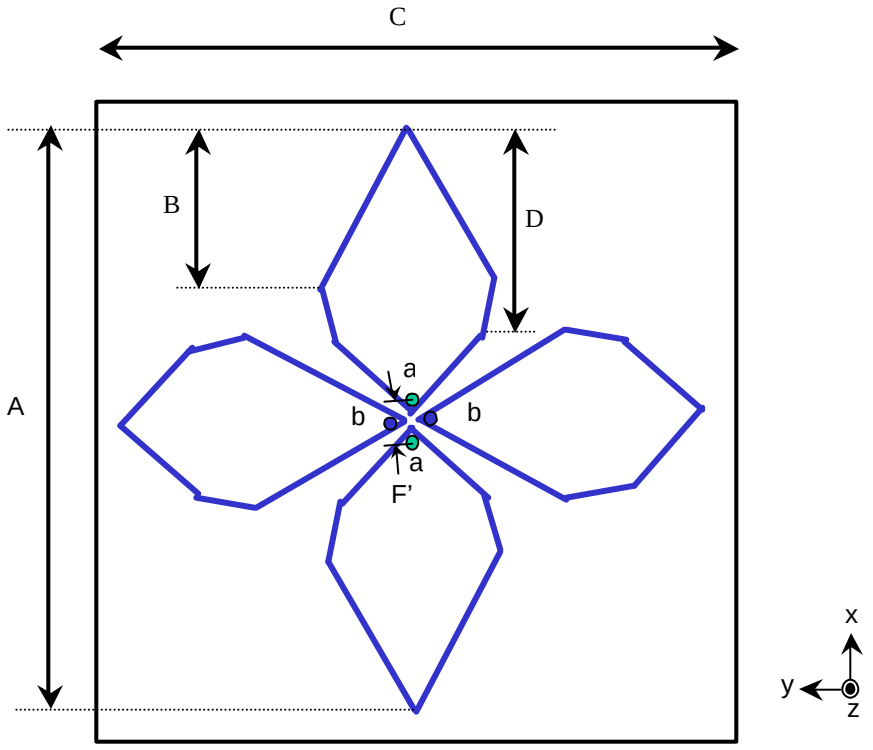

(a) Radiating element of the modified Fourtear antenna.

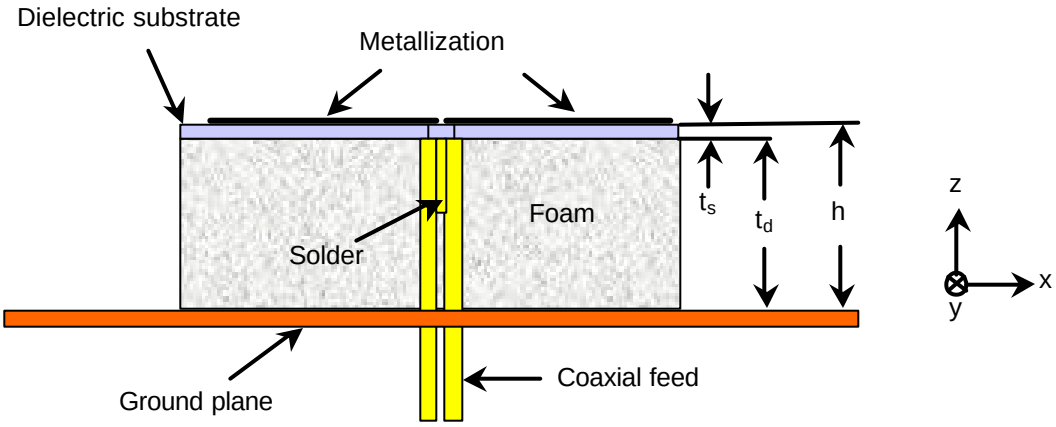

(b) Side view of the modified Fourtear antenna.

Figure 5.18 Geometry of the modified Fourtear antenna.

Table 5.5

Geometry of the modified Fourtear Antenna of Fig. 5.18.

Description	Symbol	Size
Element side length	A	157.5 mm (6.2”)
Length B	B	41.3 mm (1.63”)
Substrate side length	C	165.1 mm (6.5”)
Length D	D	57.15 mm (2.25”)
Substrate thickness	t_s	0.76 mm (30 mils)
Foam thickness	t_d	37.34 mm (1.47”)
Element height above ground plane	h	38.1 mm (1.5”)
Feed positions distance	F’	3.56 mm (0.14”)

5.5.1 Antenna Impedance and VSWR

The measured antenna impedance and VSWR (referenced to 150-Ω) of the test model were compared for each feed configuration as shown in Fig. 5.19. Due to the very similar shape of the radiating elements, the impedance characteristics of the two feed configurations are also nearly identical. The VSWR of the modified Fourtear antenna is not as good as the Fourtear antenna discussed in Section 5.4, but it is acceptable. The antenna impedances, however, are very similar for each feed configuration over the whole band, which is necessary for employing polarization diversity. The modified Fourtear antenna has a resistance level of about 150-Ω for both feed configuration. And the reactance is varying near the 0-Ω, which is very ideal for wideband antenna. Note that the value, 150-Ω is the average value of the resistance levels measured in the Fourtear antenna for each feed configurations discussed in Section 5.4; that is 100-Ω for a-a’ feed configuration and 200-Ω for b-b’ feed configuration. Note that the width of feeding tip in the radiating element of the modified Fourtear antenna is also between the widths of the tips for a-a’ feed configuration and b-b’ feed configuration in the Fourtear antenna discussed in Section 5.4. The experimental results are very correlated with the

phenomenon observed in the microstrip, stripline or transmission line [5.5]. The investigation results demonstrate that the overall level of the antenna impedance is determined by the width of the tip for feed the antenna. The resistance level is inversely proportional to the width of the tip for antenna feed; that is, a wide tip provides lower resistance than the narrow tip.

The impedance bandwidth of the modified Fourtear antenna is compatible with the self-complementary antenna in [5.6] [5.7]. In theory, the self-complementary antenna operating in free space (i.e. no ground plane present) has input impedance of 188.5 + $j0$ Ω. In practice, the measured impedance is lower (between 100-Ω and 188.5-Ω) than the value in theory, due to the finite thickness of metallization and the presence of the coaxial feed line [5.6]. The impedance characteristics (close to 150-Ω) of the modified Fourtear antenna are analogous to the practically measured self-complementary antenna. More investigation is required to find the relationship to the self-complementary antenna.

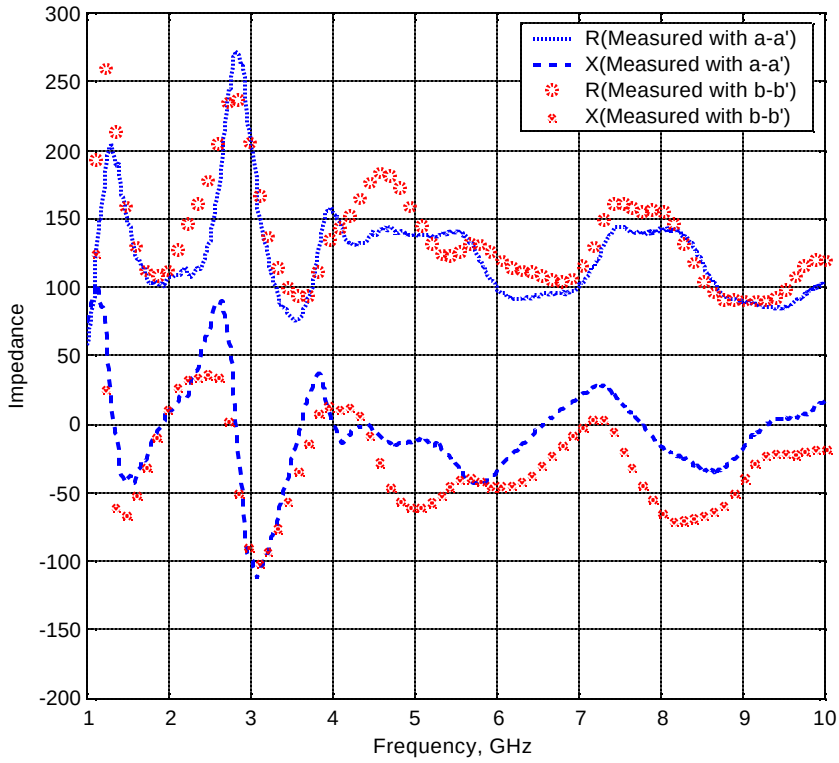

(a) Impedance curves of modified Fourtear antenna with a-a' (solid and dash) and b-b' (circle and cross) feed configurations.

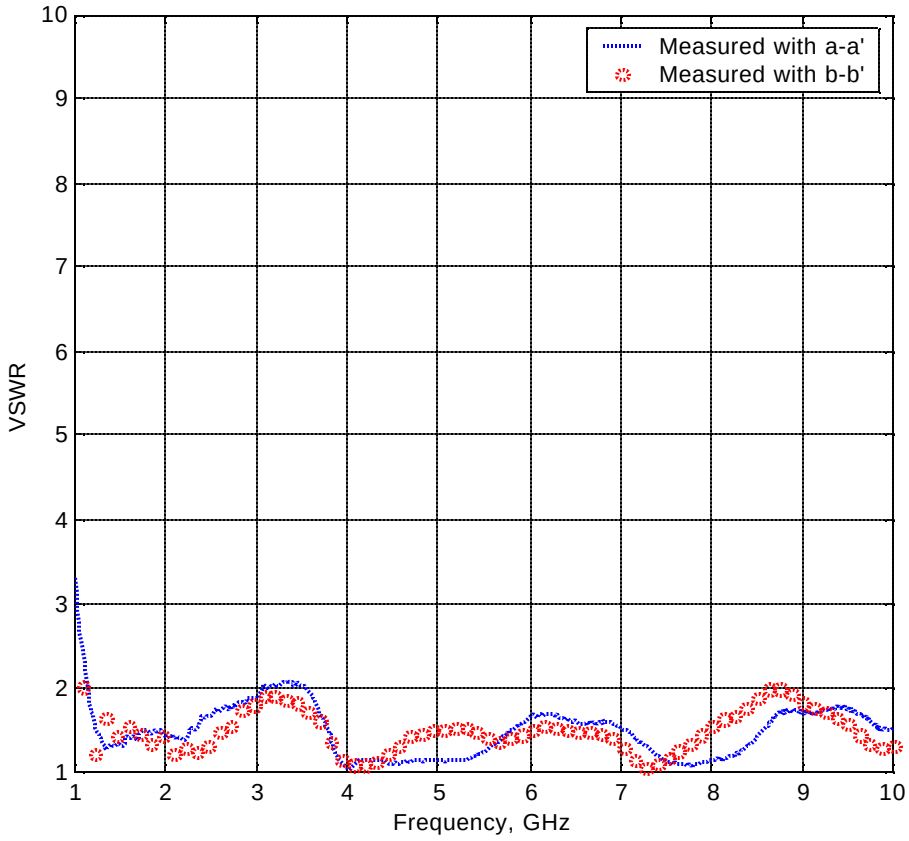

(b) VSWR referenced to 150-Ω of modified Fourtear antenna with a-a' (solid) and b-b' (circle) feed configurations.

Figure 5.19 Comparison of the measured modified Fourtear antenna performance (with ground plane) of a-a' and b-b' feed configuration with the dimensions of Table 5.5.

5.5.2 Radiation Patterns

The radiation patterns of the modified Fourtear antenna were also measured for both feed configurations. They have almost identical radiation patterns over the whole band. Therefore, only measured patterns for b-b' feed configuration are presented in Fig. 5.20 at selected frequencies from 1.0 to 8.0 GHz. And additional patterns from 2.2 – 2.8 GHz are presented in Fig. 5.21 to check at what frequency the dip is appeared. The dip begins to appear at a frequency of 2.4 GHz but the patterns are acceptable up to 2.6 GHz.

Computed maximum gain vs. frequency plot is presented in Fig. B2 in Appendix B. Gain patterns can be directly obtained by adding the maximum gain number to the normalized radiation patterns.

5.5.3 Summary

A modified Fourtear antenna was investigated on behalf of improving the performance of the Fourtear antenna. The measured impedance and radiation patterns demonstrate that the modified Fourtear antenna has almost identical antenna characteristics for both feed configurations with wide bandwidth. The modified Fourtear antenna described in this section has a hexagon shape as an example model, but other shapes such as octagon, pentagon, etc are possible to achieve the identical antenna performance for both feed configurations.

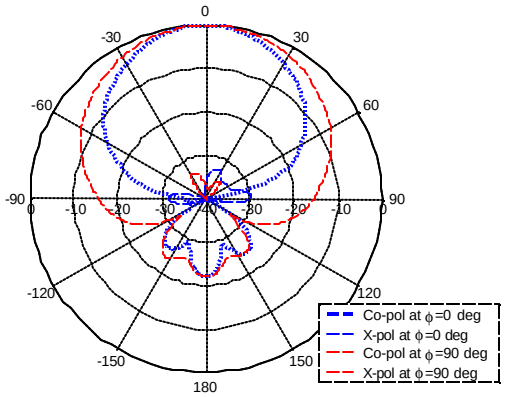

(a) 1.0 GHz (h = λ/8)

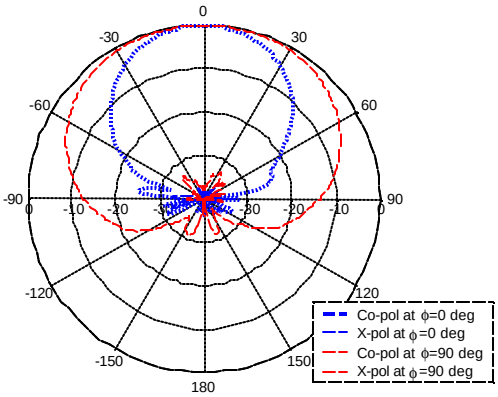

(b) 2.0 GHz (h = λ/4)

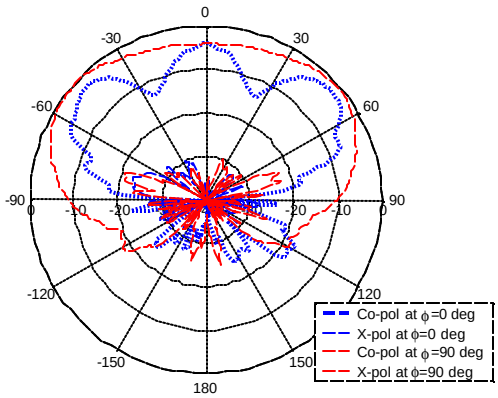

(c) 3.0 GHz (h = 3λ/8)

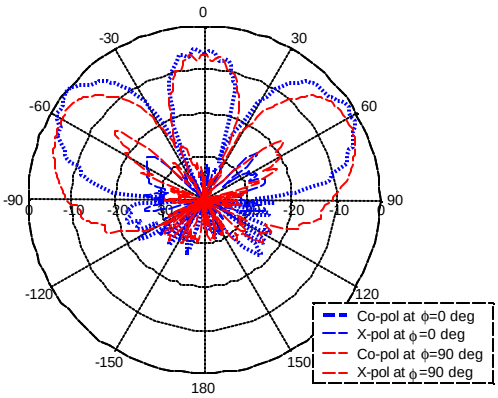

(d) 4.0 GHz (h = λ/2)

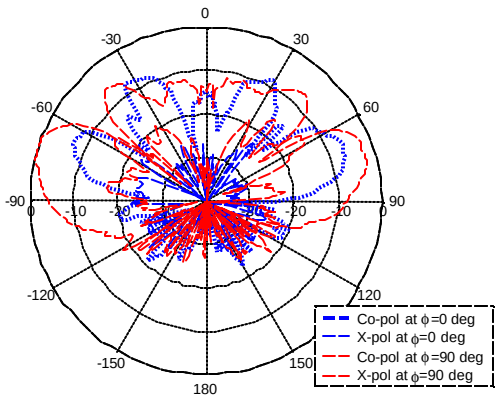

(e) 6.0 GHz (h = 3λ/4)

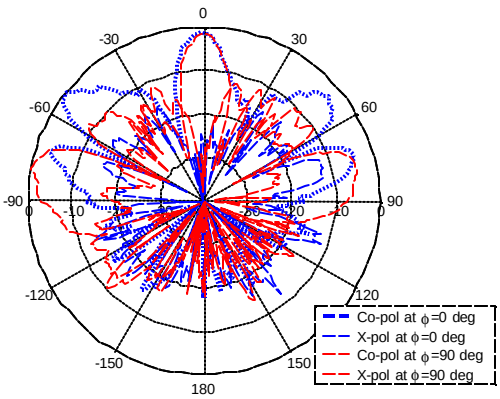

(f) 8.0 GHz (h = λ)

Figure 5.20 Measured radiation patterns of the modified Fourtear antenna in Figs. 5.17 and 5.18 with b-b' feed configuration with the dimensions of Table 5.5.

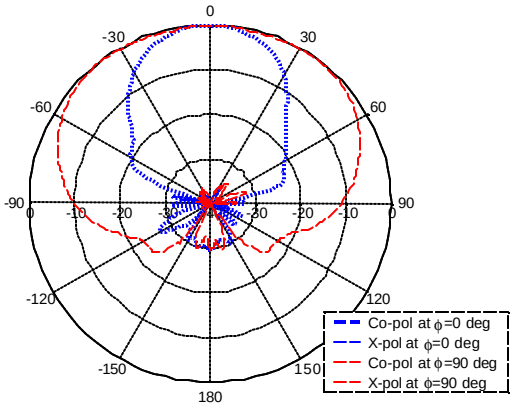

(a) 2.2 GHz

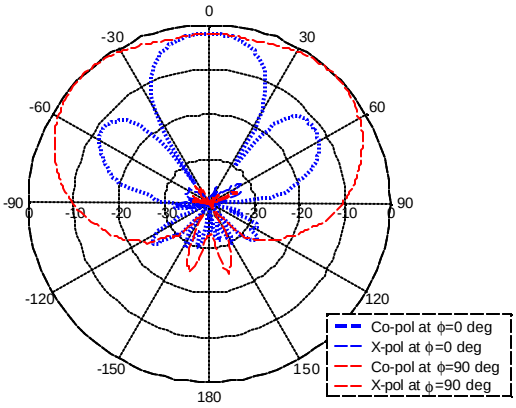

(b) 2.4 GHz

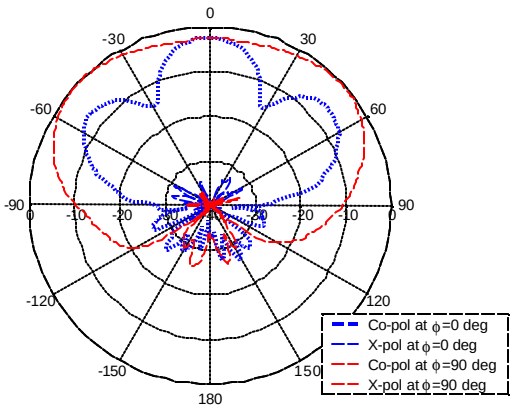

(c) 2.6 GHz

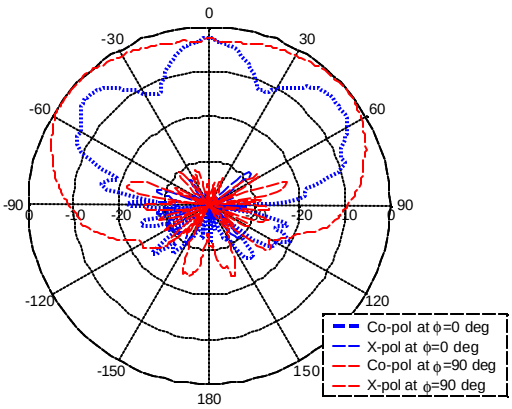

(d) 2.8 GHz

Figure 5.21 Measured radiation patterns of the Fourtear antenna in Figs. 5.17 and 5.18 from 2.2 to 2.8 GHz with b-b' feed configuration with the dimensions of Table 5.5. The radiating elements are rotated 90° from the Fig. 5.18 (a) to obtain the E-plane pattern in the direction of the feed direction.

5.6 Summary

In this chapter a new antenna, the Fourtear antenna, was introduced. The Fourtear antenna is a generalized version of the Foursquare and Fourpoint antennas. It has very wide impedance bandwidth, providing dual-linear polarization in a low-profile geometry. Its impedance bandwidth is similar to that of a frequency independent antenna. However, the drawback of the Fourtear antenna is that it has different antenna impedances for the different feed configurations due to the asymmetrical shape of the radiating element. This problem was resolved using the modified Fourtear antenna discussed in Section 5.5. The modified Fourtear antenna provides more than 10:1 impedance bandwidth and about 2.6:1 pattern bandwidth. The radiation pattern can be improved by modifying the geometry of the ground plane to achieve constant electrical height over wide impedance bandwidth. Note that the Fourtear and the modified Fourtear antenna do not use a tuning plate as was used in Fourpoint antenna. Therefore, it is easy to construct the Fourtear antenna.

References

[5.1] J. D. Kraus, *Antennas*, McGraw Hill, New York, 1950, pp. 9, Chap 1.

[5.2] N. E. Lindenblad, "Antennas and Transmission Lines at the Empire State Television Station," *Communications*, pp.10-26, April, 1941.

[5.3] W. L. Stutzman and G.A. Thiele, *Antenna Theory and Design 2nd edition*, John Wiley & Sons, New York, 1998.

[5.4] Balanis, *Antenna Theory: Analysis and Design 2nd edition*, pp. 175-181, John Wiley &Sons, New York, 1997.

[5.5] Pozar, *Microwave Engineering 2nd edition*, pp. 470-471, John Wiley &Sons, New York, 1998.

[5.6] G. A. Deschamps, "Impedance Properties of Complementary Multiterminal Planar Structures," *IRE Trans. on Antennas and Propagation*, pp. 371-378, Dec. 1959.

[5.7] Y. Mushiake, *Self-complementary Antennas*, Springer-Verlag, Berlin, 1996.

Chapter 6

Planar Inverted Cone Antenna (PICA)

6.1 Introduction

The need for wideband antennas with omni-directional coverage is increasing in both military and commercial applications. Thin antennas are preferred in most situations. The classic solution is to obtain an omni-directional pattern using a thin wire dipole or its counterpart monopole version with a ground plane (if a half-space is to be illuminated). However, the wire dipole and monopole suffer from narrow impedance bandwidth. The bandwidth can be widened using flat metal rather than a thin wire structure [6.1]. Many flat radiator geometries have been explored over several decades, as discussed in the Section 2.7. However, these antennas suffer from pattern degradation at the high end of their impedance bandwidth [6.2].

Crossed half circle flat radiators as discussed in the Section 2.7.4 appear to provide better pattern bandwidth within their impedance bandwidth [6.3], but a simulation result at VTAG revealed that they have high cross polarization over the entire band due to the interaction between flat elements.

This chapter presents a new wideband, omni-directional, flat antenna called a Planar Inverted Cone Antenna (PICA). The PICA antenna is evolved from the teardrop antenna and monopole disc antenna discussed in Sections 2.4 and 2.7. The PICA is composed of single flat element vertically mounted above a ground plane. The antenna geometry is very simple yet provides outstanding impedance and radiation pattern performance. The impedance bandwidth of more than 20:1 has been confirmed through extensive simulations and experiments. Radiation pattern improvement achieved by adding two circular holes inside of the element. The radiation pattern of the PICA is acceptable over a bandwidth up to 6:1 and has very low cross polarization of 20 dB or less [6.4]. The simulation and experiment results of the PICA antenna are presented in terms of VSWR plots and radiation patterns.

6.2 The Antenna Structure

The basic geometry of the PICA antenna is shown in Fig. 6.1. It is based on the conventional circular disc antenna of Fig. 2.12 in the Section 2.7.1 [6.5]. The top part of the circular disc was trimmed to the shape of a planar inverted cone. The PICA (Planar Inverted Cone Antenna) name is based on the shape of the element. The PICA antenna provides wider radiation pattern bandwidth than the circular disc antenna with similar impedance bandwidth in a smaller antenna: see Section 6.3.

Figure 6.1 (a) is the general geometry of the PICA antenna. Dimension P1 could have an arbitrary shape and size to customize performance to the specific application. However, edge P2 should be tapered to circular, elliptical or exponential shapes to obtain broad impedance bandwidth and an omni-directional antenna pattern. The height of the PICA antenna is about quarter wavelength of the low-end operating frequency. The cone angle α and dimensions L1, L2 and L3 in Fig. 6.1 (b) can be varied to obtain optimum performance. The basic geometry was modified to teardrop shape by tapering the straight line between vertex and curve as shown in Fig. 6.1 (c). Note that the teardrop PICA antenna in Fig. 6.1 (c) is an inverted version of the teardrop antenna shown in Fig. 5.7 (a). In Figure 5.7 (a), the ground plane of the teardrop antenna is gradually tapered to obtain wide impedance bandwidth, but in the PICA of Fig. 6.1 (c) the radiating element has a round shape at the bottom of the element to compromise the gradually tapered ground plane. The antenna geometry of Fig. 6.1 (d) with two circular holes was developed as a result of extensive investigation of the PICA antenna to find geometries improved with radiation patterns. Even though the circular holes are tried only, another shape may be used for any specific application.

Hardware test models with the Figs. 6.5 and 6.10 were constructed and measured. The results revealed that they have an extremely wide impedance bandwidth of more than 10:1 and wide radiation pattern bandwidth of about 6:1. The difference between the PICA element and the other disc elements discussed in Section 2.7 is that the geometry of the PICA antenna leads to an improved radiation pattern, while maintaining similar impedance characteristics with smaller antenna size. The next section describes the investigation results of the PICA antenna with several hardware test models.

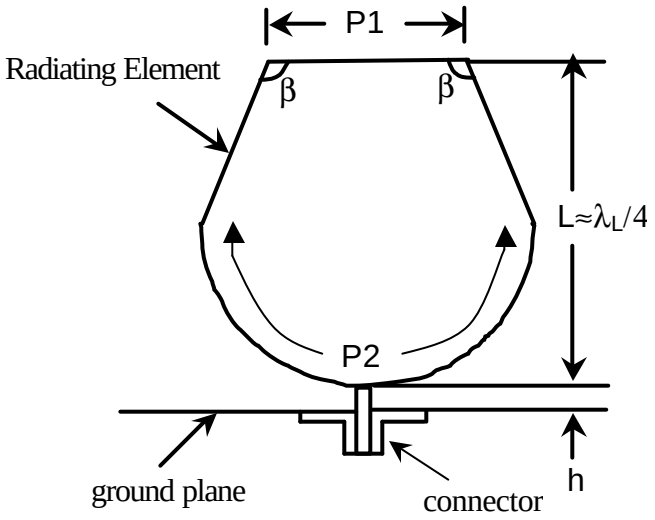

(a) Geometry of general shape of PICA antenna.

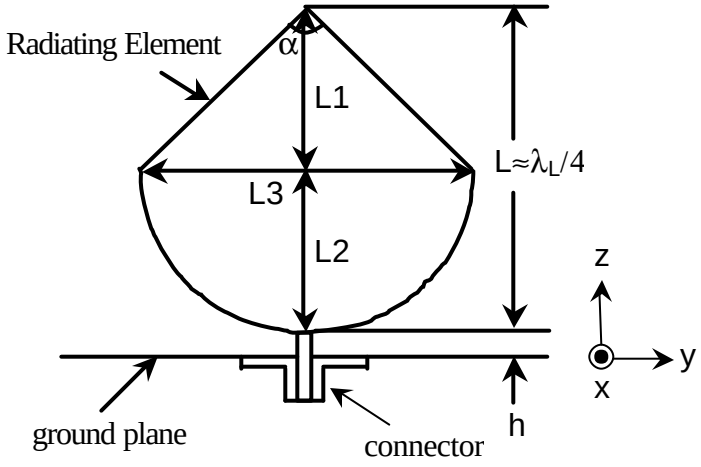

(b) Geometry of a shape of PICA antenna.

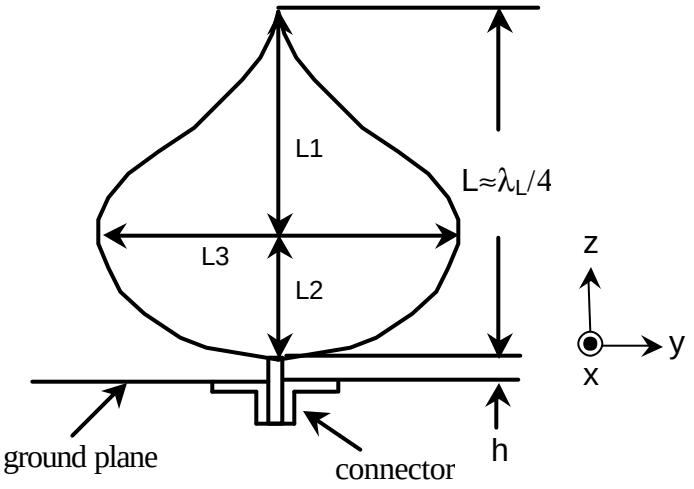

(c) Geometry of a PICA antenna having a shape of teardrop.

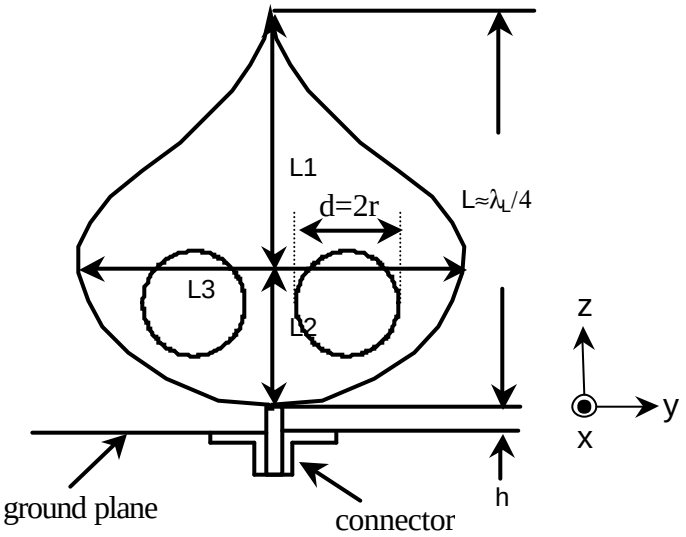

(d) Geometry of a PICA antenna having a shape of teardrop with two circular holes.

Figure 6.1 Geometries of the Planar Inverted Cone Antenna (PICA).
(λ_L is wavelength at the lowest operating frequency.)

6.3 A PICA Hardware Test Model I of Figure 6.1 (b)

A test model of the PICA antenna in Figure 6.1 (b) was investigated using both simulations and measurements. The PICA antenna described in this section is the first prototype of the PICA antenna. A PICA antenna that is 50.8 mm (2.0") high is simulated for operating at a low-end frequency of 1.50 GHz. The dimensions for this antenna are listed in Table 6.1. A circular ground plane having a diameter of 406.4 mm (16.0") was used in measurement of VSWR and an infinite ground plane was employed in the simulation for computational simplicity. Radiation patterns were not measured for the PICA hardware model described in this section, but extensive pattern measurements were performed and presented using the other PICA hardware models in Sections 6.4 and 6.5. The computed radiation patterns, however, are compared in Section 6.3.2 with the patterns of circular and half disc antenna discussed in Section 2.7.

Table 6.1

Dimensions of a PICA Hardware Test Model I of Figure 6.1 (b).

Description	Symbol	Size
Length L1	L1	25.4 mm (1.0")
Length L2	L2	25.4 mm (1.0")
Height of the element	L	50.8 mm (2.0")
Width of the element	L3	50.8 mm (2.0")
Cone angle	α	90°
Feed length	h	0.64 mm (0.025")

6.3.1 VSWR Computations and Measurements

The VSWR of the PICA antenna was computed and measured using Fidelity and HP 8720C network analyzer, respectively, and are compared in Fig. 6.2. Simulations and measurements agree. The agreement between measured and calculated results indicates that accurate design studies can be performed by simulation. The VSWR curves are referenced to a 50-Ω input impedance in both simulation and measurement. In addition, the VSWRs are well below 2:1 from 1.5 to 20 GHz for an impedance bandwidth of 13:1 (f_U/f_L). The wide impedance bandwidth was achieved by tapering the bottom of the element in a circular fashion [6.5]. The electrical size of the PICA antenna at 1.5 GHz is about $\lambda/4$, i.e. $L=\lambda_L/4$..

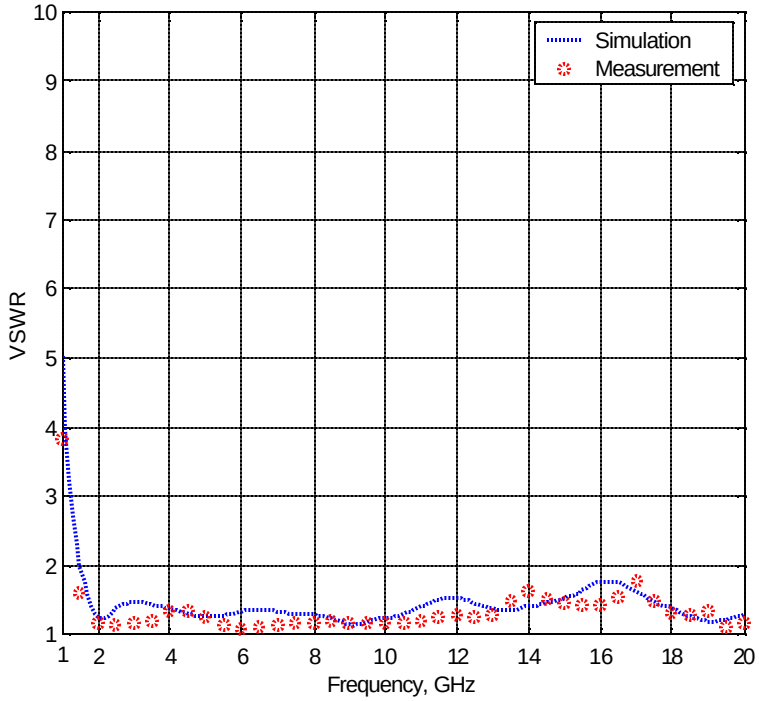

Figure 6.2 Computed (solid curve) and measured (dot curve) VSWR (referenced to 50-Ω) for the PICA antenna of Fig. 6.1 (b) with the dimensions listed in Table 6.1.

6.3.2 Radiation Patterns

Far field radiation patterns were computed for the PICA antenna in Fig. 6.1 (b), as well as the circular disc and half disc antennas. The geometry of each antenna element is presented in Fig. 6.3. The antenna size, L, and feed height, h, above the ground plane are set to 50.8 mm (2.0") and 0.64 mm (0.025"), respectively, for all cases. Therefore, the circular disc has a radius of L3 = 25.4 mm (1.0") and the half disc has a radius of L3 = 50.8 mm (2.0") without top of circular disc. The PICA antenna has the dimensions listed in Table 6.1. Very thin metal plate was employed in simulation. The radiation patterns of the three antennas are compared in Fig. 6.4 at selected frequencies.

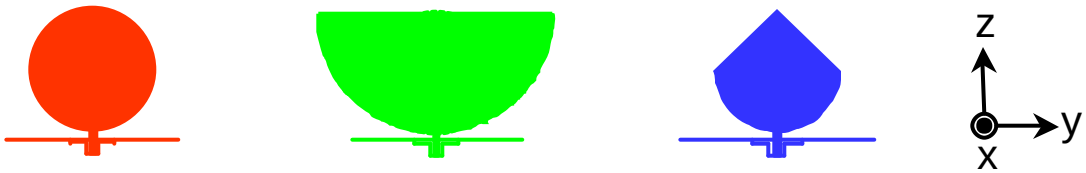

(a) Circular-disc antenna (b) Half-disc antenna (c) PICA antenna

Figure 6.3 Antenna geometries used in simulation.

The computed radiation patterns are compared in Fig. 6.4 for several frequencies. The elevation patterns for the antennas were computed in the xz-plane (ϕ = 0°). Cross-polarized patterns of the antennas are also displayed. The level of the cross-polarization is about 20 dB below the co-polarized pattern. Azimuth patterns at θ=60° were also presented for the three antennas (circular-disc, half-disc, and PICA antenna).

These patterns show that the half disc antenna suffers from pattern degradation as frequency increases beyond 3:1 impedance bandwidth, while there is no significant pattern variation with the circular-disc antenna and PICA up to a 6:1 bandwidth. In addition, the PICA antenna, provides better radiation pattern shape than the circular-disc antenna in a smaller dimension [6.4].

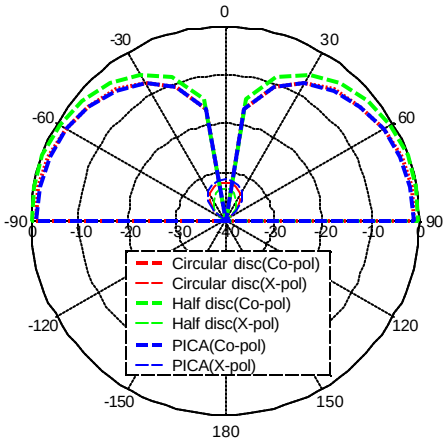

(a) Elevation pattern at 2.0 GHz

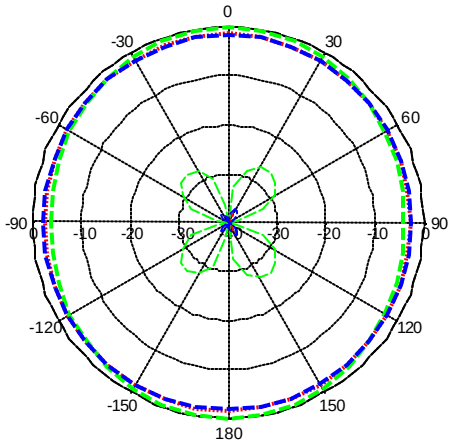

(b) Azimuth pattern at θ = 60° at 2.0 GHz

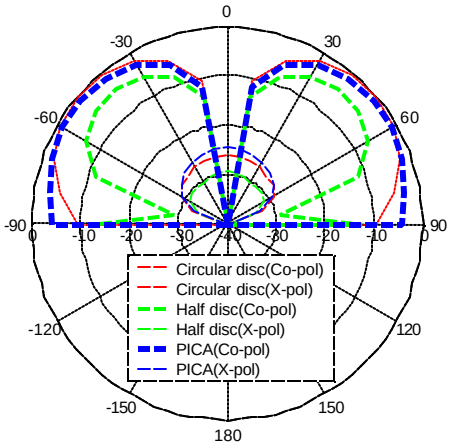

(c) Elevation pattern at 5.0 GHz

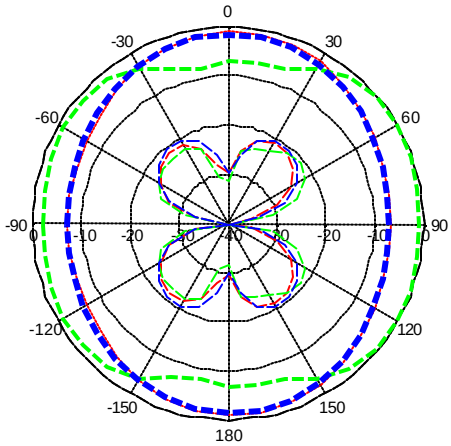

(d) Azimuth pattern at θ = 60° at 5.0 GHz

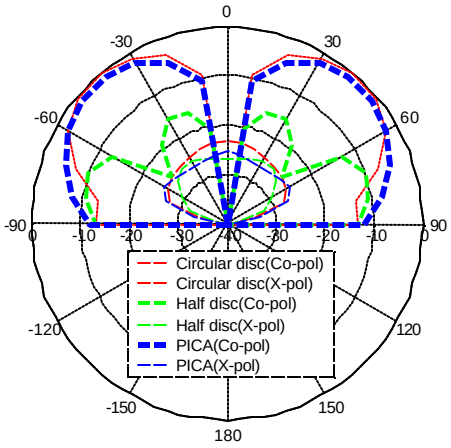

(e) Elevation pattern at 7.0 GHz

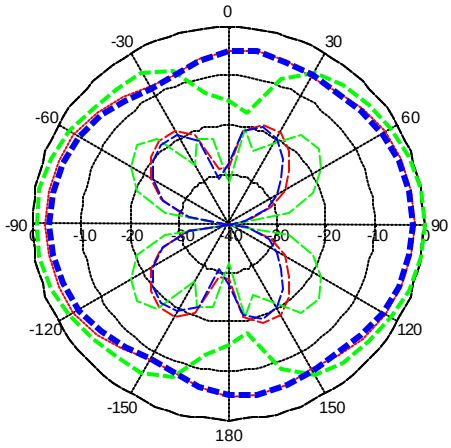

(f) Azimuth pattern at θ = 60° at 7.0 GHz

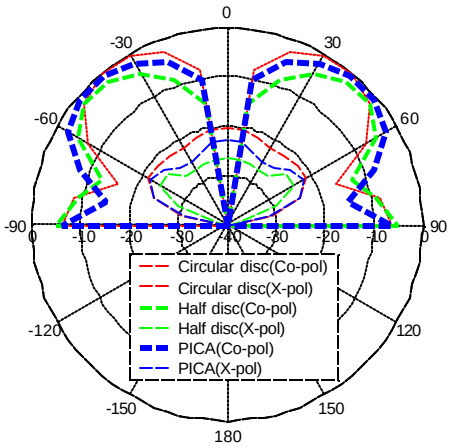

(g) Elevation pattern at 9.0 GHz

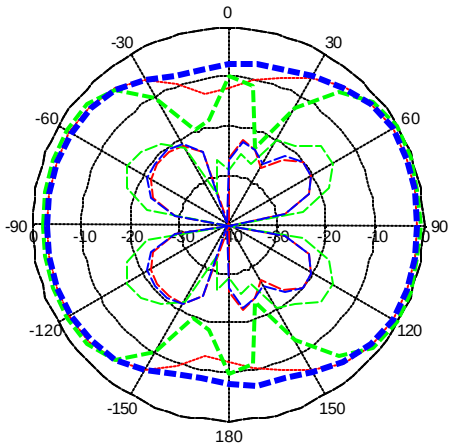

(h) Azimuth pattern at θ = 60° at 9.0 GHz

Figure 6.4 Computed radiation patterns of disc antennas such as the circular disc, half disc, and PICA antennas at several frequencies.

6.3.3 Summary

The PICA antenna shown in Fig. 6.1 (b) was computed and measured. The measured VSWR of the PICA antenna demonstrates extremely wide impedance bandwidth. The tapered curve of the bottom of the element is the most important parameter in determining the wide impedance bandwidth [6.5]. The feed length, h is also another important parameter in tuning the antenna impedance [6.2]. The PICA antenna has similar impedance characteristics with the circular disc antenna and half-disc antenna. Computed radiation patterns, however, demonstrate that the PICA antenna provides better radiation pattern in a smaller dimension than the circular disc antenna and half-disc antenna. More investigation results will be discussed in Sections 6.4 and 6.5 using another hardware test models.

6.4 The Teardrop PICA Antenna

Models for the teardrop PICA antenna in Fig. 6.1 (c) were computed and measured. A photo of the PICA antenna is presented in Fig. 6.5 and the dimensions of the antenna element is displayed in Fig. 6.6. Note that the width of the PICA is almost same as the height of the antenna. The size of the PICA element is 76.2 mm (L = 3.0") and it was mounted with a feed length of 0.64 mm (h=0.025") above an aluminum ground plane of 609.6 mm x 609.6 mm (24" × 24"). The PICA element was designed with a size of L1 = 47 mm (1.85"), L2 = 29.2 mm (1.15") and L3 = 76.2 mm (3.0"). Note that the ratio of the L1/L2 is 1.609, which is close the golden ratio (or Sacred section) of 1.618 [6.6]. The ground plane used in this section is larger than the ground plane used in Section 6.3. The radiating element was etched on a substrate with a dielectric constant of 2.33 with a thickness of 0.79 mm (31 mils).

Figure 6.5 A teardrop PICA antenna.

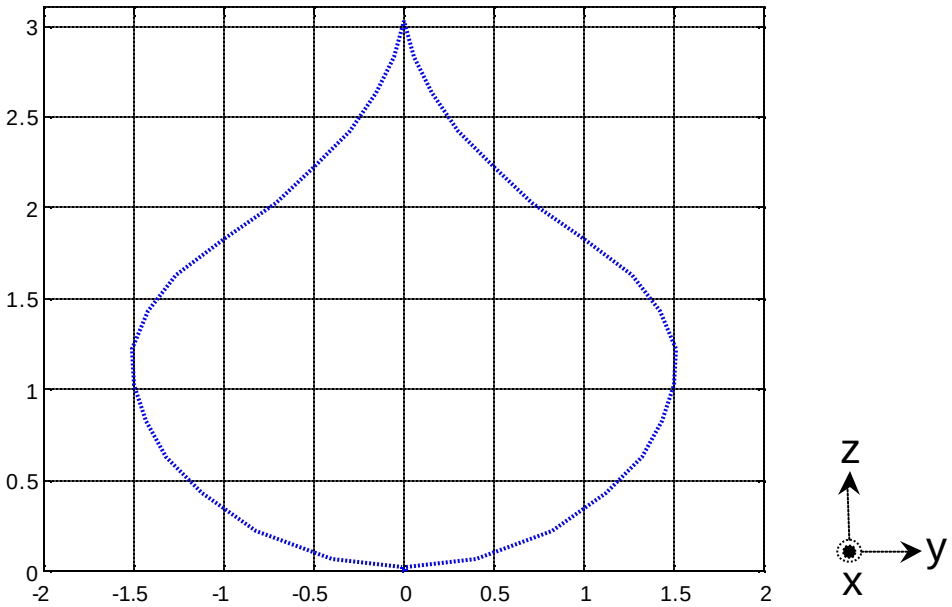

Figure 6.6 Size and geometry of a teardrop PICA antenna. The coordinate values are in inches.

6.4.1 VSWR

The VSWR of the teardrop PICA antenna was computed using a commercial code Fidelity and measured using a network analyzer, HP 8720C in the anechoic chamber in Virginia Tech Antenna Group (VTAG). The results computed and measured VSWR referenced to 50-Ω are shown in Fig. 6.7. At the high frequencies a difference in simulation and measurement data deviate. This difference could be caused by construction errors such as inaccurate feed length and the substrate effects. In spite of the difference, the PICA antenna demonstrated wide impedance bandwidth. Note that the teardrop PICA antenna impedance is very sensitive to the feed length 'h' at high frequency [6.2]. The impedance at high frequency can be tuned by changing the height 'h'.

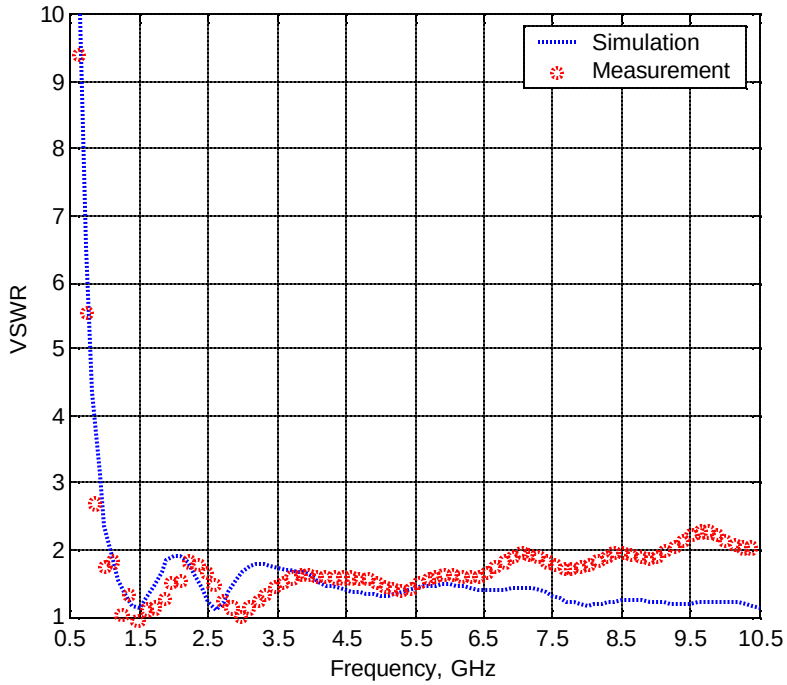

Figure 6.7 Computed and measured VSWR (referenced to 50-Ω) of a teardrop PICA antenna in Fig. 6.1 (c) with L = 76.2 mm (3.0") and h=0.64 mm (0.025").

6.4.2 Radiation Patterns

Radiation patterns were computed and measured at several frequencies over the bandwidth from 1 to 8 GHz. The patterns were computed using the FDTD commercial code Fidelity. An infinite ground plane was used in computing the PICA antenna to save computation time. In the experiment, a 609.6 mm x 609.6 mm (24" × 24") aluminum finite ground plane was used to measure the teardrop PICA antenna. Ground plane size difference may cause some differences in the simulation and measurement data. The patterns are measured using a near field scanner built by Antcom system at VTAG.

Computed radiation patterns at 1.0, 3.4 and 6.0 GHz are presented in Fig. 6.8. Measured radiation patterns are presented in Fig. 6.9 for the some frequencies plus several additional one. The elevation patterns are presented for the two principal planes of $\phi = 0°$ (xz-plane) and $\phi = 90°$ (yz-plane). The azimuth patterns are presented at an angle of $\theta = 60°$ and the 0° azimuth angle corresponds to the x-axis direction. When we consider the difference in the size of the ground plane between the simulation and measurement, the agreement can be reasonably matched well.

The PICA antenna tends to radiate energy omni-directionally for first 4:1 portion of the bandwidth. But beyond the initial 4:1 bandwidth, the antenna tends to radiate more in the direction of $\phi = 90°$ (yz-plane). A slot between the element and ground plane contributes to radiate at the high frequency. The measured radiation patterns demonstrate that at the low end of the operating band, the currents are well distributed over the PICA antenna plate so the patterns are omni-directional. But at high end of the operating band, the currents are concentrated near the slot, so the fields radiate in the direction of yz-plane mainly through the slot [6.7].

Regardless of the gain differences in the principal planes, the elevation patterns at the xz-plane ($\phi = 0°$) are useful up to 6.0 GHz if an acceptable gain is achieved. Gain measurement have not been performed, but acceptable gain is to be expected. Note that the elevation patterns in the yz-plane ($\phi = 90°$) are acceptable over a very wide band extending up to 8:1 bandwidth. The good elevation patterns in the yz-plane ($\phi = 90°$) are mainly obtained due to the slot between the radiating element and the ground plane,

which is also be observed in the Tapered Slot Antennas (TSA) such as the Vivaldi antenna [6.8]-[6.9].

The measured azimuth patterns at $\theta = 60°$ demonstrate that the PICA antenna provides good omni-directional coverage from 1.0 GHz to 4.0 GHz. However, the azimuth pattern becomes much less omni-directional as the frequency increases beyond 4.0 GHz.

Computed maximum gain vs. frequency plot is presented in Fig. B3 in Appendix B. Gain patterns can be directly obtained by adding the maximum gain number to the normalized radiation patterns.

6.4.3 Summary

The PICA antenna was etched on the dielectric material having a shape of teardrop. Measurement results for the teardrop PICA demonstrated very wide impedance bandwidth and a good radiating performance in a thin metal plate. The teardrop PICA antenna, however, experiences pattern degradation in the direction of xz-plane ($\phi = 0°$) as the frequency increases. Beyond, however, the pattern in the direction of yz-plane ($\phi = 90°$) is not degraded as the frequency increases even up to 8:1 bandwidth. The good elevation patterns at the yz-plane ($\phi = 90°$) are obtained due to the slot between the radiating element and the ground plane. The good radiation patterns and the wide impedance bandwidth of the PICA antenna demonstrate its great potential for the use of wideband antenna. An other enhancement of the PICA antenna using circular holes in the PICA element is discussed in the next section..

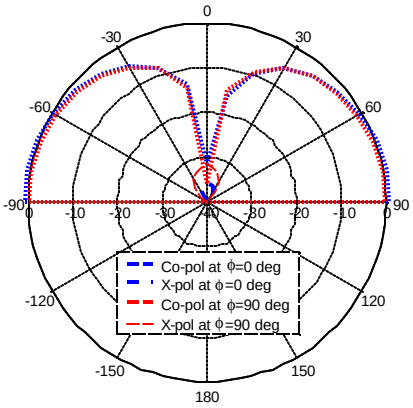

(a) Elevation pattern at 1.0 GHz

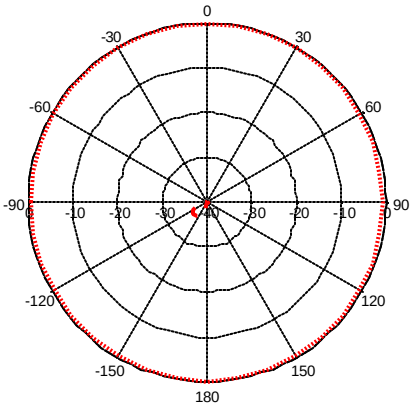

(b) Azimuth pattern at θ = 60° at 1.0 GHz

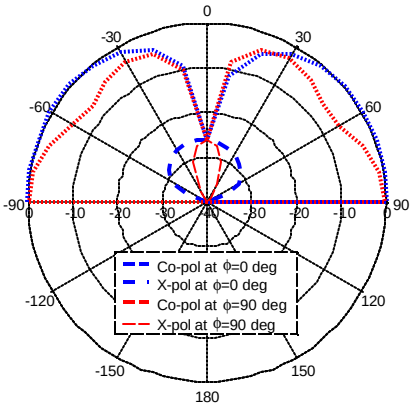

(c) Elevation pattern at 3.4 GHz

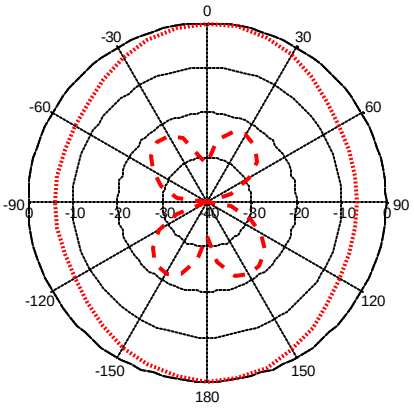

(d) Azimuth pattern at θ = 60° at 3.4 GHz

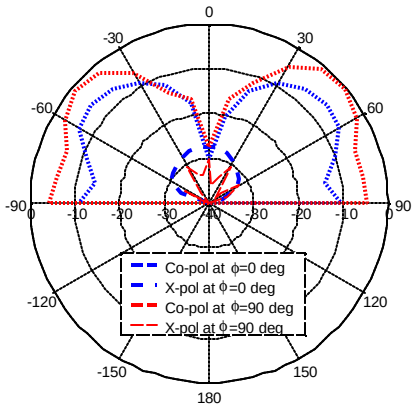

(e) Elevation pattern at 6.0 GHz

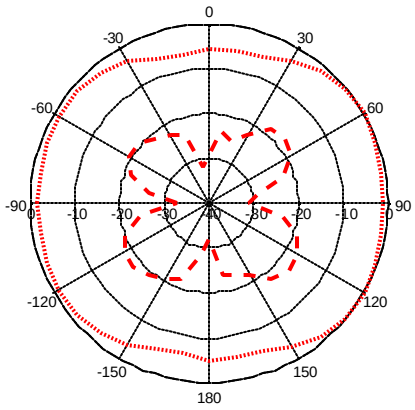

(f) Azimuth pattern at θ = 60° at 6.0 GHz

Figure 6.8 Computed radiation patterns for the teardrop PICA hardware test model in Fig. 6.1 (c). The azimuth angle 0° angle corresponds to the x-direction in Fig. 6.1 (c). The 0° elevation angle corresponds to the z-axis direction in Fig. 6.1 (c).

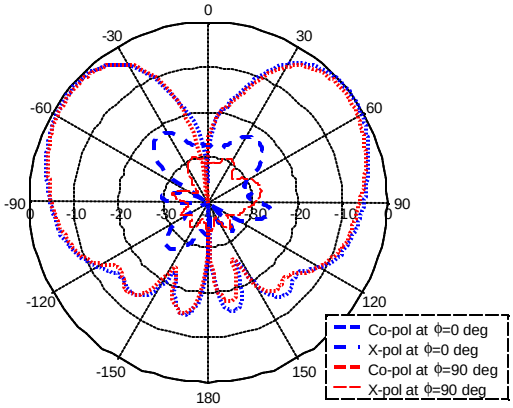

(a) Elevation pattern at 1.0 GHz

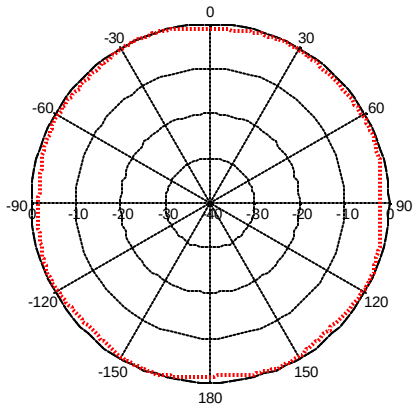

(b) Azimuth pattern at θ = 60° at 1.0 GHz

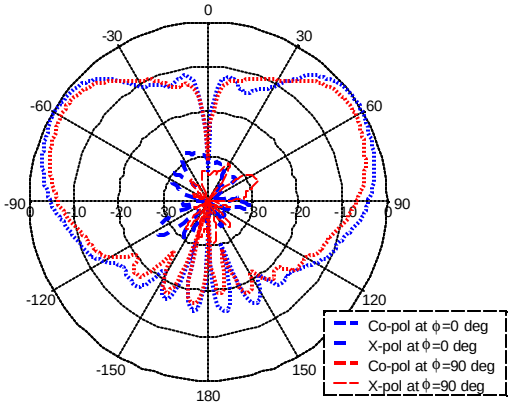

(c) Elevation pattern at 1.6 GHz

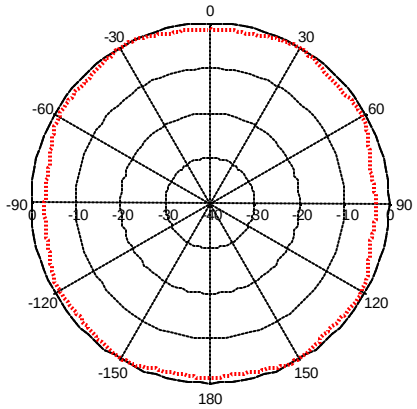

(d) Azimuth pattern at θ = 60° at 1.6 GHz

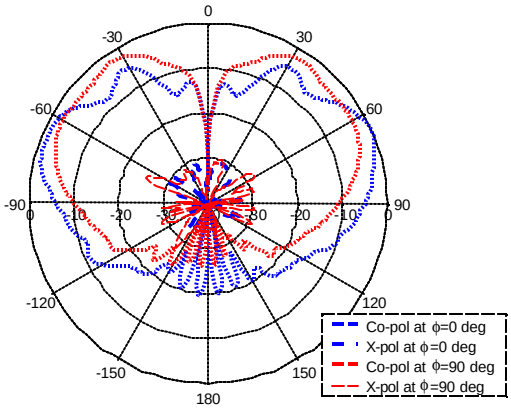

(e) Elevation pattern at 2.2 GHz

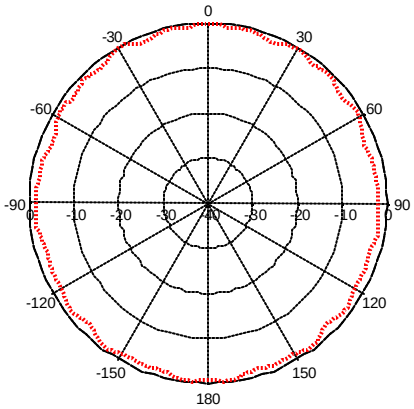

(f) Azimuth pattern at θ = 60° at 2.2 GHz

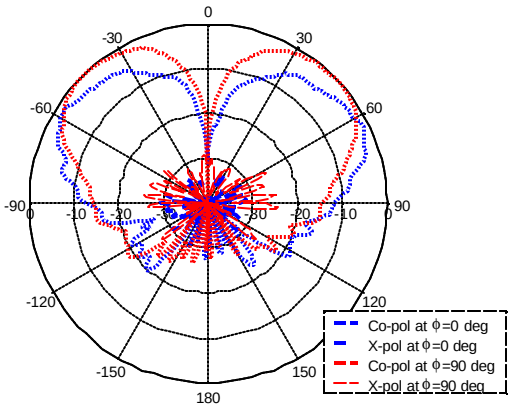

(g) Elevation pattern at 2.8 GHz

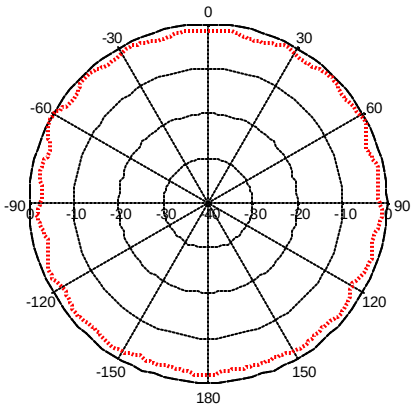

(h) Azimuth pattern at θ = 60° at 2.8 GHz

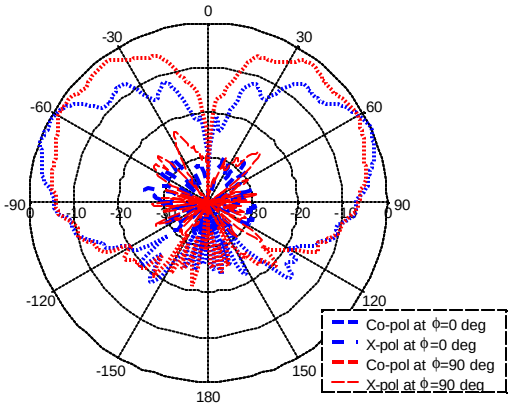

(i) Elevation pattern at 3.4 GHz

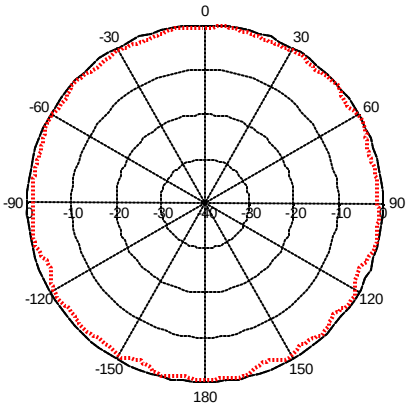

(j) Azimuth pattern at θ = 60° at 3.4 GHz

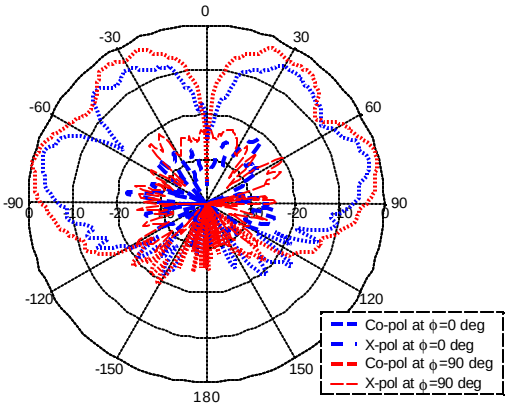

(k) Elevation pattern at 4.0 GHz

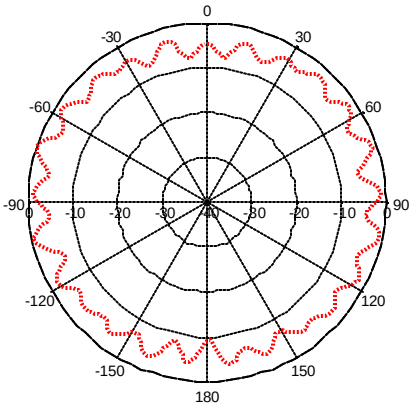

(l) Azimuth pattern at θ = 60° at 4.0 GHz

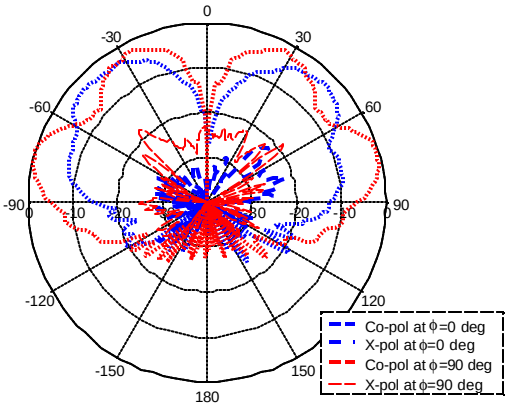

(m) Elevation pattern at 4.5 GHz

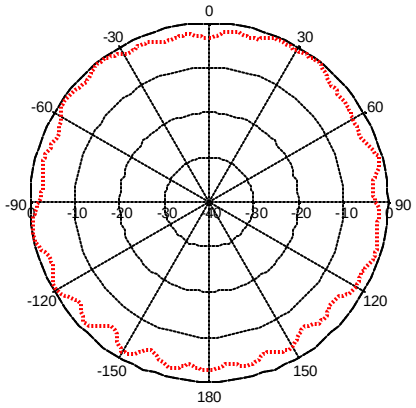

(n) Azimuth pattern at θ = 60° at 4.5 GHz

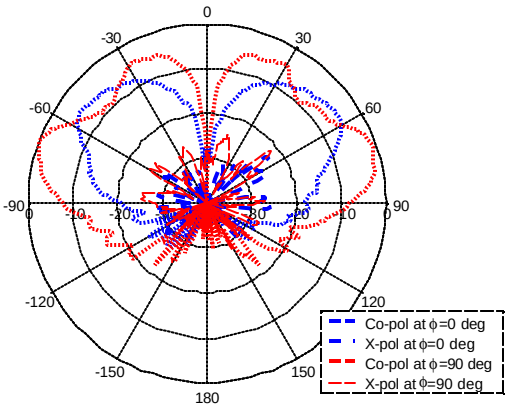

(o) Elevation pattern at 5.0 GHz

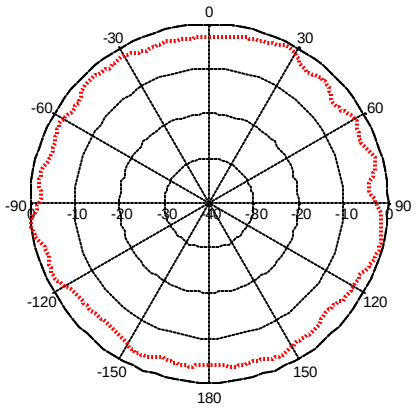

(p) Azimuth pattern at θ = 60° at 5.0 GHz

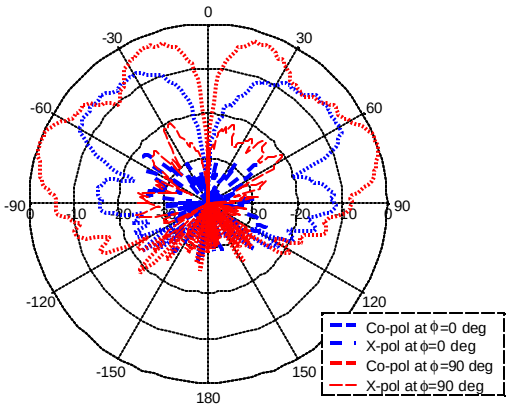

(q) Elevation pattern at 5.5 GHz

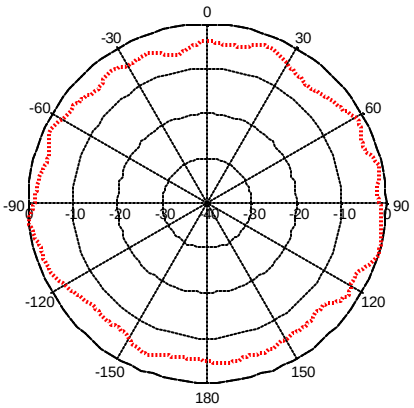

(r) Azimuth pattern at θ = 60° at 5.5 GHz

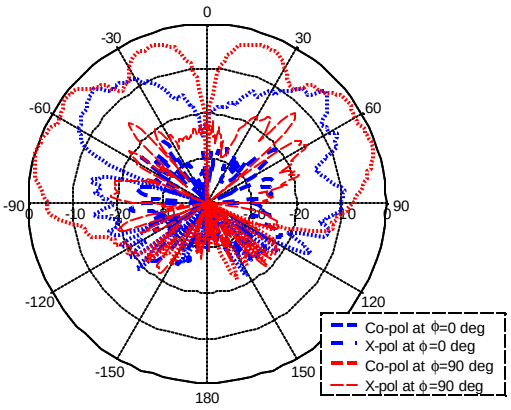

(s) Elevation pattern at 6.0 GHz

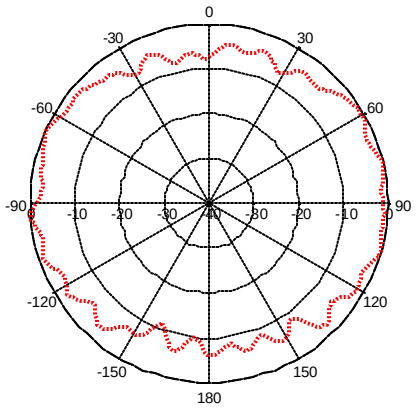

(t) Azimuth pattern at θ = 60° at 6.0 GHz

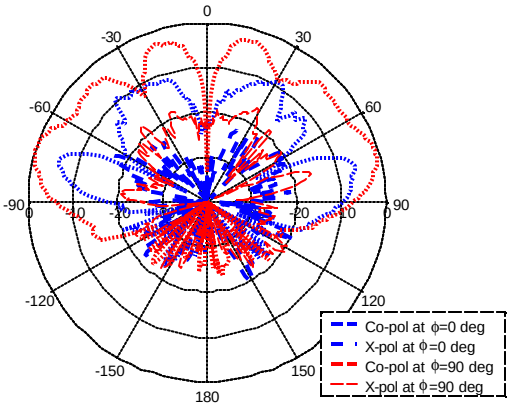

(u) Elevation pattern at 7.0 GHz

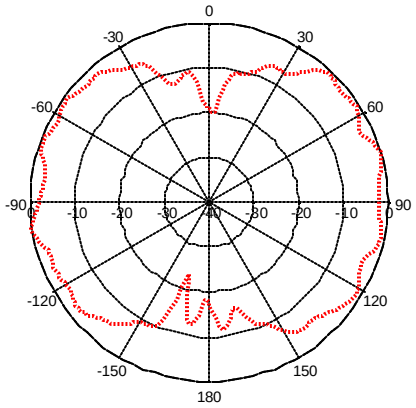

(v) Azimuth pattern at θ = 60° at 7.0 GHz

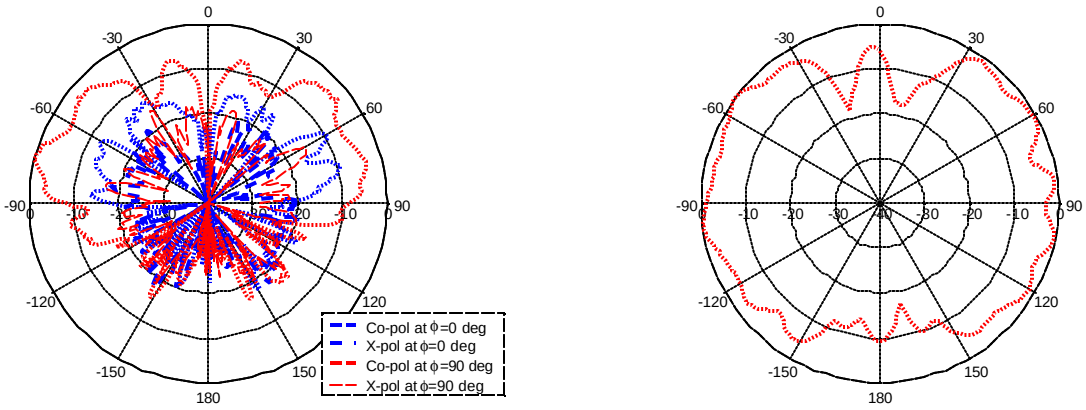

(w) Elevation pattern at 8.0 GHz (x) Azimuth pattern at θ = 60° at 8.0 GHz

Figure 6.9 Measured radiation patterns for the teardrop PICA antenna in Fig. 6.1 (c). The azimuth angle 0° angle corresponds to the x-direction in Fig. 6.1 (c). The 0° elevation angle corresponds to the z-axis direction in Fig. 6.1 (c).

6.5 The Two-circular-hole PICA Antenna

The PICA antenna with two circular holes in Fig. 6.1 (d) was converted to experimentally to see if holes in the element enhance the radiation pattern without degrading the impedance performance. There are two symmetric circular holes inside of the metal as shown in Fig. 6.10 and the radiating element was etched on a substrate with a dielectric constant of 2.33 and a thickness of 0.79 mm (31 mils). The size and the location of the circular holes are also shown in Fig. 6.11. The same element size of L=76.2 mm (3.0") was used as the teardrop PICA antenna in Section 6.4 and it was also mounted with h=0.64 mm (0.025") above a ground plane of 609.6 mm x 609.6 mm (24" × 24") aluminum plate. The PICA element was designed with the same size with the PICA antenna in Section 6.4 of L1 = 47 mm (1.85"), L2 = 29.2 mm (1.15") and L3 = 76.2 mm (3.0"). Note that the ratio of the L1/L2 is 1.609, which is close the golden ratio (or Sacred section) of 1.618 [6.6]. Only results for two circular holes are presented in this section, but several another shapes of holes are possible.

Figure 6.10 A PICA Hardware Test Model III.

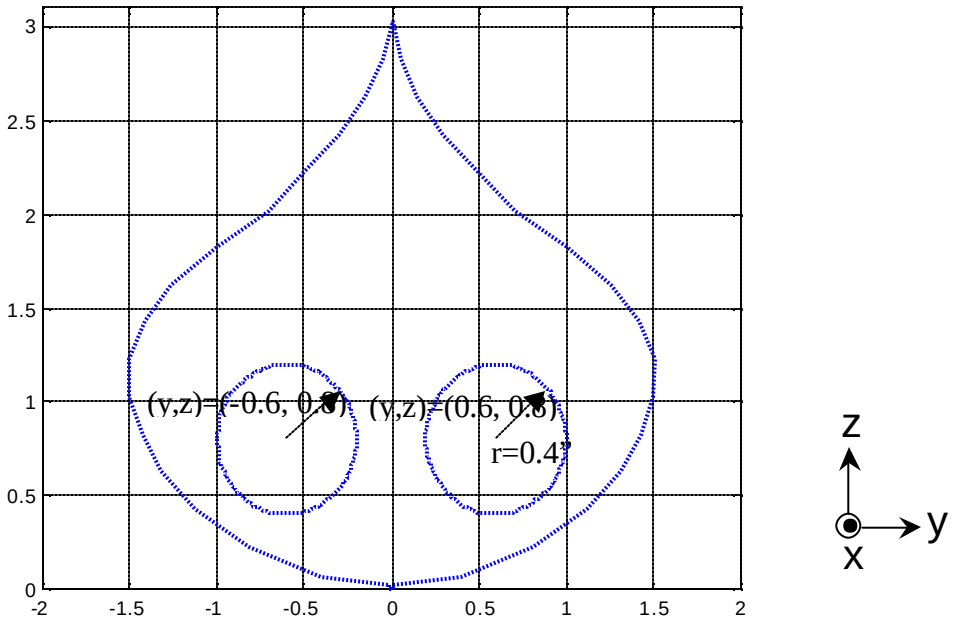

Figure 6.11 Size and geometry of a PICA antenna with two circular holes. The coordinate value represents inches.

6.5.1 Impedance properties of the two-circular-hole PICA antenna

The VSWR of the PICA antenna with two circular holes was both computed and measured at VTAG. The results presented in Fig. 6.12 in terms of VSWR are referenced to 50-Ω indicate that there is a good match over a wide band. The computed and measured results demonstrate that two circular holes in the test model do not adversely affect the antenna impedance at all but the current distribution must be changed due to the circular holes. The PICA antenna with two circular holes has more than 10:1 impedance bandwidth as well.

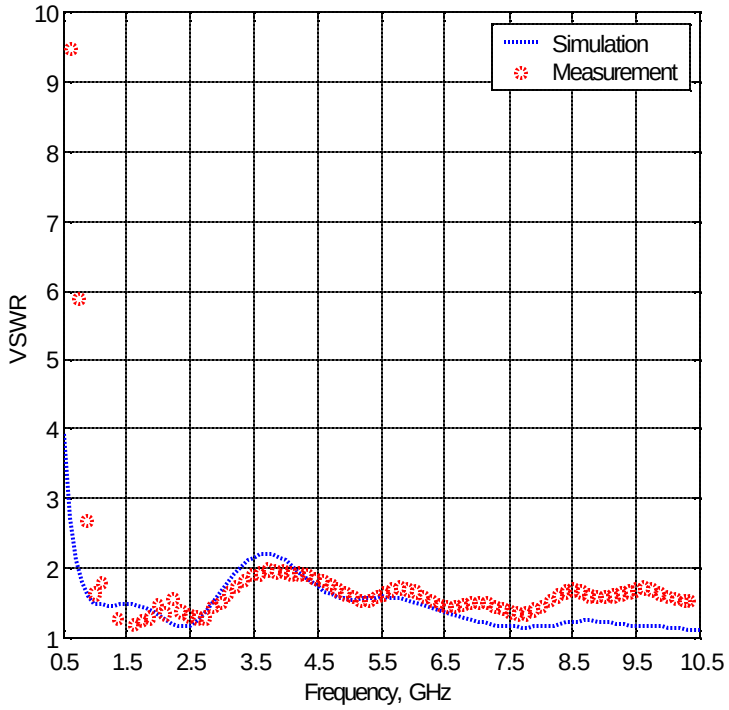

Figure 6.12 Computed and measured VSWR of a two-circular-hole PICA antenna in Figs. 6.10 and 6.11 with L = 76.2 mm (3.0”) and h = 0.64 mm (0.025”).

6.5.2 Radiation Patterns

Having demonstrated in the previous subsection that the PICA antenna impedance is not degraded by the two circular holes, we now examines the radiation patterns of the two-circular-holes PICA antenna of Figs. 6.10 and 6.11. Extensive radiation pattern measurements were made from 1 to 8 GHz. The measurement set up is exactly the same as the setup in the Section 6.4.2, except that the plain PICA radiating element was replaced by the PICA antenna in Fig. 6.10. Pattern were also computed using the Fidelity code and good agreement to the measured pattern was obtained. Only the measured results are presented here.

The measured radiation patterns of the two-circular-hole PICA antenna are very similar to the patterns of the PICA antenna without holes (see Fig. 6.9) up to 4.0 GHz. At the high frequencies, however, the two-circular-hole PICA antenna radiates in a different way with the PICA antenna without holes. The pattern plots in Fig. 6.13 demonstrate that two holes in the PICA antenna help to enhance the radiation patterns in the direction of xz-plane ($\phi = 0°$); compare the pattern plots in Figs. 6.9 and 6.13. The radiation patterns in the direction of yz-plane ($\phi = 90°$), however, are not affected significantly by the holes. The holes affect only the xz-plane patterns, which is the direction of the plane of the metal. Thus, the two-circular-hole PICA antenna has good omni-directional pattern behavior over an 8:1 bandwidth. It is important to reemphasizing that the holes do not impair the impedance performance of the PICA antenna, as shown in Fig. 6.12.

Investigation results of the PICA antenna with two circular holes demonstrate that the holes control the flow of the current in the metal plate so that the frequency response of the element is improved without deteriorating the impedance performance. Even though only two holes are tested in this section, several another shapes of holes can be applied to appropriate position on behalf of enhancing the radiation performance.

Computed maximum gain vs. frequency plot is presented in Fig. B4 in Appendix B. Gain patterns can be directly obtained by adding the maximum gain number to the normalized radiation patterns.

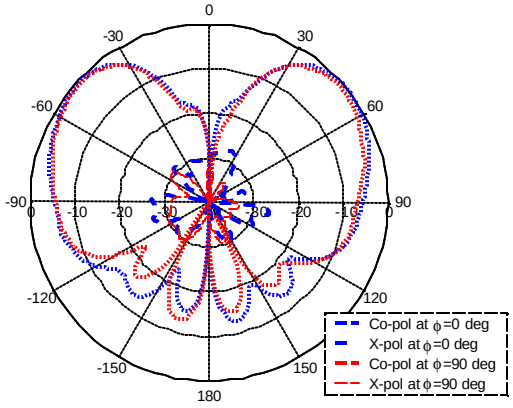

(a) Elevation pattern at 1.0 GHz

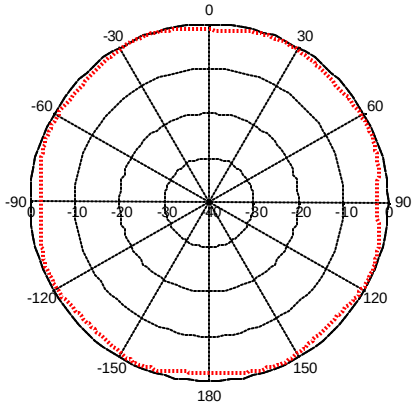

(b) Azimuth pattern at θ = 60° at 1.0 GHz

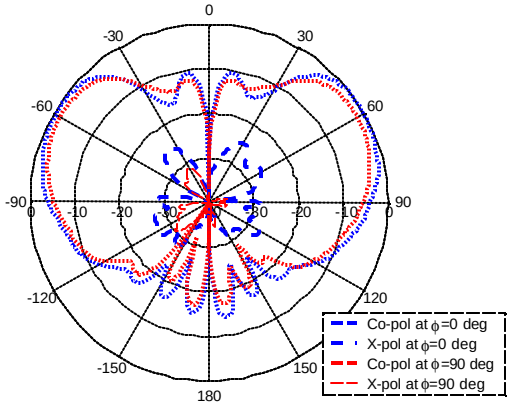

(c) Elevation pattern at 1.6 GHz

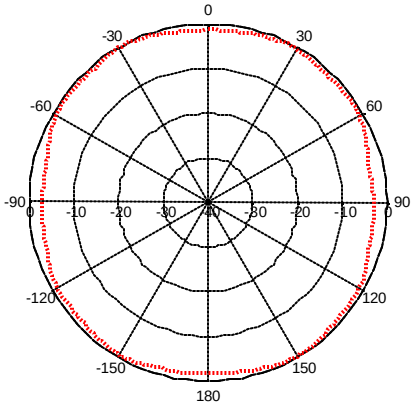

(d) Azimuth pattern at θ = 60° at 1.6 GHz

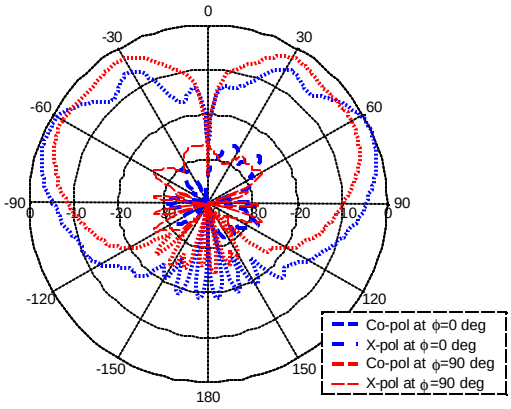

(e) Elevation pattern at 2.2 GHz

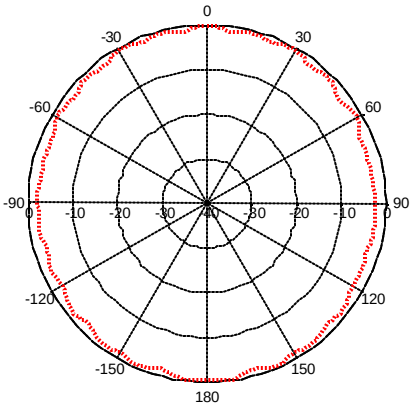

(f) Azimuth pattern at θ = 60° at 2.2 GHz

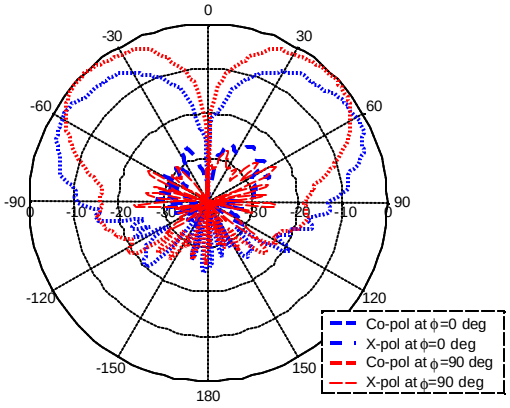

(g) Elevation pattern at 2.8 GHz

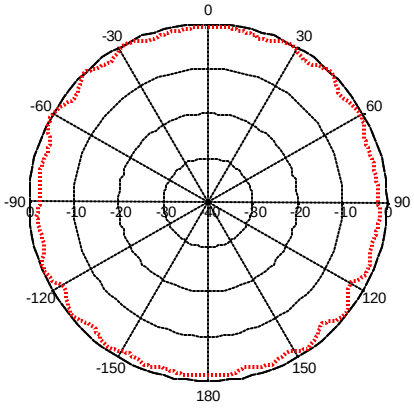

(h) Azimuth pattern at θ = 60° at 2.8 GHz

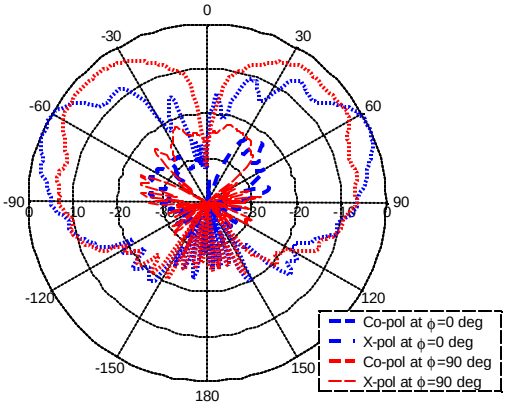

(i) Elevation pattern at 3.4 GHz

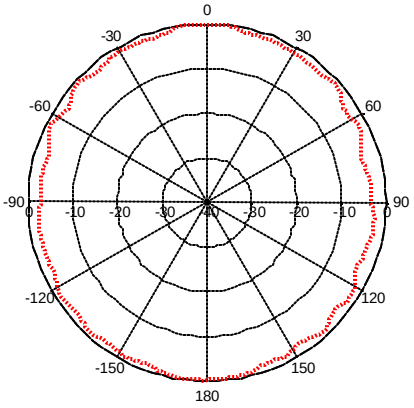

(j) Azimuth pattern at θ = 60° at 3.4 GHz

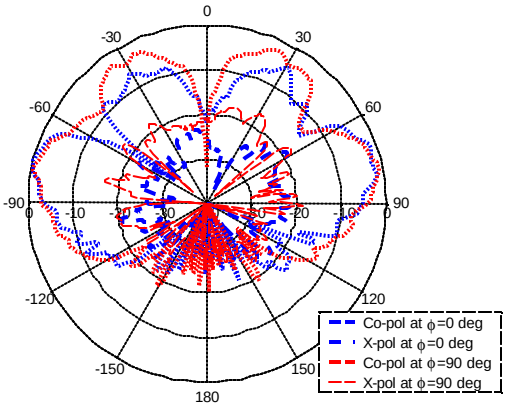

(k) Elevation pattern at 4.0 GHz

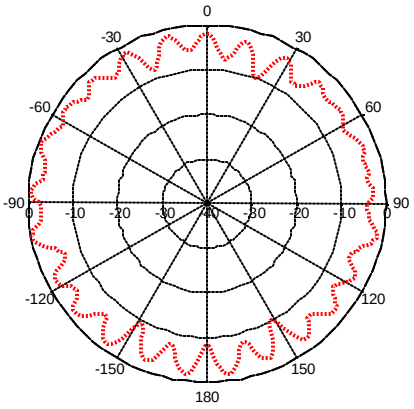

(l) Azimuth pattern at θ = 60° at 4.0 GHz

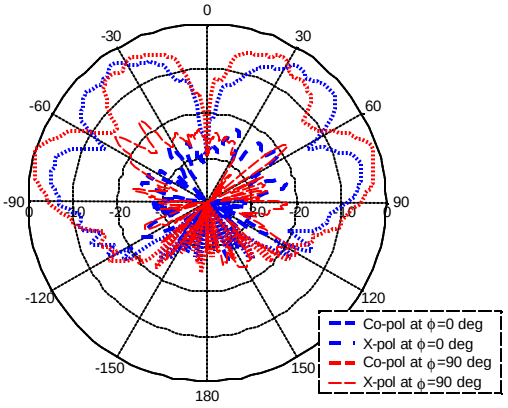

(m) Elevation pattern at 4.5 GHz

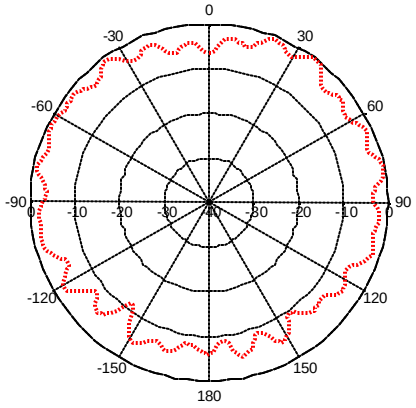

(n) Azimuth pattern at θ = 60° at 4.5 GHz

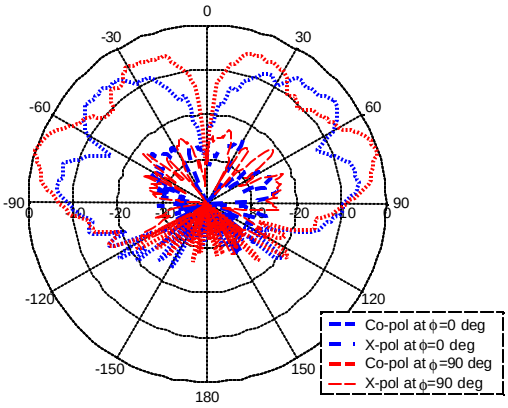

(o) Elevation pattern at 5.0 GHz

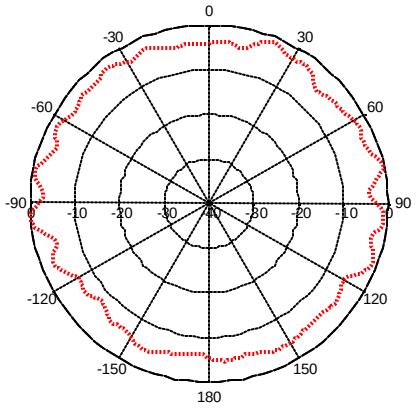

(p) Azimuth pattern at θ = 60° at 5.0 GHz

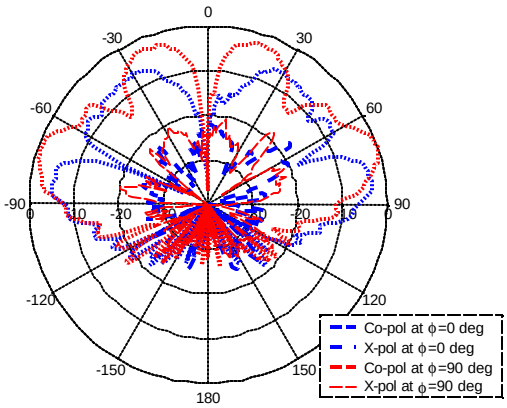

(q) Elevation pattern at 5.5 GHz

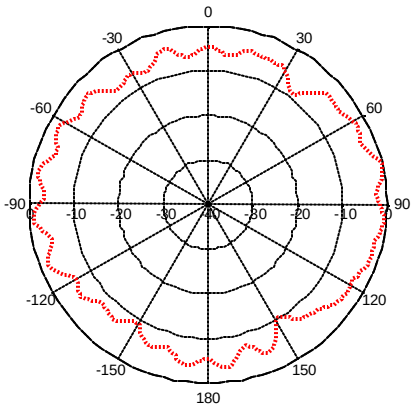

(r) Azimuth pattern at θ = 60° at 5.5 GHz

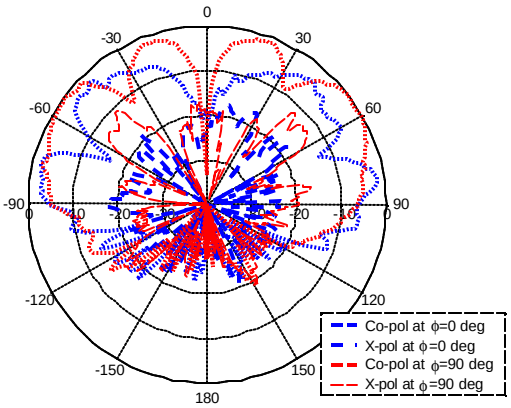

(s) Elevation pattern at 6.0 GHz

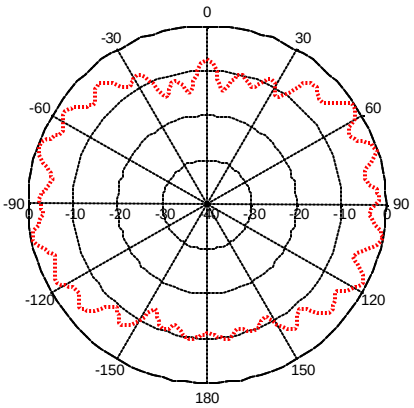

(t) Azimuth pattern at θ = 60° at 6.0 GHz

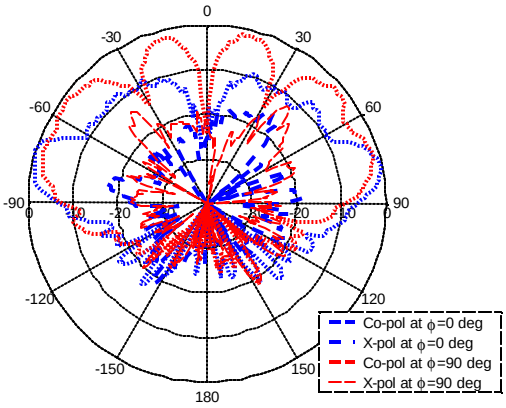

(u) Elevation pattern at 7.0 GHz

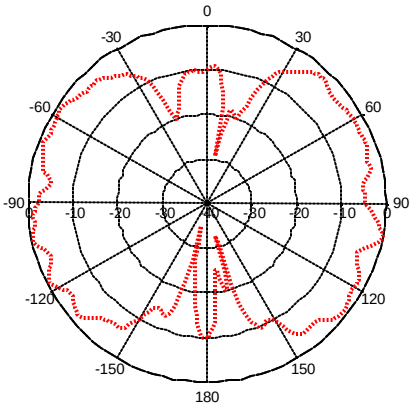

(v) Azimuth pattern at θ = 60° at 7.0 GHz

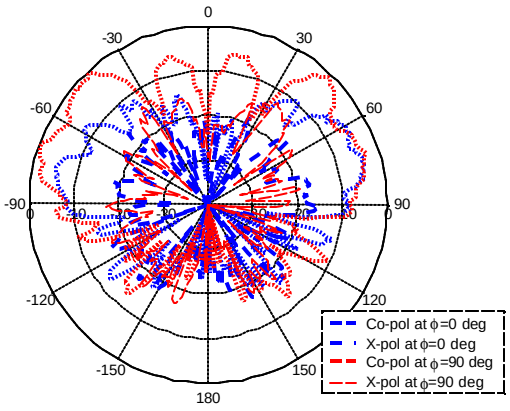

(w) Elevation pattern at 8.0 GHz

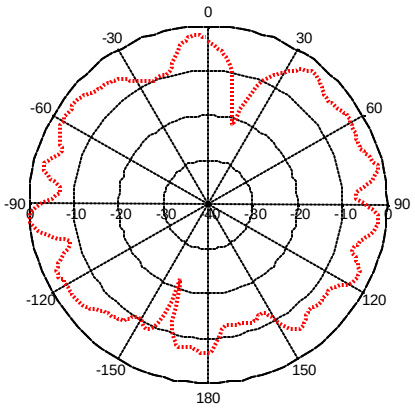

(x) Azimuth pattern at θ = 60° at 8.0 GHz

Figure 6.13 Measured radiation patterns of a two-circular-hole PICA antenna in Figs. 6.10 and 6.11. The azimuth angle 0° angle corresponds to the x-direction in Fig. 6.1 (c). The 0° elevation angle corresponds to the z-axis direction in Fig. 6.1 (c).

6.6 Summary

A newly invented PICA antenna was investigated through extensive simulations and experiments in this chapter. The PICA antenna has very wide impedance bandwidth, up to more than 10:1, and can provide acceptable radiation pattern bandwidth of about 8:1. Three PICA geometries were investigated, the plain, teardrop, and two-circular hole PICAs; see Fig. 6.1. The teardrop PICA antenna was designed with a golden ratio, 1.618 in determining the ratio of L1/L2 [6.6]. More investigation is necessary for the ratio effect of L1/L2 on the antenna performance. The two-circular-hole in the teardrop PICA antenna does not impair the antenna impedance. But they enhance the radiation pattern by changing the current distribution in the antenna element. The PICA antennas provide omni-directional pattern over very wideband; 4:1 for the teardrop PICA antenna and 8:1 for the two-circular-hole PICA antenna.

Based on the features of the PICA antenna, the PICA antenna is an excellent candidate antenna element for the Ultra Wideband (UWB) Antenna application, which requires to efficiently propagate the monocycle pulses with minimal distortion; in other words, ultra wide band should be covered in a single antenna element. In many UWB applications, the modified Vivaldi antenna is used such as a shape of rabbit ears or Mickey Mouse ears [6.10]. When the PICA antenna is modified into dipole version and the direction of the yz-plane is used for antenna propagation, the geometry is very similar to the UWB antenna, Mickey Mouse antenna. More detail investigation should be performed for the UWB application as a future work.

The investigated PICA antennas are summarized in Table 6.2.

Table 6.2

Summary of PICA Antenna discussed in Chapter 6.

Antenna	**Characteristics**	
	Impedance Bandwidth for VSWR < 2	**Pattern Bandwidth**
PICA (Section 6.3)	> 20:1 (measured)	6:1 (computed)
Teardrop PICA (Section 6.4)	> 10:1 (measured)	4:1 (measured)
Two-circular-hole PICA (Section 6.5)	> 10:1 (measured)	8:1 (measured)

References

[6.1] W. L. Stutzman and G.A. Thiele, *Antenna Theory and Design 2nd edition*, John Wiley & Sons, New York, 1981.

[6.2] P. P. Hammoud and F. Colomel, " Matching the input impedance of a broadband disc monopole," *Electronics Letters*, Vol. 29, pp. 406-407, Feb. 1993.

[6.3] R. M. Taylor, "A broadband Omni-directional Antenna," *IEEE Antennas and Propagation Society International Symposium Digest (Seattle)*, Vol. 2, pp. 1294 – 1297, June 1994

[6.4] Seong-Youp Suh and Warren L. Stutzman, "A Planar Inverted Cone Antenna," *VTIP disclosure No. 00-130*, http://www.vtip.org/Licensing/disclosures/00-130.htm, September 8, 2000

[6.5] N. P. Agrawall, G. Kumar, and K. P. Ray, "Wide-band Planar Monopole Antennas," *IEEE Transactions on Antennas and Propagation*, Vol. 46, No. 2, pp.294-295, Feb. 1998.

[6.6] S Vajda, *Fibonacci and Lucas numbers, and the Golden Section: Theory and Applications*, Halsted Press, New York, 1989.

[6.7] B. J. Lamberty, "*A class of low gain broadband antennas*," *1958 IRE Wescon Convention Record*, pp. 251-259, August 1958.

[6.8] L. R. Lewis, M. Fasset and J. Hunt, "A Broadband Stripline Array Element," *Digest of 1974 IEEE Ant. And Prop. Sym.*, pp. 335-337.

[6.9] J. D. S. Langley, P.S. Hall and P. Newham, "Novel Ultrawide-bandwith Vivaldi antenna with low crosspolarization," *Electron. Letter*, vol. 29, no. 23, pp2004-2005, 1993.

[6.10] Adams, J. C., Gregorwich, W., Capots, L., Liccardo, D., "Ultra-wideband for Navigation and Communications," *Aerospace Conference, 2001, IEEE Proceedings*, Vol. 2, pp. 2/785 – 2/792, 2001.

Chapter 7

Wideband Low-profile Dipole Planar Inverted Cone Antenna (LPdiPICA)

7.1 Introduction

The well-known monopole antenna is easily related to the dipole antenna through image theory [7.1]. In a similar fashion, the monopole PICA antenna in Chapter 6 has a dipole version of the PICA antenna called the diPICA. Applications for the dipole PICA are those that requires full spheroidal volume (omni-directional) coverage, rather than hemispherical omni-directional radiation obtained with the (monopole) PICA. A software test model demonstrated that the diPICA antenna behaves like several segment half-wave dipoles in a single element, giving ultra wide impedance and pattern bandwidth.

However, for many situations a unidirectional beam is required. With a conventional dipole, this is accomplished by introducing a ground plane parallel to and a $\lambda/4$ behind the dipole. We refer to this as a Low-Profile Dipole Planar Inverted Cone Antenna (LPdiPICA). The LPdiPICA is a wideband compact antenna with a unidirectional pattern and is easy to apply to implement in an array element.

We saw in Chapters 3 and 5 that the Fourpoint and Fourtear antennas can provide dual-linear or circular polarization by proper feed implementations. The low-profile diPICA antenna, however, has only a single polarization because it has only two opposing arms whereas the Fourpoint or Fourtear antenna has two parts of opposing radiating arms. In this chapter, the unique features of the low-profile diPICA antenna are discussed by examining antenna impedance and radiation patterns.

The low-profile diPICA antenna was extensively investigated using multiple software simulation codes and hardware test models. It was observed that the low-profile diPICA antenna has very similar pattern characteristics to the infinitesimal dipole antenna above a perfect ground plane with varying height [7.2]. The study was started by investigating the characteristics of the diPICA antenna, i.e. LPdiPICA without a ground plane.

Based on the investigation of the LPdiPICA antenna, the LPdiPICA antenna patterns are degraded as the frequency increases toward high end of the band. As an attempt to enhance the radiation patterns at the high end of the band, several ground plane geometries are proposed and one of them (exponentially-tapered ground plane) was simulated using the Fidelity code. The simulation results demonstrate that the exponentially-tapered ground plane enhanced the radiation patterns at the high end of frequency. The basic concept of these efforts is to keep the electrical height above the ground plane as about $\lambda/4$ at all frequencies [7.2]. The detail investigation should be done as a future work.

Figure 7.1 presents the antenna geometries investigated in this chapter.

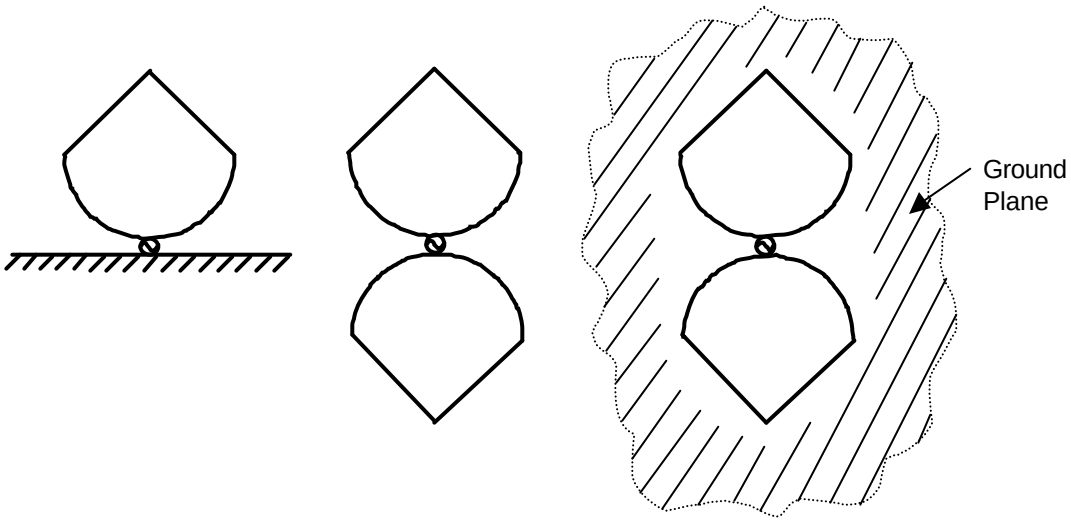

(a) PICA (b) diPICA (c) LPdiPICA

Figure 7.1 Antenna geometries of the PICA antenna family discussed in this chapter.

7.2 A diPICA antenna without Ground Plane

The monopole PICA antenna discussed in Chapter 6 can be easily constructed to a dipole PICA antenna (called diPICA) using the concept of the image theory [7.1] and the diPICA antenna is presented in Fig. 7.2. The dimensions are described in the figure. The geometry of the two-circular-hole PICA antenna was used as a test model for the diPICA antenna. The coordinate system is adjusted to compare the radiation pattern with the typical dipole antenna vertically positioned.

7.2.1 Impedance Properties of the diPICA antenna

The Fidelity code was used in simulating the diPICA antenna without ground plane. The computed antenna impedance and the radiation patterns are presented in Figs. 7.3 and 7.4. The antenna impedance characteristics are close to one of a frequency independent antenna, which have more than 10:1 impedance bandwidth [7.1]. The resistive component maintains near 100-Ω and the reactive component is within ± 50-Ω, which characteristics are resulted in excellent VSWR performance over the entire band as shown in Fig. 7.3 (b). The VSWR is referenced to 100-Ω.

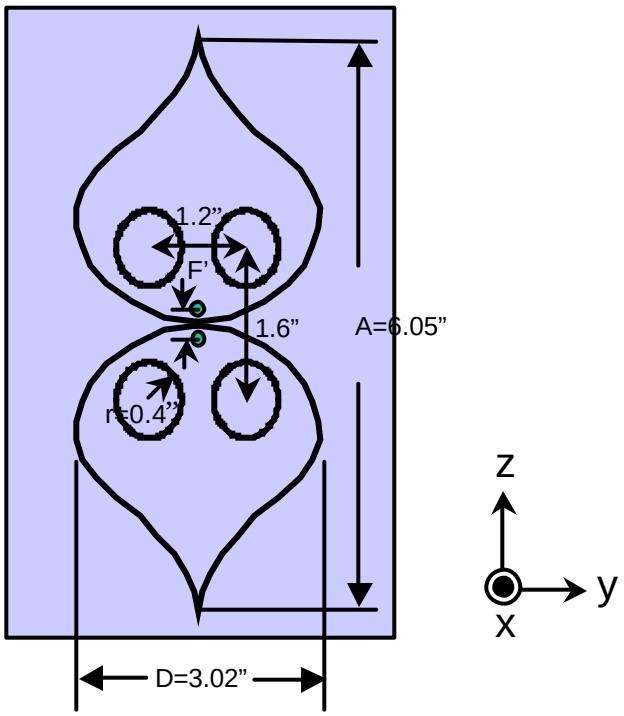

(a) Geometry at xz-plane.

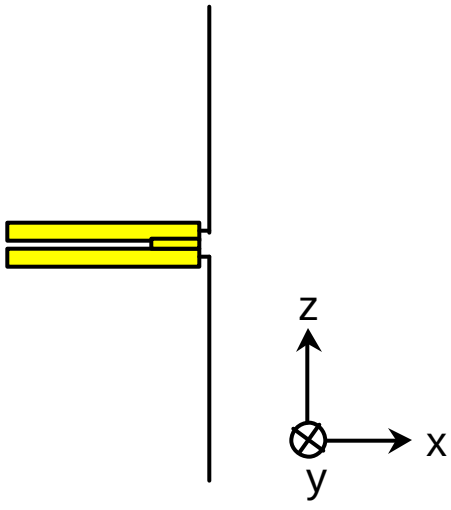

(b) Geometry at yz-plane.

Figure 7.2 A diPICA antenna without ground plane (F’ = 2.3 mm (0.09”)).

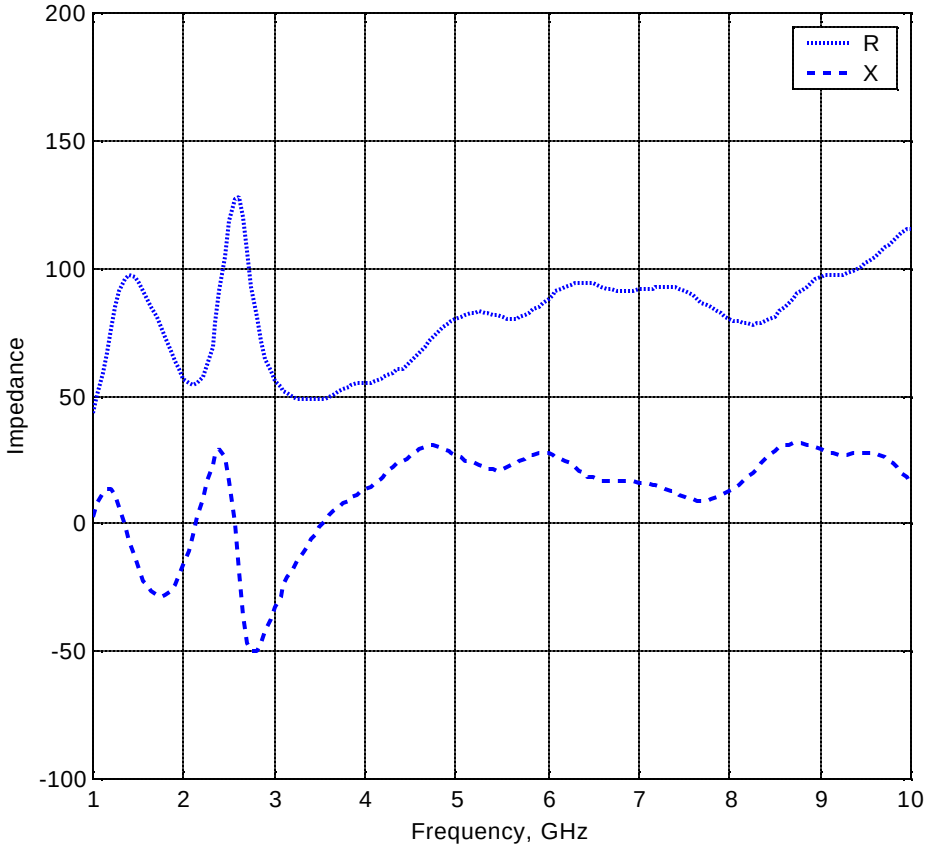

(a) Computed antenna impedance of the diPICA antennas without ground plane.

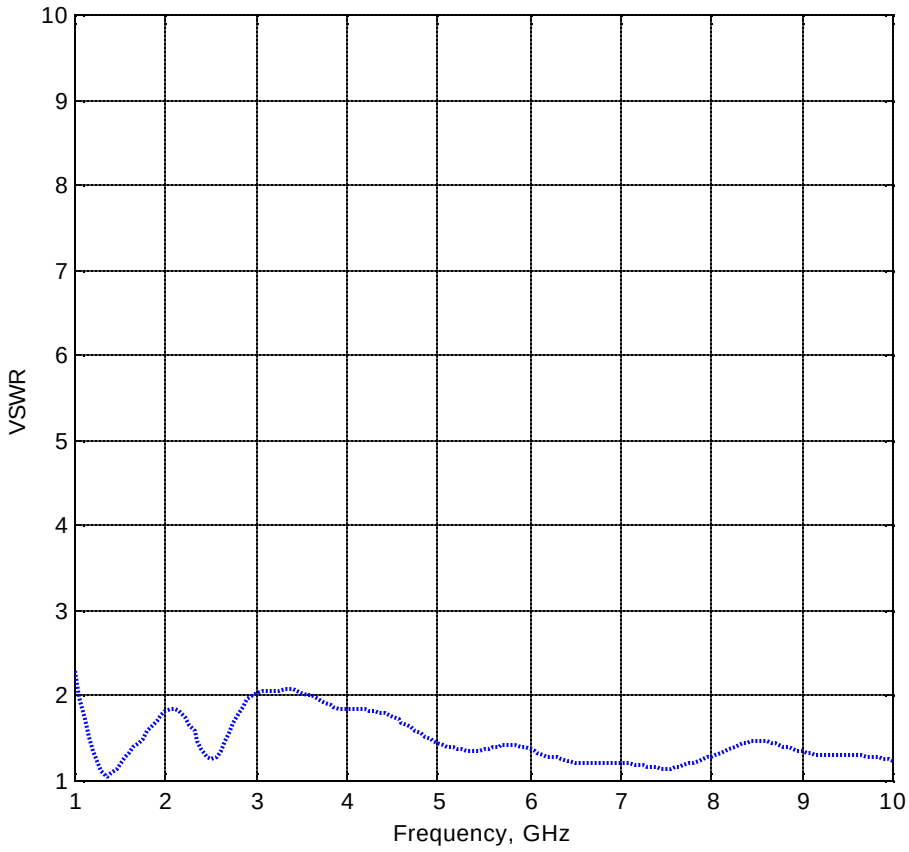

(b) Computed VSWR (referenced to 100-Ω) of the diPICA antenna without ground plane.

Figure 7.3 Computed antenna impedance and VSWR (referenced to 100-Ω) of the diPICA antenna without ground plane in Fig. 7.2.

7.2.2 Radiation Pattern of the diPICA antenna

Computed radiation patterns of the diPICA antenna are presented at some selected frequencies in Fig. 7.4. The elevation patterns are computed at the E-plane (xz-plane, ϕ = 0°) and H-plane (yz-plane, ϕ = 90°) as described in Fig. 7.2. The azimuth patterns of the diPICA antenna are also presented for an angle computed at θ = 60°. The diPICA antenna provides good omni-directional patterns from the frequency of 1.0 GHz up to 4.0 GHz, but the patterns are degraded as the frequency increases beyond 4.0 GHz. Several lobes are generated at the high end of the frequency as shown in Fig. 7.4 (i) and (k). The several lobes and broad beam will decrease the directivity of the diPICA antenna at the high end of the frequency. However, the patterns at the high frequency are still useful for the wireless communication. The cross-pol level is less than 20 dB for the entire band.

The simulation results demonstrate that the diPICA antenna provides excellent antenna performance in antenna impedance and radiation patterns. The diPICA antenna is just like the several segment of typical dipole antenna tuned at several frequencies in a single element.

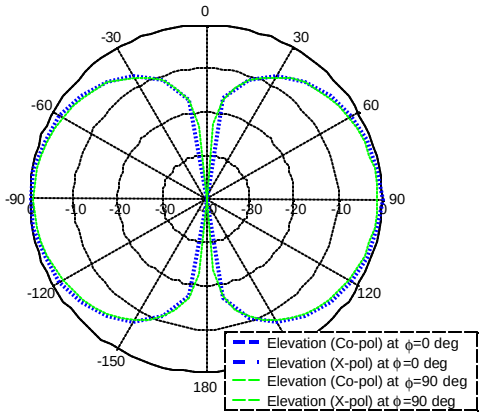

(a) Elevation pattern at 1.0 GHz

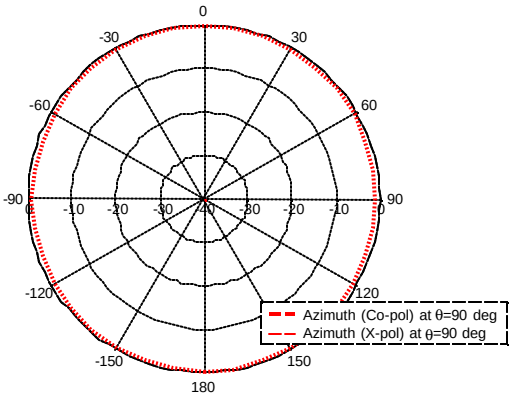

(b) Azimuth pattern at 1.0 GHz

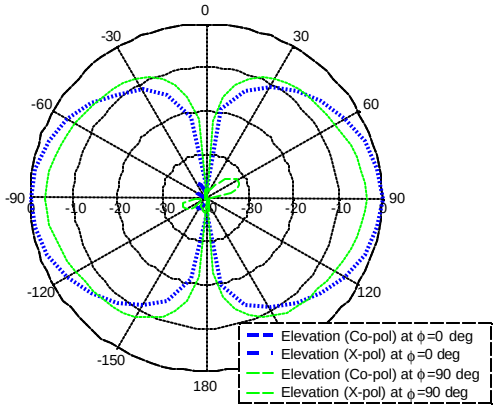

(c) Elevation pattern at 2.0 GHz

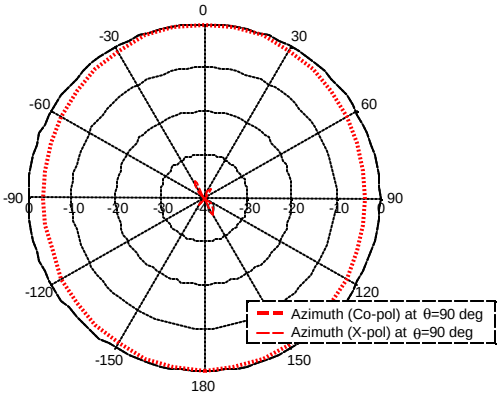

(d) Azimuth pattern at 2.0 GHz

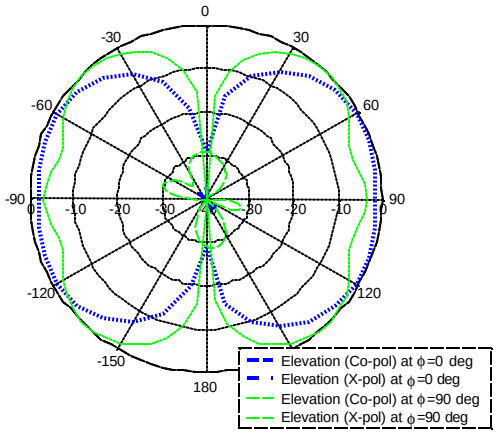

(e) Elevation pattern at 3.0 GHz

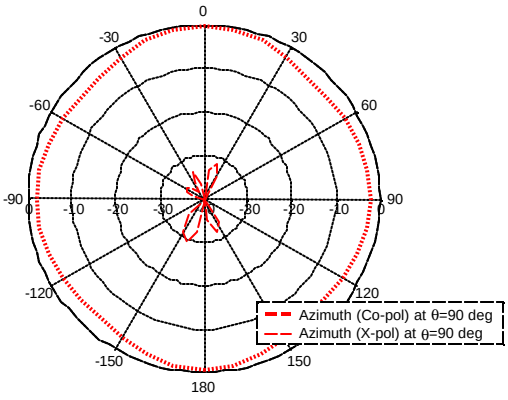

(f) Azimuth pattern at 3.0 GHz

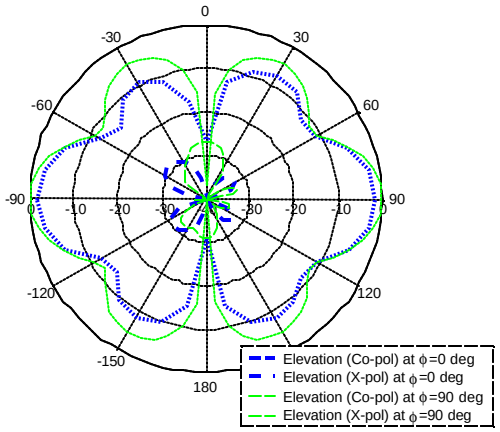

(g) Elevation pattern at 4.0 GHz

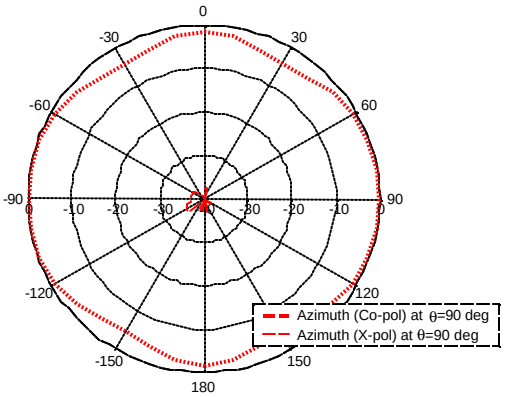

(h) Azimuth pattern at 4.0 GHz

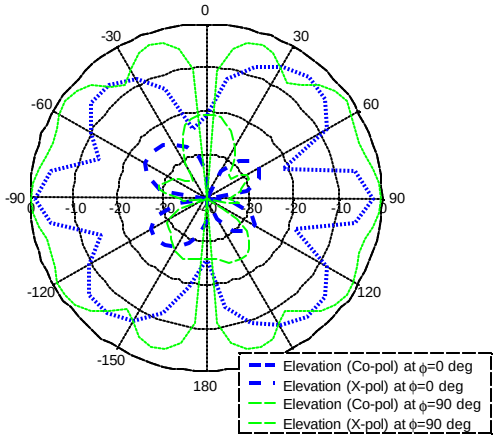

(i) Elevation pattern at 6.0 GHz

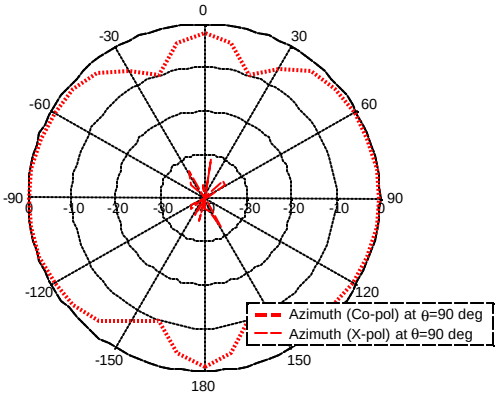

(j) Azimuth pattern at 6.0 GHz

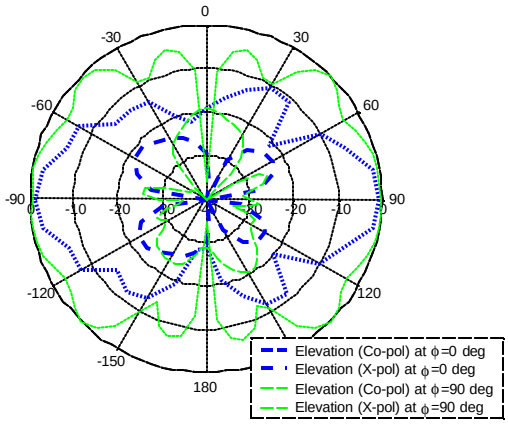

(k) Elevation pattern at 8.0 GHz

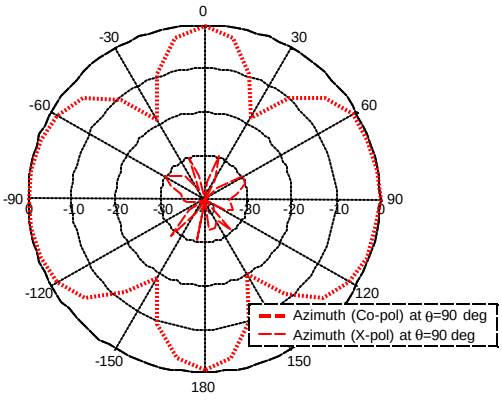

(l) Azimuth pattern at 8.0 GHz

Figure 7.4 Computed radiation patterns of the diPICA antenna without ground plane.

7.3 A Low-Profile diPICA Antenna Test Model I

Many dipole antennas also can be constructed to a low-profile dipole antenna to obtain a unidirectional pattern. In a similar fashion, the diPICA antenna can be modified to the low-profile diPICA antenna (called LPdiPICA) by backing a ground plane parallel to the diPICA antenna like the Fourpoint and Fourtear antennas discussed in Chapters 3 and 5.

7.3.1 Antenna Structure of the LPdiPICA Model I

The basic antenna structure of the low-profile diPICA (LPdiPICA) antenna is shown in Fig. 7.5. The top view of the LPdiPICA antenna is the dipole version of the PICA antenna discussed in Section 7.1 (see Fig. 7.1(b)) and the side view of the antenna structure is the same geometry with one of the Fourpoint and Fourtear antennas in Fig. 3.1. The radiating element in Fig. 7.5 can be replaced other valid geometry of the PICA element as discussed in Section 6.2. Note that the radiating elements in Fig. 7.5 do not have parasitic elements, unlike the Fourpoint or Fourtear antennas and has only single linear polarization. The shape of the tapered slot and the distance between two radiating elements are the critical parameters in determining the antenna impedance. The height, 'h' between the radiating element and the ground plane is to be adjusted to achieve maximum pattern bandwidth just as with the wideband half-wave dipole antenna reported by Bailey [7.3]. Generally the height is set to $\lambda/4$ at the high end of the frequency band, but at the same time the height should be properly determined to meet the VSWR requirement.

The coordinate system used in Fig. 7.5 (a) of the LPdiPICA leads to an xz-plane as E-plane for description of radiation patterns. The H-plane is the orthogonal plane of the E-plane as shown in Fig. 7.5(a).

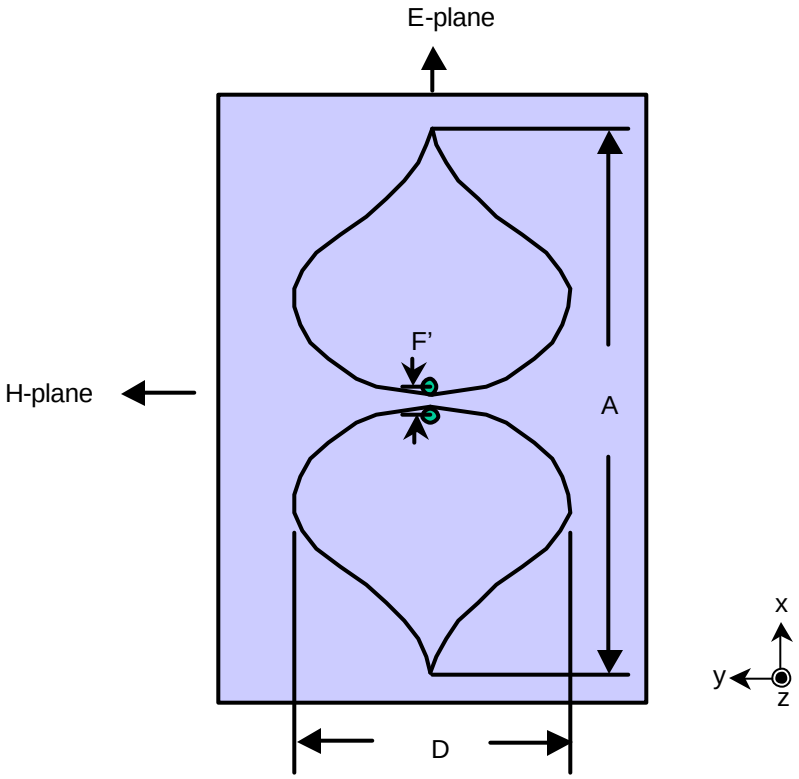

(a) Top view.

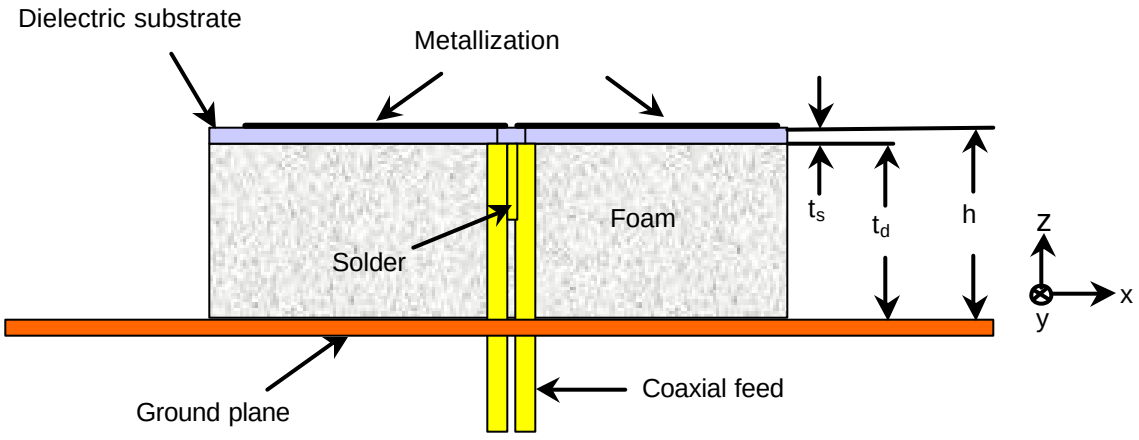

(b) Side view.

Figure 7.5 The structure of the low-profile diPICA antenna (LPdiPICA).

7.3.2 Dimensions of the LPdiPICA Hardware Test model I

A hardware test model of the wideband LPdiPICA antenna shown in Fig. 7.6 was constructed and tested. The dimensions are listed in Table 7.1. The outer dimension of the antenna is 153.67 mm x 76.7 mm (6.05" x 3.02"). The radiating element was etched on a dielectric material (ε_r=2.33) of Duroid 5870 from Rogers Co. The antenna was investigated using both simulations and measurements performed by the Virginia Tech Antenna Group. The hardware test model was simulated using the commercial FDTD code Fidelity. Measurement was made using a network analyzer HP 8720C and an Antcom near field scanner system for the impedance and radiation patterns, respectively. Note that an infinite ground plane was employed in simulations for reasons of the computational simplicity, but a 431.8 mm x 431.8 mm (17" x 17") aluminum ground plane was used in the measurements. The electrical size of the ground plane is about 1.42 λ x 1.42 λ at the lowest operating frequency of 1.0 GHz. A semi-rigid cable of RG 405 /U was used as a coaxial feed with a characteristic impedance of 50-Ω. The outer diameter of the cable is about 2.2 mm (0.087").

Figure 7.6 A LPdiPICA antenna hardware test model I.

Table 7.1

Dimensions of the LPdiPICA antenna model I of Figs. 7.5 and 7.6.

Description	Symbol	Size
Element vertical length	A	153.67 mm (6.05”)
Element horizontal length	D	76.7 mm (3.02”)
Substrate thickness	t_s	0.79mm (0.031”)
Foam thickness	t_d	37.3 mm (1.47”)
Element height above ground plane	h	38.1 mm (1.50”)
Feed positions distance	F’	2.3 mm (0.09”)
Feed (Semi-Rigid Coaxial Cable)	RG 405 /U	Outer diameter: 2.2 mm (0.087”)

7.3.3 Impedance Properties of the LPdiPICA model I

The VSWR of the LPdiPICA model I was measured using two different methods, a 2-port method and a 1-port method. The 2-port method is a method of measuring S-parameters for 2-port and computes antenna impedance using the S-parameter data with the equation (2-6) in Section 2.8.2.1. (The 2-port method uses a 100-Ω reference input impedance.)

The 1-port method employs a wideband 180° hybrid that operates over 1-18 GHz as shown in Fig. 7.7. In order to obtain 180° phase difference at the two input ports, the difference (Δ) port of the hybrid was used as an input port and the sum (Σ) port was terminated with a 50-Ω load. Each port of the hybrid has an input impedance of 50-Ω, so in order to match the impedance of the port connecting the hybrid and antenna input, each port of the antenna should have an impedance of 50-Ω as shown in Fig. 7.7. Hence when we use the wideband hybrid with input impedance of 50-Ω, the antenna VSWR should be referenced to 100-Ω. Note that the low-profile diPICA antenna was also referenced to 100-Ω when the VSWR was measured using the 2-port method. Therefore, the measured data from both methods can be compared directly.

The impedance properties are presented in Fig. 7.8(a) with computed and measured data. They are agreed very well each other. The resistive component is near the 100-Ω and the reactive component is within ±50-Ω so that the LPdiPICA antenna provides extremely wide impedance bandwidth.

Figure 7.8(b) shows the comparison of the measured VSWR data using the two different methods. Also shown is the results computed using the Fidelity simulation code. Note that the antenna impedance data is not provided for the 1-port measurement method. All three results agreed very well each other. The results presented in Fig. 7.8 confirmed that the low-profile diPICA antenna has more than 10:1 impedance bandwidth for VSWR<2.

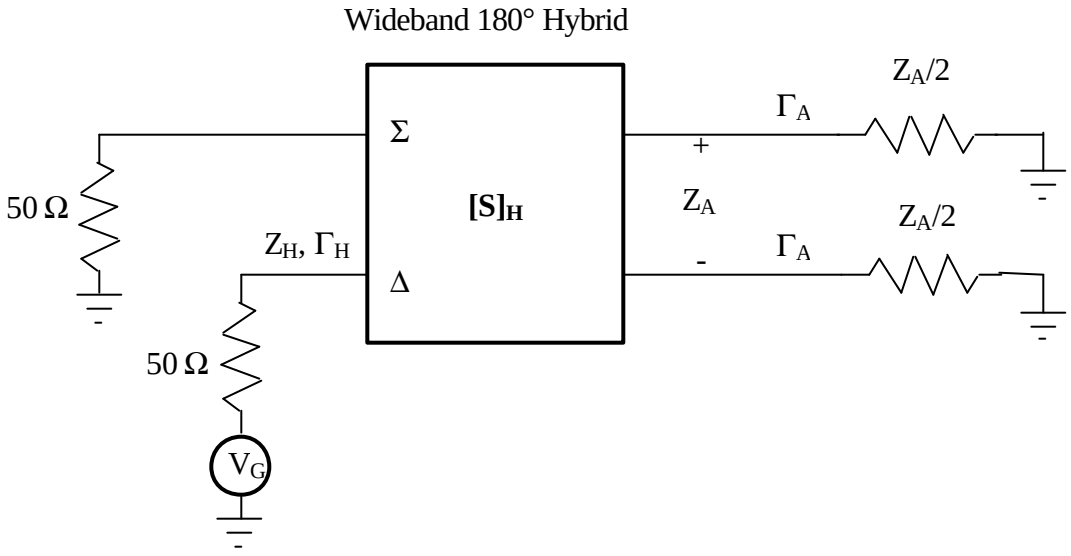

(a) Schematics of the 1-port measurement method.

(b) A hardware test model using the 1-port measurement method.

Figure 7.7 A 1-port measurement method using a wideband 180° hybrid.

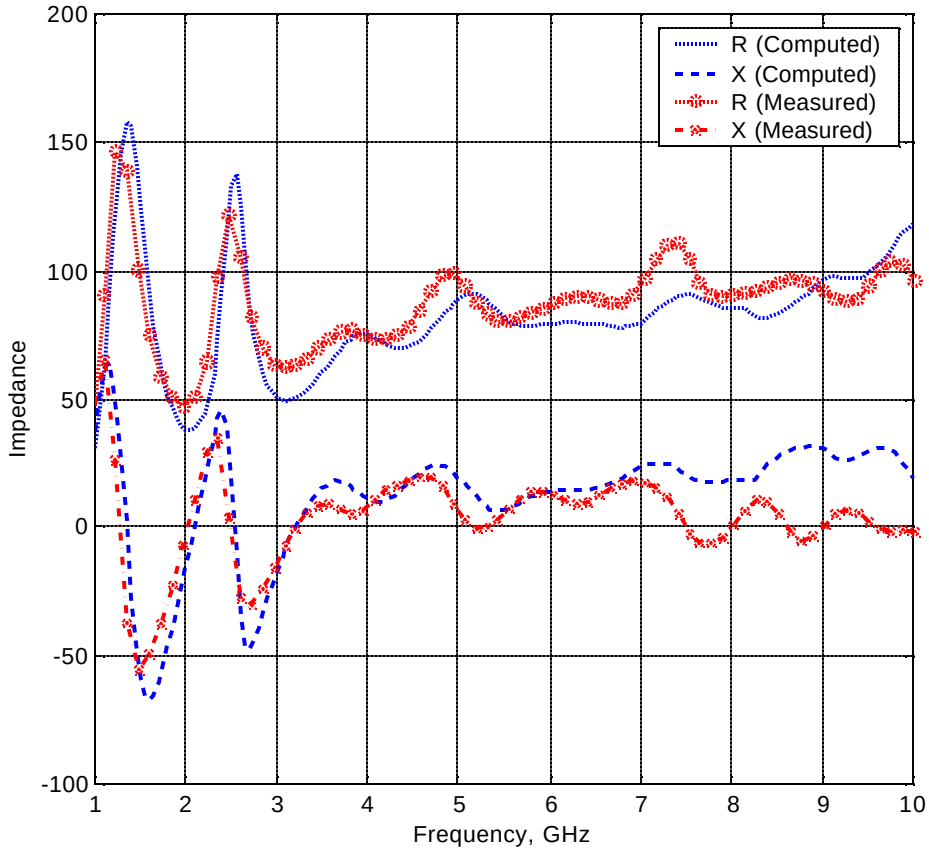

(a) Computed and measured (2-port method) antenna impedance of the LPdiPICA antenna in Figs. 7.5 and 7.6 with the dimensions listed in Table 7.1.

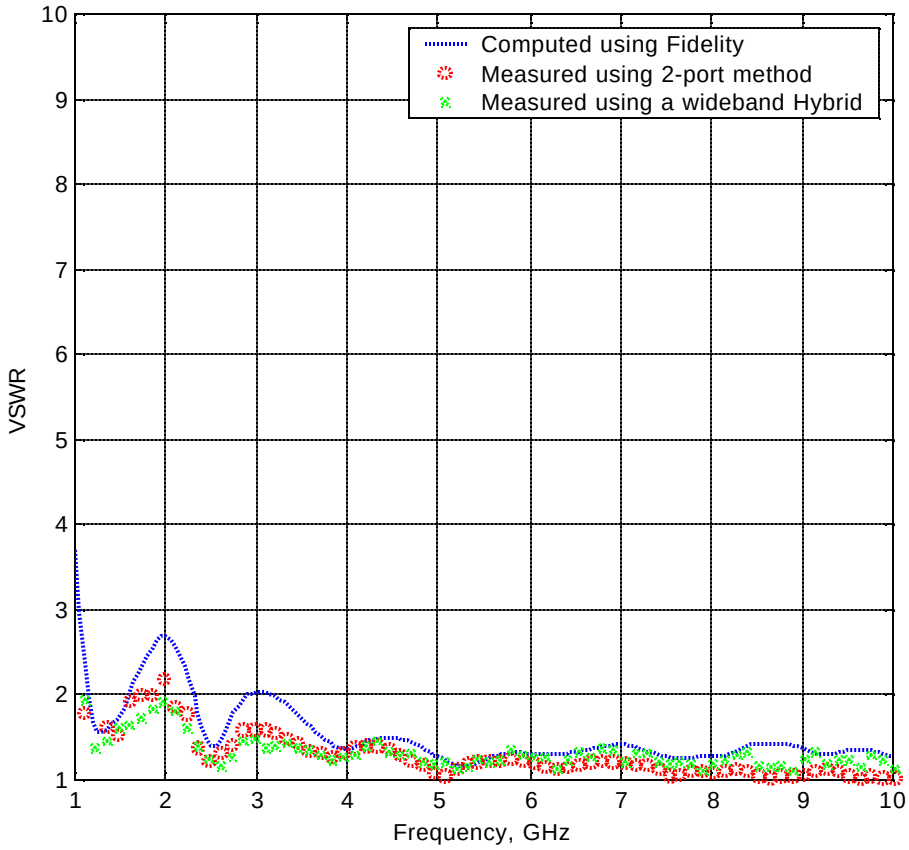

(b) Computed and measured (2-port and 1-port methods) VSWR (referenced to 100-Ω) of the LPdiPICA antenna in Figs. 7.5 and 7.6 with the dimensions listed in Table 7.1.

Figure 7.8 Computed and measured antenna impedance and VSWR (referenced to 100-Ω) of the LPdiPICA antenna in Figs. 7.5 and 7.6 with the dimensions listed in Table 7.1.

7.3.4 Radiation Pattern of the LPdiPICA model I

The same computational and experimental techniques were used for the low-profile diPICA antenna as were used for the Fourtear antenna; see Chapter 5. Many radiation patterns of the LPdiPICA antenna were computed and measured over the wide bandwidth from 1 to 8 GHz. An infinite ground plane was used for simulating the low-profile diPICA antenna with Fidelity to save the computational time.

In the experiments, a 431.8 mm x 431.8 mm (17" × 17") finite ground plane was used, which is equivalent to 1.4 λ x 1.4 λ at the low frequency of 1.0 GHz. The size of the ground plane is large enough to obtain an acceptable unidirectional pattern from the low-profile diPICA antenna.

Selected computed radiation patterns at the frequencies of 1.0, 2.0, 3.0, 4.0, 6.0 and 8.0 GHz are presented in Fig. 7.9. The measured radiation patterns for the low-profile diPICA are presented in Fig. 7.10 at the same frequencies plus several more. When we consider the difference in the size of the ground plane between simulation and measurement, they can be considered to agree reasonably well. The radiation patterns are presented at two principal planes of $\phi = 0°$ (xz-plane) and $\phi = 90°$ (yz-plane), i.e. the E- and H-planes; see Fig. 7.5.

The results show that the radiation patterns are changing as the frequency increases. In other words as the electrical height of the radiating element above the ground plane increases, the radiation patterns are changing due to a diverse field interaction between direct and reflected wave components near the radiating element. It can be analyzed using an image theory [7.1]. The effect of electrical height on the elevation pattern was investigated in [7.2] using an infinitesimal dipole antenna above an infinite perfect ground plane. Note that the elevation patterns of the diPICA antenna at frequencies of 1.0, 2.0, 3.0, 4.0 and 8.0 GHz are similar to the patterns of an infinitesimal electric dipole at electrical height of λ/8, λ/4, 3λ/8, λ/2 and λ above an infinite perfect ground plane. And the actual electrical height, 'h' of the low-profile diPICA antenna at the each frequency (1.0, 2.0, 3.0, 4.0 and 8.0 GHz) is very close to the electrical height above (λ/8, λ/4, 3λ/8, λ/2 and λ) respectively.

The low-profile diPICA antenna provides excellent unidirectional pattern from 1.0 to 2.2 GHz, which is corresponding to the electrical height of h = $\lambda/8 \sim \lambda/4$. Beyond the frequency, a null was generated at bore-sight and it was deepen as the frequency increases up to 3.6 GHz. Specifically, at 3.6 GHz which is 0.46λ in electrical length (close to $\lambda/2$), the perfect field cancellation was occurred at the bore-sight so very deep null was generated in the direction of the bore-sight. The experimental results demonstrate that the image theory is exactly applied to the LPdiPICA antenna.

At the higher frequency, from 4.0 to 8.0 GHz, additional lobes were generated and the number of lobes is increasing as the frequency increases. The number of lobes at the frequencies is similar to the estimated number of lobes described in [7.2].

Computed maximum gain vs. frequency plot is presented in Fig. B5 in Appendix B. Gain patterns can be directly obtained by adding the maximum gain number to the normalized radiation patterns.

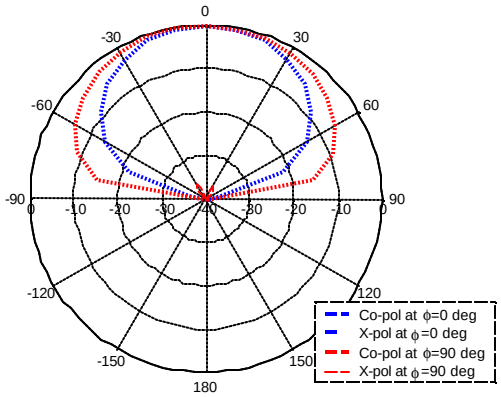

(a) 1.0 GHz (h = λ/8)

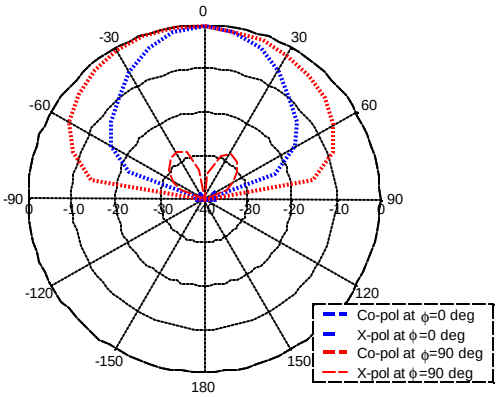

(b) 2.0 GHz (h = λ/4)

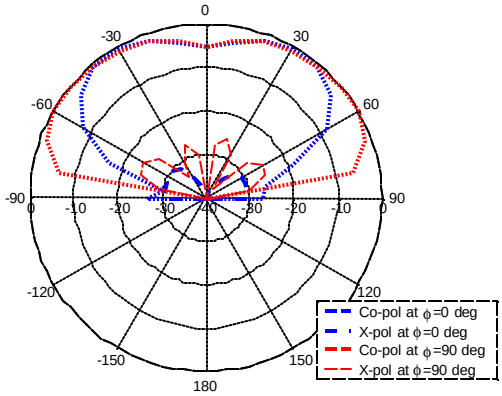

(c) 3.0 GHz (h = 3λ/8)

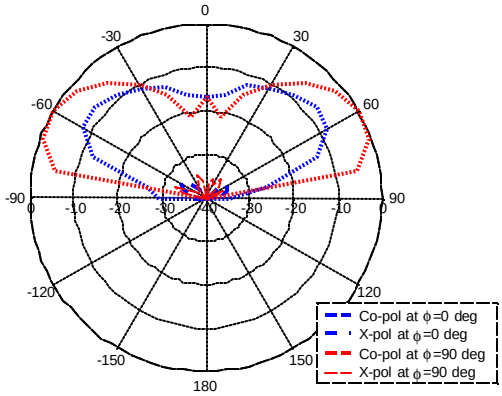

(d) 4.0 GHz (h = λ/2)

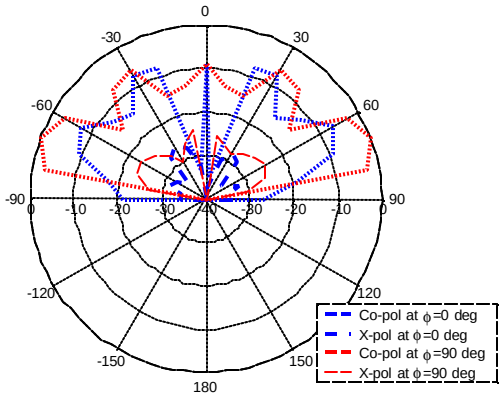

(e) 6.0 GHz (h = 3λ/4)

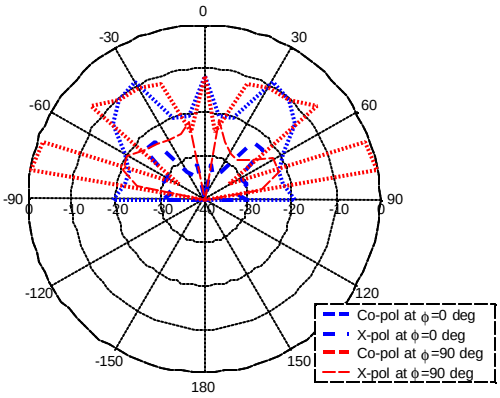

(f) 8.0 GHz (h = λ)

Figure 7.9 Computed radiation patterns of a LPdiPICA antenna model I in Figs. 7.5 and 7.6 with h=1.5".

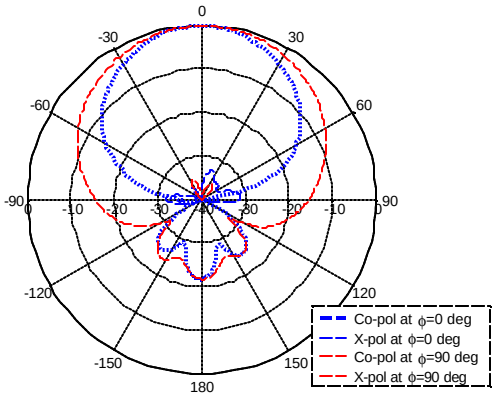

(a) 1.0 GHz (h = λ/8)

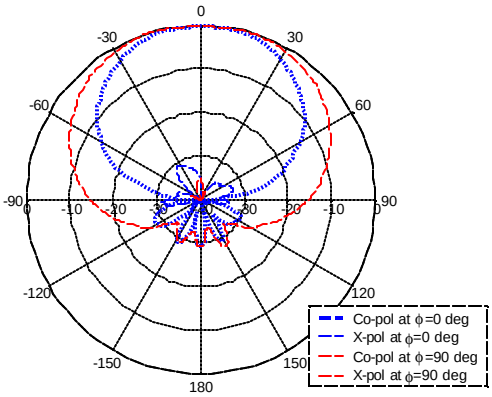

(b) 1.4 GHz

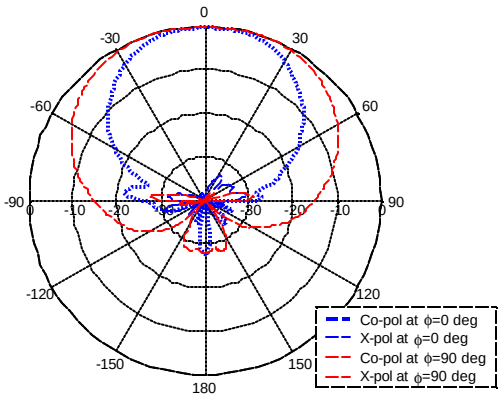

(c) 1.8 GHz

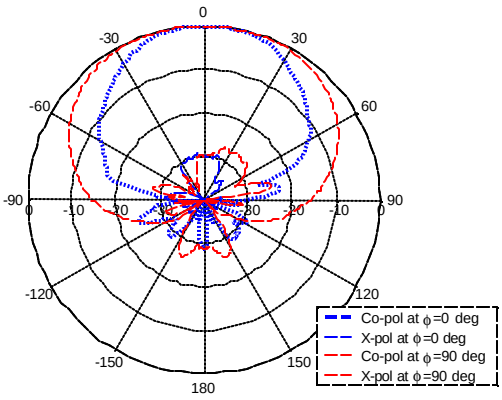

(d) 2.0 GHz (h = λ/4)

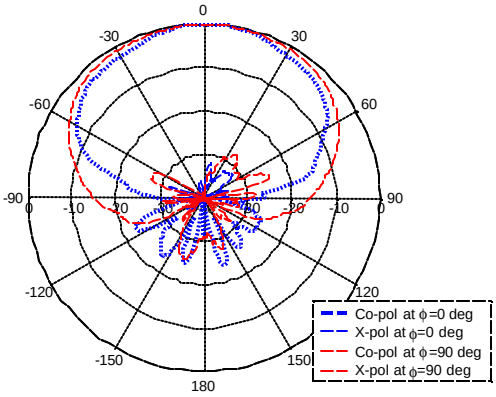

(e) 2.2 GHz

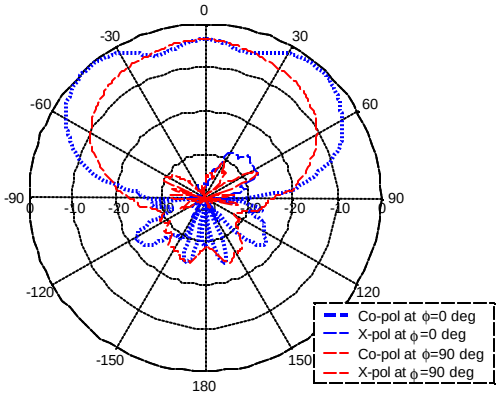

(f) 2.4 GHz

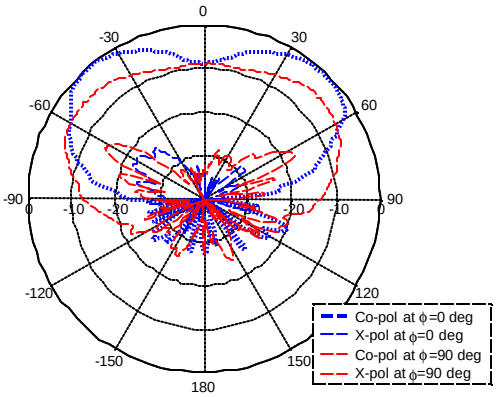

(g) 2.8 GHz

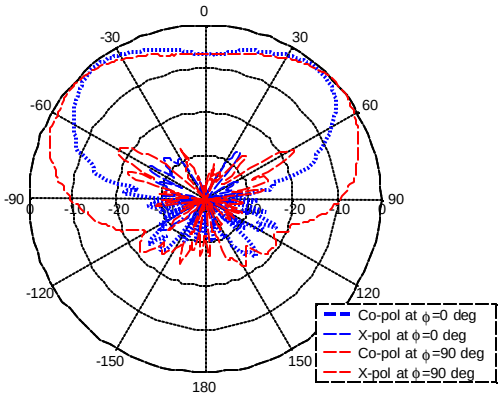

(h) 3.0 GHz (h = 3λ/8)

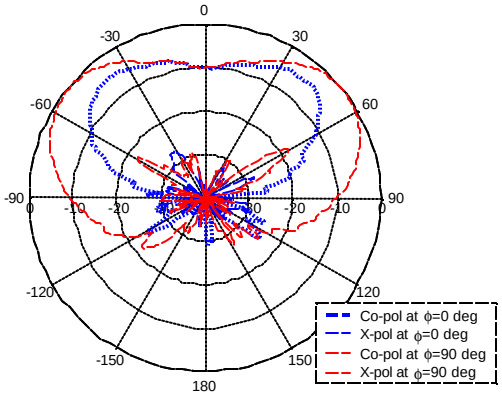

(i) 3.2 GHz

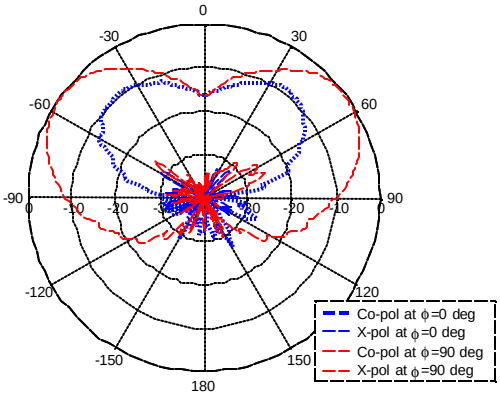

(j) 3.4 GHz

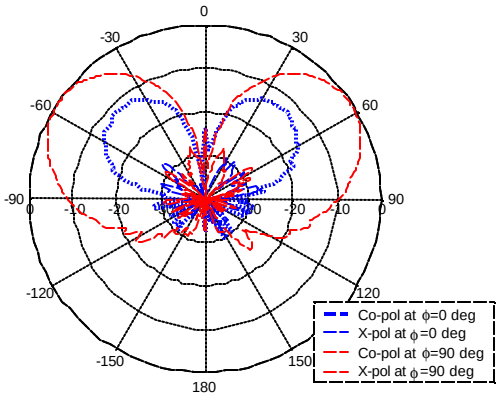

(k) 3.6 GHz

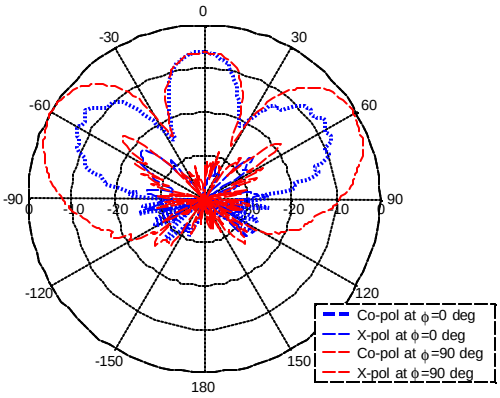

(l) 4.0 GHz (h = λ/2)

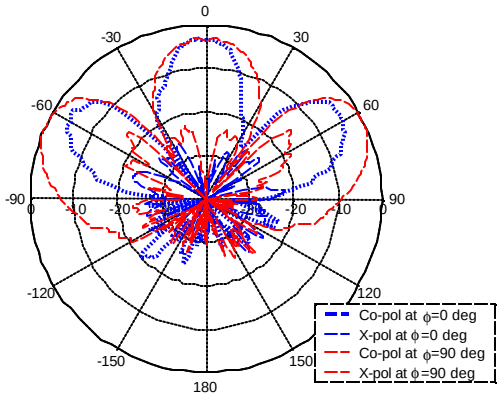

(m) 4.5 GHz

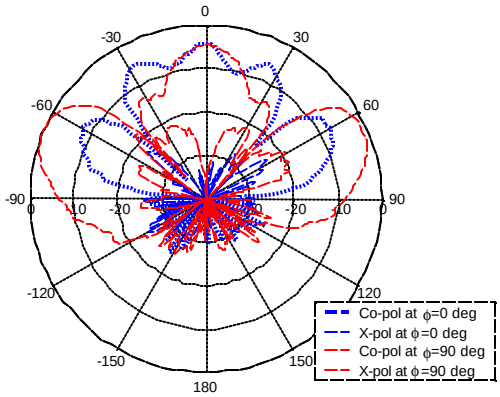

(n) 5.0 GHz

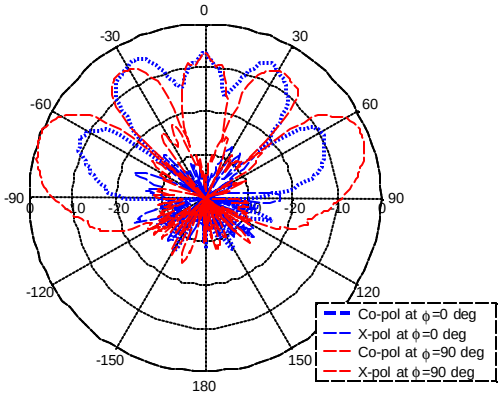

(o) 5.5 GHz

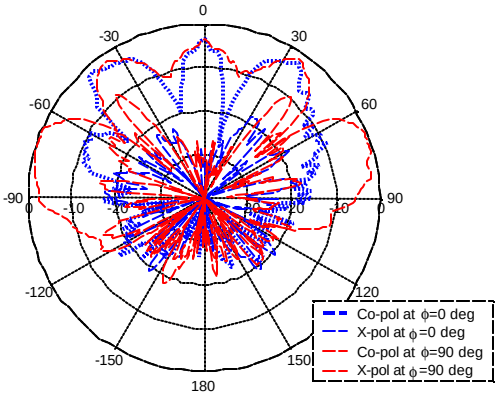

(p) 6.0 GHz (h = 3λ/4)

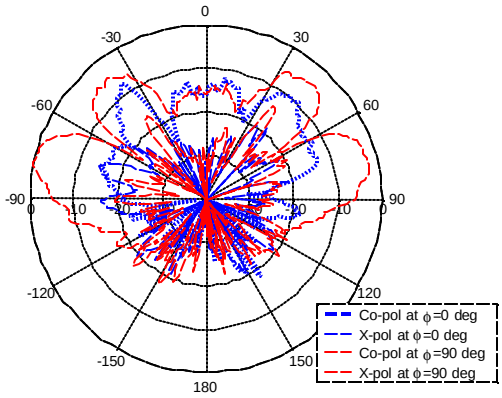

(q) 7.0 GHz

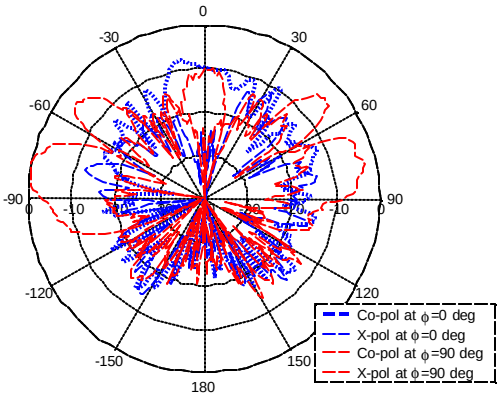

(r) 8.0 GHz (h = λ)

Figure 7.10 Measured radiation patterns of a LPdiPICA antenna model I in Figs. 7.5 and 7.6 with h=1.5".

7.3.5 Summary

The LPdiPICA antenna discussed in this section provides extremely wide impedance bandwidth of more than 10:1, but the radiation patterns are degraded as the frequency increases. The pattern degradation at high end of the band is caused by increase of electrical height as the frequency increases. Based on the investigation of the radiation pattern, the radiation patterns of the LPdiPICA antenna is similar to the one of an infinitesimal dipole antenna for various heights above the ground plane. Similar pattern changing phenomenon was observed in both antennas. The computed and measured results of the LPdiPICA antenna demonstrate that the LPdiPICA antenna operates like the several segment of the dipole antenna in a single element. So the LPdiPICA antenna has a great potential to be used as a wideband antenna providing omni-directional pattern.

In Section 7.4, the height effect in the LPdiPICA was examined by reducing the element height to half (h = 0.75") of the height, 1.5" used in this section.

7.4 A Low-Profile diPICA Antenna Test Model II

In order to examine the effect of the height 'h', a reduced height, h = 0.75" was examined to the LPdiPICA antenna whereas the height h = 1.50" was used in the Section 7.3 (see Table 7.1). Other than the height, the rest of the dimensions are same with the ones of LPdiPICA discussed in Section7.3.

The LPdiPICA with h = 0.75" was computed with the Fidelity code. The computed antenna impedance and the radiation patterns are presented in Figs. 7.11 and 7.12, respectively. The computed antenna impedance are compared with the LPdiPICA with h = 1.50" in Fig. 7.11(a). The impedance characteristics are very similar each other except at the frequency band of from 1.0 to 4.0 GHz. For the LPdiPICA with h = 0.75", the variation of the impedance level is more severe than the LPdiPICA with h = 1.50" so that the VSWR of the LPdiPICA with h = 0.75" was degraded than the LPdiPICA with h = 1.50". However, the radiation patterns of the LPdiPICA with h = 0.75"are improved at high frequency such as at 3.0 – 6.0 GHz as shown in Fig. 7.12. Note that the electrical height in the parenthesis is half of the electrical height parenthesized in Fig. 7.9. There is a trade-off relationship between VSWR and radiation patterns as the height has been reduced.

The simulation results demonstrate that the performance of the LPdiPICA antenna is dependent on the height of the element above the ground plane. When the electrical height is kept as $\lambda/4$ over entire band, the LPdiPICA antenna should be able to enhance the radiation pattern toward high end of the band without degrading the impedance performance. A possible method for accomplishing the constant electrical height is to employ a tapered ground plane from top to bottom. The detail investigation will be discussed in Section 7.6.

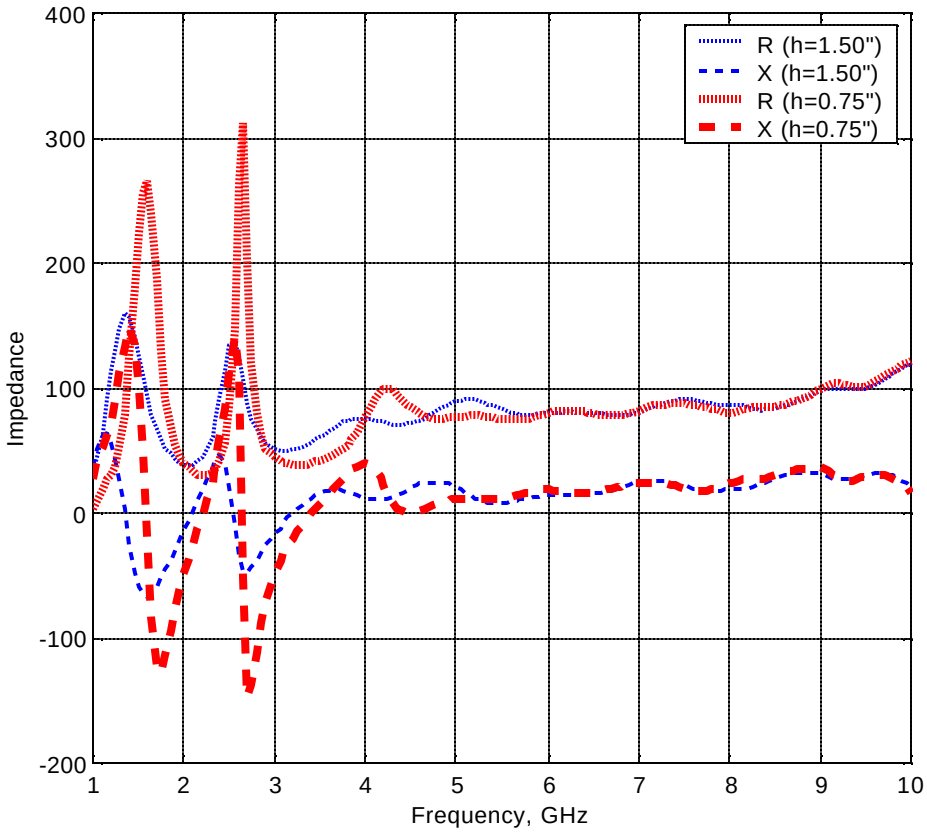

(a) Antenna impedance.

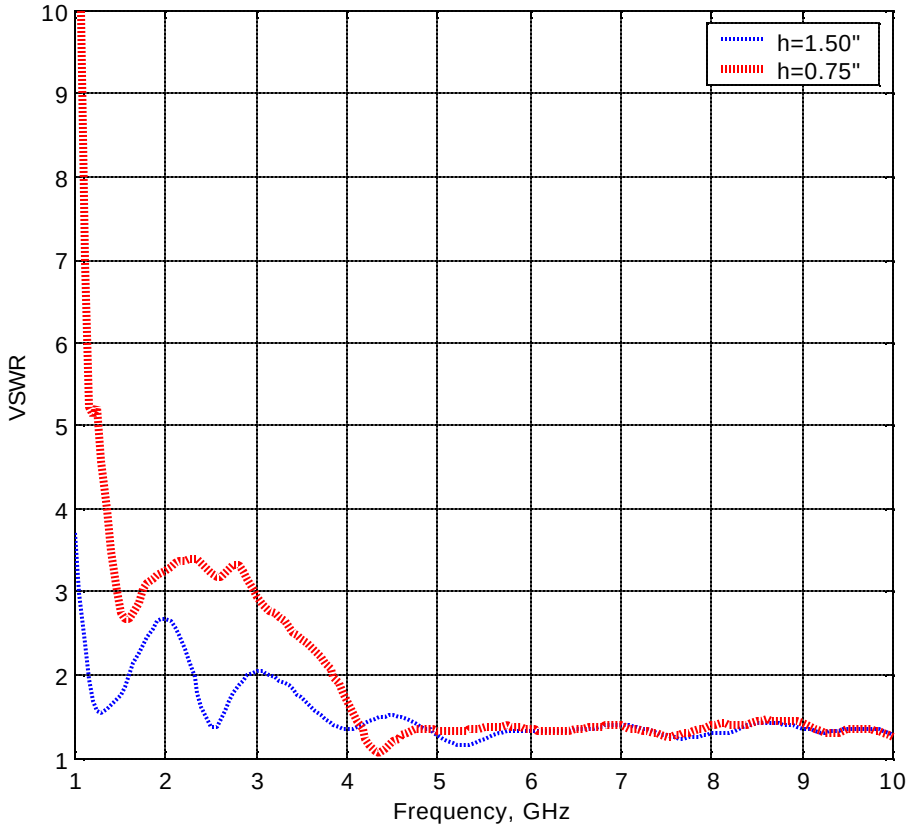

(b) VSWR referenced to 100-Ω.

Figure 7.11 Computed antenna impedance and VSWR (referenced to 100-Ω) of the LPdiPICA antenna model II in Figs. 7.5 and 7.6 with h=0.75" (thick curve) and 1.50" (thin curve).

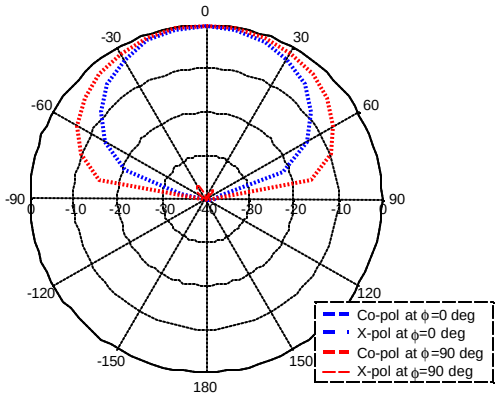

(a) 1.0 GHz (h = λ/16)

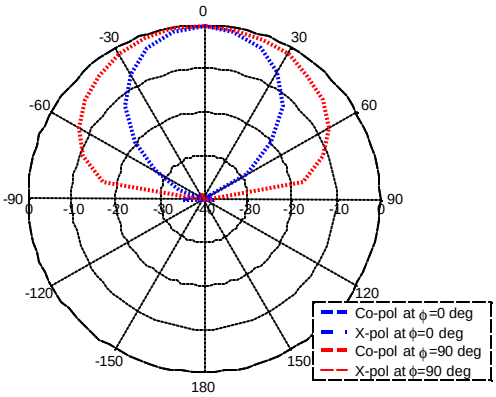

(b) 2.0 GHz (h = λ/8)

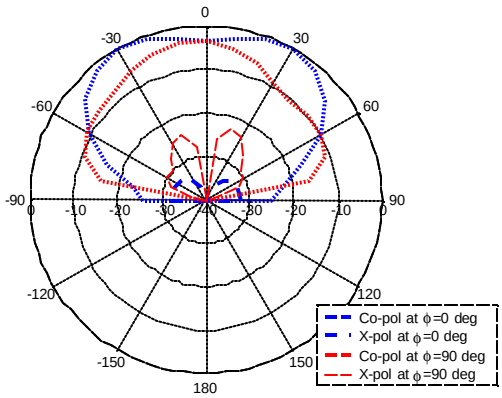

(c) 3.0 GHz (h = 3λ/16)

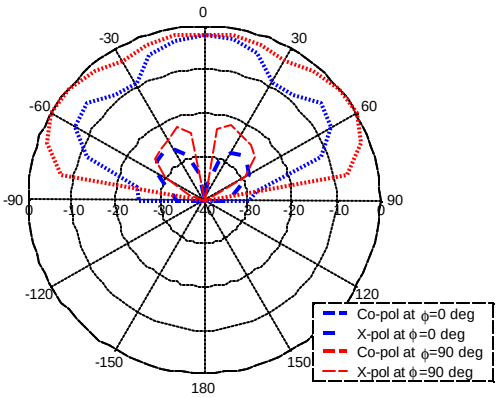

(d) 4.0 GHz (h = λ/4)

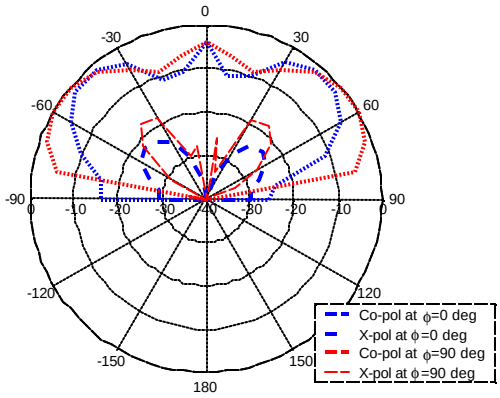

(e) 6.0 GHz (h = 6λ/16)

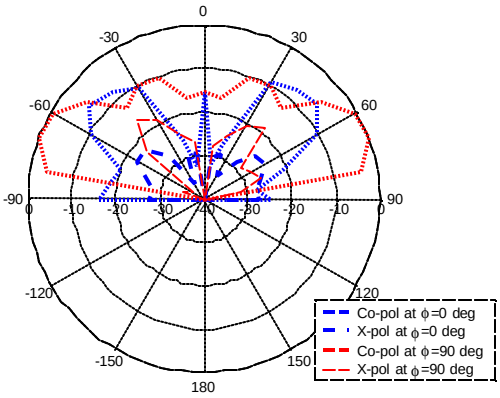

(f) 8.0 GHz (h = λ/2)

Figure 7.12 Computed radiation patterns of the LPdiPICA antenna model II in Figs. 7.5 and 7.6 with h=0.75".

7.5 A Low-Profile diPICA Antenna Test Model III

Another hard ware test model of the wideband low-profile diPICA antenna is presented in Fig. 7.13 with the dimensions listed in Table 7.1. The antenna structure is described in Fig. 7.14. The two-circular-hole diPICA antenna was used for the radiating element with the dimensions displayed in Fig. 7.2. The two-circular-hole diPICA antenna was backing with a finite ground plane with the size of 431.8 mm x 431.8 mm (17" x 17"). The radiating element is mounted above the ground plane with the height of 1.5". The two-circular-hole LPdiPICA antenna was constructed and measured using the same technique described in Section 7.3.

The two-circular-hole LPdiPICA antenna was simulated using the Fidelity code. Measurement were made using HP 8720C network analyzer and an Antcom near field system for the impedance and radiation patterns, respectively. Same computational and experimental set ups were used as presented in Section 7.3.2.

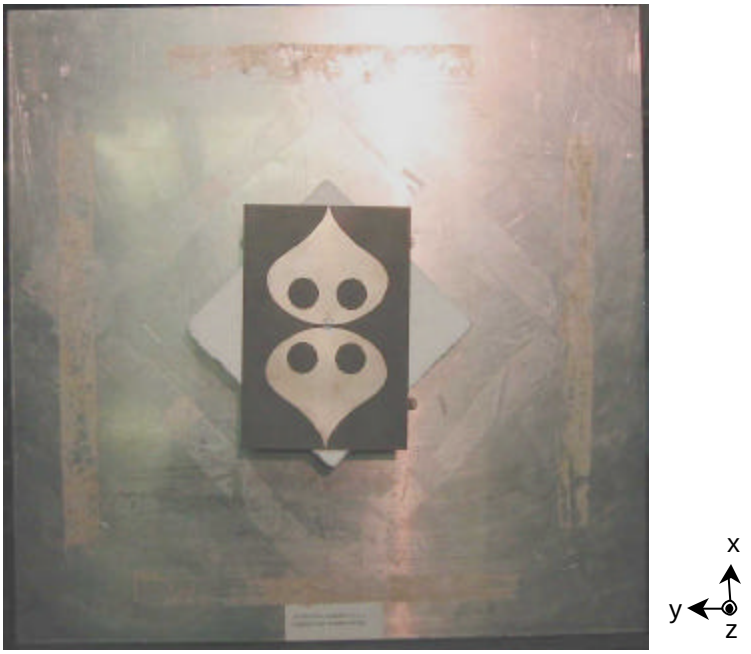

Figure 7.13 A two-circular-hole LPdiPICA antenna hardware test model III.

Table 7.2

Dimensions of the two-circular-hole LPdiPICA antenna model III of Figs. 7.13 and 7.14.

Description	Symbol	Size
Element vertical length	A	153.67 mm (6.05”)
Element horizontal length	D	76.7 mm (3.02”)
Diameter of the circular hole	d	20.32 mm (0.8”)
Vertical distance of the circular holes	S1	40.64 mm (1.6”)
Horizontal distance of the circular holes	S2	30.48 mm (1.2”)
Substrate thickness	t_s	0.79 mm (0.031”)
Foam thickness	t_d	37.3 mm (1.47”)
Element height above ground plane	h	38.1 mm (1.50”)
Feed positions distance	F’	2.3 mm (0.09”)
Feed (Semi-Rigid Coaxial Cable)	RG 405 /U	Outer diameter: 2.2 mm (0.087”)

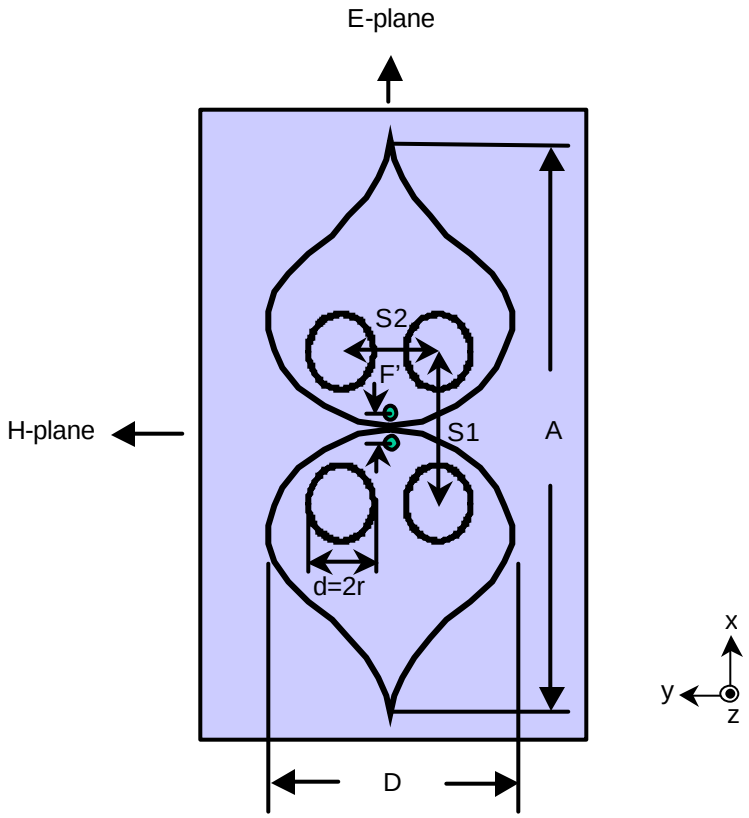

(a) Top view.

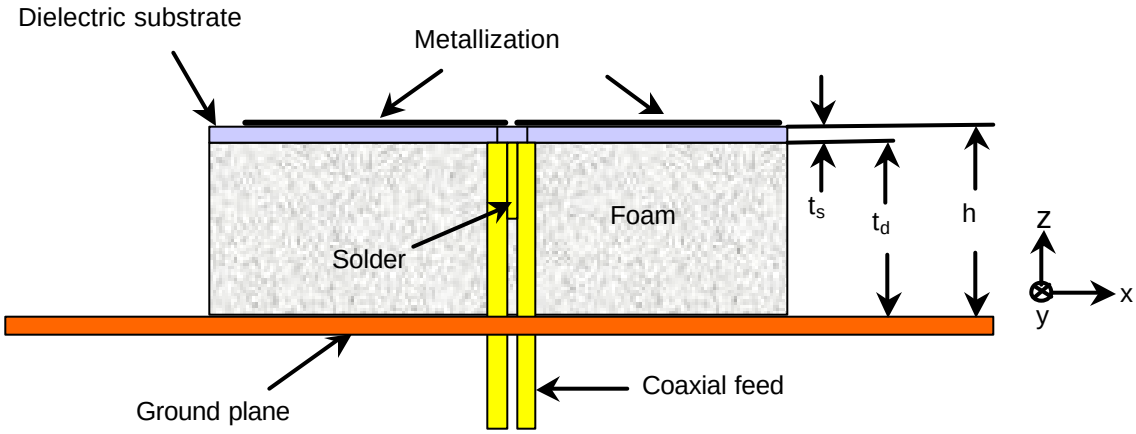

(b) Side view.

Figure 7.14 The structure of the two-circular-hole LPdiPICA antenna.

7.5.1 Impedance Properties of the LPdiPICA model III

The impedance properties are presented in Fig. 7.15(a) with computed and measured data. They are agreed very well each other. The antenna characteristics are very similar to the LPdiPICA antenna discussed in Section 7.3.3 (see Fig. 7.8). The resistive component is near the 100-Ω and the reactive component is within ±50-Ω so that the two-circular-hole LPdiPICA antenna provides extremely wide impedance bandwidth.

The VSWR of the two-circular-hole LPdiPICA antenna was also measured with both 2-port method and 1-port method (using the wideband 180° hybrid) as discussed in Section 7.3.3 so that the measured data can be confirmed each other. The computed VSWR is compared with the two measured data in Fig. 7.15 (b). All three data are agreed very well each other giving more than 10:1 impedance bandwidth. VSWR were referenced to 100-Ω.

The experimental results are similar to the ones of the LPdiPICA antenna without holes presented in Fig. 7.8. It means that the properly positioned circular holes in the LPdiPICA antenna minimally affect on the antenna impedance.

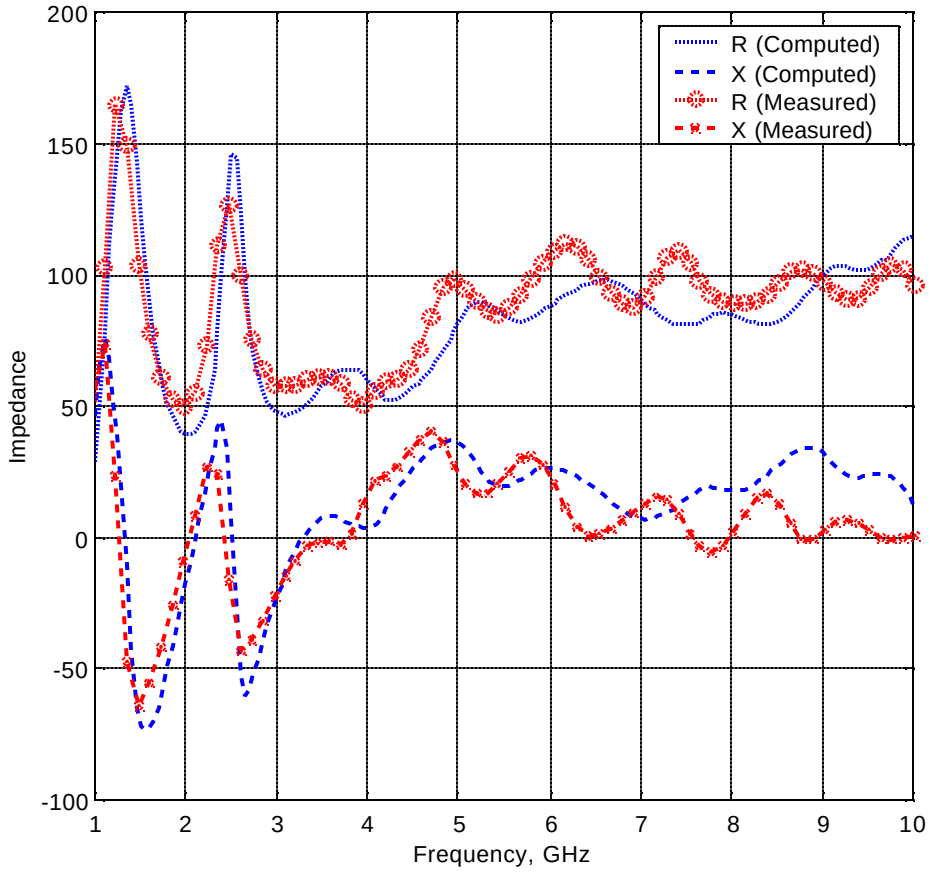

(a) Computed and measured (2-port method) antenna impedance.

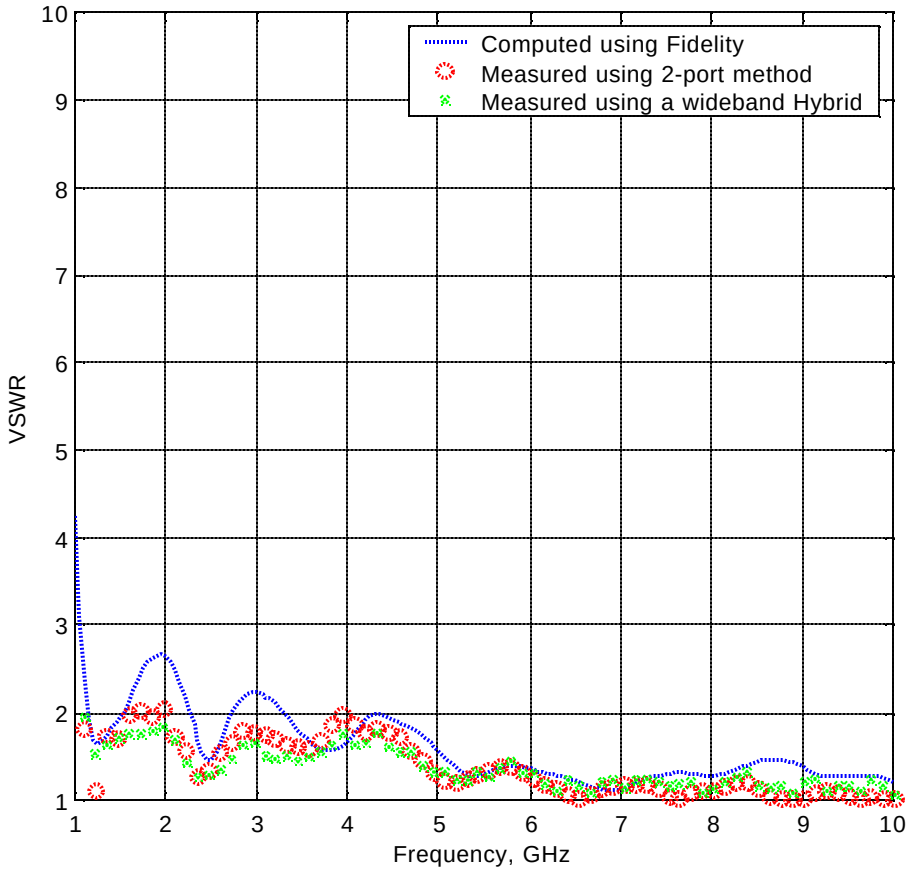

(b) Computed and measured (2-port and 1-port methods) VSWR referenced to 100-Ω.

Figure 7.15 Computed and measured antenna impedance and VSWR (referenced to 100-Ω) of the two-circular-hole LPdiPICA antenna in Figs. 7.13 and 7.14 with the dimensions displayed in Table 7.2.

7.5.2 Radiation Pattern of the LPdiPICA model III

Radiation patterns of the two-circular-hole LPdiPICA antenna were computed and measured at the several frequencies. The same experimental set up and computational techniques are used as the LPdiPICA antenna in Section 7.3. Selected computed radiation patterns of 1.0, 2.0, 3.0, 4.0, 6.0 and 8.0 GHz are presented in Fig. 7.16. Measured elevation patterns are presented in Fig. 7.17 at the same frequencies plus several more. The electrical height between the ground plane and the radiating element is also noted in the Figure using a parenthesis. Note that the mechanical height, h is 1.50". Even though an infinite ground plane was employed in simulation, a finite ground plane with a dimension of 431.8 mm x 431.8 mm (17" x 17") was used in measurement. When we consider the difference in the size of the ground plane, the radiation patterns in Figs. 7.16 and 7.17 are relatively agreed well each other.

The two-circular-hole LPdiPICA antenna provides excellent unidirectional pattern from 1.0 to 2.2 GHz, which is corresponding to the electrical height of $\lambda/8 \sim \lambda/4$. The elevation patterns of the two-circular-hole LPdiPICA are changing as the frequency increases just as the LPdiPICA antenna without the holes discussed in Section 7.3. At the similar frequency, the null and lobes are generated in the similar direction.

A difference, however, is observed in the pattern of the two-circular-hole LPdiPICA antenna; that is beyond the frequency of 4.0 GHz, the lobe in the direction of the bore-sight is noticeably stronger than the LPdiPICA antenna without circular holes; compare Fig. 7.10 (l)-(q) and Fig. 7.17 (l)-(q). The experimental results demonstrate that the circular holes in the LPdiPICA antenna affected on the radiation pattern positively in the direction of bore-sight. Even though only the simple circular holes are examined in this section, more extensive investigations are necessary for enhancing the radiation patterns using various geometries of the holes at several positions as a future work.

Computed maximum gain vs. frequency plot is presented in Fig. B6 in Appendix B. Gain patterns can be directly obtained by adding the maximum gain number to the normalized radiation patterns.

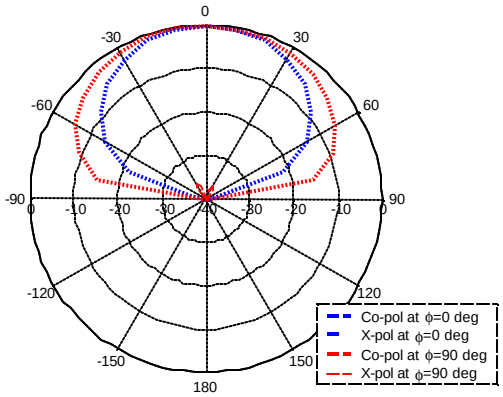

(a) 1.0 GHz (h = λ/8)

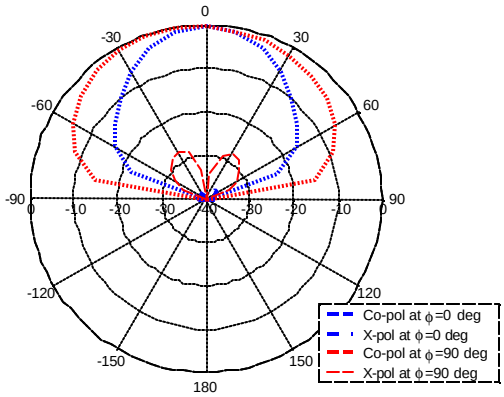

(b) 2.0 GHz (h = λ/4)

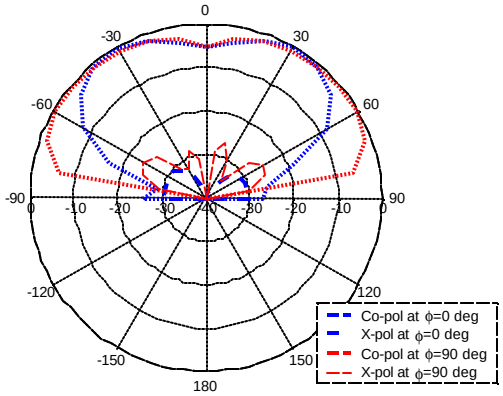

(c) 3.0 GHz (h = 3λ/8)

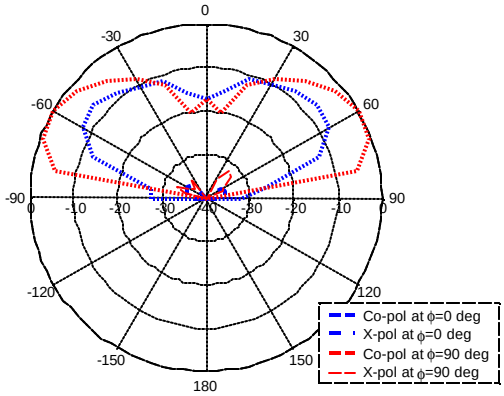

(d) 4.0 GHz (h = λ/2)

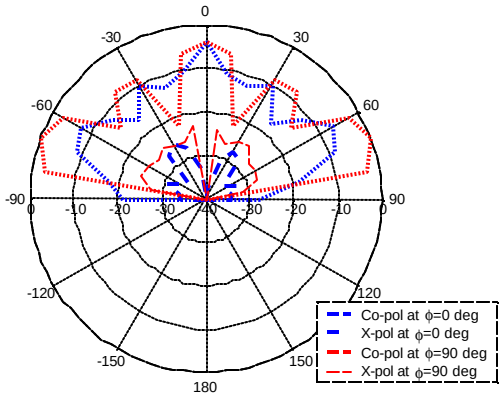

(e) 6.0 GHz (h = 3λ/4)

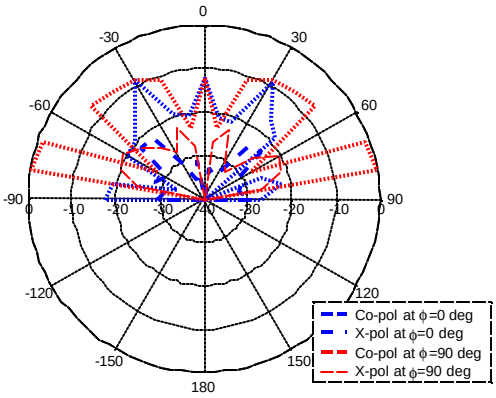

(f) 8.0 GHz (h = λ)

Figure 7.16 Computed radiation patterns of the two-circular-hole LPdiPICA antenna in Figs. 7.13 and 7.14 with the dimensions listed in Table 7.2.

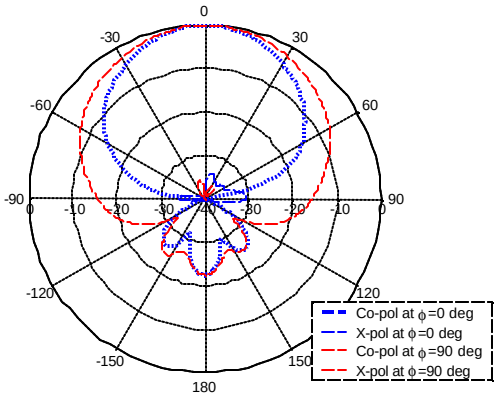

(a) 1.0 GHz (h = λ/8)

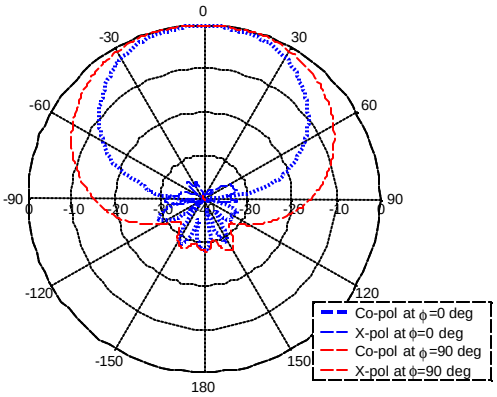

(b) 1.4 GHz

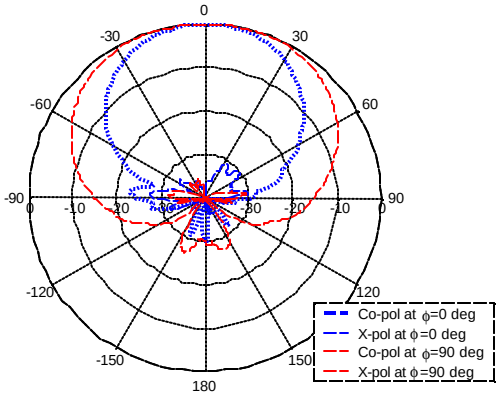

(c) 1.8 GHz

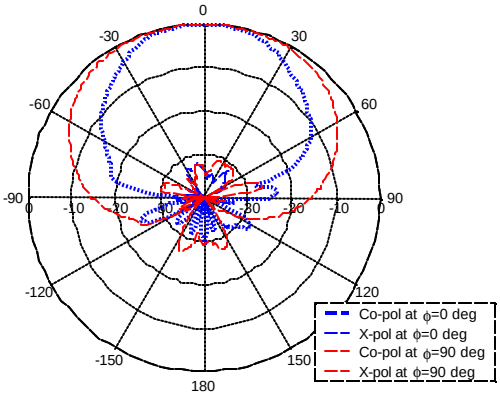

(d) 2.0 GHz (h = λ/4)

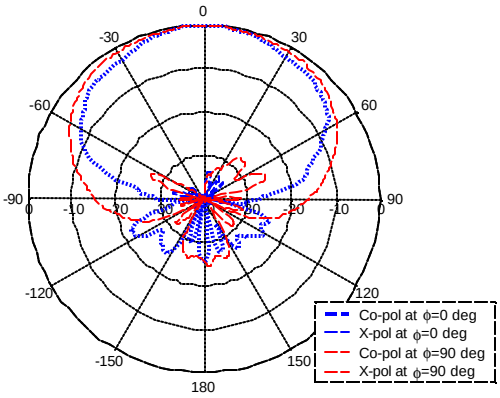

(e) 2.2 GHz

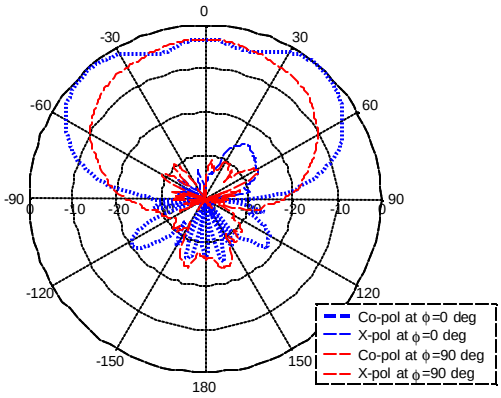

(f) 2.4 GHz

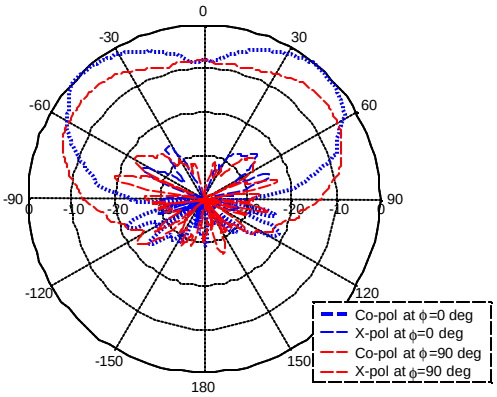

(g) 2.8 GHz

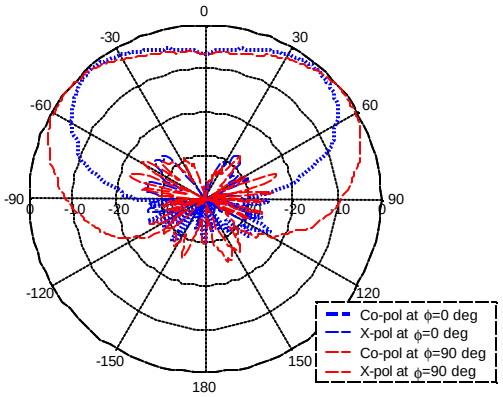

(h) 3.0 GHz (h = 3λ/8)

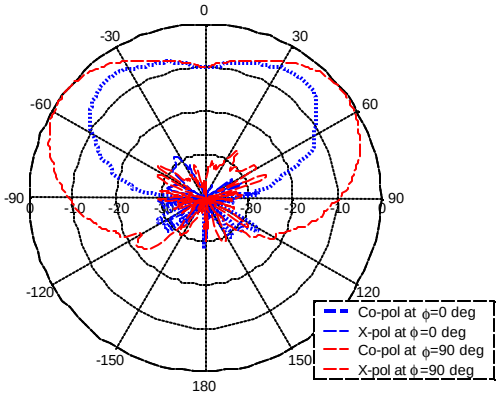

(i) 3.2 GHz

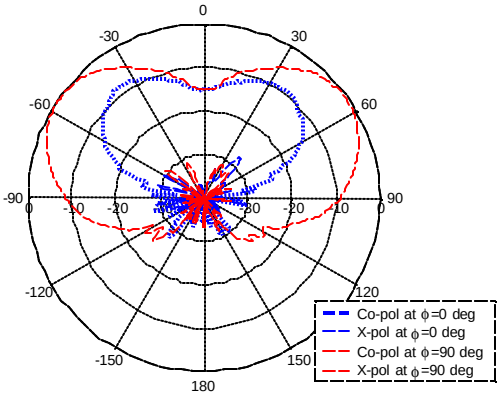

(j) 3.4 GHz

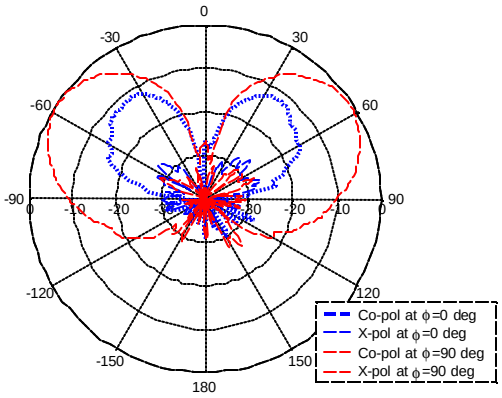

(k) 3.6 GHz

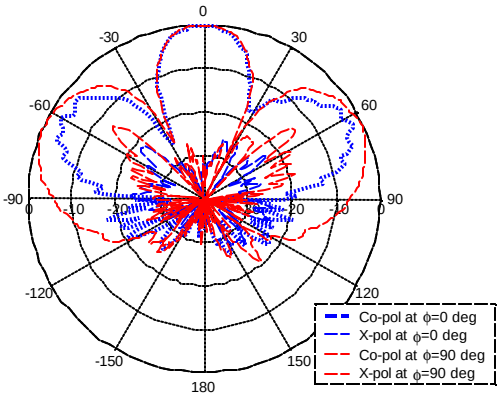

(l) 4.0 GHz (h = λ/2)

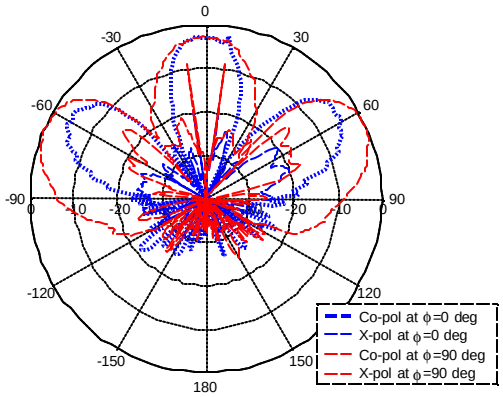

(m) 4.5 GHz

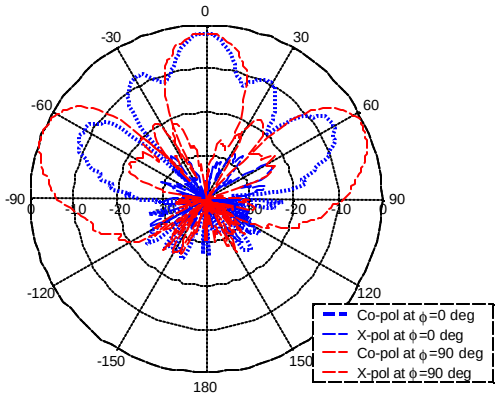

(n) 5.0 GHz

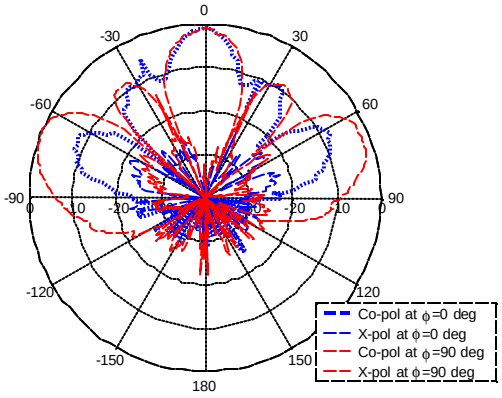

(o) 5.5 GHz

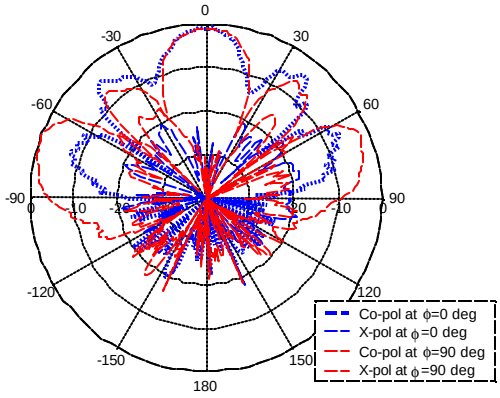

(p) 6.0 GHz

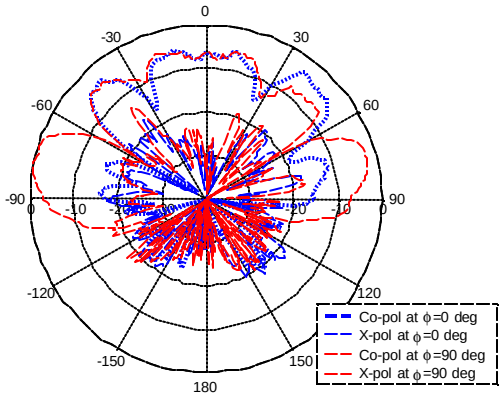

(q) 7.0 GHz

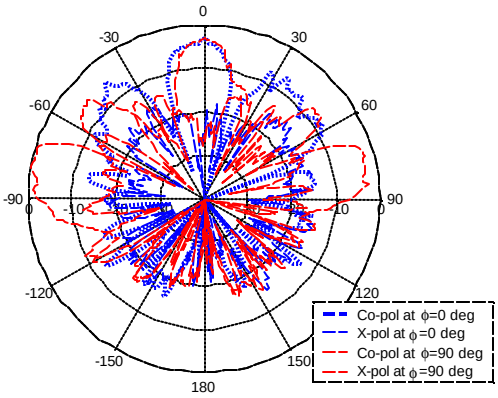

(r) 8.0 GHz (h = λ)

Figure 7.17 Measured radiation patterns of the two-circular-hole LPdiPICA antenna in Figs. 7.13 and 7.14 with the dimensions listed in Table 7.2.

7.6 A Low-Profile diPICA Antenna Test Model IV

Several LPdiPICA antenna models were investigated in the previous sections. The LPdiPICA antennas provide more than 10:1 impedance bandwidth for VSWR<2, but the radiation patterns are degraded as the frequency increases due to the increased electrical height above the flat ground plane at the high frequency. Generally, the good unidirectional patterns are obtained at the electrical height of $\lambda/4$. With the fixed and flat ground plane, the electrical height easily exceed the height of $\lambda/4$ at the mid and high frequencies.

As an attempt to obtain acceptable unidirectional pattern over the wide impedance bandwidth of 10:1, several tapered ground planes were proposed in this section rather than the fixed and flat ground plane and one of them is simulated using the Fidelity code. Basic concept of the tapered ground plane is for providing constant electrical height of $\lambda/4$ over entire impedance bandwidth.

The tapered ground planes are presented in Fig. 7.18. They are tapered in a various fashions such as linear, lognormal, exponential or multiple ground plane, etc. In order to examine the tapered ground plane effect, exponentially tapered ground plane was simulated with the two-circular-hole LPdiPICA antenna as shown in Fig. 7.19. The dimensions of the radiating element are listed in Table 7.2 and a slope of 1.5 e^{-2x} was used for the exponentially tapered ground plane. The Fidelity code was used to simulate the two-circular-hole LPdiPICA antenna with the exponentially tapered ground plane.

The simulation results are presented in Figs. 7.20 and 7.21 for the impedance and radiation patterns, respectively. Two cases (flat and exponentially tapered ground plane) are compared in the impedance and VSWR plot as shown in Fig. 7.20. The same radiating element is used in the simulation of two-circular-hole LPdiPICA as discussed in Section 7.5. The comparison data demonstrate that the exponentially tapered ground plane does not degrade the impedance performance at all. The VSWR are referenced to 100-Ω for both cases.

Meanwhile, the radiation patterns are improved at the high end of the band; compare the patterns at 6.0 and 8.0 GHz in Fig. 7.16 (e), (f) and 7.21 (e), (f) for flat and exponentially tapered ground planes, respectively. The patterns at the frequency of 6.0 and 8.0 GHz are much more acceptable to use for unidirectional pattern.

The simulation results in this section demonstrate that the exponentially tapered ground plane improved the radiation pattern without degrading the impedance performance. More investigation is necessary for enhancing the radiation pattern at the mid band by modifying the geometry of the exponentially tapered ground plane. Another geometry of the tapered ground plane proposed in Fig. 7.18 should be done as a future work.

Another possible method for enhancing the radiation pattern is the several layers of Frequency Selective Surfaces (FSS) in the LPdiPICA antenna. The Frequency Selective Surface operates as a ground plane at a desired frequency only. Otherwise the FSS is nothing but a free space. In order to utilize the FSS in the LPdiPICA antenna, the FSS should be placed in the order of FSS tuned at upper band to FSS tuned at lower band as presented in Fig. 7.22 [7.4]. The idea of using the FSS is to be investigated as a future work.

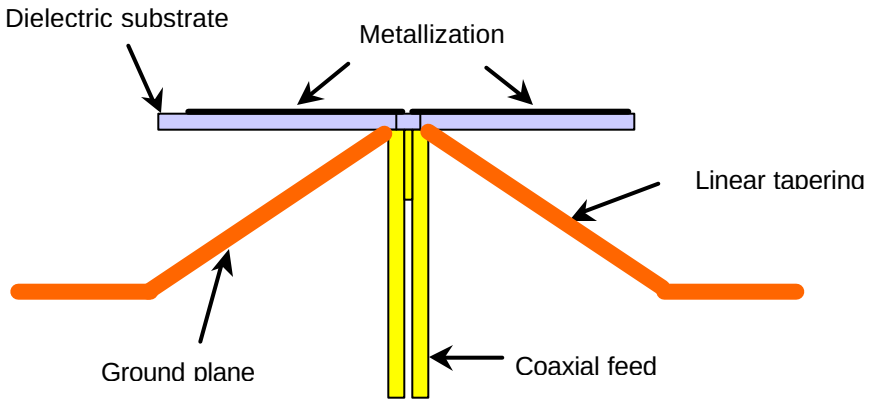

(a) Linearly tapered ground plane.

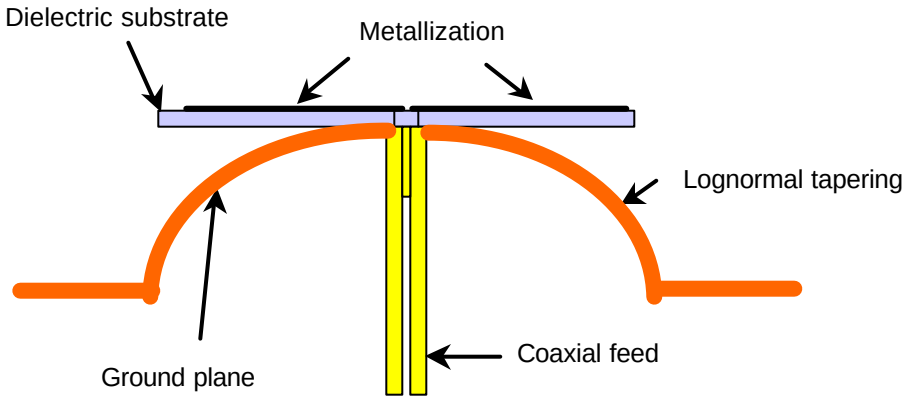

(b) Lognormally tapered ground plane.

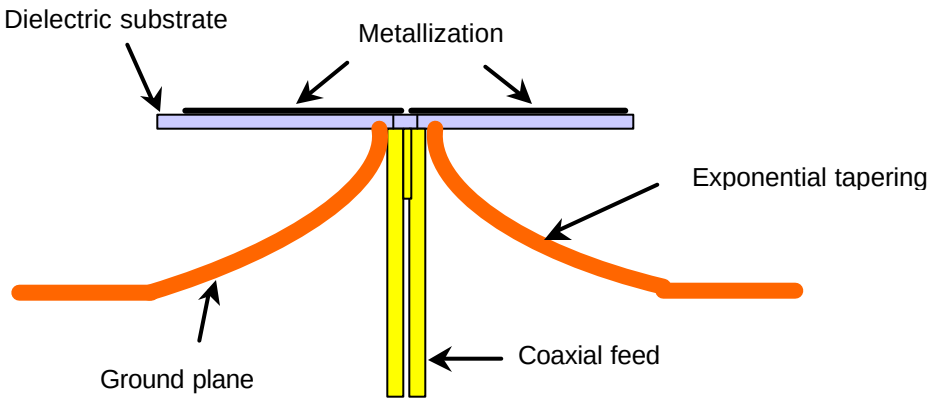

(c) Exponentially tapered ground plane.

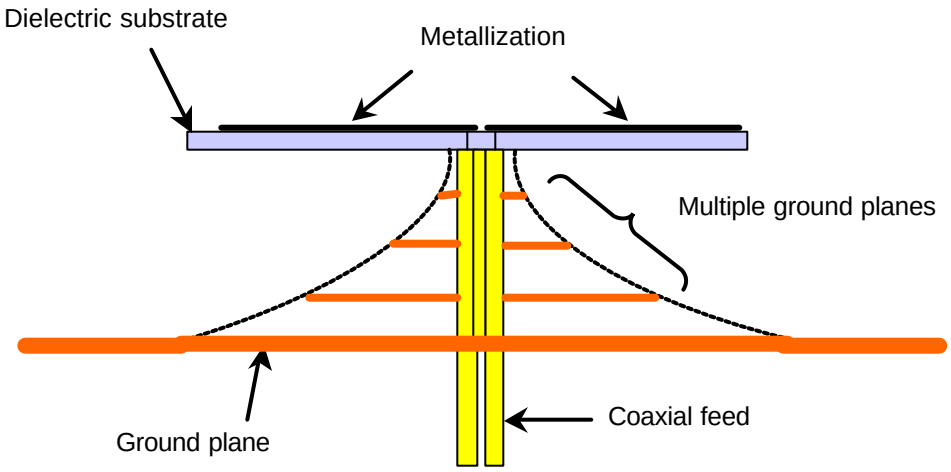

(d) Multiple ground planes.

Figure 7.18 Several tapered ground planes for the low-profile diPICA antenna.

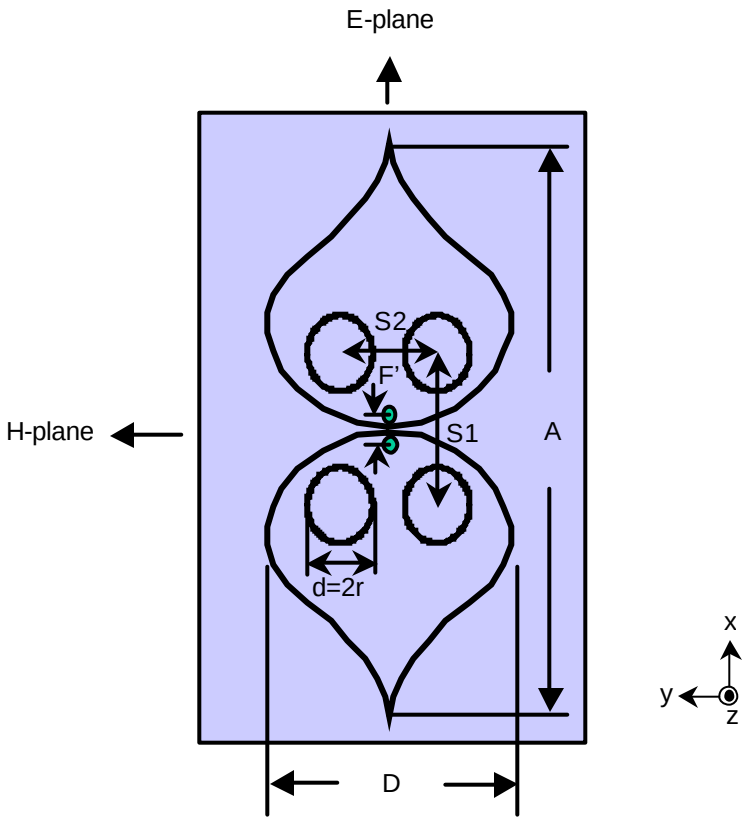

(a) Top view with the dimensions listed in Table 7.2.

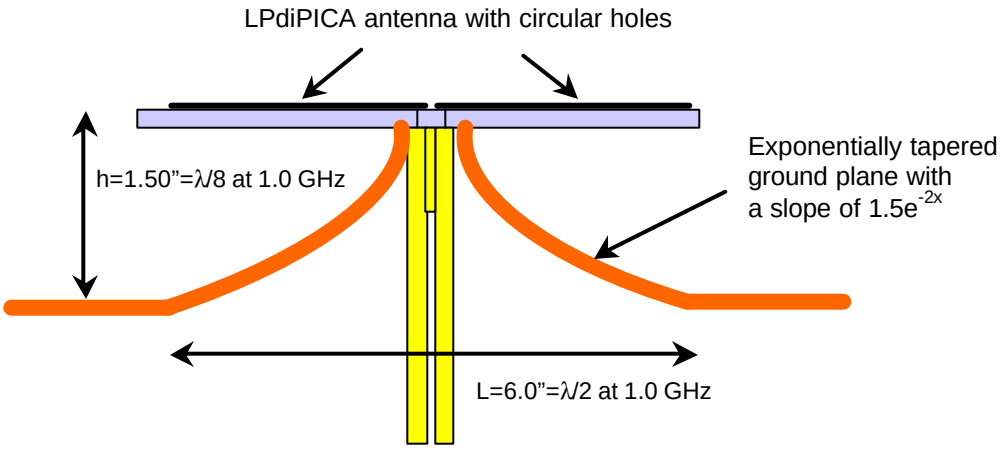

(b) Side view.

Figure 7.19 A two-circular-hole LPdiPICA antenna with the dimensions listed in Table 7.2 and with an exponentially tapered ground plane with a slope of 1.5 e^{-2x}.

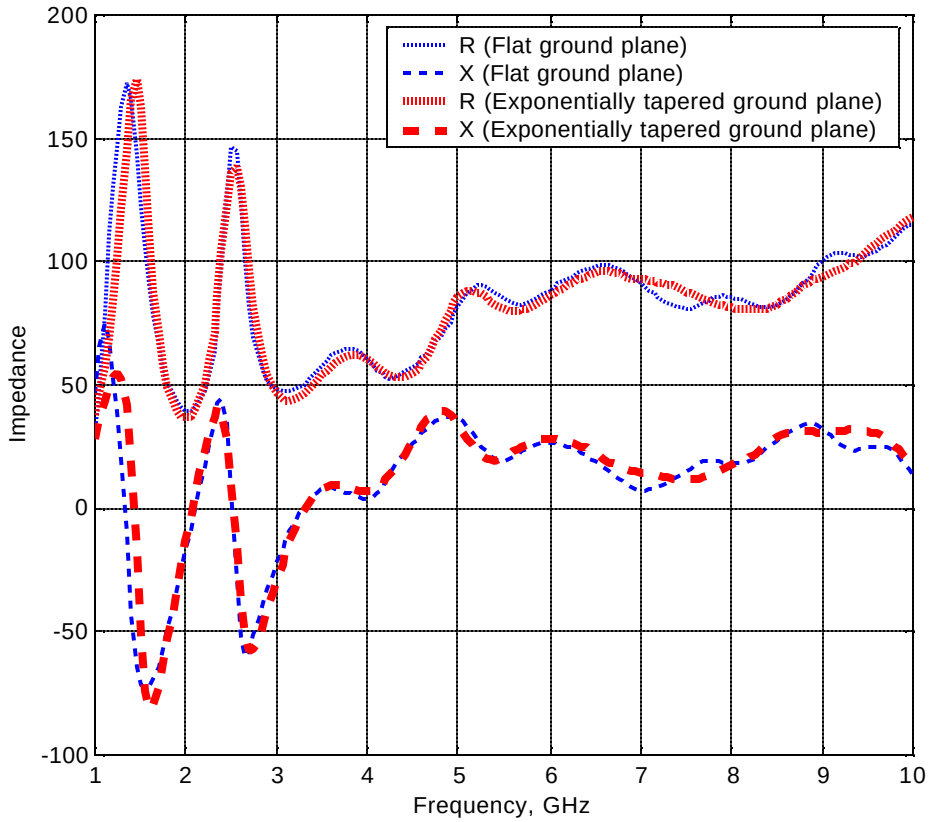

(a) Antenna impedance.

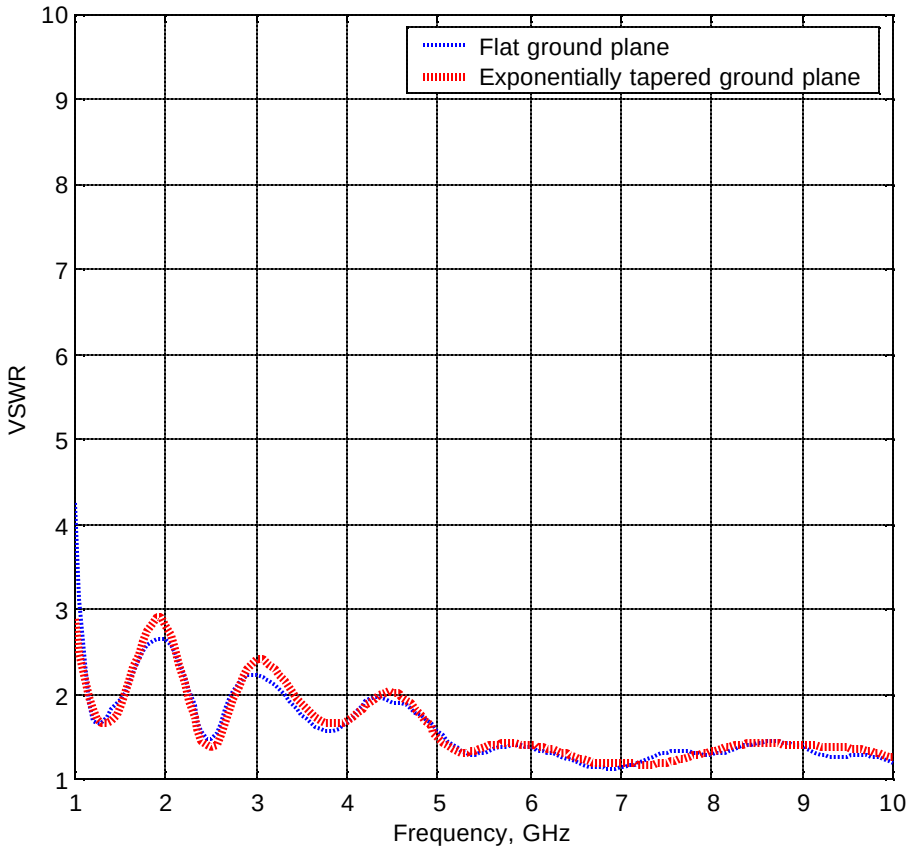

(b) VSWR referenced to 100-Ω.

Figure 7.20 Computed antenna impedance and VSWR (referenced to 100-Ω) of a LPdiPICA antenna with an exponentially tapered ground plane with a slope of 1.5 e^{-2x}.

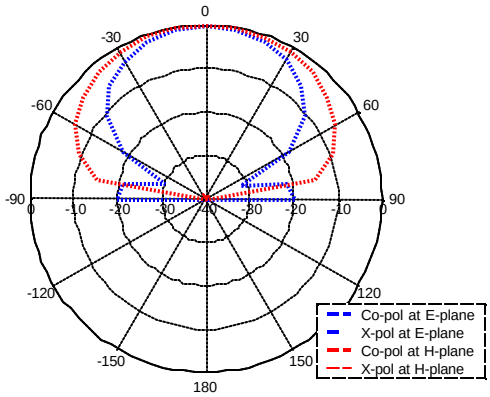

(a) 1.0 GHz (h = λ/8)

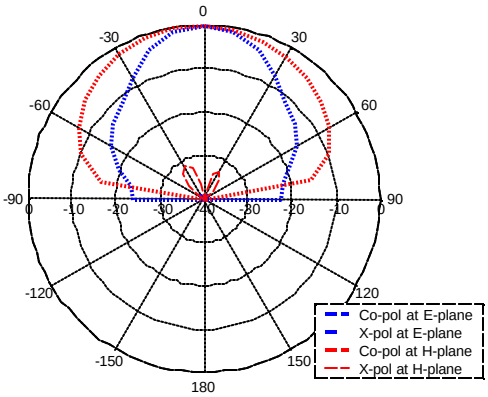

(b) 2.0 GHz (h = λ/4)

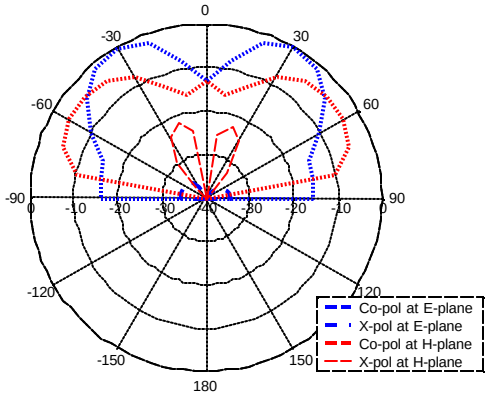

(c) 3.0 GHz (h = 3λ/8)

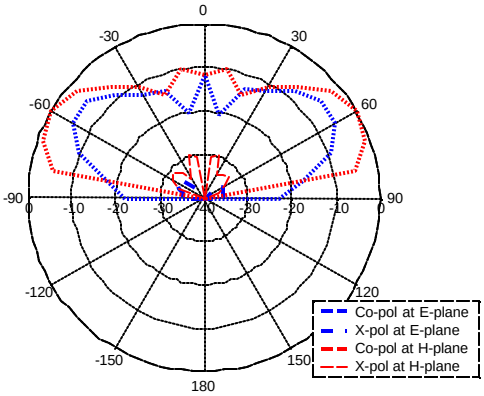

(d) 4.0 GHz (h = λ/2)

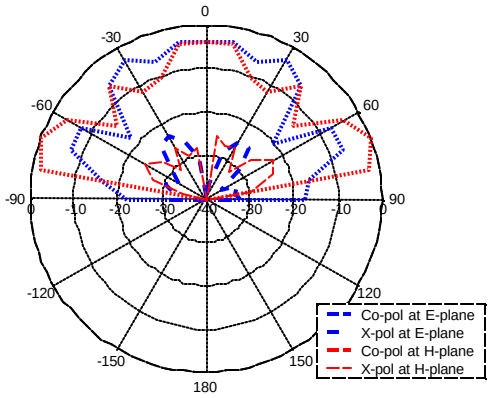

(e) 6.0 GHz (h = 3λ/4)

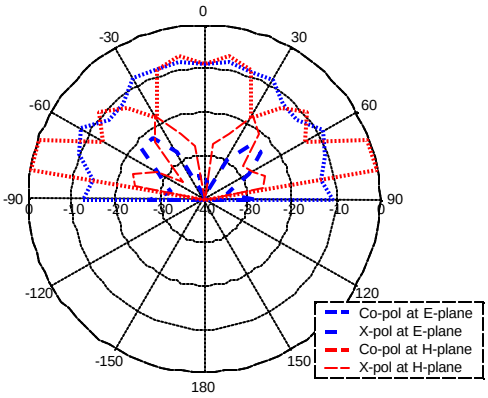

(f) 8.0 GHz (h = λ)

Figure 7.21 Computed radiation patterns of a low-profile diPICA antenna with an exponentially tapered ground plane with a slope of 1.5 e^{-2x}.

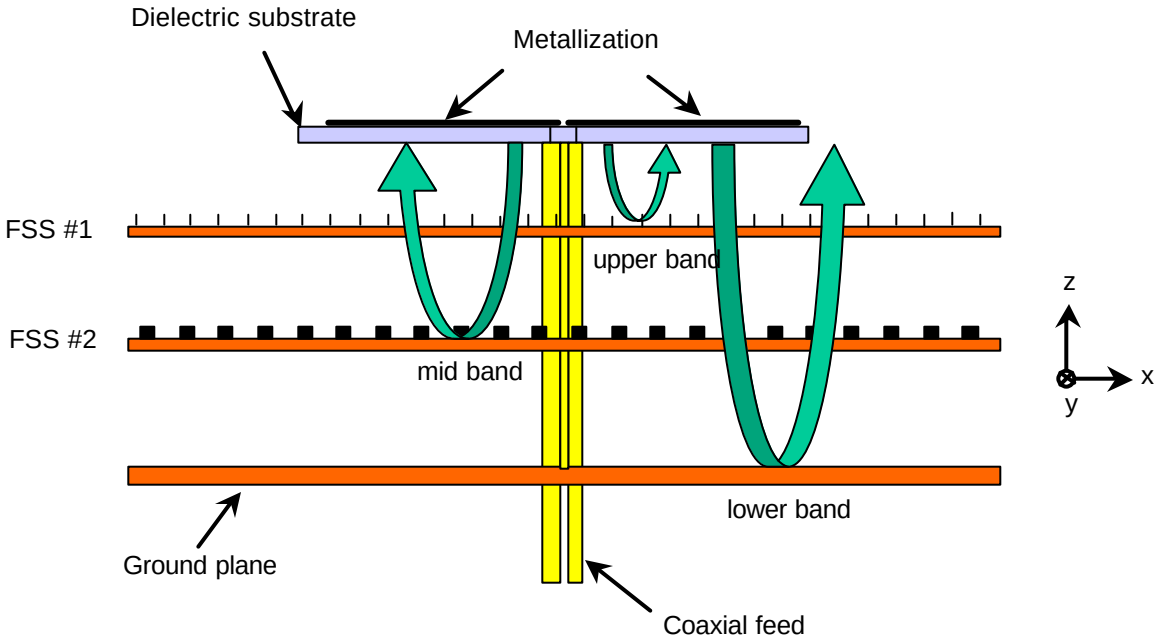

Figure 7.22 A functional schematic diagram of a wideband and passive ground plane using several layers of the Frequency Selective Surfaces [7.4].

7.7 Summary

In this section, diPICA, LPdiPICA with flat ground plane and LPdiPICA antenna with exponentially tapered ground plane were investigated using simulations and several hardware test models.

The dipole PICA antenna (called diPICA) was naturally constructed from the (monopole) PICA antenna discussed in Chapter 6. A software test model demonstrated that the diPICA antenna behaves like several segment half-wave dipoles in a single element, giving ultra wide impedance and pattern bandwidth; see Section 7.2.

With the diPICA antenna, a low-profile diPICA (called LPdiPICA) antenna was accomplished by introducing a ground plane parallel to and behind the diPICA. The LPdiPICA provides more than 10:1 impedance bandwidth and a unidirectional pattern with a ratio bandwidth of 2.2:1 in a compact size. The radiation patterns of the LPdiPICA antenna are degraded as the frequency increases due to the increased electrical height at high frequency. Two hardware test models were examined for the investigation.

As an attempt to enhance the radiation pattern at high frequency, exponentially tapered ground plane was simulated in Section 7.6 rather than flat ground plane. The exponentially tapered ground plane improved the radiation patterns at the high end of the band without degrading the impedance performance at all. Some other tapered ground plane was proposed in Fig. 7.18. Frequency Selective Surface (FSS) was also proposed for improving the radiation pattern. More investigation is necessary with the proposed ground planes for enhancing the performance of the LPdiPICA antenna.

The LPdiPICA antenna has only a single polarization because it has only two opposing arms whereas the Fourpoint or Fourtear antenna has two parts of opposing radiating arms providing dual-polarization. The LPdiPICA antenna, however, provides very wide bandwidth in a low-profile and compact size, which features are suitable for wideband array system and wideband commercial or military applications.

Table 7.3 summarized the performance of the LPdiPICA antenna discussed in this chapter.

Table 7.3

Summary of the antennas discussed in Chapter 7.

Antenna	**Impedance Bandwidth (for VSWR <2)**	**Pattern Bandwidth**
Two-circular-hole diPICA (Section 7.2)	> 10:1	Good omni-directional patterns up to 4:1. Acceptable pattern up to 8:1
Low-profile diPICA (LPdiPICA) with h=1.50" (Section 7.3)	> 10:1	2.2:1
Low-profile diPICA (LPdiPICA) with h=0.75" (Section 7.4)	for 1- 4 GHz, VSWR<3.3. for 4.0 - 10.0 GHz, VSWR < 2.0. (See Fig. 7.11)	4:1
Two-circular-hole LPdiPICA with h=1.50" (Section 7.5)	> 10:1	2.2:1 (Strong lobe in the bore-sight direction at high end of the band)
Two-circular-hole LPdiPICA with exponentially tapered ground plane (Section 7.6)	> 10:1	Good unidirectional patterns at low end and high end of the band such as at $1f_{low}$-$2f_{low}$ and $6f_{low}$-$8f_{low}$. Impaired pattern at the mid-band. Improved pattern is expected with modified tapered ground plane

References

[7.1] W. L. Stutzman and G.A. Thiele, *Antenna Theory and Design 2nd edition*, John Wiley & Sons, New York, 1998.

[7.2] Balanis, *Antenna Theory: Analysis and Design 2nd edition*, pp. 175-181, John Wiley &Sons, New York, 1997.

[7.3] M. C. Bailey, "Broad-Band Half-Wave Dipole," *IEEE Transactions on Antennas and Propagation*," Vol. AP-32, No. 4, pp. 410-412, April 1984.

[7.4] Sanders, R. Gilbert, et. al. "Structually-Integrated Optically-Reconfigurable Antenna Array," *Proc. of Antenna Applications Symposium*, Sept. 1995.

Chapter 8

Conclusions and Future Work

8.1 Summary and Conclusions

This dissertation reported on results from an investigation of several new wideband antennas. Three types of new antennas were invented. These antennas are shown in Table 8.1 along with their electrical characteristics and geometry type. The three types with their subtypes are:

Fourpoint type (Type I)

Fourpoint antenna (I.1)

Fourpoint antenna with tuning plate (I.2)

Fourtear type (Type II)

Fourtear antenna (II.1, II.2)

Modified Fourtear antenna (II.3, II.4)

Planar Inverted Cone Antenna (PICA) type (Type III)

PICA (III.1)

Two-circular-hole PICA (III.2)

Dipole PICA (diPICA) (III.3)

Low-profile diPICA (LPdiPICA) (III.4)

Two-circular hole, low-profile diPICA (LPdiPICA) (III.5)

Two-circular hole, low-profile diPICA with experimentally tapered ground plane (III. 6)

The antenna geometries are all based on a planar radiating structure. They can be printed on a substrate for ease of construction. Or, they can be stamped to avoid the cost of dielectric materials.

There are three pattern shapes represented by the antennas:

Unidirectional (I.1, I.2, II.1, II.2, II.3, II.4, III.4, III.5, III.6)

A single wide main beam perpendicular to the planar structures directed away from the ground plane with nearly equal principal plane beamwidths.

Monopole type (III.1, III.2)

Omni-directional in the plane of the ground plane and a null perpendicular to the ground plane.

Dipole type (III.3)

Omni-directional in the plane perpendicular to the structure.

With the exception of the original Fourpoint antenna, all of the antennas have very wide impedance bandwidth, 10:1 or more. The Fourtear and PICA structures all have 10:1 or more impedance bandwidth. Many of the PICA structures have more than a 10:1 impedance bandwidth and more than a 8:1 pattern bandwidth. In general, the bandwidth is limited by pattern performance rather than impedance performance as is usually the case with wideband antennas.

Table 8.1

Summary of the Wideband Antennas Investigated

Type	Antenna	Impedance bandwidth	Pattern bandwidth	Pattern	Polarization	Geometry
I.1	Fourpoint antenna backed with ground plane 	40.6 % (1.51:1)	40.6 % (1.51:1)	Uni-directional	Dual-linear and Circular	Low-profile
I.2	Fourpoint antenna with tuning plate backed with ground plane 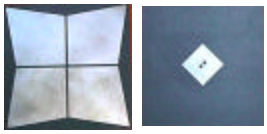	2.75:1	~ 2:1	Uni-directional	Dual-linear and Circular	Low-profile
II.1	Fourtear antenna backed with ground plane (a-a' feed configuration) 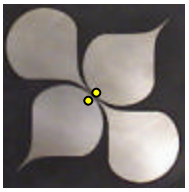	> 10:1	~ 2.2:1	Uni-directional	Dual-linear	Low-profile
II.2	Fourtear antenna backed with ground plane (b-b' feed configuration) 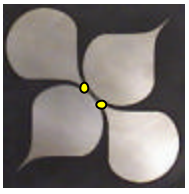	> 10:1	~ 2.2:1	Uni-directional	Dual-linear	Low-profile

Table 8.1 (Continued)

	Antenna	Impedance bandwidth	Pattern bandwidth	Pattern	Polarization	Geometry
II.3	Modified Fourtear antenna backed with ground plane (a-a' feed configuration) 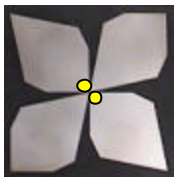	> 10:1	~ 2.6:1	Uni-directional	Dual-linear and Circular	Low-profile
II.4	Modified Fourtear antenna backed with ground plane (b-b' feed configuration) 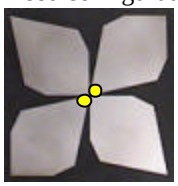	> 10:1	~ 2.6:1	Uni-directional	Dual-linear and Circular	Low-profile
III.1	Planar Inverted Cone Antenna (PICA) mounted on the ground plane perpendicularly 	> 10:1	~ 6:1	Monopole type omni-directional	Linear	Monopole
III.2	Two-circular-hole Planar Inverted Cone Antenna (PICA) mounted on the ground plane perpendicularly 	> 10:1	~ 8:1 (Better pattern than III.1)	Monopole type omni-directional	Linear	Monopole

Table 8.1 (Continued)

	Antenna	Impedance bandwidth	Pattern bandwidth	Pattern	Polarization	Geometry
III.3	Dipole PICA (diPICA) without ground plane 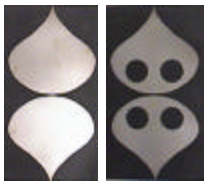	> 10:1	~ 8:1	Dipole type omni-directional	Linear	Dipole
III.4	Low-profile diPICA (LPdiPICA) backed with ground plane 	> 10:1	~ 2.2:1	Uni-directional	Linear	Low-profile
III.5	Two-circular-hole low-profile diPICA (LPdiPICA) backed with ground plane 	> 10:1	~ 2.2:1	Uni-directional	Linear	Low-profile
III.6	Two-circular-hole low-profile diPICA (LPdiPICA) with exponentially tapered ground plane. 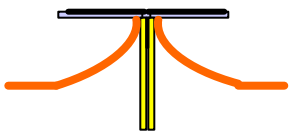	> 10:1	~ 2.2:1 and good pattern at high end of band	Uni-directional	Linear	Low-profile

All of the antennas were thoroughly investigated using both simulations and measurements. Prototypes were constructed and measured, and simulations were performed using a FDTD commercial code, Fidelity. The measured data agreed very well with the simulated data for all the antennas, demonstrating that antenna designs are possible with the computational tool alone.

8.1.1 Fourpoint Antennas

The Fourpoint antenna described in Chapter 3 is a first generation evolution from the Foursquare antenna [8.1], [8.2]. The Fourpoint antenna has enhanced impedance bandwidth that is more than twice that of the Foursquare antenna of the same physical size. The Fourpoint antenna has smaller reactance variations over bandwidth compared to the Foursquare antenna, which is accomplished by eliminating the corner of the Foursquare antenna element. The Fourpoint antenna provides acceptable unidirectional radiation patterns over the impedance bandwidth of about 40 %.

The bandwidth of the Fourpoint and Foursquare antennas was extended even further by adding a tuning plate to the feed structure, but without increasing the antenna size. The tuning plate was devised through extensive antenna simulations as described in Chapter 4. The tuning plate adds a second impedance resonance to the Fourpoint antenna at the high frequency end of the operating band. The tuning plate provides flexibility for tuning the antenna to a desired frequency characteristic; dual-band operation or continuous wideband antenna, etc [8.3]. The tuning plate increases the impedance bandwidth of the Fourpoint antenna to 3:1. The radiation patterns, however, degrade with increasing frequency.

Simulation results demonstrate that the tuning plate is also effective when used with the Foursquare antenna by improving its impedance bandwidth. A numerical model operating in the 5.65 - 10.5 GHz band was simulated; see Section 4.2. A practical Fourpoint antenna was constructed with a tuning plate with the design goal of application as a commercial base-station antenna. The Fourpoint antenna with the tuning plate covers AMPS, GSM, DCS and PCS bands (805 – 2190 MHz) in a single element, providing dual-linear polarization in a low-profile geometry. The Fourpoint antenna element is a very promising element candidate for use in base-station array antennas.

8.1.2 Fourtear Antennas

The next step in the evolution from Fourpoint to Fourtear geometries is the Fourtear antenna (Type II in Table 8.1). Investigation of the gap effect in the Fourpoint antenna leads to Fourtear antenna design. Three gap shapes were examined in Chapter 5: uniform, linearly tapered and non-linearly tapered gaps. The tapered gaps in the Fourpoint antenna enhanced the impedance bandwidth dramatically and were thus employed in the Fourtear antenna also. The Fourtear antenna (II.1 and II.2 in Table 8.1) provides more than 10:1 impedance bandwidth and 2.2:1 pattern bandwidth. Different antenna characteristics for each feed terminal are observed due to the asymmetric geometry in the radiating element. The modified Fourtear antenna (II.3 and II.4) with hexagonal radiating elements has lower impedance variation with frequency for the two feed configurations. The modified Fourtear antenna (II.3 and II.4) provides more than 10:1 impedance bandwidth and a pattern bandwidth of 2.6:1, which is slightly more that of the Fourtear antenna (II.1 and II.2). Based on the investigation, the antennas appear to radiate in the metal part of the radiating element up to the bandwidth of 2.0 ~ 2.5:1. However, at the upper band beyond 3.0:1 bandwidth, most radiation occurs through gaps between the metals, so most of the patterns beyond 3.0:1 bandwidth degraded very fast as the frequency increases. The bandwidth of 2.5 ~ 3.0:1 seems a transition band, changing radiation path from metal to gap. Abrupt change in the impedance level is easily observed in every impedance curves between 2.5 ~ 3.0:1 bandwidth (see Figs.5.10, 5.13 and 5.19). Such phenomenon is one of evidence explaining the transition band.

8.1.3 PICA Antennas

The Planar Inverted Cone Antenna (PICA), Type III antenna is an evolution from the well-known solid teardrop antenna [8.4]. The PICA antenna has more than 10:1 impedance bandwidth and 8:1 pattern bandwidth, as discussed in Chapter 6. Better radiation patterns are observed in the direction of the yz-plane than the pattern in the xz-plane (see Fig. 6.1). The two-circular-hole PICA antenna (III.2) has even better radiation patterns in the direction of the xz-plane without degrading the impedance performance.

The dipole PICA (diPICA) antenna is a modification of monopole PICA antenna. The low-profile diPICA (LPdiPICA) is a further modification of the diPICA antenna to obtain a unidirectional radiation pattern. Investigation results using two hardware test models of the diPICA antennas were discussed in Chapter 7. They provide more than 10:1 impedance bandwidth and 2.2:1 pattern bandwidth. An exponentially tapered ground plane with the two-circular-hole LPdiPICA antenna (III.6) enhanced the radiation patterns at high end of the band without degrading impedance performance. Simulation results demonstrate that the LPdiPICA antenna patterns can be enhanced further at the mid and upper bands by modifying the ground geometry.

8.1.4 Evolution of the Investigated Antennas

The three antenna types developed during the course of this research program can be related to each other with an evolutional chain. It is speculated that the wideband antennas in this dissertation evolved from the PICA antenna. This evolutional process follows these (see Fig. 8.1):

(a) PICA (III.1)

The start point is the PICA which is a monopole type antenna that evolved from a planar form of the teardrop antenna (see Section 2.4 and Fig. 2.8 (b))

(b) diPICA (III.3)

Modification from monopole PICA to dipole PICA (diPICA) is a natural antenna transition using the image concept.

(c) LPdiPICA (III.4)

LPdiPICA antenna is low-profile version of the diPICA obtained by backing the ground plane below the diPICA antenna to obtain a unidirectional pattern.

(d) Fourtear antenna (II.1 and II.2)

The Fourtear antenna evolved by adding parasitic elements perpendicular to the diPICA antenna with identical radiating element but 180° rotated.

(e) Modified Fourtear antenna (II.3 and II.4)

The Fourtear antenna has different antenna characteristics for each feed configuration. Minimizing these differences in the Fourtear antenna characteristics leads to the modified Fourtear antenna.

(f) Fourpoint antenna (I.1)

Fourpoint antenna is one example of the modified Fourtear antenna providing identical antenna characteristics for different feed configurations with lower impedance bandwidth than that of the modified Fourtear antenna.

(g) Fourpoint antenna with tuning plate (I.2)

The impedance bandwidth of the Fourpoint antenna (I.1) was enhanced nearly up to 3:1 with the help of tuning plate. The Fourpoint antenna with tuning plate provides wide bandwidth and identical antenna characteristics for two feed configurations.

Note that the modified Fourtear antenna has electrical characteristics that are strikingly similar to those of self-complementary antenna [8.5]. In theory, self-complementary antenna operating in free space (i.e. no ground plane present) has input impedance of 188.5 + $j0$ Ω. In practice, the measured impedance is lower (between 100-Ω and 188.5-Ω) than the value in theory, due to the finite thickness of metallization and the presence of the coaxial feed line [8.5]. The impedance characteristics (close to 150-Ω) of the modified Fourtear antenna are analogous to the practically measured self-complementary antenna. A more detail investigation is necessary to explain the relationship between the Fourtear antenna and the self-complementary antenna.

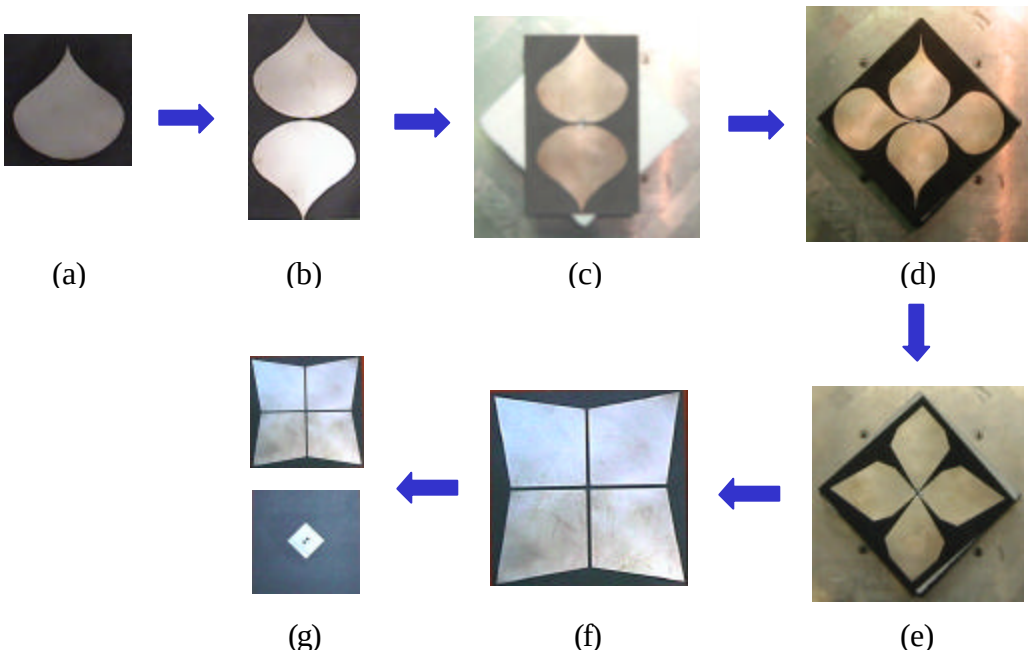

Figure 8.1 An evolution process of the wideband antennas.

8.2 Summary of Original Contributions

The original contributions in this dissertation are following:

- The Fourpoint antenna (I.1) was introduced as a modification of the Foursquare antenna that was invented previously in VTAG. The Fourpoint antenna increases the bandwidth of the Foursquare from 19.7 % to 40.6 % in the same size structure.
- A tuning plate was added to the Foursquare and Fourpoint antennas without increasing the physical antenna size and increased the impedance bandwidth of both. The Fourpoint antenna with tuning plate (I.2) was investigated in detail.
- The Fourtear antenna was developed as a generalization of the concept of the Foursquare and Fourpoint antennas.
- The modified Fourtear antenna (II.3, II.4) was developed and has the similar impedance characteristics for its two feed configurations.
- The PICA antenna (III.1, III.2) was developed and has enhanced radiation pattern performance compared to circular or half-circular monopole disc antennas.
- The low-profile diPICA (LPdiPICA) antenna (III.4, III.5) was developed. It has unidirectional pattern with wide impedance bandwidth, 10:1.
- An exponentially tapered ground plane was added to the LPdiPICA to enhance radiation pattern at upper frequency (III.6). Simulation results of the exponentially tapered ground plane demonstrate the possibility of the radiation pattern enhancement in the wideband antennas with shaped ground planes.
- An evolution process was proposed to explain the relationship between the wideband antennas; see Sec. 8.1.4.
- Three provisional patents have been filed based on this research: the PICA antenna [8.10], the Fourpoint antenna [8.11], and the Fourtear antenna [8.12].

8.3 Future Work

There are several research opportunities that build on this research wideband antenna:

- Extensive current distribution studies could be performed to understand how the antennas work.
- As discussed in Section 8.1, the wideband antennas seem to have close relationship to each other. A logical and mathematical explanation could be developed.
- The modified Fourtear antenna provides an input impedance of 150-Ω close to theoretical value (188.5-Ω) of the self-complementary antenna. A more detail investigation is necessary to explain the relationship between the Fourtear antenna and the self-complementary antenna.
- Self-similarity study was attempted in the PICA antenna. Figure 8.2 shows the prototype of a PICA family antenna and its preliminary measured data demonstrates that the prototype seems to have a self-similarity characteristic. Extensive investigation of the self-similarity in the PICA antenna will be a valuable research for understanding the PICA antenna and further application to wireless communications.
- In designing the PICA antenna, the ratio (L1/L2 = 1.609) of length in the triangle section (L1) and curved section (L2) is close to the golden ratio, 1.618 [8.6]; see Sections 6.4 and 6.5. The golden ratio is found in many natural things such as the human body, animals, plants, DNA, solar system, etc [8.7]. Pyramids are also designed with the golden ratio. There are many other applications using the golden ratio in architecture, sound, and electromagnetics (Windharp) [8.8]. A golden ratio antenna is presented in [8.9], but has very little information. More investigation of the golden ratio lead to a new antenna design concept.

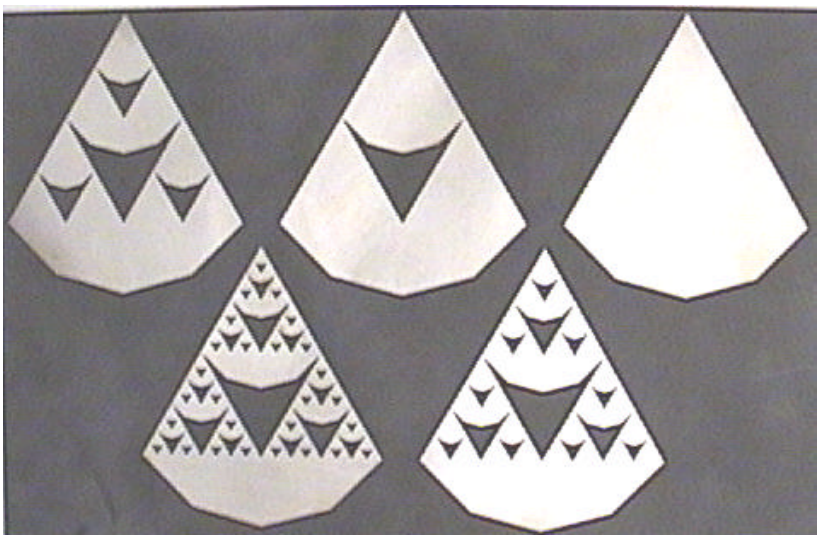

Figure 8.2 Prototypes of the PICA Family etched on a dielectric material with self-similarity.

- The radiating elements of the LPdiPICA antenna can be repositioned to enhance the radiation pattern bandwidth. In other words, when the planar region (xz-plane; see Fig. 7.1) faces upward, the radiation patterns are degraded as the frequency increases in the bore-sight direction and only single polarization is available. However, when the radiating elements are rotated 90° so that the slot region (yz-plane) facing upward, very wide pattern bandwidth is expected. Moreover, dual-linear polarization is also possible by adding another element perpendicular to the radiating element. In addition, the crossed diPICA antenna is easily fed by microstrip lines etched on the same plane as the radiating element. The crossed diPICA antenna with a ground plane can be applied to the multi-band, dual-polarization base-station antenna covering AMPS, GSM, DCS and PCS bands. The crossed diP ICA antenna can also be used in wideband phased array antennas.

- Simulations of the tapered ground plane demonstrates that the tapered ground plane improves the radiation patterns at the high end of the band. More investigations could be performed in attempt to enhance the radiation patterns not only at the high end but also over all the impedance bandwidth.
- Wideband multiple layer Frequency Selective Surface (FSS) ground plane [8.13] could be used as an alternative of the tapered ground plane for the LPdiPICA antenna. The FSS ground plane can also be applied to the low-profile wideband antenna such as the Fourpoint and Fourtear antenna. Investigation is necessary to see if the multiple FSS ground plane can provide wide pattern bandwidth without degrading the impedance performance.
- All of the wideband antennas discussed in this dissertation are excellent candidate elements for wideband phased array antennas because of their features, such as the low-profile geometry and wide antenna bandwidth. The study of wideband array antenna using the proposed elements could be fruitful.

References

[8.1] J. R. Nealy, "Foursquare Antenna Radiating Element," *U.S. Patent No. 5,926,137*, July 20, 1999. VTIP Ref. 96-056. http://www.vtip.org.

[8.2] Randall Nealy, Warren Stutzman, J. Matthew Monkevich, William Davis, "Improvements to the Foursquare Radiating Element-Trimmed Foursquare," *U.S. Patent No. 6,057,802*, May 2, 2000. VTIP Ref. 98-001. http://www.vtip.org.

[8.3] S. A. Bokhari, Jean-Francois Z?rcher, Juan R. Mosig, Fred E. Gardiol, "A small Microstrip Patch Antenna with a Convenient Tuning Option," *IEEE Trans. Antennas Propagation*., vol. 44, No. 11, pp. 1521-1528, Nov. 1996.

[8.4] N. E. Lindenblad, "Antennas and Transmission Lines at the Empire State Television Station," *Communications*, pp.10-26, April, 1941.

[8.5] G. A. Deschamps, "Impedance Properties of Complementary Multiterminal Planar Structures," *IRE Trans. on Antennas and Propagation*, pp. 371-378, Dec. 1959.

[8.6] S Vajda, *Fibonacci and Lucas numbers, and the Golden Section: Theory and Applications*, Halsted Press: New York, 1989.

[8.7] http://goldennumber.net/.

[8.8] http://www.soundscapesinternational.com/index.htm.

[8.9] http://ncatark.uark.edu/~rondav/georgek/index/Goldenratio.htm.

[8.10] Seong-Youp Suh and Warren L. Stutzman, "*A Planar Inverted Cone Antenna*," VTIP Disclosure No. 00-130, http://www.vtip.org/Licensing/disclosures/00-130.htm, September 8, 2000.

[8.11] Seong-Youp Suh and Warren L. Stutzman, "*A Fourpoint Antenna*," VTIP Disclosure No. 00-141, http://www.vtip.org/Licensing/disclosures/00-141.htm, September 28, 2000.

[8.12] Seong-Youp Suh and Warren L. Stutzman, "*A Fourtear Antenna*," VTIP Disclosure No. 01-078, http://www.vtip.org/Licensing/disclosures/01-078.htm, July 17, 2001.

[8.13] Sanders, R. Gilbert, et. al. "Structually-Integrated Optically-Reconfigurable Antenna Array," *Proc. of Antenna Applications Symposium*, Sept. 1995.

Appendix A
Pattern Measurement of a Balanced Antenna Using a Balun

In pattern measurement, many balanced antennas employ balun (0°/180° hybrid or 180° power divider) to create a balanced feed as shown in Fig. A1. If the 0°/180° hybrid is used, the sum port in the hybrid should be terminated with the characteristic impedance, Z_0. The balun transmits 180° out-of-phase signals to the each port of the antenna with the same amplitude. Losses exist during the signal transmission due to impedance mismatch between the balun and the antenna. And the insertion loss of the balun exists too. The shape of the antenna pattern, however, can be obtained by normalizing the measured pattern with maximum gain. Therefore, the normalized radiation pattern can be directly measured regardless of the presence of the impedance mismatch and insertion losses. In other words, no matter what the antenna impedance, the normalized radiation pattern can be measured with the balun (0°/180° hybrid or 180° power divider).

Gain measurement, however, needs complicate procedures such as compensation of mismatch and insertion losses. Generally, the hybrid (or the power divider) has a characteristic impedance of Z_0=50-Ω, so the impedance at the balanced end (antenna element feed point) is $2Z_0$=100-Ω, which is the sum of Z_0 at two balanced ports (see Fig. A1). Except for a condition that the antenna has an input impedance of $2Z_0$=100-Ω over whole band, there are always loss in the balun and the antenna due to the impedance mismatch between the balun and the antenna. Not only the impedance mismatch, but the insertion loss exists always due to the loss caused when the balun is inserted between the

antenna and power source. Realized antenna gain can be obtained only if the losses are compensated from the directly measured gain.

Loss from impedance mismatch can be calculated using VSWR value from the measured element impedance with referenced to the balun impedance of 100-Ω. Insertion loss can be found in the technical brochure of the balun.

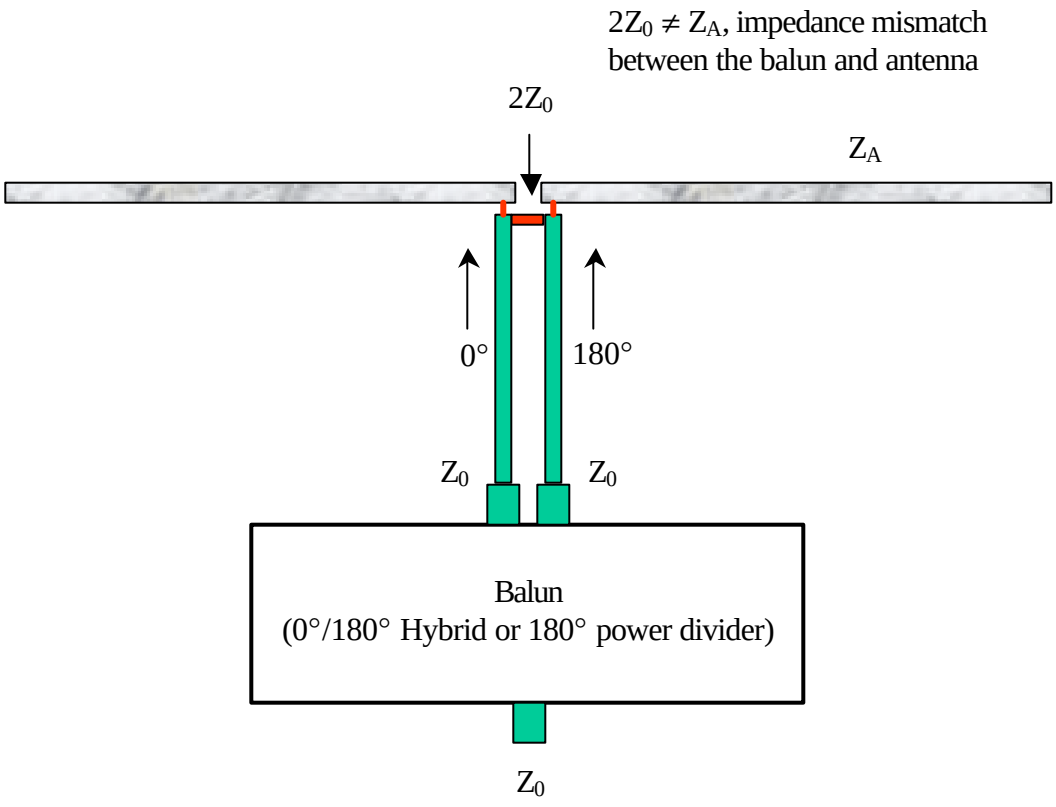

Figure A.1 Balanced antenna with a balun.

Appendix B
Gain vs. Frequency Plots

This appendix presents gain versus frequency plots for some typical antennas discussed in this dissertation. Figures B.1 to B.6 show plots for the following antennas: Fourpoint, modified Fourtear, PICA, two-circular-hole PICA, LPdiPICA and two-circular-hole LPdiPICA antennas. The maximum gain is presented at frequencies in the impedance bandwidth. Gain patterns can be directly obtained by adding the maximum gain number to the normalized radiation pattern of each antenna.

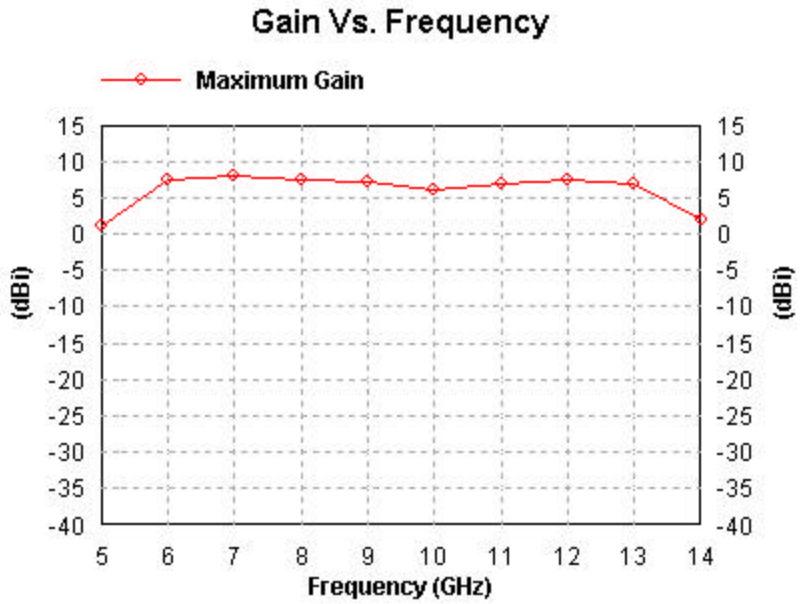

Figure B.1 Computed gain plot of Fourpoint antenna discussed in Section 3.6. (see the normalized patterns in Fig. 3.8)

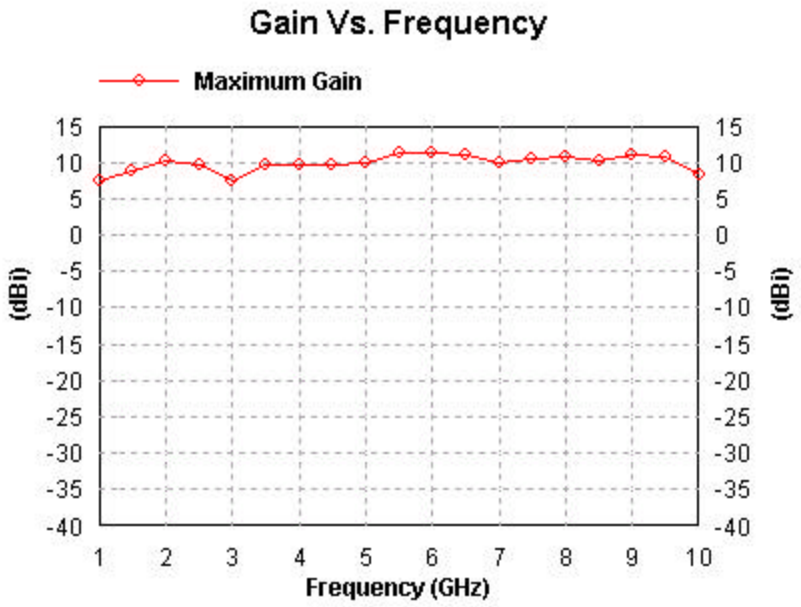

Figure B.2 Computed gain plot of modified Fourtear antenna (b-b' feed) discussed in Section 5.5. (see the normalized patterns in Figs. 5.20 and 5.21)

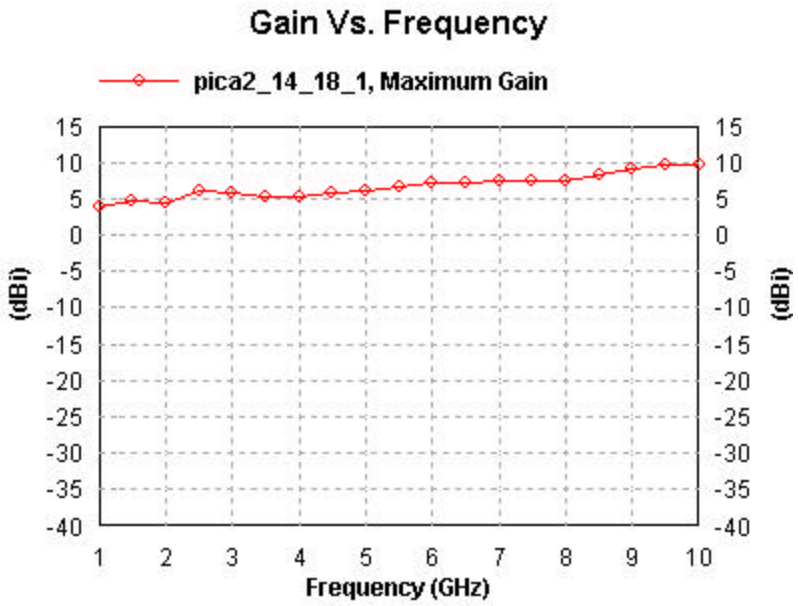

Figure B.3 Computed gain plot of PICA discussed in Section 6.4.

(see the normalized patterns in Fig. 6.9)

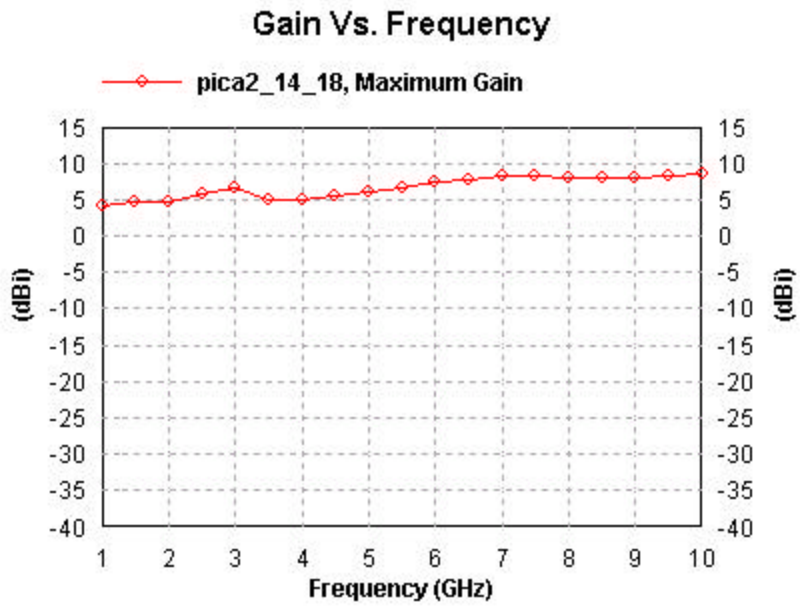

Figure B.4 Computed gain plot of two-circular-hole PICA discussed in Section 6.5.
(see the normalized patterns in Fig. 6.13)

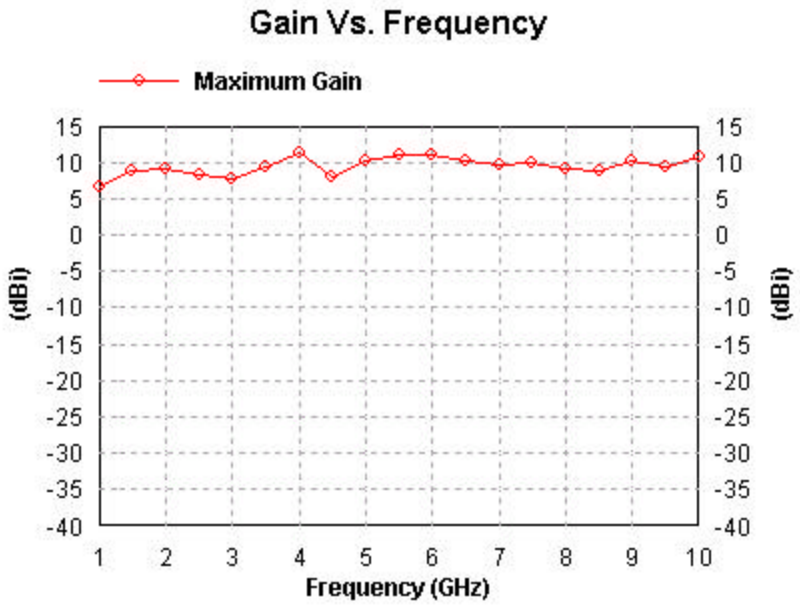

Figure B.5 Computed gain plot of LPdiPICA discussed in Section 7.3.
(see the normalized patterns in Fig. 7.10)

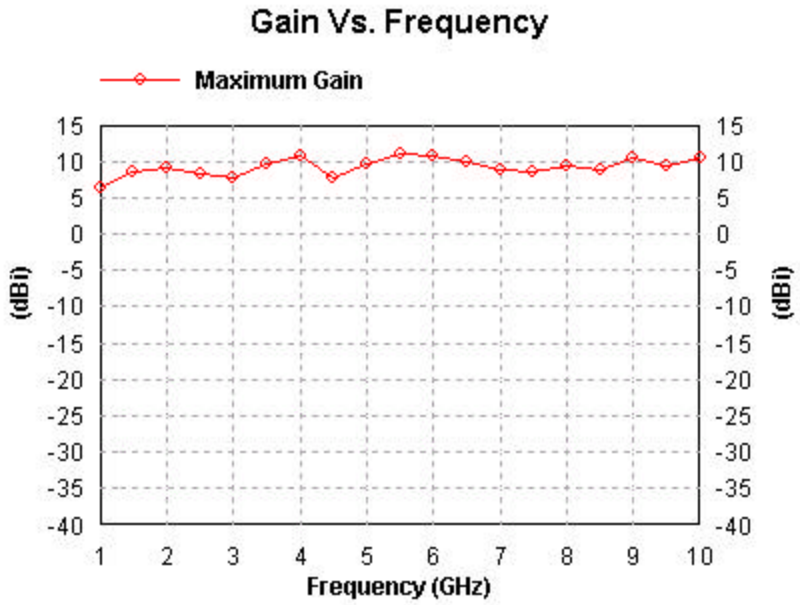

Figure B.6 Computed gain plot of LPdiPICA discussed in Section 7.5.
(see the normalized patterns in Fig. 7.17)

VITA

Seong-Youp Suh
suh@vt.edu

Seong-Youp Suh was born in Chonbuk, Republic of Korea on February 17, 1968. He attended the Chonbuk National University in JeonJu, Republic of Korea from March 1986 through February 1990 where he received the Bachelor of Engineering degree. Following graduation, he worked as a researcher for Agency for Defense Development in Daejeon, Republic of Korea from 1990 to 1996. While a researcher at the Agency for Defense Development, he worked in the EMI/EMC design group.

In August of 1996, Seong-Youp joined the Virginia Tech Antenna Group to pursue a Master's degree. He studied propagation for land mobile satellite communications and developed a simulator. He obtained his Master's degree on May 1998.

Seong-Youp continued his Ph.D. program at Virginia Tech as a graduate research assistant in Virginia Tech Antenna Group. His research interests are wideband antenna design and antenna propagation.